

UC Irvine

UC Irvine Electronic Theses and Dissertations

Title

Validation of a Human Vascularized Micro-Tumor Model

Permalink

<https://escholarship.org/uc/item/7mq5z49d>

Author

Hachey, Stephanie Jeanelle

Publication Date

2019

Peer reviewed|Thesis/dissertation

UNIVERSITY OF CALIFORNIA,
IRVINE

Validation of a Human Vascularized Micro-Tumor Model

DISSERTATION

submitted in partial satisfaction of the requirements
for the degree of

DOCTOR OF PHILOSOPHY

in Molecular Biology and Biochemistry

by

Stephanie J. Hachey

Dissertation Committee:
Christopher Hughes, Chair
Marian Waterman
David Fruman
Jennifer Prescher

2019

DEDICATION

To my son Noah, who is my inspiration and motivation every single day.

TABLE OF CONTENTS

	Page
LIST OF FIGURES	vii
LIST OF TABLES	ix
ACKNOWLEDGMENTS	x
CURRICULUM VITAE	xiii
ABSTRACT OF THE DISSERTATION	xvii
1 Introduction	1
1.1 Background	1
1.2 Strengths and Limitations of Standard Preclinical Models	4
1.3 Overview of the Tumor Microenvironment	9
1.4 Microphysiological Systems for Cancer Research	12
1.4.1 Tumor Chips	14
1.4.2 Integrated Tumor-Organ-Chip Systems: Toxicity, PK-PD Modeling, and Metastasis Studies	28
1.4.3 Personalized Medicine Applications	31
1.4.4 Design of Tumor Chips	39
1.5 Future Considerations	42
1.6 Closing Remarks	44
1.7 Foreword	44
2 Recapitulating the Tumor Microenvironment <i>In Vitro</i> Using a Vascularized Micro- Tumor Model	47
2.1 Abstract	47
2.2 Introduction	48
2.3 Materials and Methods	50
2.3.1 Cell culture.	50
2.3.2 Microfluidic device fabrication.	50
2.3.3 Loading the microfluidic device.	51
2.3.4 Generation of tumor spheroids.	51
2.3.5 Drug treatment.	52
2.3.6 Immunofluorescence staining.	53

2.3.7	Fluorescence imaging and analyses.	53
2.3.8	Finite element simulation.	54
2.3.9	Cell sorting.	55
2.3.10	Animal studies.	55
2.3.11	NanoString PanCancer Human Pathways Assay.	57
2.3.12	Xenograft tumors for single-cell sequencing and cell anchoring.	58
2.3.13	SW480 xenograft dissociation for single cell sequencing.	58
2.3.14	Single-cell sequencing.	59
2.3.15	Transcriptome alignment and data processing.	59
2.3.16	Ligand-receptor interaction analyses.	60
2.3.17	Single cell genotyping analyses.	61
2.3.18	Pathway analyses.	63
2.3.19	Cell anchoring.	63
2.3.20	Statistical analyses.	63
2.4	Results	64
2.4.1	The vascularized micro-tumor (VMT) serves as a high throughput platform for realistic tumor modeling and direct visualization of the tumor microenvironment.	64
2.4.2	Vessels in the VMT are irregular and leaky, hallmarks of <i>in vivo</i> tumors.	66
2.4.3	Transcriptomic comparison of cancer cells grown as monolayer culture, in the VMT and as xenograft tumors shows high correlation in gene expression between VMT and xenograft tumors, with significant divergence from monolayer cultures.	69
2.4.4	The VMT recapitulates xenograft tumor growth and response to standard of care therapy, whereas monolayer cultures show significantly different growth patterns and drug sensitivity.	71
2.4.5	Single-cell mRNA sequencing reveals that the transcriptome of stromal and tumor cells in the VMT retain features of <i>in vivo</i> tumor cell populations not seen in monolayer or spheroid cultures.	74
2.4.6	HCT116 colorectal cancer (CRC) cell-derived VMT and matched monolayer cultures.	74
2.4.7	SW480 CRC cell-derived VMT, tumor spheroids and matched monolayer cultures.	79
2.4.8	Lineage hierarchy reconstruction reveals a unique VMT-derived HCT116 tumor population with characteristics of invasive CRC.	81
2.4.9	Pathways implicated in tumor progression are upregulated in CRC cells grown in the VMT when compared to cells grown as 2-dimensional (2D) or 3-dimensional (3D) monocultures.	84
2.4.10	Dynamic intercellular cross talk within the VMT promotes extracellular matrix remodeling characteristic of malignancy.	87
2.4.11	VMT-derived stroma model clinical characteristics of reactive stroma in CRC.	89
2.4.12	VMT-derived SW480 CRC cells better model <i>in vivo</i> tumor heterogeneity than 2D and 3D monocultures.	92
2.5	Discussion	93

2.6	Conclusion	96
3	Automated Image Processing for a Vascularized Micro-Tumor Model Using ImageJ Scripting and Macros	97
3.1	Abstract	97
3.2	Introduction	98
3.3	Materials and methods	99
3.3.1	Script development	99
3.3.2	Script installation	100
3.3.3	Device fabrication	102
3.3.4	Cell culture	103
3.3.5	VMO/VMT establishment	103
3.3.6	Fluorescent imaging, perfusion and bead tracking	104
3.3.7	COMSOL Multiphysics simulation	105
3.3.8	Statistical analysis	105
3.4	Results	106
3.4.1	Overview	106
3.4.2	Functionality	107
3.4.3	Convert ND2	110
3.4.4	Color and Merge Images Module	111
3.4.5	Segment Tumor Images Module	112
3.4.6	Measure Tumor Gray Level	113
3.4.7	Threshold Vessel Images	113
3.4.8	Measure Vessel Diameter	114
3.5	Discussion	121
3.6	Conclusion	122
4	A Vascularized Micro-Tumor Model to Study Patient-Derived Colorectal Cancer Cells	124
4.1	Introduction	124
4.2	Methods	127
4.2.1	Sample collection	127
4.2.2	Tissue processing	127
4.2.3	Cell culture	128
4.2.4	Immunofluorescent staining	130
4.2.5	Fluorescent imaging	130
4.2.6	Fluorescent image analysis	131
4.2.7	Microfluidic device fabrication	132
4.2.8	Loading the microfluidic device	132
4.2.9	DNA and RNA isolation	133
4.3	Results	133
4.3.1	The VMT model supports the growth of patient-derived tumor tissue.	133
4.3.2	Fluorescence lifetime imaging microscopy (FLIM) detects metabolomic heterogeneity in pVMT.	136
4.4	Discussion	138

4.5	Conclusion	141
5	Considerations	143
5.1	Establishment of culture conditions	143
5.1.1	Oxygen tension	143
5.1.2	Human-derived serum	144
5.1.3	Treatment with bevacizumab	145
6	Future Directions	150
6.1	Significance	150
6.2	Aims	153
6.2.1	Aim 1: Promote enhanced immune cell infiltration into the tumor via vascular normalization.	154
6.2.2	Aim 2: Analyze transcriptome of CRC tumor-immune microenviron- ment at single cell resolution to derive novel immunotherapy targets.	157
6.3	Conclusion	158
	Bibliography	160

LIST OF FIGURES

	Page
1.1	Vascularized micro-tumor model 15
1.2	Tumor cell extravasation from <i>in vitro</i> microvessels 19
1.3	Cancer type-specific modeling on-chip 21
1.4	Examples of onco-immuno chips 26
2.1	Cells in the VMT can be isolated via flow assisted cell sorting (FACS). 56
2.2	Cell cycle gene visualization for HCT116. 61
2.3	Cell cycle gene visualization for SW480. 62
2.4	Vascularized micro-tumors (VMTs) form in response to gravity-driven flow within a microfluidic platform arrayed for high throughput experiments 65
2.5	VMT-associated stroma model key features of <i>in vivo</i> tumors 67
2.6	Collagen tracks revealed within the VMT 69
2.7	Distinct changes in gene expression and tumor heterogeneity that better model <i>in vivo</i> tumors occur when cells previously grown in 2D monocultures are grown in the VMT 73
2.8	Distinct changes in gene expression that better model <i>in vivo</i> tumors occur when cells previously grown in 2D monocultures are grown in the VMT 75
2.9	Single nucleotide variation and copy number variation analyses for HCT116 77
2.10	Distinct changes in tumor heterogeneity that better model <i>in vivo</i> tumors occur when cells previously grown in 2D monocultures are grown in the VMT 78
2.11	VMT-associated stroma model key features of <i>in vivo</i> tumors 80
2.12	VMT-associated stroma model key features of <i>in vivo</i> tumors 82
2.13	Differential tumor states observed in VMT derived from SW480 and HCT116 83
2.14	VMT-associated stroma model key features of <i>in vivo</i> tumors 84
2.15	Pathway enrichment for VMT-derived cells. 86
2.16	VMT-associated stroma model key features of <i>in vivo</i> tumors 90
2.17	TGF- β signaling promotes CRC progression. 91
3.1	Options presented during installation of Hughes Lab Tools 101
3.2	Hughes Lab Tools Menu. 102
3.3	Hughes Lab Tools User Interface 108
3.4	ND2 Convert tool log window 111
3.5	Color and Merge Images function 112
3.6	Tumor Segmentation and Measurement function 113
3.7	Vessel Thresholding function 114

3.8	An Automated Method of Measuring Vessel Diameter is Comparable to Manual Methods.	116
3.9	Thrombin-induced vascular leak in the vascularized micro-organ (VMO) .	119
3.10	Streamline profile and bead tracking simulation using thresholded vessel images	120
4.1	Isolation of primary colorectal cancer-initiating cells	134
4.2	Primary CRC cells grow in a vascularized micro-tumor model arrayed for high throughput experiments	135
4.3	Wide chamber design allows ease of CCIC loading	136
4.4	The VMT supports the survival and growth of patient-derived CRC cells from different individuals	137
4.5	pVMTs model histological and growth characteristics of primary tumors from which they were derived	138
4.6	FLIM metabolomics imaging of pVMT reveals heterogeneity	139
5.1	Oxygen tension affects growth of CRC cells within the VMT	144
5.2	Human serum in place of FBS promotes differential growth of CRC-derived VMT	146
5.3	Bevacizumab shows no significant anti-angiogenic or anti-tumor effects in the VMT	147
5.4	Dual chamber device supports angiogenic sprouting toward tumor cells .	149

LIST OF TABLES

	Page
1.1 Applications of Tumor Chip Technology	12
2.1 Results from reference-based integration of SW480 scRNAseq datasets . . .	92
4.1 CCIC basal media	128
4.2 CCIC complete media	129

ACKNOWLEDGMENTS

I would like to thank my mom, Cynthia, first and foremost for giving so wholly and selflessly of herself, for always being there and prioritizing our family above all else, and for the huge heart she constantly gives from. She's the one who's made it possible for me to pursue my dreams and I would not have been able to finish my degree without her. She's the best mom and now a wonderful grandma to my son. I hope that someday I will be able to give back to her even a small fraction of what she's given us.

I'm deeply appreciative to all the support my dad, Peter, has provided me throughout my life to help me achieve my goals, and he is such an amazing grandpa. I'd also like to thank my brother, Michael, for his support and for being there in times of need – my son loves his Uncle Mikey.

Thank you to my precious sweet Noah Bear, the light and joy of my life, for teaching me what's truly important and giving me the most incredible purpose. Every moment with you is magic and I'm so excited about what the future holds. You've grown so much and it blows me away how brilliant and fun you are.

Thank you to my partner, Alex, for loving and supporting me unconditionally. You do so much for us without any expectations and I appreciate that so much. I love our journey, you make it so much fun, and I'm excited about where it will take us.

My family is my rock, through good times and bad, my reliable source of support and reprieve, and for that there are no words that can describe the depth of my love and appreciation. I feel extremely fortunate for being presented with the opportunities that I have.

I'd like to thank my mentor Dr. Chris Hughes, without whom I wouldn't have been able to take part in such amazing, groundbreaking research and had the opportunity to further my career in the ways that I have. I'm truly grateful to his dedication to his students, and that he supports my professional as well as personal goals. Chris always encourages us to think outside the box and be creative about how we approach problems - the sky is never the limit. He's helped me to grow as a scientist, writer, communicator and critical problem-solver.

I'd like to thank those on my committee: Dr. Marian Waterman, for providing sound scientific feedback and collaboration, Dr. David Fruman, for his thoughtful and thorough feedback on my dissertation and projects, for helping to foster my professional development and for promoting me in my career aspirations through the GPS-Biomed program, and to Dr. Jason Zell, for acting as a second mentor to me, continually advocating for our studies, and supporting me throughout my journey as a translational researcher. Thank you to Dr. Jennifer Prescher for acting as oversight member for these studies and providing helpful feedback.

I am grateful for the help of the physicians who have dedicated their time to this study, particularly the members of the gastrointestinal disease oriented team at UCI medical center. Thank you to the following physicians for making collection of patient samples possible: Dr. Jason Zell, Dr. John Lee, Dr. Dorna Jafari, Dr. Robert Edwards, Dr. Yung Lyou and Dr. Samuel Klempner. Thank you to Chang Shim and Corrinne Maton, clinical research coordinators, for facilitating collections. Many thanks to the numerous other research and clinical staff who have assisted in these studies. A special thank you to the patients who agree to donate their tissues to research purposes to make these types of studies possible for the betterment of humanity.

Thank you to everyone in lab, past and present, who've helped with this study and provided support. I've grown so much during my time here and am so grateful to all those people who supported me in achieving my goals, either directly or indirectly. Thank you to Dr. Jennifer Fang for providing scientific, professional and personal advice, for developing the macro for perfusion and diameter measurements in Chapter 3, for writing the methods for those functions and producing Figure 3.8, providing edits and feedback on manuscript drafts and feedback on my defense; Dr. Hugh Bender for feedback on my defense and manuscript drafts and providing scientific advice; Dr. Duc Phan for providing feedback and advice; Damie Juat for help with culturing and validating cells, ordering reagents and general support in the lab; Hannah Bone for fabricating devices and providing general support in the lab; Brittany Pham for providing feedback on my defense, providing scientific feedback and general support; Sebastian Piombo for helping with cell sources and providing scientific feedback; Dr. Satomi Matsumoto for providing feedback on my defense and providing scientific feedback; and Makena Ewald and William Van Trigt for providing feedback on my defense, as well as scientific feedback.

Thank you to the following past lab members: Dr. Agua Sobrino, for helping with patient-derived tissues and drug screening in the VMT, for performing FLIM analyses, for writing methods and providing scientific feedback; Dr. Monica Romero-Lopez for helping with imaging and analyses and providing scientific feedback; Dr. Nan Hultgren and Dr. Ashley Fong for providing scientific feedback and professional advice, and Michaela Hatch, for assisting with establishment of xenograft tumors and training me how to work with mice.

Thank you to the undergraduate students who have helped me over the course of my time in the lab. A special thank you for all your work with cell culture, fabrication, imaging, image analysis, and general project support: Silva Movsesyan, Elizabeth Celaya, Ani Tankanzyan, Giselle Burton Sojo and Samantha Gomez.

Thank you to our collaborators in the following labs: Dr. Marian Waterman, Dr. Abraham Lee, Dr. Steven George, Dr. Kai Kessenbrock, and Dr. Devon Lawson. Thank you to: Da Zhao, Lee lab, for help with VMO/VMT simulations, fabrication and methods; Quy Nguyen, Kessenbrock lab, for help with single cell RNA sequencing data processing and analyses, coding, figures and methods; Kevin Nee, Kessenbrock lab, for help with ligand-receptor interaction analyses and methods; Nick Pervolarakis, Kessenbrock lab, for single cell RNA sequencing analyses and coding; Ryan Davis, Lawson lab, for help with copy number

variation analyses; and George Chen, Waterman lab, for allowing us use of his single cell RNA sequencing dataset and providing methods.

Thank you to Dr. Jenny Wu for bioinformatics support to carry out the single nucleotide variation analyses, cell anchoring, coding and methods; and Dr. Tuyen Hoang for biostatistics assistance with bulk RNA sequencing data analyses. Thank you to Vanessa Scarfone for support with FACS.

Thank you to the organizations and funding sources that have supported this research and my career development: Center for Complex Biological Systems (CCBS) Opportunity Award, ARCS Fellowship, Chancellor's Club Fellowship, Institute for Clinical and Translational Science (ICTS) Pilot Award, Edwards LifeSciences Cardiovascular Technology Fellowship, Chao Family Comprehensive Cancer Center (CFCCC) Kure-It Award, School of Medicine (SOM) Chair Award, National Institutes of Health (NIH) UH2/UH3 TR000481, NIH R01-PQD5 CA180122 and NIH U54 CA217378-01A1.

Thank you to the Royal Society of Chemistry for allowing the use of published work in its entirety for dissertation purposes (Chapter 1 - Introduction, published review).

CURRICULUM VITAE

Stephanie J. Hachey

EXPERIENCE

Graduate Student Researcher, Hughes Lab University of California, Irvine	2015–2019
Graduate Professional Success in Biomedical Sciences Program University of California, Irvine	2016–2019
Invention Transfer Group Fellow University of California, Irvine	2018
Teaching Assistant University of California, Irvine	2016–2017
Lab Assistant II, Boiko Lab University of California, Irvine	2013–2014
Lab Assistant II, Chen Lab University of California, Irvine	2010–2012
Lab Assistant I, Strome Lab University of California, Santa Cruz	2008–2010

EDUCATION

Doctor of Philosophy, Molecular Biology and Biochemistry University of California, Irvine	2019
Master of Science, Biomedical and Translational Science University of California, Irvine	2014
Bachelor of Science, Molecular, Cell, and Developmental Biology University of California, Santa Cruz	2009

HONOR SOCIETIES

Graduate Women in Science Member	2017 – Present
Golden Key Honor Society Member	2013 – Present

CERTIFICATES

BioInformatics Stanford University	In Progress – 2020
Data Science University of California, Irvine	In Progress – 2019
Professional Development University of California, Irvine	In Progress – 2019
Scientific Writing and Publishing Nature Masterclasses, Nature Publishing Group	2017
Effective Communications University of California, Irvine	2017

FELLOWSHIPS, FUNDING AND AWARDS

Center for Complex Biological Systems Opportunity Award University of California, Irvine	2019
Chancellor’s Club Excellence Fellowship University of California, Irvine	2019
Grad Slam 2nd Place Award University of California, Irvine	2019
Institute for Clinical and Translational Science Pilot Award University of California, Irvine	2018–2019
ARCS Scholar Award University of California, Irvine	2017–2019
Edwards Lifesciences Center for Advanced Cardiovascular Technology Fellowship University of California, Irvine	2017–2018
Chao Comprehensive Cancer Center Kure It Grant University of California, Irvine	2017–2018
School of Medicine Chair Award University of California, Irvine	2015–2016

PUBLICATIONS (ACCEPTED)

Applications of Tumor Chip Technology, S. J. Hachey, C. C. W. Hughes, Lab Chip. 18(19):2893-2912 September 26, 2018 doi:10.1039/c8lc00330k

Deep Learning for Drug Discovery and Cancer Research: Automated Analysis of Vascularization Images, G. Urban, K. M. Bache, D. Phan, A. Sobrino, A. K. Shmakov, S. J. Hachey, C. C. W. Hughes, P. Baldi, *IEEE/ACM Trans. Comput. Biol. Bioinform.* 16(3):1029-1035 May 29, 2018 doi:10.1109/TCBB.2018.2841396

Blood-brain barrier-on-a-chip: Microphysiological systems that capture the complexity of the blood-central nervous system interface, D. T. T. Phan, R. H. F. Bender, J. W. Andrejcsk, A. Sobrino, S. J. Hachey, S. C. George, C. C. W. Hughes, *Exp. Biol. Med.* 242(17):1669-1678 January 1, 2017 doi:10.1177/1535370217694100

3D microtumors in vitro supported by perfused vascular networks, A. Sobrino, D. T. T. Phan, R. Datta, X. Wang, S. J. Hachey, M. Romero-López, E. Gratton, A. P. Lee, S. C. George, C. C. W. Hughes, *Sci. Rep.* 6(1):31589 August 23, 2016 doi:10.1038/srep31589

Antibody Therapy Targeting CD47 and CD271 Effectively Suppresses Melanoma Metastasis in Patient-Derived Xenografts, M. Ngo, A. Han, A. Lakatos, D. Sahoo, S. J. Hachey, K. Weiskopf, A. H. Beck, I. L. Weissman, A. D. Boiko, *Cell Rep.* 16(6):1701-1716 August 9, 2016 doi:10.1016/j.celrep.2016.07.004

Therapeutic Implications of Melanoma Heterogeneity, S. J. Hachey, A. D. Boiko, *Experimental Dermatology.* 25(7):497-500 July 25, 2016 doi:10.1111/exd.13002

Preeclampsia up-regulates angiogenesis-associated microRNA (i.e., miR-17, -20a, and -20b) that target ephrin-B2 and EPHB4 in human placenta. , W. Wang, L. Feng, H. Zhang, S. J. Hachey, S. Satohisa, L. C. Laurent, M. Parast, J. Zheng, D. Chen, *J. Clin. Endocrinol. Metab.* 97(6):E1051-E1059 June 2012 doi:10.1210/jc.2011-3131

P granules extend the nuclear pore complex environment in the C. elegans germ line, D. L. Updike, S. J. Hachey, J. Kreher, S. Strome, *J. Cell Biol.* 192(6):939-948 March 21, 2011 doi:10.1083/jcb.201010104

PUBLICATIONS (IN PREPARATION)

Validation of a Vascularized Micro-Tumor Model, S. J. Hachey, S. Movsesyan, A. Tankanzyan, G. B. Sojo, M. S. Hatch, C. W. W. Hughes — Planned submission *PNAS*, June 2019

Automated Image Processing of Vascularized Micro-Tumor Micrographs Using ImageJ, S. J. Hachey, J. Fang, D. Zhao, C. C. W. Hughes — Planned submission *Journal of Cell Biology*, June 2019

Recapitulating Tumor Heterogeneity *In Vitro* Using Patient-Derived Colorectal Cancer Cells in a Vascularized Micro-Tumor Model, S. J. Hachey, G.B. Sojo, C. C. W. Hughes, J. A. Zell — Planned submission *Nature*, August 2019

A Microfluidic Device to Culture Multi-Type 3D *In Vitro* Tissues to Study Tumor Angiogenesis, D. Zhao, S. J. Hachey, J. Fang, C. C. W. Hughes, A. Lee — Planned submission Lab on a Chip, August 2019

PRESENTATIONS

Recapitulating Tumor Heterogeneity *In Vitro* Using a Vascularized Micro-Tumor Model, S. J. Hachey, S. Movsesyan, A. Tankazyan, G. B. Sojo, J. A. Zell and C. C. W. Hughes

- Oral Presentation – 2019 Molecular Biology and Biochemistry Departmental Retreat – University of California, Irvine

Validation of a Microfluidic Device to Study Patient-Derived Colon Cancer Cells and Determine Clinical Predictive Value, S. J. Hachey, A. Sobrino-Gregorio, E. Celaya, D. Phan, M. Romero-Lopez, R. Datta, E. Gratton, A. Lee, S. Klempner, J. A. Zell and C. C. W. Hughes

- Oral presentation – 2016 19th Annual Cancer Center Retreat – University of California, Irvine
- Oral presentation – 2017 Molecular Biology and Biochemistry Departmental Retreat – University of California, Irvine
- Oral and poster presentation – 2017 9th Annual Translational Science Day – University of California, Irvine

A Pilot Study to Establish Proof-of-Concept That Patient-Specific Tumor Tissue Can Be Maintained in the Novel Tumor-on-a-Chip Model, S. J. Hachey, A. Sobrino-Gregorio, D. Phan, M. Romero-Lopez, R. Datta, E. Gratton, A. Lee, S. Klempner, J. A. Zell and C. C. W. Hughes

- Poster presentation – 2015 18th Annual Cancer Center Retreat – University of California, Irvine

Effect of BRAF V600E Heterogeneity on Melanoma Pathogenesis, S. J. Hachey, D. Gillen, W. Chen, and A. Boiko

- Poster presentation – 2015 17th Annual Cancer Center Retreat – University of California, Irvine

Targeting CD271+ Melanoma Tumor Initiating Cells Synergizes with CD47 Blockade to Prevent Multiple Organ Metastasis *In Vivo*, M. Ngo, S. J. Hachey, K. Weiskopf, A. Aziladeh, I. Weissman, and A. Boiko

- Poster presentation – 2013 16th Annual Cancer Center Retreat – University of California, Irvine

S-Nitrosylation of Cofilin-1 is a Novel Pathway for Endothelial Cytoskeleton Remodeling, H. Zhang, S. J. Hachey, S. Park, and D. Chen

- Poster presentation – 2011 SSR Annual Meeting – Portland, Oregon

ABSTRACT OF THE DISSERTATION

Validation of a Human Vascularized Micro-Tumor Model

By

Stephanie J. Hachey

Doctor of Philosophy in Molecular Biology and Biochemistry

University of California, Irvine, 2019

Christopher Hughes, Chair

About 95% of anti-cancer drugs that show promise during preclinical study fail to gain FDA-approval for clinical use. The gap between *in vitro* and *in vivo* preclinical study calls for physiologically relevant *in vitro* models that can better serve as a reliable drug-screening tool. The vascularized micro-tumor (VMT) is a novel three-dimensional model system that recapitulates the complex tumor microenvironment within a transparent microfluidic device that allows real-time study of drug response and tumor-stromal interactions. Here we validate our model system by showing that gene expression, tumor heterogeneity, and treatment response in the VMT more closely model tumor clinicopathology than current standard drug screening modalities.

Chapter 1

Introduction

1.1 Background

Cancer is the second leading cause of death in the United States, with 1,500 people dying from the disease every day[216]. The high rate of mortality and morbidity for this disease highlights the need for more effective therapies. Despite the high incidence, drug discovery has been slow to translate into clinical benefit for patients and the paucity of effective treatments in oncology is consequent to the high attrition rate during drug development[128]. Indeed, oncology has the lowest success rate of any therapeutic area with only 5.1% of anti-cancer drugs entering phase I clinical trials ultimately gaining FDA approval[223]. For every 10,000 compounds that proceed through research and development, only 1 will ultimately become FDA-approved for market use[128, 269]. To bring a new drug to market for any disease indication can take in excess of 10 years and \$2.5 billion[55]. Despite promising preclinical data, the majority of drugs fail during clinical stages due to issues with efficacy (>50%) and/or safety (>10%)[125]. One of the main reasons for such a high attrition rate is that current methods for disease modeling and drug screening are

poor predictors of human outcomes. Given the fact that about two thirds of drug development cost occurs during clinical trial phases, the ability to more accurately identify lead candidates and eliminate ineffective drugs earlier in the process will save a significant amount of time and resources, reduce human risk, and accelerate the translation of effective therapies to the clinic[268, 282].

While animal models have advanced our understanding of complex diseases such as cancer and provide essential readouts of organism-level drug effects *in vivo*, these same models are expensive, time consuming and often fail to predict human responses during clinical trials[175, 146]. In fact, it is estimated that less than 8% of successful animal trials for cancer drugs translate to successful human clinical trials, primarily due to species-specific differences in physiology and cell biology[282]. Furthermore, animal models allow only limited manipulation to study the mechanisms at play during disease progression or therapeutic response[219, 250]. On the other hand, while standard 2D cell monocultures used for drug screening are cost-efficient and simple to use, such monolayer cultures fail to recapitulate the 3D cellular spatial arrangement and microenvironment of *in vivo* tissues leading to poor predictive power. Cell growth in 2D versus 3D environments not only promotes changes in cellular morphology, function, response to stimuli, and gene expression patterns, but also leads to drug responses that vary dramatically from the *in vivo* situation[232]. Translation of results obtained from cell culture studies into animal trials during preclinical stages of drug development is difficult because of the inability of these oversimplified *in vitro* models to simulate the complex and heterogeneous tissue architectures of their *in vivo* counterparts.

To bridge the translational gap between current preclinical models and clinical outcomes, *in vitro* platforms that better mimic native tissue physiology are undergoing rapid evolution. Advances in tissue engineering have assisted the development of functional, miniaturized human healthy or diseased organs termed microphysiological systems (MPS, also

known as 'organ-on-a-chip', organ chip or tissue chip)[282, 15, 142]. MPS integrate microfluidics, microfabrication techniques, biomaterials and tissue engineering to create tissue or organ constructs via co-culture of multiple cell types, often embedded in a hydrogel or extracellular matrix (ECM), within a palm-sized device. By leveraging microfluidics technology, physiological relevance can be built into the MPS to model the dynamic microenvironment and inter-cellular interactions of complex tissues or organ-systems. High-fidelity modeling of essentially any tissue in the human body to reproduce corresponding functional units is now possible. For example, microscaled platforms have been developed to model lung[95], liver [11], brain[178], endocrine tissues[278], intestine[120], kidney[275, 103], and heart[92], among many others. In addition to these micro-organ platforms, MPS technology offers new opportunities for building and applying functional 3D *in vitro* human tumor models for oncology research.

Besides 3D cellular assembly, the tumor microenvironment consists of a complex combination of ECM, stromal cells and interstitial fluids. This complex composition influences the tumor cell phenotype via mechanical and biochemical factors that ultimately contribute to tumor growth[203]. To recreate the tumor microenvironment, tumor chip models have been engineered to incorporate stromal cells such as pericytes[122], cancer associated fibroblasts[107], smooth muscle cells and myofibroblasts[88], mesenchymal stem cells[53], as well as endothelial cells[12, 164] to form a vascular compartment, either self-organized[12, 225, 90, 160, 281, 35, 36, 264, 129], or spatially organized by design[261, 30]. Rudimentary (natural) immune systems have also been incorporated into tumor chips through the addition of macrophages[88], dendritic cells[171] and T cells[105, 174]. Fully autologous systems are still on the horizon. Tumor chips have been arrayed for high throughput drug screening applications[180], optimized for cancer metastasis studies such as tumor cell extravasation and micrometastasis generation[37], and populated with patient-specific cells for personalized medicine approaches[105]. Organotypic tumor chips capable of recapitulating complex organ-level patterns of cancer growth, dissemination and

therapeutic response observed in patients are quickly advancing[84, 150]. Multi-MPS have been generated for the detailed study of drug pharmacokinetics (PK), pharmacodynamics (PD) and toxicity[142, 238, 215, 251]. In particular, tumor chip models allow experimental manipulation and well-controlled real-time study of dynamic interactions among tumor cells, stromal cells and the tumor microenvironment, which is less simple to accomplish using regular tissue culture and animal models.

In this introduction, we first briefly describe the strengths and limitations of current model systems and highlight critical features of the tumor microenvironment that contribute to disease progression. We then review the current state-of-the-art in 3D tissue-engineering models developed for cancer research and outline how the technology is revolutionizing disease modeling, drug screening and personalized medicine for oncology. Within this context, we critically evaluate limitations in current tumor chip models and address challenges in the field by proposing solutions to accelerate the translation of tumor chips into mainstream use.

1.2 Strengths and Limitations of Standard Preclinical Models

2D Monocultures

While assays derived from 2D monolayers of cell lines grown on plastic are low cost, easy to use and high throughput, these same models have limited predictive capability since they fail to mimic natural human physiology[55, 60]. Differences in cell morphology, differentiation, proliferation, viability, response to stimuli, metabolism, gene/protein expression and drug sensitivity are observed when cells, previously cultured in 2D, are

moved to a 3D environment[86, 19, 138]. This is not surprising considering that, with few exceptions, human organs develop and maintain their specific functions owing to the 3D structure they adopt. 2D cell cultures have vastly different substrate topography, stiffness, and architecture than *in vivo* counterparts, and fail to recapitulate the cell-cell and cell-matrix interactions of endogenous tissues[18]. Furthermore, 2D culture places a selective pressure on cells that can cause genetic drift and loss of heterogeneity, resulting in substantial changes to their original phenotypes[13].

Another major limitation of 2D assays is that artificial *in vitro* conditions for growing cells on plastic dishes prevents investigation and therapeutic targeting of many cell behaviors that lead to disease progression and treatment failure, such as immune suppression and metastasis[232]. Moreover, 2D assay properties may lead to false-positive selection of drugs that have only limited efficacy *in vivo*, often due to the greater heterogeneity seen in more complex environments, where stem cells and quiescent cells may cycle more slowly and demonstrate resistance to cell cycle arrest[279]. Since the tumor microenvironment and tumor-stromal interactions that create a barrier to drug delivery *in vivo* are not modeled in 2D cell culture, drugs that look promising in cell assays may not be able to reach target cells *in vivo*[233]. Drug screening is typically performed in 2D on cells growing as monocultures, despite evidence that direct association of tumor cells with stroma renders populations of cancer cells resistant to chemotherapeutic drugs[262, 274, 6, 245, 46]. The intrinsic limitations of 2D cell culture models have prompted the development of 3D models that can provide a cellular microenvironment and physiologic context that more closely mimics the microenvironment observed in native tissues. This feature is critical for drug testing since environmental cues can have profound effects on cell functions, which often affect cellular responses to drugs. Therefore, drugs often demonstrate greater efficacy in 2D cultures than in 3D or *in vivo* systems; conversely, compounds that are only effective in 3D will be missed by traditional screening assays.

3D Spheroids

By maintaining tumor cells in a native 3D conformation, spheroid cultures address certain limitations in 2D cell models. Spheroids develop distinct areas of rapidly dividing cells on the outer layer vs necrotic and slow cycling cells at the center and intermediate layers, respectively[239]. In this regard, spheroid cultures more accurately mimic the metabolic gradients and drug resistance of *in vivo* tumors than standard 2D cultures[242]. These models have progressively evolved from the simplest form comprising homogeneous epithelial cell populations to 3D co-cultures that can be embedded in matrix with variable ECM properties and derived from numerous cell sources (such as established cell lines, patient-derived cells, and stem cells). 3D models provide sound insight into the differences between normal and malignant epithelial cells and serve as an excellent basis for determining the intermediate steps that are responsible for the transition from a normal to a malignant fate[64].

While spheroid cultures can recapitulate disease characteristics such as chemo-/radio-resistance[241], some aspects of tumor cell heterogeneity and invasive/migratory potential of tumor cells[257], there are several limitations in these models. Spheroids are useful models of avascular tumors but lack the structure and complexity seen in vascularized tumors *in vivo*[72]. As a result, spheroid cultures are not able to fully recapitulate the spectrum of cell phenotypes within the tumor milieu. Due to static culture conditions, cells in spheroid models do not experience the same mechanical forces that would be expected *in vivo* and lack of dynamic flow also prevents long-term culture for drug sensitivity and toxicity studies[183]. Thus several important factors of the tumor microenvironment are not reproduced and cannot be studied in these models. Another significant limitation is that many tumor types, especially those with a highly invasive phenotype, do not readily form spheroids and so cannot be assayed in these cultures (e.g. MDA-MB-231 breast cancer cell line). To address these shortcomings, tumor chips represent more sophisticated

tissue-based culture models that mimic critical features not represented in traditional monolayer or spheroid cultures.

Animal Models

Animal surrogates of human disease are a necessary component in the drug development pipeline because these *in vivo* models can emulate physiological complexity at the whole-organism level. Although animal studies have advanced our understanding of complex diseases such as cancer, a major shortcoming of these models is that they often have only limited translatability to humans. This is evidenced by the fact that >90% of drugs that show promise during animal studies fail in clinical trials, suggesting that current animal models fail in critical ways to fully recapitulate the human disease condition[65]. Species-specific differences between mouse and human in physiology, and cell biology, variations in the homology of molecular targets, and differences in the number of required key mutations to develop tumors can impede clinical translation of preclinical results[165]. Further, immunological and inflammatory response vastly differs in the murine model[158, 209]. During preclinical drug development, tumor cells are often injected subcutaneously into the flanks of severely immunocompromised mice to generate xenograft tumors for *in vivo* testing of candidate drugs. This procedure greatly facilitates tumor monitoring by palpation and visual inspection, but is poorly representative of tumor development in the native tissue microenvironment. Less commonly, transplants are generated orthotopically, or in the original site of cancer, to better mimic tumor-specific disease evolution, although these procedures can present technical challenges both in establishing and monitoring the xenograft tumor[202]. Moreover, tumors generated from transplantation in mice will inherently contain non-human host cells. In contrast, tumor chips can be composed entirely of human cells and tissue-specific factors of the microenvironment can be readily incorporated into the chip by design to better mimic the organ site of tumor origin.

To better replicate the heterogeneity of human tumors, patient-derived xenograft (PDX) tumor models that are established from transplantation of primary tumors are increasingly being adopted for drug screening, disease modeling and personalized medicine applications[202, 187]. These models are limited by the small amounts of patient-derived tissue available, thus it can take months to expand and serially transplant PDX to generate sufficient replicates for *in vivo* drug testing, and many primary tumors simply fail to engraft from the outset. While there have been increasing efforts to use PDX as models to study drug response, recent evidence suggests that PDX may not recapitulate parent tumor characteristics as faithfully as initially assumed[63]. Indeed, Ben-David et al[13] assessed copy number alterations (CNA) in 1,100 PDX samples derived from 24 cancer types and analyzed PDX genomic stability through the process of serial engraftment, compared to human primary tumors and primary-derived cell lines. Interestingly, individual PDX models often gained or lost CNAs and mutations in cancer-related genes during PDX passage, quickly diverging genomically from the parental tumors from which they derived. These changes in genomic landscape were comparable to those observed in primary-derived cells maintained and passaged *in vitro*, which included loss of recurrent chromosomal aberrations that are believed to have casual roles in tumor progression and therapy response. These results suggest that primary-derived cells are critically influenced by the amount of time maintained outside of the body, and that MPS can address this limitation by providing an *in vivo*-like environment amenable to more rapid analysis.

While severely immunocompromised mice are necessary to allow engraftment of human tumors, such models preclude the study and therapeutic targeting of interactions between adaptive immune cells and tumor cell populations. Humanized mouse models are being developed to address this concern, whereby human immune components are incorporated to partially reconstitute the immune-inflammatory response during disease progression[286, 158]. Still, appropriate mouse models may not be readily available for certain applications and are impractical for routine drug screening[68, 242]. Another im-

portant limitation of animal models is that only limited experimental manipulation can be performed to interrogate mechanisms of disease progression, due to the complexity of generating knockout animals and difficulty investigating dynamic cell-cell interactions *in vivo*. Furthermore, spatially random and temporally rapid events such as tumor cell intravasation that can be easily visualized in real-time using tumor chips cannot be easily interrogated using animal models. Transgenic mouse models have been genetically engineered to partially recapitulate aspects of human carcinogenesis *in situ*, however evidence suggests key differences in the signaling requirements for transformation of mouse and human cells[190, 83]. Additional considerations for the use of different types of mouse models in cancer research have been reviewed previously[29, 45, 132].

Although animal models represent a necessary component in the drug development pipeline and have provided useful information on disease processes, these same models require tremendous time and resources and thus represent a low throughput model system. Even so, approximately 27 million vertebrate animals are used for research purposes in the US every year, highlighting the ethical burden associated with these studies[4]. Indeed, the US National Research Council recommends that animal model based tests be replaced as soon as possible with an increased emphasis on epidemiology, *in silico* models and *in vitro* human cell-based assays, including MPS[146]. This is in accordance with federal and ethical guidelines originating from the 3R's initiative to replace, reduce and refine the use of animals in scientific and medical research[244].

1.3 Overview of the Tumor Microenvironment

To create a realistic tumor model, several key features of an actual tumor must be replicated. A tumor comprises numerous cell types in a dynamic tumor microenvironment wherein a host of biochemical and biophysical cues dictate cellular responses. Although

tumor genetic heterogeneity remains a significant barrier to effective cancer eradication, it is now widely recognized that the tumor microenvironment plays an equally critical role in cancer initiation, progression and drug resistance, thus representing an attractive therapeutic target independent of the myriad genomic aberrations unique to each tumor[246, 233, 262, 197, 83]. The tumor microenvironment serves as a complex ecosystem containing diverse cellular and non-cellular components that modulate the proliferation, function and fate of cancer cells via bi-directional communication[184, 147]. Cell signaling within the tumor microenvironment occurs through release of soluble factors in the interstitial fluid, cell-cell or cell-ECM adhesion, and mechanical forces. These mechanical forces are generated by fluid forces, shear stresses, interstitial flow and ECM organization, composition and stiffness[258, 183, 133]. The functional association of tumor cells with surrounding tissues leads to the development of a new pathological 'organ' that continually changes as malignancy progresses and in response to treatment[147].

Like normal tissues, tumors require delivery of oxygen and nutrients, and elimination of metabolic wastes, via the vascular supply. In the absence of new vasculature, central necrosis will develop in a solid tumor due to limited diffusion of oxygen to the tumor core resulting in hypoxia, high acidity and the accumulation of wastes[257]. Before undergoing cell death, cells at the core adapt their metabolism and become quiescent in order to maintain homeostasis. Quiescent tumor cells are difficult to eradicate with conventional therapies that target rapidly proliferating cells, such as radiation and chemotherapy[150]. Gradients of nutrients, oxygen and cytokines develop as the tumor mass grows, often leading to zonation within the tumor whereby viable, proliferating cells survive at the periphery of the tumor while quiescent and necrotic cells are harbored at the center. Necrotic cells can also release growth-stimulating factors, such as IL-1 α , that can directly stimulate neighboring cells to proliferate, thus contributing to disease progression[83]. Overexpression of hypoxia inducible factors such as HIF-1 promotes the expression of hypoxia-inducible genes that enhance cell survival, alter glucose metabolism, increase

vascular permeability and inflammation, and induce new vessel sprouting via angiogenesis[184]. Such genes include phosphoglycerate kinase 1 (PGK-1), glucose transporter 1 (Glut-1), lactate dehydrogenase A (LdhA), glyceraldehyde-3-phosphate dehydrogenase (GAPDH), vascular endothelial growth factor (VEGF) and nitric oxide synthetase (iNOS)[208]. Hypoxia also promotes cancer metastasis of solid tumors via a step-wise, physical process that is heavily influenced by the ECM density and composition of the surrounding tumor microenvironment. Synergistic interactions between malignant cells and the tumor microenvironment lead to active ECM remodeling that further promotes the recruitment of fibroblasts, immune-inflammatory cells, and perivascular cells to facilitate cancer cell dissemination and invasion to distant organs[46].

Bissell and colleagues demonstrated the importance of faithfully recapitulating the tissue-specific tumor microenvironment in a series of seminal studies[134, 99, 138, 19]. When mammary epithelial cells were cultured on laminin-rich reconstituted basement membrane, the cells self-assembled into spherical structures with a central lumen and produced milk protein in response to stimuli, similar to normal mammary acini. However, when the same mammary luminal epithelial cells were cultured in 3D collagen I gels, the self-assembled spheres failed to form a central lumen, demonstrated inverse cell polarity and did not produce milk protein. Interestingly, the physiological phenotype (i.e. lumen formation and cell polarity) could be restored if the mammary luminal epithelial cells were co-cultured with myoepithelial cells that could deposit the basement membrane *in situ*, suggesting that the composition of the ECM is a critical determinant of tissue structure and function[46]. Further, our work has demonstrated the profound effect of ECM composition and stiffness on cell behavior within the tumor microenvironment. By extracting and comparing ECM from normal human colon tissue and colon tumor metastases, we found differences in protein composition and stiffness between the two reconstituted matrices with overrepresentation of a number of ECM proteins (e.g. collagens IV and XIV, laminin) in the tumor ECM as well as a 3-fold increase in stiffness compared to normal ECM[197]. In

Disease modeling	Drug Screening	Personalized Medicine
<ul style="list-style-type: none"> • Metastasis modeling <ul style="list-style-type: none"> • Invasion/intravasation • Survival/dormancy • Extravasation • Metastatic niche • Epithelial-mesenchymal transition • Tumor heterogeneity/evolution • Mechanical forces • Tumor-ECM interactions • Tumor-stromal interactions • Organ-specific microenvironments • Immuno-oncology studies • Species-specific models 	<ul style="list-style-type: none"> • PK-PD modeling <ul style="list-style-type: none"> • Absorption • Distribution • Metabolism • Excretion • Toxicity • High-throughput designs • Efficacy testing • Novel compound validation • Tumor resistance/sensitivity • Mechanistic studies 	<ul style="list-style-type: none"> • Incorporation of primary cells <ul style="list-style-type: none"> • Induced pluripotent stem (iPS) cells • Adult tissue resident stem cells • Biopsy-, blood- or tissue-derived cells • Cancer stem cells • Patient-derived organoids • Genetically modified cells • Integration with Big Data <ul style="list-style-type: none"> • ‘Omics’ signatures/readouts • Genome wide association studies (GWAS) • Computational modeling • Biomarker discovery/validation • Individualized trials-on-chip • Tailored clinical management

Table 1.1 – Applications of Tumor Chip Technology

an *in vitro* assay of vascularized tumors whereby tumor cells were co-cultured with endothelial cells and fibroblasts in the reconstituted matrices, vascular network formation and tumor growth were significantly increased in the tumor ECM compared to normal ECM, and tumor cells exhibited increased glycolysis. When introduced *in vivo*, tumor ECM promoted enhanced vascularization to the cancer cells[197]. These findings highlight the importance of studying tumor cells in the correct context. A better understanding of interactions within the tumor microenvironment, gained through use of appropriate experimental models such as MPS, will be critical to overcome treatment resistance through the development of successful targeted therapeutics.

1.4 Microphysiological Systems for Cancer Research

The ability to rapidly screen drugs and study disease mechanisms within a physiologically relevant context is critically important to facilitate clinical translation of preclinical findings. To address current limitations in preclinical models, multiple research groups

have focused on innovating MPS that model both normal and pathological human tissue functions *in vitro*[9, 98]. By utilizing advanced microfabrication, microfluidic and tissue engineering techniques, physiological relevance can be designed into MPS to emulate the important functions of practically any human tissue or organ in corresponding microscale configurations. Major advantages of on-chip tissue models are that they recapitulate both the 3D organization and multicellular complexity of tissues and at the same time enable enhanced dynamic control over the cellular microenvironment to accommodate systematic experimental intervention[15]. Furthermore, organ-on-a-chip platforms are composed exclusively of human cells and require fewer cells and drug volumes than standard pre-clinical models since assays are performed on a microscale. Microfabrication techniques such as soft lithography and replica molding are often used to manufacture tissue chips based on precise microfluidic designs. These bioengineering approaches allow manipulation of fluids at ultralow volumes (i.e. nanoliter and below) to simulate physiological flow, shear stress, nutrient delivery and drug exposure[183, 227, 182, 214]. Furthermore, on-chip devices enable careful spatiotemporal control over cell growth to better model complex tissue structure and function within micrometer-sized channels. Since fluid flow in microfluidic channels is laminar, it can be easily mathematically modeled, allowing theoretical predictions of complex biological phenomena[238] that, when coupled with experimental analysis, provide a robust *in vitro* system for understanding tissue function and testing promising approaches for treating disease.

Microfluidic devices for biomedical purposes are often fabricated using poly (dimethylsiloxane) (PDMS), an elastic silicone-based polymer that is biocompatible, oxygen-permeable, and optically transparent, allowing for continuous observation of tissue constructs by microscopy for real-time assessment of cell behavior and response to treatment[205]. Recent advances have allowed continuous *in situ* monitoring of biochemical, physical and optical responses via fully integrated sensing platforms on chip[282, 109]. Physical properties of individual organs can be modeled on-chip via cyclic deformations (to model

breathing or peristaltic motions [84, 120]), mechanical loading (to mimic the weight of the body on the musculoskeletal system [151]) or contractile forces (such as those important for heart function [92]). Current on-chip approaches mainly rely on combining pre-differentiated cells in particular ratios, often within an ECM or hydrogel that acts as scaffolding for cell growth, to emulate the native tissue composition[242]. Cells are often fluorescently labeled, labeled with dye or immunofluorescently stained to facilitate tracking by fluorescence microscopy, but other sensitive, non-invasive imaging methods have also been applied to these systems[225]. By integrating microfluidic assays, advanced microscopy and computational modeling, single events can be investigated with unprecedented temporal and spatial resolution as part of the complex biological processes that define pathophysiological responses. Based on advances in tissue-engineering strategies, individual organ-on-a-chip platforms are now being linked together to generate multi-organ systems for the study of drug pharmacokinetics, pharmacodynamics and toxicity[268, 238, 220, 16, 59, 251, 285, 199, 237]. With knowledge gained in the field of stem cells, human induced pluripotent stem (iPS) cells or adult tissue resident stem cells can be differentiated into patient-specific cell populations for incorporation into tissue chips to achieve personalized medicine approaches[242, 92, 154, 155]. On-chip devices are anticipated to enhance preclinical predictability of drug responses by more accurately mimicking complex tissue- and disease-specific microenvironments than standard models.

1.4.1 Tumor Chips

Organ-on-a-chip platforms are rapidly evolving as powerful tools for oncology research (see Table 1.1). By replacing healthy cells and associated ECMS in tissue-specific constructs with those of cancer origins, so called tumor-on-a-chip or tumor chip systems have emerged. Tumor chips can ideally reproduce specific key aspects of the tumor mi-

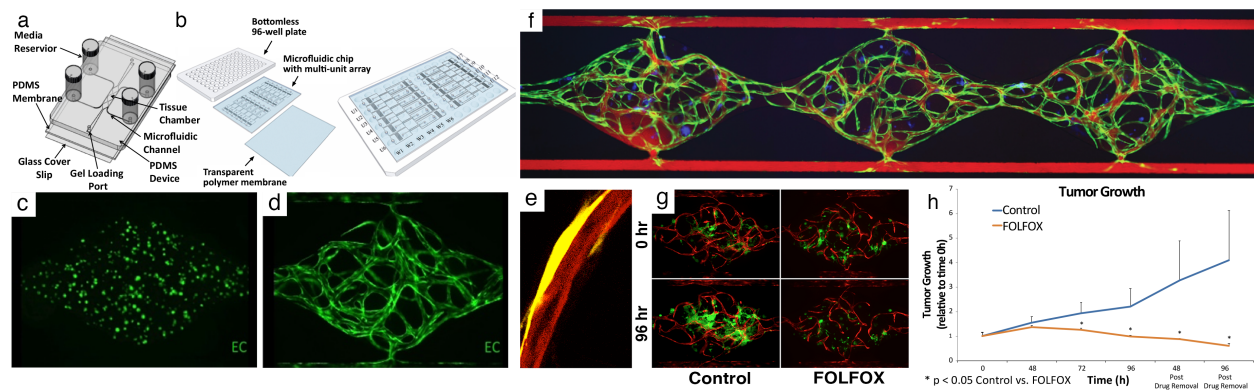


Figure 1.1 – Vascularized micro-tumor model VMT (a) A schematic of the microfluidic platform with a single unit. Three tissue chambers ($1\text{ mm} \times 1\text{ mm} \times 0.1\text{ mm}$) constitute 1 unit. Different levels of medium in the four vials drive flow. (b) A schematic of the microfluidic platform with 12 units/plate. (c) GFP+ EC at day 0. (d) A fully-formed vascular network at day 7. (e) A vessel (mCherry, red) wrapped by a pericyte (YFP, yellow) (f) 70 kDa rhodamine dextran flowing through the capillary network (green) formed within the three tissue chambers showing tight barrier function. Tumor cells are labeled in blue. (g) HCT116 colorectal cancer cells (GFP) with vessels (mCherry) are either non-treated (control) or treated with FOLFOX standard chemotherapy on day 7 (0 hour) and imaged every 24 hours. (h) Quantitation of FOLFOX treatment in HCT116 VMT. Tumor significantly regresses with treatment compared to control. Reproduced from Sobrino et al[225] and Phan et al[178] with permission from Nature Publishing Group and the Royal Society of Chemistry.

environment, such as biochemical gradients and niche factors, dynamic cell-cell and cell-matrix interactions, and complex tissue structure comprised of tumor and stromal cells. Moreover, tumor chips are able to reproduce cell confinement, a parameter imposed on cell movement in the interstitial space of tissues that is totally absent in 2D assays yet essential for studying the behavior of motile cells such as immune and cancer cells[171].

Vascularized Tumor Chips

Nearly every tissue in the human body, including those of malignant origin, depends for survival on a supply of oxygen and nutrients delivered through blood vessels. Angiogenesis refers to the sprouting of new vessels from pre-existing vasculature, and vasculogenesis occurs when vessels form *de novo* from progenitor cells. In combination they represent the fundamental processes by which new blood vessels are formed (reviewed in [70, 43, 185]) and are critical during physiological processes such as tissue homeostasis, wound healing,

pregnancy and fetal development. However, during malignant progression angiogenesis and, to a lesser degree, vasculogenesis are co-opted to feed the growing tumor mass, while also providing a means for metastasis. Metastasis is a primary reason for therapy failure and accounts for >90% of cancer deaths[118]. Thus, tumor-associated vasculature represents an important component of the tumor niche and an attractive therapeutic target. Indeed, anti-angiogenic drugs have been developed extensively for use in cancer but with mixed clinical trial outcomes and oftentimes marginal survival gains[185]. Elucidating the factors that contribute to therapy failure will ultimately lead to more effective therapies. Furthermore, approximately 25% of drugs entering clinical trials fail due to pharmacological issues such as lack of absorption or penetration into the tumor[146]. High efficacy drug delivery to cancer remains a challenge primarily due to the heterogeneity and complexity of the tumor microenvironment, therefore models that mimic physiological barriers to drug or gene delivery will facilitate translation of *in vitro* results to *in vivo* studies.

To advance drug development in this area, our group and others have designed microvascularized tissue constructs on-chip in which vascular and perivascular cells self-organize *de novo* into a living and perfused vascular network in response to fluid flow and shear stress[225, 123, 119, 272]. Incorporation of these microvascular networks into tumor chips is a breakthrough for several reasons: 1) it better mimics the structure, function and disease processes of a vascularized tumor mass *in vivo*; 2) it models key steps of metastasis, which involve tumor-endothelial and stromal cell interactions that are poorly understood and difficult to investigate in current preclinical models; 3) it more accurately establishes physiologically selective barriers to nutrient and drug delivery in target tissues allowing for more realistic pharmaceutical screening; and, 4) drugs with anti-angiogenic and anti-metastatic capabilities can be directly assessed in such a system.

For realistic tumor modeling and anti-cancer drug screening, our group has adapted our base VMO platform[38, 90, 160] for cancer studies by incorporating tumor cells into the

model to generate vascularized micro-tumors, or VMTs (Figure 1.1)[225, 180]. We have previously validated our VMO model by demonstrating that perfused, living microvessels that self-assemble within the microfluidic device (Figure 1.1a, 1.1b) model the physiology of blood vessels *in vivo*. In response to gravity-driven physiologic flow, VMO microvessels derived from EC (Figure 1.1c) form tight junctions by day 5 of culture (Figure 1.1d). Stromal cells seeded with EC in the tissue chambers acquire a pericyte phenotype (NG2+, PDGFR β +) with tight appositions to vessels (Figure 1.1e), and once established, vessels rapidly lay down a collagen IV rich basement membrane that increases in density over time. Importantly, the VMT recapitulates the barrier functions of tumor-associated vessels *in vivo* (Figure 1.1f). We then created biomimetic VMT models for CRC using HCT116 (Figure 1.1g), SW620 and SW480 cell lines, breast cancer (MCF7 and MDA-MB-231) and melanoma (MNT1) by introducing each cancer cell line mixed with stromal cells, EC and ECM into the three tissue chambers of the device. Interestingly, tumor cells showed reproducibly different growth patterns, with SW480 and MCF7 growing as tight spheroids and MDA-MB-231 and MNT1 showing highly diffuse, invasive phenotypes reminiscent of their *in vivo* behaviors. Differences in growth rate, vessel development, and collagen synthesis suggests that each tumor cell line uniquely remodels the tumor microenvironment within the VMT.

We next performed drug screening to test VMT response to FDA-approved chemotherapeutics and small molecule receptor tyrosine kinase (RTK) inhibitors representing both anti-cancer and anti-angiogenic drugs, including the standard-of-care therapies indicated for specific tumor types[225]. By treating VMTs with physiologically-relevant doses, we demonstrated that the IC₅₀ in our VMT model is higher than for 2D cultures (i.e. cancer cells are more resistant to treatment in VMTs) and better representative of the IC₅₀ observed *in vivo* or in patients based on effective plasma concentration dose. This indicates that 2D models fail to accurately model certain critical features of *in vivo* tumors and that certain survival-signaling pathways essential for tumor progression *in vivo* are not activated in 2D culture. In response to FOLFOX, a chemotherapeutic regimen indicated for

CRC, HCT116 tumors displayed marked regression after 48 hours of treatment vs control, whereas the already established vasculature remained intact (Figure 1.1g, 1.1h). Tumor regression continued even 96 hours post-drug removal, confirming the cytotoxic effect of FOLFOX treatment. The anti-angiogenic multi-kinase inhibitors sorafenib and pazopanib were also tested in the VMT model and induced marked vascular regression in response to treatment. Both drugs target VEGFR2 and PDGFR β with similar efficacy, but pazopanib additionally targets VEGFR1 and caused a greater degree of vascular regression in the platform, whereas sorafenib induced greater tumor regression due to its targeting of RAF. Additional drug screening results indicate that the VMT robustly recapitulates anticipated drug response based on mechanism of action, animal studies and clinical trial results[225]. We have now arrayed our platform for high-throughput experiments to facilitate drug-screening studies as well as to enable downstream molecular biology techniques that are difficult to perform using standard microfluidic platforms[180].

Recent contributions by Kamm and colleagues[35, 272, 106, 119] have provided an unprecedented, high-resolution view of tumor cell extravasation through microvessels formed in a microfluidic device (Figure 1.2). The authors employed a *de novo* vascularized platform to study the process of tumor cell extravasation from within *in vitro* microvessels and were able to track each step in real-time. Suspended human umbilical vein endothelial cells (HUVEC) and normal human lung fibroblasts (NHLF) (Figure 1.2a) cultured under dynamic gravity-driven flow conditions in the two-gel channel device (Figure 1.2b) self-organize to form stable, functional and perfused microvessels via paracrine signaling across the central media channel (Figure 1.2c–1.2e). The microvessels formed tight cell-cell endothelial junctions, deposited basement membrane and demonstrated physiologic vascular permeability. Breast cancer cells (MDA-MB-231) were introduced into the device and high-resolution time-lapse microscopy revealed the highly dynamic nature of extravasation events (Figure 1.2f). The cancer cells first penetrated the EC barrier by extending thin filipodial protrusions that continued to increase and branch out while the remain-

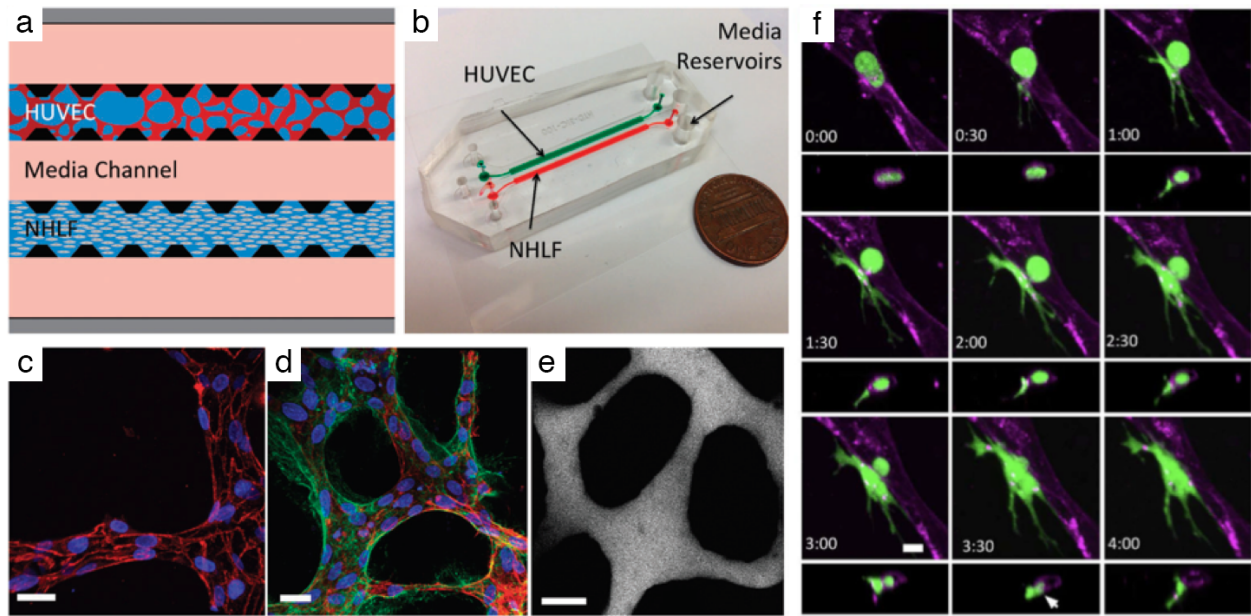


Figure 1.2 – Tumor cell extravasation from *in vitro* microvessels. (a) A schematic of a microfluidic device and cell-seeding configuration. Suspended HUVECs form microvascular networks in a gel matrix via paracrine signaling with NHLFs across the central media channel. (b) Photograph of 2-channel microfluidic device. (c) Visualization of VE-cadherin (red) at 60X reveals continuous cell-cell junctions. (d) Collagen IV basement membrane deposition (green) around the lumen (red) and in the perivascular space suggests vessel maturation. (e) Perfusion of vessels with 70 kDa dextran reveals patent lumens void of local leaks. Scale bars are 20 μm . (f) High resolution time-lapse confocal microscopy (40X) of an extravasating entrapped MDA-MB-231 (green). Lumens were labeled with a far-red plasma membrane stain (purple). Tumor cells transmigrate through the endothelium and into the 3D matrix over a period of 4 h. The white arrow at 3:30 h indicates the location of a vessel opening at the site of tumor cell extravasation. Reproduced from Chen et al[37] with permission from the Royal Society of Chemistry.

ing body on the apical side of the lumen maintained its sphericity, even as the nucleus traversed the vessel. Throughout the process, tumor cells underwent significant shape changes as the cell body extruded through a gap in the microvessel of subnuclear dimensions. Interestingly, staining for VE-cadherin revealed that EC cell-cell junctions remained largely intact. Employing this assay, the authors found that $\text{TNF}\alpha$ stimulation impaired endothelial barrier function and increased tumor cell extravasation efficiency, and noted positive correlations between the metastatic potentials of MDA-MB-231, HT1080 and MCF10a cancer cells and their extravasation capabilities. These results indicate that human tumor cells exhibiting different metastatic potentials exit the vascular system with different efficiencies, and that the platform possesses the sensitivity to detect such variations.

Cancer Type Modeling On-Chip

Cancer progresses via dynamic organ- and tissue-specific interactions; therefore, accurately modeling tissue-specific factors of the tumor microenvironment is crucial to creating physiologically and clinically relevant *in vitro* platforms for cancer research. In a recent study, Hassell et al[84] created a sophisticated *in vitro* human orthotopic model of non-small cell lung cancer (NSCLC) using a biomimetic microsystem of the alveolar-capillary interface in the human lung (Figure 1.3a)[95, 94]. The lung alveolar chip consists of two closely-aposed upper and lower channels separated by a thin, flexible and porous ECM-coated PDMS membrane that serves as the alveolar-capillary interface, or can serve as an airway-capillary interface. NSCLC tumor cells were cultured on the upper surface of the membrane containing primary human lung alveolar or small airway epithelial cells and human lung microvascular EC lined all four walls of the lower channel, forming a hollow vascular lumen. Physiological breathing motions were mimicked on-chip by applying cyclic suction to two parallel side chambers that rhythmically deformed the adherent lung tissues. Interestingly, NSCLC cells proliferated rapidly when cultured in the human alveolus chip, yet displayed a relatively dormant phenotype when cultured in the airway chip, reflecting organ microenvironment-specific lung cancer growth observed in human patients *in vivo*. Surprisingly, when NSCLC cells were cultured in the presence of cyclic mechanical strain to mimic physiological breathing motions, lung cancer growth was significantly suppressed by >50%. Without breathing motions on-chip, the tumor cells expanded to replace large regions of the epithelium and invaded into the epithelial layer, whereas the same tumor cells remained limited to smaller localized regions of the epithelium when grown with cyclic deformation. The authors note the possibility that *in vivo* obstruction of lung motion due to filling of alveolar spaces by growing cancer cells or other causes could produce a positive feedback loop to further enhance tumor growth. NSCLC cells also displayed decreased sensitivity to tyrosine kinase inhibitors (TKI) when treated

under mechanical stimulation due to significantly reduced EGFR expression and phosphorylation, as well as an increase in both expression and phosphorylation of c-Met. Thus, it was concluded that mechanical breathing motions may suppress NSCLC cell response to TKI therapy by altering signaling pathway activation. These studies reveal that mechanical cues within the tumor microenvironment can significantly influence NSCLC growth, drug sensitivity and tumor dormancy *in vitro* to mimic unique NSCLC tumor growth patterns that are observed in human patients.

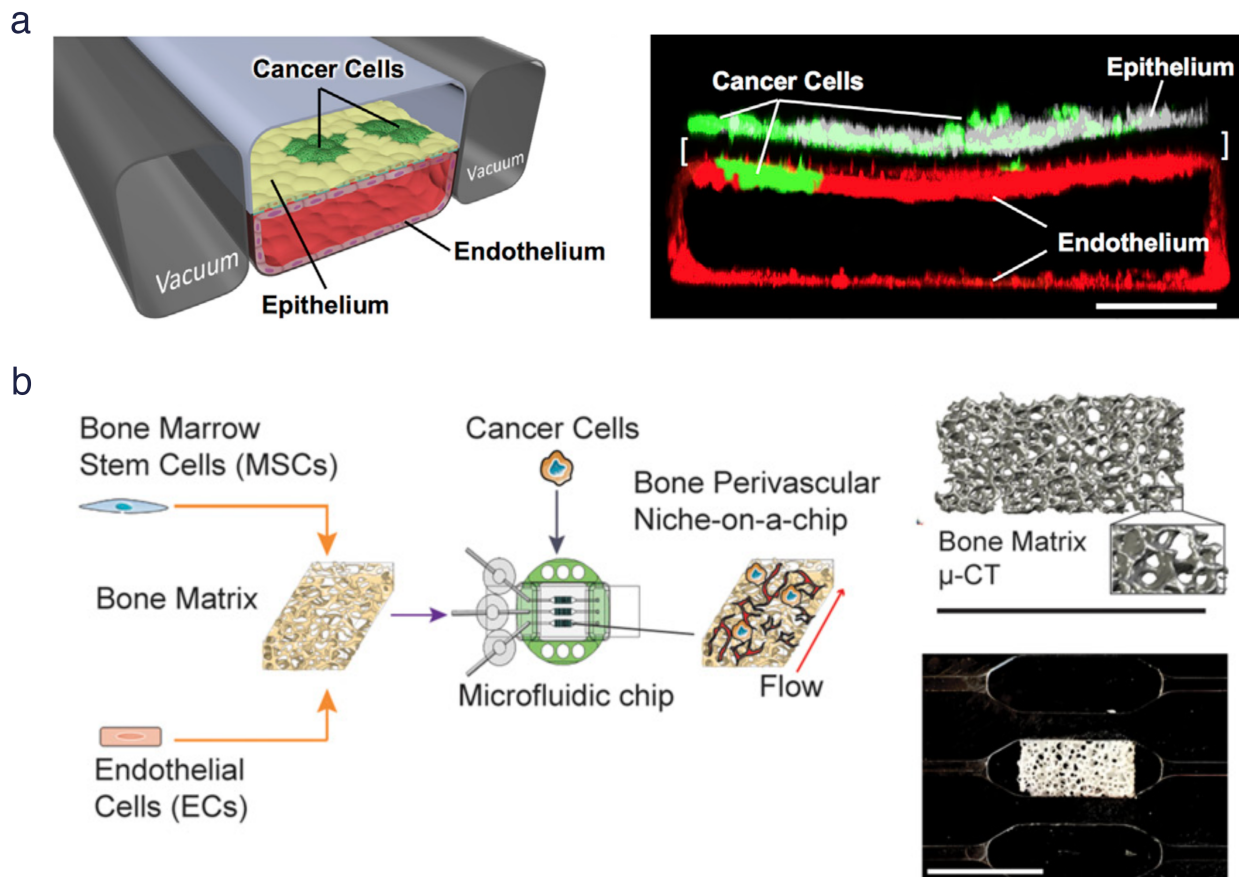


Figure 1.3 - Cancer type-specific modeling on-chip. (a) (Left) Schematic diagram of a cross-section through 2-channel microfluidic lung-on-a-chip device. (Right) Confocal fluorescence micrograph of a cross-section of the two central cell-lined channels of an alveolus chip. NSCLC cells are labeled with GFP and endothelium with RFP, as shown. Reproduced from Hassell et al[84] with permission from Cell Press. (b) (Left) Workflow for generating bone perivascular (BoPV) niche for studies of breast cancer colonization. (Right Top) Bone tissue reconstruction based on micro-computed tomography (μ -CT) data. (Right Bottom) Rectangular-shaped bone matrix in microfluidic chip. Reproduced from Marturano-Kruik et al[150] with permission from the National Academy of Sciences.

Metastases can arise months or even years after a patient is treated for primary disease due to residual disseminated tumor cells that enter dormancy and evade therapies[228]. Tissue-specific experimental models of the metastatic niche are needed to identify critical factors leading to metastatic-cell homing and colonization at distant sites, as well as tumor latency and resistance to treatment. Tumor chips are uniquely primed to elucidate the roles of stromal cells, secreted factors, exosomes and ECM proteins in niche priming and reveal therapeutic targets that may prevent metastatic progression[3]. To investigate breast cancer metastatic colonization and drug resistance, Marturano-Kruik et al[150] developed a functional human triculture that formed stable vascular networks within a 3D native bone matrix cultured on a microfluidic chip, termed the bone perivascular (BoPV) niche-on-a-chip (Figure 1.3b). Human endothelial and bone marrow-derived mesenchymal stem cells were seeded into decellularized bone and exposed on-chip to physiologically relevant interstitial flow and oxygen gradients. Recreation of these niche factors on-chip allowed the long-term maintenance of self-assembled microvascular networks without continuous addition of angiogenic factors. Interestingly, breast cancer cells that were introduced into the BoPV niche-on-a-chip under physiologic flow conditions showed a 4-fold reduction in cell numbers after 1 week in culture compared to static BoPV niche-on-a-chip cultures. Furthermore, treatment with the RTK inhibitor sunitinib, which is commonly used to target proliferative cancer cells and vasculature, was effective only in the static BoPV niche-on-a-chip. Cancer cell growth was inhibited by 50% following drug treatment in the absence of flow, whereas slowly-proliferating cancer cells in the perfused niche showed no response to sunitinib treatment. This study reveals the importance of recapitulating key cancer-specific characteristics of the tumor microenvironment to reveal physiologic mechanisms of drug resistance *in vitro*. It also demonstrates how tumor chips provide the unique capability to manipulate the host microenvironment to study the contribution of each niche component to tumor cell dormancy and drug sensitivity.

Onco-Immuno Chips

Cancer is well recognized as an immunogenic disease that stimulates complex immune responses via activation of both immune-inflammatory and immune-suppressive signaling pathways. Cancer cells hijack immune checkpoint signals (including upregulation of PDL1 and PDL2) to evade immune surveillance, while concurrently recruiting immune-inflammatory tumor-associated immunosuppressive cells that actively contribute to malignant progression and metastasis[68]. The tumor microenvironment itself plays a critical role in influencing tumor-immune interactions and response to immunotherapy[108]. For example, desmoplastic stroma within the tumor microenvironment can function as a barrier to T cell infiltration to foster a permissive, tumor-promoting environment[108]. By mobilizing the host immune system against malignant cells, cancer immunotherapy induces long-term remissions in a subset of patients with metastatic disease and has become a clinically validated treatment for many cancers[68, 211]. However, despite the remarkable success of cancer immunotherapy, overcoming treatment resistance and the variable responses among patients remain major challenges. The interactions between the immune system and cancer cells are dynamic and constantly evolving within each individual patient – from the initial establishment of cancer to the progression to metastatic disease, which is dependent on immune evasion[211]. Immunotherapy efficacy relies on this tumor-immune crosstalk within the tumor microenvironment. Given the emerging importance of the tumor microenvironment in modulating immune cell function, more sophisticated tumor models that incorporate features of the tumor microenvironment are needed to elucidate mechanisms of response and resistance to immunotherapies. Broadening the clinical applicability of onco-immunotherapies requires an improved understanding of the mechanisms limiting therapeutic response in order to derive actionable strategies to overcome them. *Ex vivo* systems such as tumor chips that model the dynamic interactions between the immune system and cancer cells may facilitate efforts in

precision immune-oncology and the development of effective combination therapies[21]. Onco-immuno chip models, incorporating both malignant and immune components, fed through a vasculature are well positioned for these studies since they are derived entirely from human cells and the delivery of patient-based antibody therapies to the tumor occurs via tumor-associated vessels. Immune and tumor response can subsequently be assessed in real-time within the tumor microenvironment.

Microfluidic technologies hold many advantages for studying tumor-immune cell interactions since they capture the essential features of multiple cell type interactions while allowing tight control of the microenvironment and real-time monitoring. Hsu et al[88] developed a microfluidic platform that allowed cancer cells, myofibroblasts and macrophages to be cultured in each of three separate chambers connected by a Y-shaped channel equipped with microvalves that, when opened, allowed release of cell-conditioned media (CM) from myofibroblasts and/or macrophages to the cancer cells. Employing the platform, it was observed that CM from myofibroblasts and macrophages increased migration of cancer cells and that TNF α secretion by macrophages counteracted the migration-promoting effects of myofibroblasts. This study provides insights into the crosstalk between tumor and stromal cells and highlights the importance of modeling these aspects of the tumor microenvironment in disease models. In a recent contribution by Parlato et al[171], a novel platform was used to monitor behavior of patient-derived interferon- α -conditioned DCs (IFN-DCs) toward SW620 colorectal cancer cells, either untreated or exposed to an innovative anti-tumor combined treatment (termed RI). IFN-DCs moved through the microfluidic device toward RI-treated cancer cells, rather than the untreated counterparts, which was facilitated by CXCR4/CXCL12 dendritic cell-cancer cell signaling. RI-treatment of SW620 resulted in a significant increase in phagocytosis of SW620 cells as IFN-DCs modified their motion within the platform to take up more tumor antigens from drug treated cancer cells. The microfluidic device allowed real-time visualization of the dynamic tumor-immune interac-

tions involved in disease progression and treatment response, while further revealing that cancer treatment with the novel dual therapy RI facilitated anti-tumor immune function. Similarly, in a recent publication by Jenkins et al[105], *ex vivo* response to immune checkpoint blockade (ICB) was interrogated using Murine- and Patient-Derived Organotypic Tumor Spheroids (MDOTS \ PDOTS) cultured in a microfluidic device (Figure 1.4a) and validated against *in vivo* data. Primary spheroids isolated from mouse and human tumors retained autologous lymphoid and myeloid cell populations that recapitulated response and resistance to ICB within the tumor chips. Profiling of Murine-Derived Organotypic Tumor Spheroids (MDOTS) within the tumor chips revealed that TBK1/IKK ϵ inhibition enhanced response to PD-1 blockade, which effectively predicted tumor response *in vivo*. Systematic profiling of secreted cytokines in Patient-Derived Organotypic Tumor Spheroids (PDOTS) captured key features associated with response and resistance to PD-1 blockade, such as increased CCL19 and CXCL13 that facilitate recruitment of immune cells to sites of chronic inflammation to coordinate anti-tumor response. These findings were further confirmed in paired biopsy specimens collected from patients with melanoma both before and after ICB treatment. Thus, MDOTS \ PDOTS profiling represents a novel platform to evaluate ICB using established murine models as well as clinically relevant patient specimens. A 2017 study by Pavesi et al[174] describes a microfluidic model to test the antitumor efficacy of TCR-engineered T cells wherein cancer cells and T cells interact in a 3D collagen matrix on-chip (Figure 1.4b). Effector T cells introduced into medium-filled side channels encountered a central collagen-filled region (i.e. the “tissue”) containing hepatocellular carcinoma (HepG2-Env) cells expressing both hepatitis B virus (HBV) envelope protein (HBsAg) and GFP. Only T cells engineered via retroviral transduction to express a specific TCR recognizing the complex HLA-A0201 molecule and hepatitis B Env183-191 epitope (TCRe-T cells) engaged and killed the target cells upon migration into the gel. This was observed in real-time via a high resolution, 11-hour time-lapse video (Figure 1.4c).

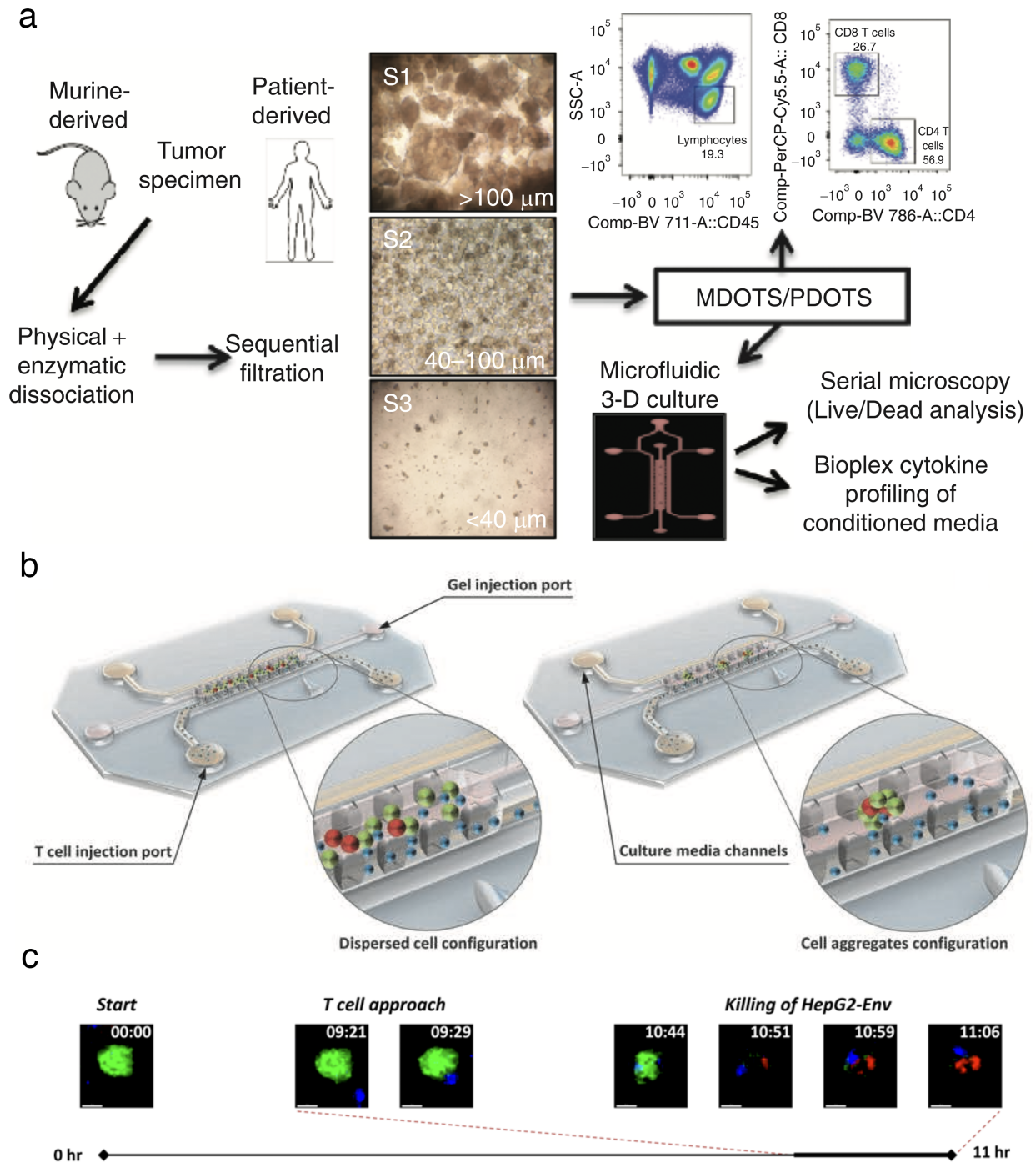


Figure 1.4 – Examples of onco-immuno chips (a) Schematic for preparation and analysis of MDOTS \PDOTS from murine or patient-derived tumor specimens. Reproduced from Jenkins et al[105] with permission from the American Association of Cancer Research. (b) 3D rendering of onco-immuno devices from Pavesi et al[174]. (c) Time-lapse video showing TCR-eT cell killing of HepG2-Env cells on-chip. Reproduced with permission from the American Society for Clinical Investigation.

Future Opportunities

Given their versatility and wide range of capabilities, microfluidic tumor chip assays could be exploited for more complex modeling of immune-cancer cell interactions by using additional cell types in 3D[21]. Stromal cells such as cancer-associated fibroblasts and macrophages should be included in future studies because of their critical role in modulating the immune response and facilitating cancer cell dissemination and invasion to distant organs[83, 18, 46]. Incorporation of a functional vascular network is also necessary to model physical barriers to drug or cell delivery, cell homing to distinct microenvironments, and trans-endothelial migration of tumor, stromal and immune cells[130, 149]. An important limitation to such studies is that incorporation of adaptive immune cells (e.g. T and B cells) would require an entirely autologous, HLA-compatible vascularized tumor chip model since human endothelial cells are highly immunogenic antigen presenting cells[93]. However, one can envision the development of patient-specific onco-immuno chips, incorporating tumor, stroma, and immune components for studying critical initiating steps in metastasis and developing novel immune-modulating therapies[21]. These individualized tumor chips are now becoming feasible with advanced cell culturing and genetic engineering techniques[69, 169].

While modeling of blood cancers-on-chip is still in its infancy, a recent study by Bruce et al[24] demonstrates a reductionist bone marrow-on-a-chip for study of acute lymphoblastic leukemia. It was shown that co-culture of primary human bone marrow stromal cells, osteoblasts and human leukemic cells in a 3D collagen matrix under dynamic flow conditions within the platform conferred enhanced cell viability and chemoresistance to the cancer cells compared to 2D and 3D static models. In a study by Torisawa et al[248], an *in vivo* engineered organotypic bone marrow-on-a-chip that recapitulates the structural, cellular and physical complexity of the hematopoietic niche *in vitro* is described. Bone marrow-on-a-chip can be used not only for study of toxicity/drug response and solid

tumor colonization within the metastatic niche, these models can also be developed to study leukemia, myeloma, myeloproliferative neoplasms and lymphoma. In addition to endothelial cell self-assembly into microvessels on-chip in response to flow, lymphatic microvasculature[126] and primitive lymph node models have also been described[228, 76]. These microphysiological elements can be further integrated into novel models of blood cancers, metastatic disease and onco-immune responses to increase physiological relevance, faithfully recreate steps of cancer progression *in vitro* and interrogate mechanisms of drug resistance.

1.4.2 Integrated Tumor-Organ-Chip Systems: Toxicity, PK-PD Modeling, and Metastasis Studies

Cancer is a heterogeneous and individualized disease involving multiple systems. Each cancer is both patient-specific and tissue-specific – i.e. breast cancer is not bone cancer is not lymphoma; all will behave differently, even between individuals with the same type. Yet, all cancers require integration of multiple tissue components to create a complex tumor microenvironment for tumorigenesis to proceed. This cannot be modeled with overly reductionist models like 2D or 3D models that lack tissue structure, or in immunocompromised non-human animal models. MPS represent a physiological, humanized model that allows for customization to specific cancers and integration of multiple systems. Integration of tumors into multi-MPS platforms will allow truly predictive *in vitro* modeling of human pathophysiology. These coupled tumor-organ-chip systems can enable comprehensive studies of drug toxicity, PK-PD parameters, and complex systemic cell-cell interactions such as those influencing the establishment of distant metastases. The importance of recapitulating orthotopic tumor growth and metastasis further necessitates the use of integrated tumor-organ-chip systems. Metastasis is a physical process by which mobile cancer cells break away from the primary site, travel into lymph vessels to

seed nearby lymph nodes or squeeze through blood vessel walls to gain access to the systemic circulation. Metastatic cells can then invade distant tissues by extravasating through the resident vasculature and establishing a secondary tumor at the new site[130, 149]. Coupling of organ systems holds tremendous potential for modeling metastasis of tumor cells from primary organs to distant sites in the body, especially if the organs are interconnected by microfluidic channels lined with living, perfused vessels to mimic the blood flow pattern in the human body[237].

One of the reasons for high rates of attrition during drug development is unforeseen drug toxicity that is not revealed until the later stages of testing when the drug has progressed to clinical trials. Many drugs have even been FDA-approved and available on the market before being recalled by the FDA for unanticipated side effects[221]. Current pre-clinical and computational models are unable to fully reproduce the pharmacokinetics-pharmacodynamics (PK-PD) of drugs *in vivo*, underscoring the need for clinically relevant model systems capable of revealing drug effects prior to testing in humans. The majority of therapeutic failures attributed to toxicity in cancer treatment are accounted by cardiotoxicity, hepatotoxicity and bone marrow toxicity, although nearly every other organ/system of the body (including gastrointestinal tract, kidneys, nervous system, skeletal muscles and gonads) has been reported to have anti-cancer drug-related pathologies[86]. To date, each of these organs have been recreated on-chip and could potentially be leveraged into tumor-organ-chip systems. While single tissue chips are useful for many applications, organs and tissues in the human body are not isolated but instead highly interconnected via the vasculature, receiving biochemical signals from cells at distant sites and functioning in concert to dictate the absorption, distribution, metabolism and excretion of drugs. Since the liver is the major site of drug metabolism, tumor chips can be linked to human liver chips to emulate *in vivo* PK-PD for simultaneous preclinical efficacy and safety testing within a single platform. Toxic effects on other organs can be assessed by incorporating additional functional units onto the platform.

Organ chip systems that integrate multiple human tissues have been described extensively in the literature[268, 267, 59, 186]. Yet there are fewer integrated systems in which malignant cell populations have been incorporated to study drug response or cancer progression, suggesting that multi-organ systems are still in the developmental phases of physiologic modeling. In 2010, Sung et al[238] published a pumpless system containing liver, bone marrow and colon cancer cells that, upon treatment with the chemotherapy 5-fluorouracil (5-FU), recreated anticipated drug actions showing that metabolites generated in the liver recirculated to achieve expected outcomes in all 3 tissue compartments. While a 'human surrogate' on-chip has not yet been fully realized, recreating the entire body may not be necessary or even practical for drug screening. When considering the increased costs, time, resources, sophisticated engineering and complex experimental procedures required for establishing such body-chip systems, the advantages of these systems may be insufficient compared to simpler on-chip models[152]. Furthermore, many biological and technical challenges remain, including the need to: 1) scale organs and their associated blood supplies to produce outputs that are physiologically accurate compared to other organs[273, 237]; 2) control oxygen gradients to create areas of inter- and intra-organ zonation; 3) create a systemic and interconnected circulatory system; and, 4) feed the tissues with a universal blood surrogate providing all the necessary nutrients, growth factors and proteins in a physiologically relevant manner[199]. Therefore, simplicity must be weighed against physiological relevance and platform usability when considering the appropriate level of model complexity important to reconstitute tissue functions, disease processes or drug responses for a given application.

For screening purposes, we feel that tumor chips are best positioned for drug efficacy studies because the majority of drugs fail during development due to lack of efficacy. The predictive power of tumor chips in toxicology studies may well be limited as there is a multitude of ways a drug could manifest toxicity, in contrast to efficacy, which is a clearly-delineated endpoint. Certain aspects of organ-specific toxicity may be tested in well-

designed multi-organ chips containing malignant cells, however these studies will need to be supplemented with mathematical models, *in vivo* study, and careful cross-species and drug design considerations. We envision that the greatest commercial and clinical potential for tumor chips resides in efficacy testing, since this application requires only a single tissue unit and output for ease of production, faster readouts and higher throughput screening. The less-complicated, user-friendlier tumor units with fewer barriers to use will likely see greater and faster adoption into drug development and clinical diagnostics. On the other hand, well-designed toxicity studies, with clear hypotheses and defined endpoints, should readily yield useful data from organ chips.

1.4.3 Personalized Medicine Applications

The goal of personalized medicine (precision medicine) is to choose the most efficacious, and least toxic, therapy for each individual patient. Yet many cancer drugs fail to demonstrate clinical activity due to an inability to identify patients that are most likely to respond[100]. Instead, drugs are prescribed by an empirical, one-size-fits-all approach that yields limited efficacy and significant side effects. Lack of efficacy is a significant barrier to FDA-approval for oncology drugs, and the majority of drugs that are approved confer only marginal survival gains. Current standards for precision medicine involve performing molecular testing on patient-derived tumor tissue to identify the specific genomic aberrations present and then categorizing the subtype of cancer based on population-level genetics[7]. Patients are then treated as an ‘average patient’ based on the cohort with which their tumor characteristics most segregate – we term this one-way personalized medicine. Although these tests are routinely performed in an effort to guide targeted treatment decisions, the full promise of genome-wide association studies has not yet been realized, as tumor recurrence and high variability in disease patterns remain an important

problem. Consequently, there is a lack of clinically validated and actionable biomarkers for which to guide treatment decisions.

Each individual cancer is characterized by considerable inter- and intra-tumor heterogeneity that encompasses genetic, molecular, cellular and microenvironment diversity that evolves over time[8]. These defining aspects of actual tumors are insufficiently modeled during preclinical drug development, leading to false-positive selection of drug candidates that look promising until they reach human efficacy testing in phase II and III clinical trials[55]. Part of the problem is that established cancer cell lines are routinely used for drug testing in 2D assays and animal studies, and since these cells have been maintained in culture for decades they are no longer representative of the disease from which they were derived. Even short-term culturing can induce marked genomic changes: cells adapt to growth in 2D monolayers and thus lose the intrinsic heterogeneity of the original tumor through genetic drift, as clonal populations that cannot survive in the culture flask are lost[13]. Thus, current preclinical models based on these immortalized cell lines are oversimplified and misrepresentative models of human tumors *in vivo*. To develop more effective targeted therapy for personalized treatment, understanding of human pathophysiology is critical and requires an investigational cancer model with high clinical predictive value. Tumor chips are now emerging as promising personalized model systems for pre-clinical drug development and, in the future, may serve as diagnostic tools to inform tailored clinical management.

Cell Sources for Tumor Chips

In order to achieve precision medicine approaches, it is necessary to use human primary cells for disease modeling and drug testing applications to more faithfully recapitulate the heterogeneity inherent to human disease. Primary cells can be derived from surgical resections, biopsies, aspirates and blood specimens[169]. In culture, samples can be fur-

ther enriched for adult resident stem or progenitor cells, or reprogrammed into iPS cells, and subsequently differentiated into mature cell types[154]. Ideally, matched healthy and cancerous cells can be derived from a single source and integrated into tumor chips to allow patient-specific disease modeling, drug efficacy and toxicity studies. Tumor chips populated with tissue samples obtained from sites of resistance and matched primary and metastatic lesions are valuable resources to study tumor evolution and guide the development of treatment strategies that address tumor heterogeneity. Cutting-edge bio-engineering approaches to capture patient- and disease-specific characteristics on-chip through incorporation of renewable cell sources are described below.

Organoid Technology

Advancements in stem cell biology have facilitated the development of patient-derived 3D stem cell cultures termed organoids. Since organoids give rise to multiple lineages that self-organize to reconstitute the cellular hierarchy, heterogeneity and structure of native tissues, these stem cell-derived models are increasingly being integrated into MPS for enhanced tissue fidelity and clinical relevance[266, 121]. Robust methods that are now established to derive long-term organoid cultures from virtually any matched normal and malignant tissue, such as those originating from intestine, pancreas, liver, prostate, and breast, may also be suitable for MPS applications[196, 256, 25, 131]. Organoids derived from epithelial tumors, also known as tumoroids, have been shown to be representative of distinct molecular disease subtypes by retaining the genetic heterogeneity of the parent tumors and, consequently, are able to recapitulate some aspects of *in vivo* treatment responses[259, 135, 256]. However, physiologic relevance is limited in these models because organoid cultures lack key anatomical and functional features that contribute to cancer progression and drug resistance, such as a tissue-tissue interface, stromal cells, a vascular compartment, dynamic fluid flow and mechanical forces[72]. Adaption of organoids into

tumor chips to replace commonly used established cell lines may facilitate the long-term support of cellular heterogeneity within a physiological context, since the convergence of the two technologies has been previously shown to better model organ-specific structures and *in vivo* gene expression signatures than either model alone[111]. Alternatively, cancer stem cells can be initially positively selected in specialized stem cell media and then differentiated on-chip to reconstitute the native clonal cell populations[231]. By exploiting organoid technology for tumor chip applications, both healthy and tumor tissue can be readily generated from the same individual and tested for drugs that specifically target tumor cells while leaving healthy cells unharmed[58]. A major limitation to this approach, however, is that cells must be harvested from each represented organ to generate the healthy organoids to be used for drug toxicity screening on-chip. While it may be more reasonable to collect cells from certain tissues than for others, it is neither practical nor ethical to obtain numerous biopsies from patients. Instead, patient-specific iPS cells can be generated.

iPS Cells

iPS cells are derived from primary human somatic cells via reprogramming by transient exogenous expression of a set of transcription factors[240]. Two unique properties define iPS cells: they can be maintained in culture in a self-sustaining pluripotent state, and they can be directed to differentiate into virtually any cell type of the human body, although generating fully mature cells with full functionality is still a challenge for most tissue types[169]. As a result, iPS cells have made it possible to engineer patient-specific human *in vitro* systems by deriving every cell type needed in the system from a single iPS cell. This is particularly useful for personalized toxicity screening and to detect variants that alter response to treatment. For example, patients with a genetic variation that reduces their ability to metabolize thiopurines, the drugs most commonly used to treat acute lym-

phoblastic leukemia, will build up toxic metabolites with standard treatment unless the variant is detected in the clinic and they administered a lower dose[57]. In a recent study, cardiomyocytes derived from iPS cells from patients with breast cancer were shown to model the doxorubicin-induced cardiotoxicity manifested in the patients [27], demonstrating the potential for iPS cell-derived models to faithfully recapitulate patient-specific disease outcomes *in vitro*.

To model population-wide variation necessary to detect disease variants, large and diverse collections of iPS cells capturing a range of cancer types, genotypes and patient-specific factors such as age and gender will need to be assembled and tested on-chip. Such studies could streamline the drug development process by accurately representing population variation at preclinical and early clinical trial stages, reducing the attrition rate of promising drugs and averting human risk by informing patient selection for clinical trials[142]. Gene editing tools, such as CRISPR-Cas, have enabled researchers to introduce disease-associated mutations into iPS cells to create isogenic models of human disease and then compare them with the original, unedited cell lines[143]. These studies will allow better tractability of results from preclinical to clinical stages and will be necessary to reveal novel drug targets and biomarkers of disease progression or prognosis. While iPS cells can theoretically provide an unlimited supply of once-inaccessible human tissues for research, these models are not without limitations. Not all cell lineages can be effectively derived from the same iPS cell line, and can vary between batches[169]. In general, iPS cell-derived lineages lose epigenetic markers during derivation and, as noted above, are immature[71, 199]. To address these limitations, the development of robust protocols for iPS cell differentiation and maturation are ongoing.

Individualized Trials-On-Chip

To circumvent current barriers to personalized medicine, we suggest using one or more approaches outlined above to grow a patient's own cells within tumor chip systems. Drugs can be tested, in a high throughput manner, directly on this 'individual-on-a-chip' in order to better predict the individual response to many therapies at once. Results derived from these tumor chip models can then correctly guide an oncologist to treatments that are most likely to be of clinical benefit to that patient – an approach we term two-way personalized medicine. The goal is to determine which therapeutic regimen will most effectively target their particular cancer *before* they receive any treatments. This represents a truly personal drug screening methodology whereby tumor chips can be directly used in the clinic as a diagnostic tool. Individualized tumors-on-chip can also be used for 'micro'-clinical trials in which many unique patient-specific tumor chips are established using patient-derived cells and material[110]. Such *in vitro* trials would allow testing of multiple drug dosing and schedule regimens to inform treatment timing and sequence, guide rational combination therapies, and facilitate discovery of novel agents. Drugs that are currently only approved for treatment of specific cancer types or compounds that are not traditionally prescribed for cancer can be readily tested on tumor chips *in vitro* and repurposed for additional disease indications based on the results. This may increase the number of treatment options available for patients while facilitating our understanding of cancer type-specific resistance mechanisms to inform development of clinical biomarkers. Individualized trials-on-chip could revolutionize drug development and clinical management in oncology by allowing patient stratification based on individual characteristics without the need for large-scale clinical trials, thereby reducing human risk. Such an approach would also allow therapeutic agents to be screened on tumor chips derived from patient populations unfit to participate in standard clinical trial designs, such as patients with co-morbidities, rare cancers, recurrent or heavily pre-treated disease, and pediatric

patients. High-throughput experiments combined with molecular testing could elucidate gene-drug interactions, facilitate tumor subtype stratification in response to drugs and inform clinical trials. Such an approach will allow more accurate patient stratification based on additional tumor characteristics such as the microenvironment milieu[31].

Translational Study Design

In order to validate tumor chip models as translational tools, studies utilizing these models must be designed with translation in mind[44]. In a recent study[150], for example, Vunjak-Novakovic and colleagues validate results from a bone-mimetic tumor chip model against clinical data to unravel the contribution of mechanical strain to treatment resistance in Ewing sarcoma (ES), the second most frequent bone tumor in children and young adults. A bioengineered model of ES was generated by preparing porous 3D scaffolds from collagen I and hyaluronic acid solutions using a freeze-drying technique and then seeding the matrix with established ES cell lines or patient-derived ES xenograft tumor cells. ES-mimetic bone constructs were then placed in a bioreactor and subjected to dynamic compressive loading to model the mechanical stresses generated by body weight and muscle tension on bone. Compared to unstimulated control and 2D culture, bone-like loads increased the expression of RUNX2, a transcription factor that mediates cancer cell proliferation, survival and drug resistance of tumors that reside in the bone. Indeed, mechanical stimulation of the tumor chips led to enhanced ES resistance to treatment with clinically relevant doses of RTK inhibitors. In accordance with clinical trial data and immunohistochemical staining of ES tumor biopsies, patient-derived ES cells demonstrated increased RUNX2 expression and exhibited an enhanced degree of treatment resistance than established ES cell lines, indicating that patient-derived tumor cells better retained characteristics of the native tumor. By analyzing publicly available databases for RUNX2 expression, it was revealed that patients with tumors overexpressing RUNX2 had poorer outcomes and decreased survival.

Based on these findings, the authors suggest targeting the RUNX2 downstream effectors ERK1/2 as a rational therapeutic strategy for ES.

The vast numbers of clinically annotated ‘omics’ (genomics, transcriptomics, metabolomics, and proteomics) databases now available constitute a powerful set of research tools to identify high frequency cancer-related biological variations. However, despite significant advancements arising from these association studies, it has proven very difficult to assign causal roles to the identified “cancer-associated” variants[143, 255]. To successfully verify biomarkers of cancer progression or treatment response, realistic human cell-based cancer models that can be experimentally queried in a reproducible manner are needed. Tumor chips offer unprecedented opportunities to model cancer in a robust, physiologically relevant context that allows repeated experimentation to probe the mechanistic and functional underpinnings of ‘omics’ cancer-associated signatures. Further, tumor chips can reveal novel targets by phenotype-based drug screening.

Considerations for Personalized Medicine

Tumor chip systems are uniquely suited to facilitate the development of personalized medicine because few cells are needed from the patient and rapid, automated results can be obtained within a clinically actionable timeframe. However, several obstacles to the use and study of patient-derived tissues include: 1) the regulatory burdens and logistical issues associated with such research; 2) challenges in successful generation of primary cultures; 3) the scarce amount of viable patient-derived cells available for use after pathological analyses; and, 4) the need to form homogeneous replicates representing the functional heterogeneity of the tumor in order to compare responses under various conditions (e.g. replicates to test different compounds, concentrations and even timing or tissue location). If tumor chip models are to be embraced for precision medicine applications, they must provide reliable results despite these challenges. Close collaboration between primary

investigators, physicians, and regulatory agencies is necessary to move the field forward. Biobanks of human primary tissues can facilitate these studies, as well as collaborative efforts among independent investigators to integrate the most critical components for modeling tumor biology on-chip. Phenotypic and genotypic profiling is necessary to demonstrate that tumor chips preserve a high degree of similarity to the original patient tumors. Moreover, it has yet to be demonstrated that tumor chips accurately replicate patients' clinical outcomes. Co-clinical trials, whereby drug responses of patient-derived tumor chips are compared directly with patient drug response, must be performed to determine the clinical predictive utility of tumor chips[100]. Pharmaceutical companies and academic research institutions can design clinical trials to include *in vitro* studies performed in parallel using patient-derived biopsy tissue to complement *in vivo* findings. These studies will reveal the value of tumor chips in maximizing drug development success and patient benefit from anticancer treatment[100].

1.4.4 Design of Tumor Chips

Oxygen Control

To create biomimetic 3D models that better recapitulate tissue or organ function during physiological or pathological processes such as cancer, several important factors of the tumor microenvironment must be considered. Oxygen tension is a critical regulator of cell behavior, and in some organs (e.g. liver), tight regulation of oxygen levels across the tissue is required for function. Most adult tissues within the body typically experience 3%–8% O₂, with highly oxygenated tissues in the lungs reaching 14% O₂, capillaries around 4% O₂ and poorly perfused tumors frequently experiencing chronic or intermittent hypoxia (i.e. ~1% O₂) within the tumor microenvironment[34]. In contrast, *in vitro* studies are usually performed under atmospheric oxygen conditions (20% O₂) that do not represent

in vivo conditions. Consequently, the results from these studies may be misleading. In cancer, hypoxia is associated with poor prognosis since it promotes treatment resistance and is a major contributor to malignant progression via metastasis[2]. *In vitro* models of metastasis must further expose migrating tumor cells to varying microenvironments and oxygen gradients mimicking what occurs during the intravasation process *in vivo*[62].

Tumor chip systems have several advantages over traditional preclinical models to facilitate experimental manipulation and interrogation of molecular mechanisms of tumorigenesis. Microfluidic devices can be designed to achieve oxygen gradients with high spatial and temporal resolution for modeling physiologically relevant effects of oxygen on tumor progression and metastasis. Such control can be implemented by perfusing oxygen scavengers or carriers, or pumping oxygen or nitrogen, directly into microfluidic channels adjacent to tissue constructs or by exploiting cellular consumption of oxygen in single- or multi-layer devices or in multicellular aggregates[2, 39, 23, 61]. However, some of these designs require cumbersome external apparatuses and pumps to deliver gas or chemicals into the chip, or require multi-layer arrangements that increase fabrication complexity and impair high-resolution microscopic observations[205]. Tumor chips that incorporate living, perfused vasculature can deliver oxygen and nutrients to the tissue construct via flow of oxygenated media through the vessels, much as it would occur *in vivo*. Other options to control O₂ delivery in tumor chips include placing microfluidic platforms in controlled gas tissue incubators for simulating chronic hypoxia, or fabricating devices with oxygen-impermeable materials, such as thermoplastics, in place of PDMS, which has high oxygen permeability[39].

Fabrication Material Properties

PDMS is traditionally used for fabrication of biomedical microfluidic devices since it is relatively inexpensive, can bond reversibly and irreversibly to itself or other materials,

and is elastic, allowing for easy removal from delicate silicon molds for feature replication as well as enabling specialized designs on-chip, such as valves or thin, flexible membranes[205]. However, drug and small molecule absorption into PDMS is a major concern since hydrophobic compounds readily diffuse into or adhere to PDMS, reducing the intended drug exposure and causing undesirable mixing between adjacent channels that can confound interpretation of experimental results[61]. The hydrophobic surface properties of PDMS can be tuned to a more hydrophilic state prior to drug testing to help prevent absorption/adsorption of drugs to PDMS[10]. This is accomplished by oxidizing the PDMS to create a barrier of silicon dioxide on the surface through plasma treating or coating with proteins. Alternatively, devices can be fabricated with a different material altogether although additional considerations must then be given to the fabrication process. Polystyrene is routinely used for cell culture and thus represents a rational alternative to PDMS. Mathematical modeling approaches have also been developed to account for absorption[142, 205].

Tumor Chip Readouts

Multiple modes of analysis (e.g. biological, electrophysiological, chemical and mechanical) can now be integrated on-chip for dynamic studies of tissue responses[199]. The majority of on-chip studies exploit the optical clarity of PDMS devices to perform functional assays on live tissues using microscopy techniques. Morphological tissue features can also be visualized by *in situ* imaging of fluorescently tagged or unlabeled cells, immunofluorescent or immunohistochemical staining. Sensitive, noninvasive imaging and confocal microscopy techniques can be performed on intact tissue-chips to reveal distinct histological features, cellular populations or tumor characteristics[109]. While these tumor chip applications rely on time-consuming and involved microscopy imaging and analyses, which limit the devices in terms of automation, streamlined methods are increasingly

reported[253, 282]. To further characterize cells grown in tumor chips, RNA-expression analysis is now routinely used in combination with imaging[109]. However, preparation of the cells for genomic assays is a manual and inefficient process that may be improved by designing tissue chips compatible with the workflow of these assays. Molecular assays such as ELISA or LC/MS based techniques can be coupled to microfluidic cell culture by means of dedicated outlets to collect and analyze effluents from individual chambers and detect secretion of compounds, such as tumor-derived exosomes or pro-inflammatory cytokines[109, 152, 174]. The increased sophistication of analytical techniques applied to MPS studies warrants a critical assessment of bioengineering designs to enhance tumor chip usability, throughput and compatibility with existing technologies[109]. Ideally, designs are considered for automation and direct translation into industry settings[199]. Data derived from large-scale tumor chip studies can then be compared directly to the *in vivo* situation to establish correlations of tumor heterogeneity and treatment response.

1.5 Future Considerations

Advances in microfluidic technologies and tissue engineering have made tumor chips attractive candidates to replace traditional experimental approaches by allowing precise control over the tumor microenvironment, the ability to interrogate dynamic cell-cell and cell-ECM interactions in real time and at high resolution, and the ability to acquire rapid, automated results using high throughput arrays. Depending on tumor chip design, virtually any type of drug or drug delivery system can be tested for efficacy and toxicity within a fully humanized system, including but not limited to: cell-based therapies[84, 174], chemotherapy, anti-angiogenic treatment, targeted therapy[225], antibodies or small molecules, radiation, nanomedicine[285, 74] and electric field therapy[174]. Yet despite their tremendous experimental potential, the use of microfluidic tumor chip assays has

mostly been restricted to academic research settings and they have not yet been widely adopted in the pharmaceutical industry or clinic. One of the major reasons for this is that many tumor chip technologies have not yet been rigorously validated against *in vivo* data, either mouse or human.

Currently, many microfluidic device studies are still considered ‘proof-of-concept’[205]. Regulatory hurdles to FDA-approval for tumor chips mean that the burden for preliminary data indicating proof-of-superiority to traditional models lies mostly with the academic labs that developed the platforms. Yet global research initiatives to support and advance this cutting-edge technology are ongoing. In the US, the NIH National Center for Advancing Translational Sciences (NCATS), in collaboration with other NIH Institutes and Centers, the Defense Advanced Research Projects Agency (DARPA), and the FDA, is leading the Tissue Chip Drug Screening program. Under this program, three Tissue Chip Testing Centers have been established to test and validate tissue chip platforms, including tumor chips, independently. The goal of this program is multifaceted: to ensure wide-ranging availability of tissue chip technology, particularly for regulatory agencies and pharmaceutical companies, and to promote adoption of this technology by the broad research community.

Much work still remains before tumor chips, or organ chip models generally, are adopted into healthcare settings and mainstream drug R&D, and predominately hinges on demonstrating the functionality, reproducibility, robustness and reliability of each tissue chip platform. The current trajectory, however, is promising. For example, blood-vessel-on-chip devices have already been implemented into the clinic for the diagnosis of sickle cell disease[276], and pharmaceutical companies are now readily forming collaborations with academic centers that develop on-chip technologies. Similarly, start-up companies based on these technologies and founded by the inventors are now gaining commercial recognition as well as support from both public and private entities. Microfluidic technologies have clear potential to advance cancer research, the success of which depends on how

effectively the engineering and the biology can be integrated to create a clinically relevant *in vitro* tumor system.

1.6 Closing Remarks

Rapid technological advances have led to the development of tumor chip platforms for monitoring in real time the events linked to cancer development, progression and response to therapy. Given their close mimicry of human biology and physiology, tumor chips are anticipated to bridge the enormous gap between *in vitro* and *in vivo* preclinical studies as well as serve as a clinical diagnostic for personalized medicine applications. By surpassing the predictive accuracy of conventional 2D cell culture models, tumor chips can reduce reliance on animal models in line with the 3R's initiative and eliminate false-positive selection of ineffective or toxic drugs earlier in the drug development pipeline, thereby saving time and resources. Most importantly, better predictability of human drug response will reduce human risk and improve patient outcomes. We anticipate a paradigm shift in drug development, disease modeling and precision medicine as tumor chip models become widely adopted in academia, industry and healthcare.

1.7 Foreword

Given the current state-of-the-art in tumor chip technology, we sought to determine whether our VMT system recapitulates key features of *in vivo* tumors, including: 1) gene expression; 2) heterogeneity; and 3) drug response. To do so, we profiled tumor cells, endothelial cells and fibroblasts isolated from the VMT at single cell resolution to map heterogeneity within the tumor microenvironment. We found that the cells growing in

the VMT better model the cellular diversity and gene signatures of *in vivo* tumors. Further, the VMT captures distinct cell populations that are not observed in simple 2D or 3D monocultures, including a subpopulation undergoing epithelial to mesenchymal transition. High-resolution, time-lapse confocal microscopy allows us to visualize this rapid event as tumor cells break away from one another and intravasate into associated vasculature. By comparing gene expression data from bulk RNA sequencing performed for monolayer, VMT and xenograft tumors, we demonstrate that the VMT more faithfully recapitulates the xenograft tumor gene signature than 2D cultures. Reference-integration analyses comparing single-cell gene expression data for 2D and 3D monocultures, the VMT and xenograft tumors shows that the VMT maintains the heterogeneity observed within the xenograft more closely than the current standard culture models. Based on our single-cell RNA sequencing results, we find tumor-stromal interactions that recapitulate clinicopathological tumor features. We show that these tumor-stromal interactions can be therapeutically abrogated to suppress tumor growth, and that these interactions can not be studied or targeted in simple monocultures, further highlighting the physiologic relevance of the VMT.

We next developed automated image processing methods via scripts and macros to improve and standardize our image analyses workflow. These scripts provide flexibility to the user's needs, while allowing a range of functions to address many different research questions within the VMT or with other assays. We show the utility of these scripts to perform standard analyses and derive interpretable results in a fraction of the time that the image processing, measuring and analyses normally take when performed manually. Lastly, we show the promise of the VMT model for personalized medicine applications by demonstrating our methods for deriving patient-specific tumor tissue from freshly collected biopsies and surgical resections for maintenance within the VMT. Our aims with these studies are to position the VMT in the drug development pipeline and to gain suf-

ficient data to justify a co-clinical trial using the VMT to determine its clinical predictive value and move toward truly personalized medicine in oncology.

Chapter 2

Recapitulating the Tumor Microenvironment *In Vitro* Using a Vascularized Micro-Tumor Model

2.1 Abstract

About 95% of anti-cancer drugs that show promise during preclinical study fail to gain FDA-approval for clinical use. The gap between *in vitro* and *in vivo* preclinical study calls for physiologically relevant *in vitro* models that can better serve as a reliable drug-screening tool. The VMT is a novel three-dimensional model system that recapitulates the complex human tumor microenvironment within a transparent microfluidic device, allowing real-time study of drug response and tumor-stromal interactions. Here we validate our model system by showing that gene expression, tumor heterogeneity, and treatment response in the VMT more closely model tumor clinicopathology than current standard drug screening modalities.

2.2 Introduction

Cancer accounts for 25% of US deaths, and the majority of patients die from metastatic disease that is refractory to current therapies[217]. Less than 5% of drugs entering clinical trials ultimately receive FDA approval[96] and most anti-cancer agents fail in clinical studies despite showing promise during preclinical study, suggesting that current model systems are poor predictors of drug response in humans. Traditionally, drug candidates are first tested in 2D cell monocultures. However, cell growth in 2D versus 3D environments not only promotes phenotypic changes in cell morphology, response to stimuli, cell functions and gene expression patterns, but also alters response to therapeutic agents[163, 79, 71, 46, 198]. Indeed, both normal and cancerous cells maintain their specific functions in the body owing to the 3D conformation they adopt, encompassing heterogeneous and dynamic cell-cell and cell-matrix interactions[144, 181, 116]. Prior efforts to develop appropriate 3D tumor tissues have been limited to the generation of avascular spheroids in artificial matrix, which fail to recapitulate the structure of a vascularized tumor mass and are not viable for long-term study[67, 243]. Although animal models have significantly advanced our understanding of complex diseases such as cancer, and are important in the drug development pipeline, these same models require substantial time and resources and species-specific differences can impede clinical translation of results[5, 42].

To address the need for improved preclinical models, we have designed, fabricated and validated a microfluidic device that supports the formation of a perfused, vascularized micro-tumor (VMT) via co-culture of multiple cell types in an extracellular matrix[85, 90, 161, 226, 81]. This is a truly novel platform as it is the only one where growth of the tumor, and delivery of therapeutics to the tumor, is entirely dependent on flow through the living vascular network. Physiologic flow rate through the capillary bed formed within the device is maintained by a gravity-driven pressure differential that does not require external

pumps and valves[89]. The VMT (aka ‘tumor-on-a-chip’) represents a major breakthrough in tissue engineering by providing an environment amenable to *de novo* formation of perfused vasculature supported by stromal cells in the tissue construct, allowing long-term culture for drug sensitivity and molecular studies. Further, the platform is composed entirely of human cells, optically compatible for real-time fluorescent image analysis and arrayed for high-throughput experiments[180]. Drugs can be tested within days on limited numbers of cells expanded to form the VMTs, providing high sensitivity and rapid turnaround of results. These features are essential for developing the VMT as a drug development tool and clinical diagnostic.

CRC represents a major source of morbidity and mortality as the second leading cause of cancer-related deaths in the US and the third most common cancer worldwide, with over a million diagnoses and half a million deaths each year. The majority (75%) of patients present with localized disease (stage I and II) and undergo intentionally curative surgery. However, half of these patients will develop, and ultimately die from, metastatic disease. A 5-year survival rate for stage IV disease at merely 10% highlights the need to find more effective therapies. Accurately modeling tumor biology *in vitro* is critically important to developing therapeutic regimens to improve clinical outcomes. Here we show that CRC-derived VMT more closely model gene expression, heterogeneity, tumor growth and response to standard chemotherapy of xenograft tumors derived from the same CRC cells than those cells grown as 2D or 3D monocultures. We further interrogate the transcriptomic landscape of the VMT compared to both 2D and 3D monocultures at single cell resolution to reveal changes in cellular diversity and gene expression that arise when cells are introduced into the dynamic co-culture environment of the VMT. These studies reveal that the VMT recapitulates key features known to contribute to CRC disease progression and therapeutic failure, while also capturing unique cellular populations and expression signatures not observable in simple *in vitro* models. By characterizing distinct cell populations within the VMT via single cell mRNA sequencing, we demonstrate that

the VMT maintains the heterogeneity of tumors growing *in vivo*, distinct from the same cells growing as 2D or 3D monocultures, and that changes in gene expression within the tumor and stroma underpin drug sensitivities. Our findings support the VMT model as a powerful tool for drug development and disease modeling in oncology.

2.3 Materials and Methods

2.3.1 Cell culture.

Human endothelial colony-forming cell-derived endothelial cells (ECFC-EC) are isolated from cord blood with IRB approval. After selection for the CD31⁺ cell population, ECFC-EC are expanded on fibronectin-coated flasks and cultured in EGM2 medium (Lonza). ECFC-EC are used between passages 4–8. NHLF are purchased from Lonza and used between passages 6–10. HCT116 colorectal cancer cells were a gift from the UC Irvine Chao Family Comprehensive Cancer Center and SW480 colorectal cancer cells were clonally derived and generously provided by Dr. Marian Waterman. The ECFC-EC and cancer cells were transduced with lentivirus expressing mCherry (LeGO-C2, plasmid # 27339), green fluorescent protein (GFP) (LeGO-V2, plasmid # 27340), or azurite (pLV-Azurite, plasmid # 36086) (Addgene, Cambridge, Massachusetts)[270, 157]. Cancer cells and fibroblasts are cultured in DMEM (Corning) containing 10% FBS (Gemini Bio). All cells are cultured at 37 °C 20% O₂ 5% O₂ unless noted otherwise.

2.3.2 Microfluidic device fabrication.

Device fabrication has been described previously[226, 180]. Briefly, polydimethylsiloxane (PDMS, Sigma-Aldrich) is poured into a customized polyurethane master mold and allowed

to polymerize overnight in a 70°C oven. The PDMS replicate layer is removed and holes are punched to create inlets and outlets for the media reservoirs and loading chambers. The PDMS device is attached to a 96-well open-bottom plastic culture plate via chemical gluing and oxygen plasma bonding (Harrick Plasma Cleaner), after which a transparent 150 µm PDMS membrane is then bonded to the device using oxygenated plasma. The fully assembled high throughput device is placed in a 60°C oven overnight, covered with a standard 96-well plate polystyrene lid, and sterilized with UV light for 30 minutes prior to use.

2.3.3 Loading the microfluidic device.

EPC and LF (both 8×10^6 cells/mL) and SW480 and HCT116 CRC cells (2.5×10^6 cells/mL) were resuspended in fibrinogen solution (10 mg/mL basal medium). The cell slurry was then mixed with 1.5 µL thrombin (3 U/mL) to catalyze gel solidification and quickly loaded into the tissue chambers of each unit on the platform. Fibrin ECM was allowed to solidify at 37°C for 15 minutes prior to injecting laminin and EGM2 medium through the microfluidic channels. Laminin promotes vessel anastomosis with the outer channels. VMT were cultured at 37°C, in either a 5% CO₂ incubator (normoxic condition) for the duration of the experiment or in a 4% O₂ incubator (for low oxygen culture) after the vessel network had fully formed (by day 5).

2.3.4 Generation of tumor spheroids.

SW480 CRC cells were resuspended into 10 mg/mL solution of 70% fibrinogen at a concentration of 1×10^5 cells/mL and 50 µL of the cell solution was seeded into a 96-well plate containing 5 U of thrombin. Gels were allowed to set at 37°C for 15 minutes before addition

of 100 μ L of EGM2 medium to each well. Medium was changed every other day and drug treatment started on day 5 of spheroid formation.

2.3.5 Drug treatment.

Media is changed every other day and hydrostatic pressure restored every day in the high throughput platform. After culturing for 5 days to allow full development of each VMT, culture medium is replaced by medium containing the drugs at the desired concentration, and delivered through the microfluidic channels using the hydrostatic pressure gradient. To mimic pharmacokinetics *in vitro*, drugs were diluted into medium at maximal human plasma concentration on the first day of treatment (day 5 of VMT culture) and AUC were modeled according to average plasma clearance curves and drug half-life. Pharmaceutical grade 5-fluorouracil, leucovorin and oxaliplatin (FOLFOX) were purchased from UCI Medical Center pharmacy. Galunisertib (TGF- β R1 inhibitor) was purchased from SelleckChem. Tissues were exposed to compounds for the desired duration based on parameters defined by clinical administration and the effect on tumor growth was quantified every 48 hours for 6 days post-treatment. Cell viability in response to drugs in 2D monolayer cultures was quantified using an XTT assay according to the manufacturer's protocol (Sigma-Aldrich). Briefly, 5,000 or 10,000 cells (HCT116, SW480 or NHLF) were seeded in triplicate in a 96-well plate and allowed to grow for 24 hours prior to treatment with drugs. XTT assays were performed after 48 hours of drug exposure or at the 96 hour time point after media changed at 48 hours. Cell viability was normalized to control wells without drug treatment.

2.3.6 Immunofluorescence staining.

The VMT were fixed for immunofluorescence staining by perfusing 4% paraformaldehyde (PFA) through the medium inlet for 30 minutes at room temperature. After fixing, VMT were washed with 1x DPBS overnight at 4°C . Next, the high throughput plate was inverted and the bottom polymer membrane was carefully removed from the device. Each VMT unit was cut from the platform with a razor blade and placed in a 24-well culture plate, washed with 1x DPBS and then permeabilized for 15 minutes with 0.5% Triton-X100 diluted in DPBS. After permeabilization, VMT were blocked with 10% goat serum for 1 hour at room temperature and then incubated with primary antibody (diluted in 3% goat serum in 1x DPBS) overnight at 4°C . The following primary antibodies were used in experiments: anti-Collagen II (Abcam, ab6310), anti-EpCAM (Abcam, ab71916), and anti-Cytokeratin 5 (Abcam, ab53121). After washing with 1x DPBS, VMT were incubated with goat anti-rabbit or goat anti-mouse secondary antibody (1:2000 dilution in 5% serum) for 1 hour at room temperature before washing with DPBS and counter-staining with DAPI. Finally, anti-fade solution was added on top of each VMT before mounting with a glass coverslip. Established cell lines were seeded into multi-well cover glass chambers and processed by the same protocol.

2.3.7 Fluorescence imaging and analyses.

Fluorescence images were acquired with an Olympus IX70 inverted microscope using SPOT software (SPOT Imaging, Sterling Heights, Michigan). Confocal time-lapse series acquisition and imaging of fluorescent immunostaining was performed on a Leica TCS SP8 confocal microscope using a standard 10x air objective or 20x multi-immersion objective with digital zoom setting. AngioTool software (National Cancer Institute) was used to quantify vessel area, vessel length, number of vascular junctions and endpoints in the VMT.

ImageJ software (National Institutes of Health) was utilized to measure vessel diameter and measure the total fluorescence intensity (i.e. mean grey value) for each tumor image to quantify tumor growth. Each chamber was normalized to baseline. Vessels were perfused by adding 25 $\mu\text{g/mL}$ FITC or rhodamine-conjugated 70 kDa dextran to the medium inlet. Once the fluorescent dextran had reached the vascular network, time-lapse image sequences were acquired using a Nikon Ti-E Eclipse epifluorescent microscope with a 4x Plan Apochromat Lambda objective. Perfusion images were analyzed using ImageJ software by measuring change in fluorescence intensity within regions of the extracellular space. Permeability coefficient is calculated by using Equation 2.1:

$$P_D = \frac{1}{I_i - I_b} \left(\frac{I_f - I_i}{\Delta t} \right) \times \frac{d}{4} \quad (2.1)$$

where I_i , I_f and I_b represent the initial, final and background average intensities, respectively, Δt is the time interval between two captured images and d is the average diameter of the vessel[106].

2.3.8 Finite element simulation.

COMSOL Multiphysics®5.2a was used to perform finite element simulations for the interstitial flow inside a developed microvascular network. Thresholded vessel images were smoothed and processed into outlines using ImageJ software, then converted into a .dxf file using Img2cad software. After the vessel outline was closed, and redundant fragments were removed using AutoCAD software, the complete vessel outline was scaled and integrated into the geometry of microfluidic device. The refined CAD vessel diagram was then built into a 2D free and porous media flow model in COMSOL Multiphysics. Water was cho-

sen to model the flow of culture media through the vascular network. The porosity and permeability of fibrin gel were estimated to be 0.99 and $1.5 \times 10^{13} \text{ m}^2$ based on our published result[226]. Inlet/outlet were designated at the media reservoir boundaries, with pressure specified as 98 and 0.001 Pa, respectively, based on calculated gravity-driven pressure difference in the device, as previously described.

2.3.9 Cell sorting.

The PDMS membrane was carefully removed from the bottom of the platform to expose the VMT tissue chambers. Chambers were washed with HBSS before adding TrypLE express enzyme drop wise to each VMT unit and incubated at 37°C for 5 minutes to loosen the extra-cellular matrix from the device. Chambers were flushed with a pipette to collect cells into a conical tube and washed once with EGM2 medium to stop the digestion reaction. Next, cells were subjected to centrifugation (340×g for 3 min.) and briefly resuspended in an HBSS/collagenase type III solution (1 mg/mL) to fully digest the matrix. Finally, the single cell suspension was washed with EGM2 and put through a 70 μm filter. Cells were processed for sorting within an hour and kept on ice. Sorting was performed on the BD FACS AriaII with BD FACS Diva software version 8.0.1. Samples were sorted using a 100 μm nozzle at 20 psi with gating strategy to select for fluorescently labeled (mCherry) cancer cells (2.1).

2.3.10 Animal studies.

All animal experiments were approved by the University of California, Irvine (UCI) Institutional Animal Care and Usage Committee (IACUC). For CRC xenograft treatment experiments, male NOD scid gamma (NSG) mice (Jackson Laboratories) were injected sub-

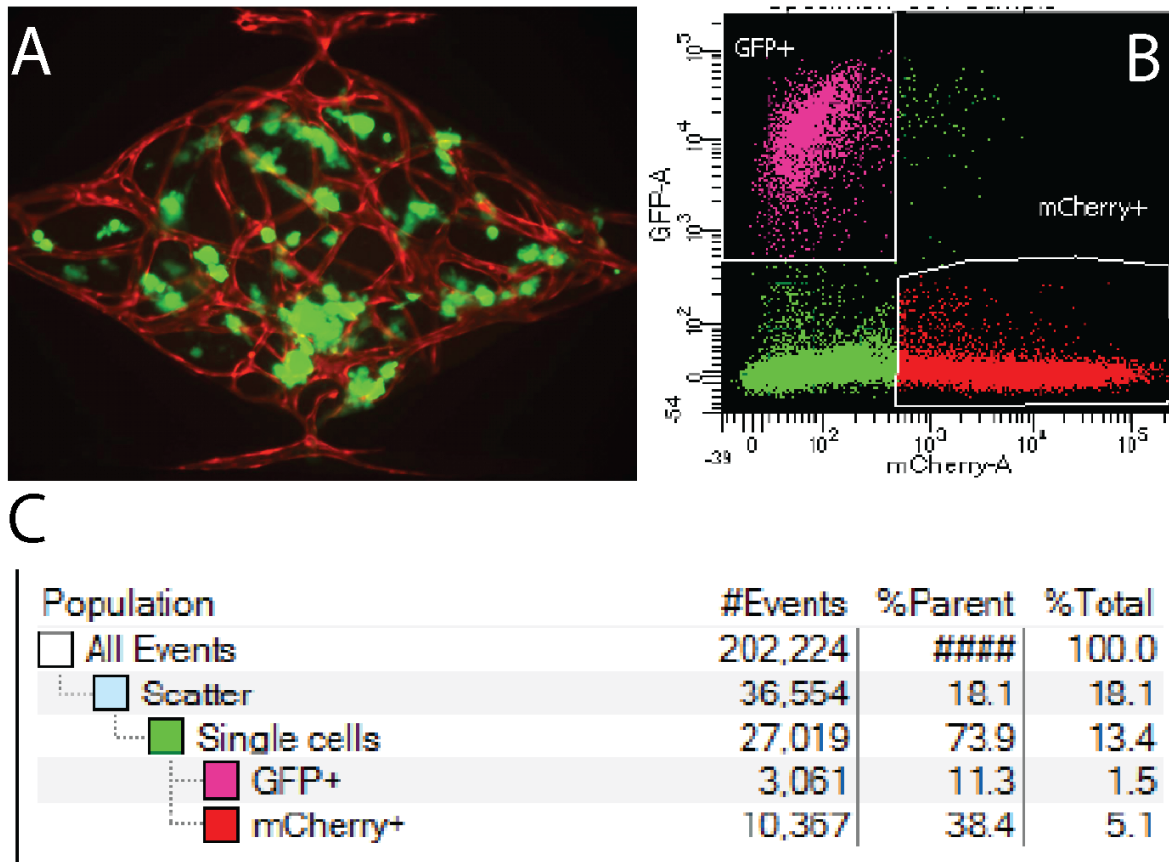


Figure 2.1 – Cells in the VMT can be isolated via fluorescence activated cell sorting FACS. (a) Representative image of SW480 VMT. CRC cells shown in GFP and vessels in mCherry. (b) Gating strategy for FACS. (c) Table showing proportions of isolated cells.

cutaneously into both flanks with a sterile culture of HCT116 or SW480 (5×10^5 cells) in 100 μ L PBS (2 injections per mouse). Tumor volume and body weight were measured every other day using a caliper and scale, respectively. Tumor volume was calculated using Equation 2.2 with length being the longest measurement of the tumor.

$$Volume = \frac{Length \times Width^2}{2} \quad (2.2)$$

When the tumors reached a volume of 150 mm³, mice in the control group received two intraperitoneal (I.P.) injections of PBS. Mice in the FOLFOX group received one I.P. injection containing a combination of leucovorin (90 mg/kg) and 5-Fluorouracil (50 mg/kg), followed by an injection of oxaliplatin (6 mg/kg) two hours later. This treatment occurred weekly for up to 6 weeks or until the tumor reached a volume of 2 cm³. For NanoString experiments, xenograft tumors were established as described. When the tumors reached a volume of 2 cm³, mice were euthanized and tumors were harvested. The tumor tissue was minced into 1 mm pieces and digested in a solution of collagenase IV, hyaluronidase and DNase I by shaking for 1–2 hours at room temperature. The single cell suspension was then processed and subjected to flow cytometry to select for mCherry labeled cancer cells as outlined above.

2.3.11 NanoString PanCancer Human Pathways Assay.

Gene expression analysis was performed using the NanoString PanCancer Human Pathways Assay. Per sample, 10,000 cells were lysed in diluted Buffer RLT (1:5 in RNase-free water) at a concentration of 2000 cells/ μ L volume. Samples were submitted to the Genomics High Throughput Core Facility at UCI. Each cell lysate was mixed with a 3' biotinylated capture probe and a 5' reporter probe tagged with a fluorescent barcode from the custom gene expression code set (list of genes provided in Supplementary Methods). Probes and target transcripts were hybridized at 65°C for 12–16 h. Hybridized samples were run on the NanoString nCounter preparation station using the recommended manufacturer protocol, in which excess capture and reporter probes were removed and transcript-specific ternary complexes were immobilized on a streptavidin-coated cartridge. The samples were scanned at maximum scan resolution on the nCounter Digital Analyzer. Data were processed using nSolver Analysis Software and the nCounter Advanced Analysis module. For gene expression analysis data were normalized using the geometric mean of house-

keeping genes selected by the GeNorm algorithm. The raw count from NanoString was subjected to background subtraction and reference gene normalization. Data were analyzed using NanoString nCounter nSolver software version 3.0 (NanoString Technologies, Seattle WA).

2.3.12 Xenograft tumors for single-cell sequencing and cell anchoring.

SW480 CRC cells were transduced with lentivirus carrying pCDH vector from System Biosciences: empty vector (Mock) or vector expressing dnLEF-1, followed by selection with 500 $\mu\text{g}/\text{mL}$ G418. Transduced cells were collected as a pool for confirmation of expression, and Wnt signaling activity was measured by a SuperTOPFlash luciferase reporter[172]. Next, 2.5×10^6 cells in PBS were injected subcutaneously into immunodeficient NSG mice. Tumors were removed after 3 weeks and dissociated for single cell sequencing. Only empty vector (Mock) samples were used for reference integration.

2.3.13 SW480 xenograft dissociation for single cell sequencing.

Tumors were excised into petri dishes containing DMEM (Corning), 1% Pen/Strep (Corning), 5% FBS (Atlas Biologicals), and 2 mg/mL Collagenase IV (Sigma-Aldrich)(DMEM-collagenase). Using razor blades, tumors were manually dissociated, the resulting suspension was collected into a 15 mL conical tube and the dish washed using additional DMEM-collagenase media, to a final volume of 10 mL. Tumors were digested on a shaker at 37°C for 1 hour. Following digestion, tubes were spun down at 1100 rpm for 5 minutes at 4°C and supernatant discarded. The pellet was washed with 10 mL HBSS (Corning) and spun down again. After discarding supernatant, the pellet was treated with 1 U/ μL DNase I (Zymo) for 5 minutes at room temperature. 2 mL of 0.05% trypsin (Corning) was added and the pellet

mechanically disturbed before incubating at 37°C for 10 minutes. 5 mL of DMEM with 10% FBS (DMEM-FBS) was added to the tube and the cells spun down at 1000 rpm for 7 minutes at 4°C. The supernatant was discarded and pellet resuspended in 5 mL DMEM-FBS and passed through a 40 micron strainer. The strainer was washed with an additional 5ml DMEM-FBS. Cells were counted prior to FACS using a Countess (ThermoFisher). Cells were resuspended to 5×10^7 cell/mL and stained with CD298-APC ($10 \mu\text{L}/10^6$ cells)(BioLegend) and Sytox Green (ThermoFisher) for 20 minutes at 4°C in the dark, prior to sorting on FACSAria II (BD) for Sytox- cells. Sorted cells were spun down and resuspended to 1×10^6 cells per mL.

2.3.14 Single-cell sequencing.

Flow cytometry sorted cells were washed in PBS with 0.04% BSA and resuspended at a concentration of 1000 cell/ μL . Cellular suspensions were loaded onto a Chromium Single Cell Instrument (10X Genomics) to generate single-cell gel beads in emulsion (GEMs). GEMs were processed to generate cDNA libraries by using 10X Genomics v2 chemistry according to the Chromium Single Cell 3' Reagents Kits v2 User Guide: CG00052 Rev B. Quantification of cDNA libraries was performed using Qubit dsDNA HS Assay Kit (Life Technologies Q32851), high-sensitivity DNA chips (Agilent 5067-4626) and KAPA qPCR (Kapa Biosystems KK4824). Libraries were sequenced on an Illumina HiSeq4000 to achieve an average of 50,000 reads per cell.

2.3.15 Transcriptome alignment and data processing.

After demultiplexing sequencing libraries to individual library FASTQ files, each library was aligned to an indexed GRCh38 reference genome using Cell Ranger (10X Genomics)

Count 2.2.0. Aligned libraries are then normalized based on mean reads per cell using Cell Ranger Aggr 2.2.0. Raw gene expression matrices were loaded into R (version 3.6.0)[201] and converted to a Seurat object using the Seurat R package (version 2.3.4)[28]. From this, the data were log-transformed and corrected for unwanted sources of variation using the ScaleData function in Seurat. Gene expression matrices were then normalized to total cellular read count and to mitochondrial read count using linear regression as implemented in Seurat's RegressOut function. For quality control filtering, we excluded libraries with less than 200 or more than 5000 genes detected, and/or over 15% UMIs (unique molecular indices) derived from mitochondrial genome. In addition, genes that were not detected in at least 3 of the cells after this trimming were also removed from further analysis. Cell cycle gene regression did not significantly influence PCs or clustering (2.2,2.3) and therefore was not performed in the final analyses.

2.3.16 Ligand-receptor interaction analyses.

In order to quantify potential cell-cell paracrine communication in the VMT, we utilized a list of published receptor-ligand interactions[222, 189]. A ligand or receptor is defined as 'expressed' if 65% of cells in a particular cell type expressed the ligand/receptor at an averaged level of 0.65. Therefore, a receptor/ligand interaction was considered to be expressed when both the receptor and ligand were expressed in 65% of cells at a level equal or greater than .65. To define these networks of interaction, we connected any two cell types where the ligand was expressed in one and the receptor in the other. To plot networks, we used the chorddiagram function in the R package 'circilize'.

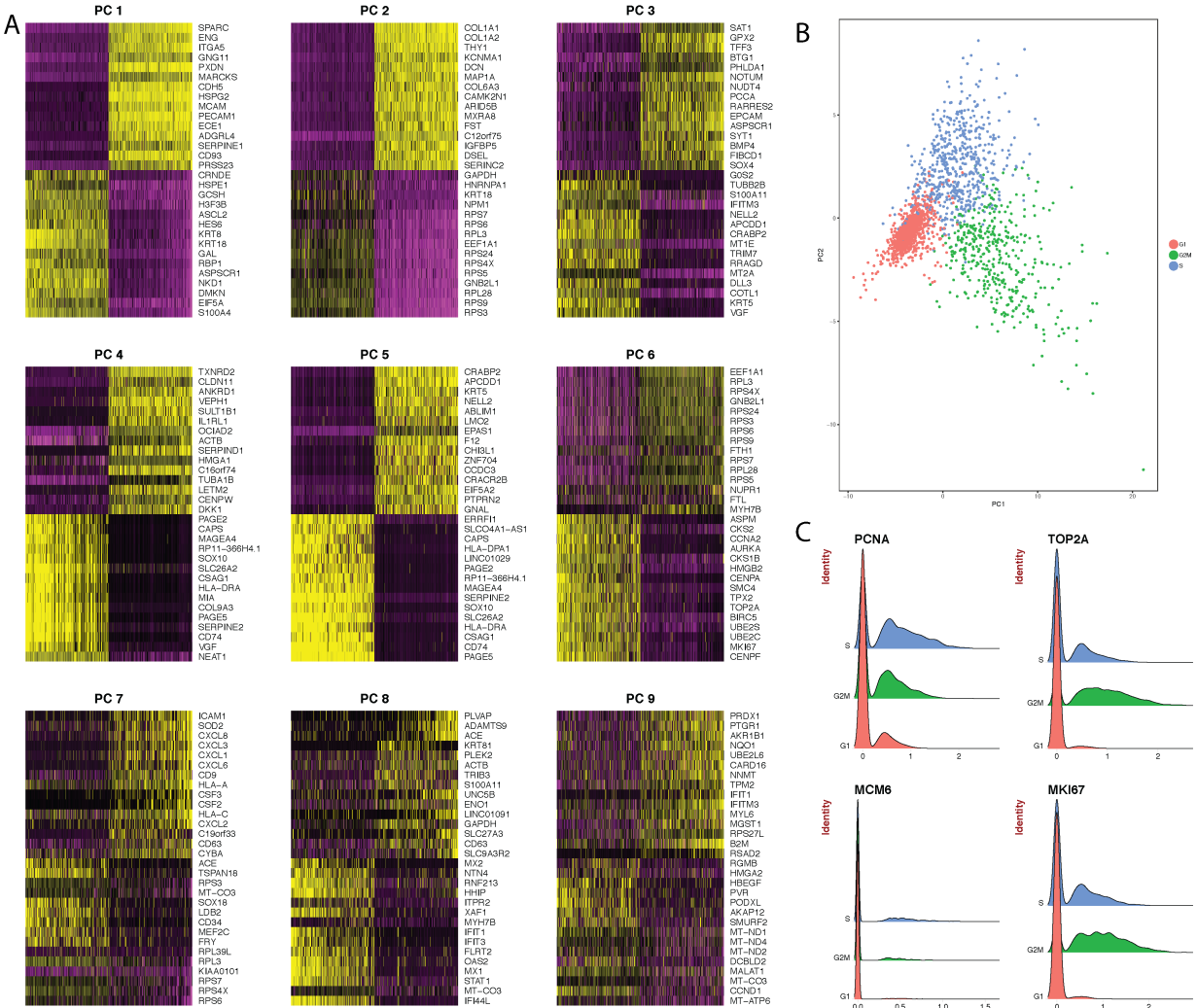


Figure 2.2 – Cell cycle gene visualization for HCT116. (a) First 9 PCs showing lack of cell cycle genes driving downstream clustering. **(b)** PC plot of cells in G1, G2M, or S phase. **(c)** Representative cell cycle genes showing marginal upregulation across the samples, with highest peak expression centered at 0 (no expression) and normal distribution with mean approximately 0.5 for expressing cell populations.

2.3.17 Single cell genotyping analyses.

In order to identify cell origin, Vartrix[1] combined with in-house scripts were used to extract single cell variant information from 10X genomics single cell data for the two HCT116 samples, VMT and monolayer. Variant information for HCT116 cell line was obtained from Broad Cancer Cell Line Encyclopedia[75] containing 39000 variants. The variant list

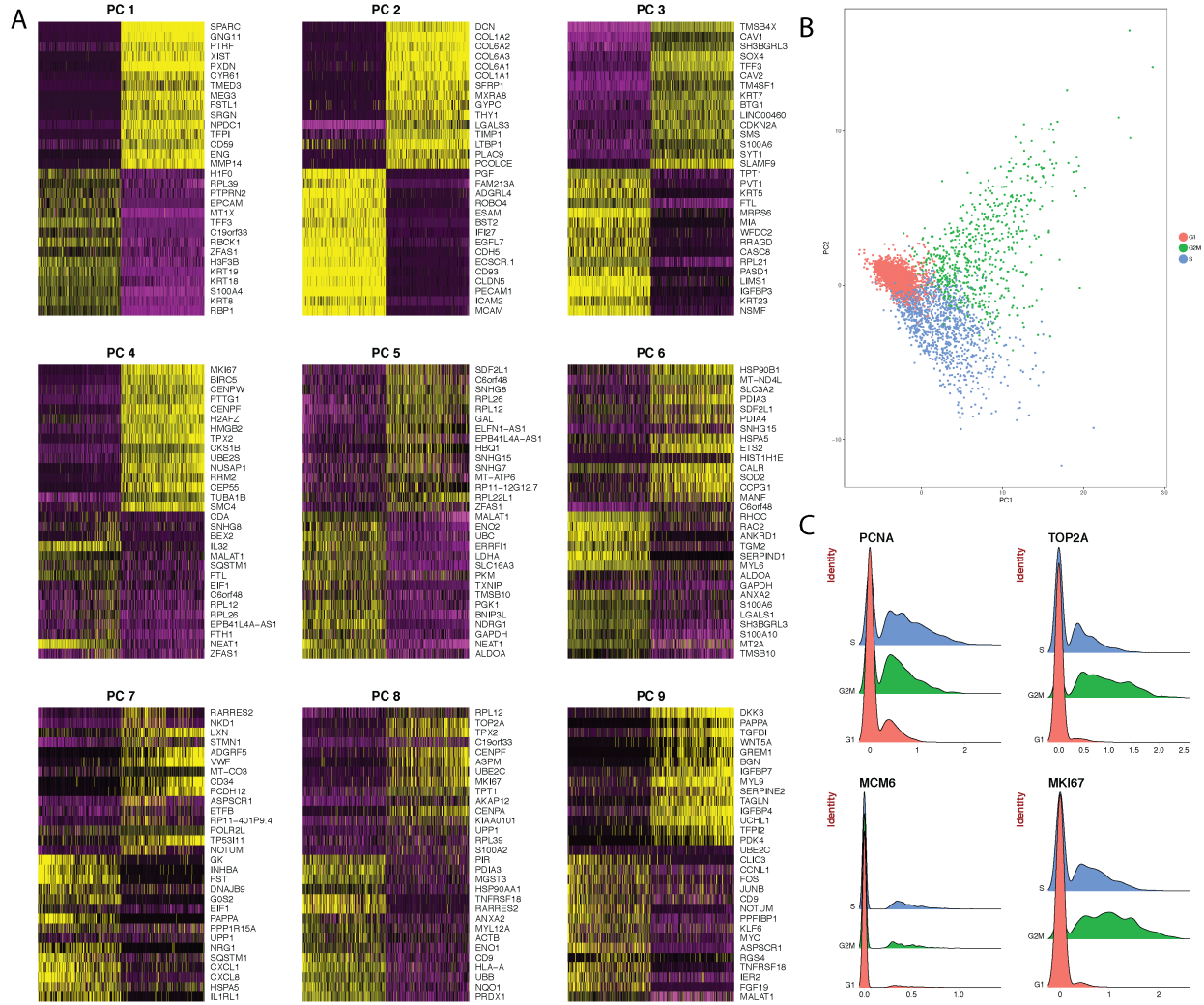


Figure 2.3 – Cell cycle gene visualization for sw480. (a) First 9 PCs showing lack of cell cycle genes driving downstream clustering. **(b)** PC plot of cells in G1, G2M, or S phase. **(c)** Representative cell cycle genes showing marginal upregulation across the samples, with highest peak expression centered at 0 (no expression) and normal distribution with mean approximately 0.5 for expressing cell populations.

was first filtered so that common variants in dbSNPs Build ID: 150[213] were excluded. For the remaining 18K SNVs, Vartrix was used to extract genotype information at each loci from the BAM files of the two samples analyzed using cellRanger (10X Genomics). For each cell in the two samples, a genotype score that the sums of the genotyping score for all 18K SNVs and then subtract the expression of all X linked genes was used to indicate the probability that the cell is derived from HCT116 . For copy number variation (CNV) analysis, we utilized a pipeline from the Broad Institute called inferCNV[247].

2.3.18 Pathway analyses.

Marker genes for each subgroup of cells were determined by Seurat following log-transformation. Based on cell type and state specific marker genes, comprehensive gene set enrichment was performed using Enrichr[104]. A p-value of 0.05 was used as a cut-off to determine significant enrichment of a pathway or annotated gene grouping.

2.3.19 Cell anchoring.

Cell anchoring was performed with Seurat version 3 using reference-based integration[235]. For these analyses, ‘Xeno’ (SW480 xenograft tumor scRNAseq dataset) was used as the ‘reference’, and all other SW480 datasets (VMT, spheroid and monolayer) were used as ‘query’. Plots were generated using Bioconductor package “projectR”[210].

2.3.20 Statistical analyses.

Data are represented as mean \pm standard error of at least three independent experiments, unless noted otherwise. Comparison between experimental groups of equal variance is analyzed using an unpaired t-test and 95% confidence interval or one-way ANOVA followed by Dunnett’s test for multiple comparisons. Statistical calculations were performed using GraphPad Prism 8.0, with the level of significance set at $p < 0.05$.

2.4 Results

2.4.1 The VMT serves as a high throughput platform for realistic tumor modeling and direct visualization of the tumor microenvironment.

We have previously validated our VMT model as a robust system for disease modeling and drug screening studies[226, 180, 81]. Multiple tissue units are incorporated within a single microfluidic device that is fitted onto a bottom-less 96-well plate to allow each VMT to be independently treated (Figure 2.4a). Since each tissue chamber is $<1 \text{ mm}^3$ in volume, few cells are needed for VMT establishment and minute volumes of reagents are required for maintenance and therapeutic testing. The microfluidic device is fabricated from transparent, biocompatible polydimethylsiloxane (PDMS) to create an optically clear platform for real-time microscopic imaging. In response to physiologic flow driven by a hydrostatic pressure gradient across the tissue, endothelial cells, fibroblasts and cancer cells introduced into each tissue unit self-organize within an extracellular matrix to form a complex tumor micro-ecosystem by day 5 of VMT culture. COMSOL Multiphysics simulation on a fully formed, anastomosed and perfused vascular network shows that the surface velocity of medium flowing through the vessels varies across the tissue, with some areas experiencing higher flow than others, mimicking blood flow through a capillary network *in vivo* (Figure 2.4b). Just like nearly all healthy tissues of the body, tumors rely on blood vessels for growth and survival via delivery of nutrients and elimination of metabolic waste. Blood vessels also serve as the conduit through which anti-cancer agents (drugs or immunotherapies) are delivered to the tumor, and a means for cancer cells to gain metastatic access to distant sites. The VMT model is the only one of its kind to incorporate living blood vessels that feed the growing tumor mass, supported by stromal cells, just as it occurs *in vivo* (Figure 2.4c). As such, we sought to determine the physiological relevance

of the VMT platform to study cancer and to bridge the gap in the drug development pipeline between *in vitro* and *in vivo* preclinical study[81].

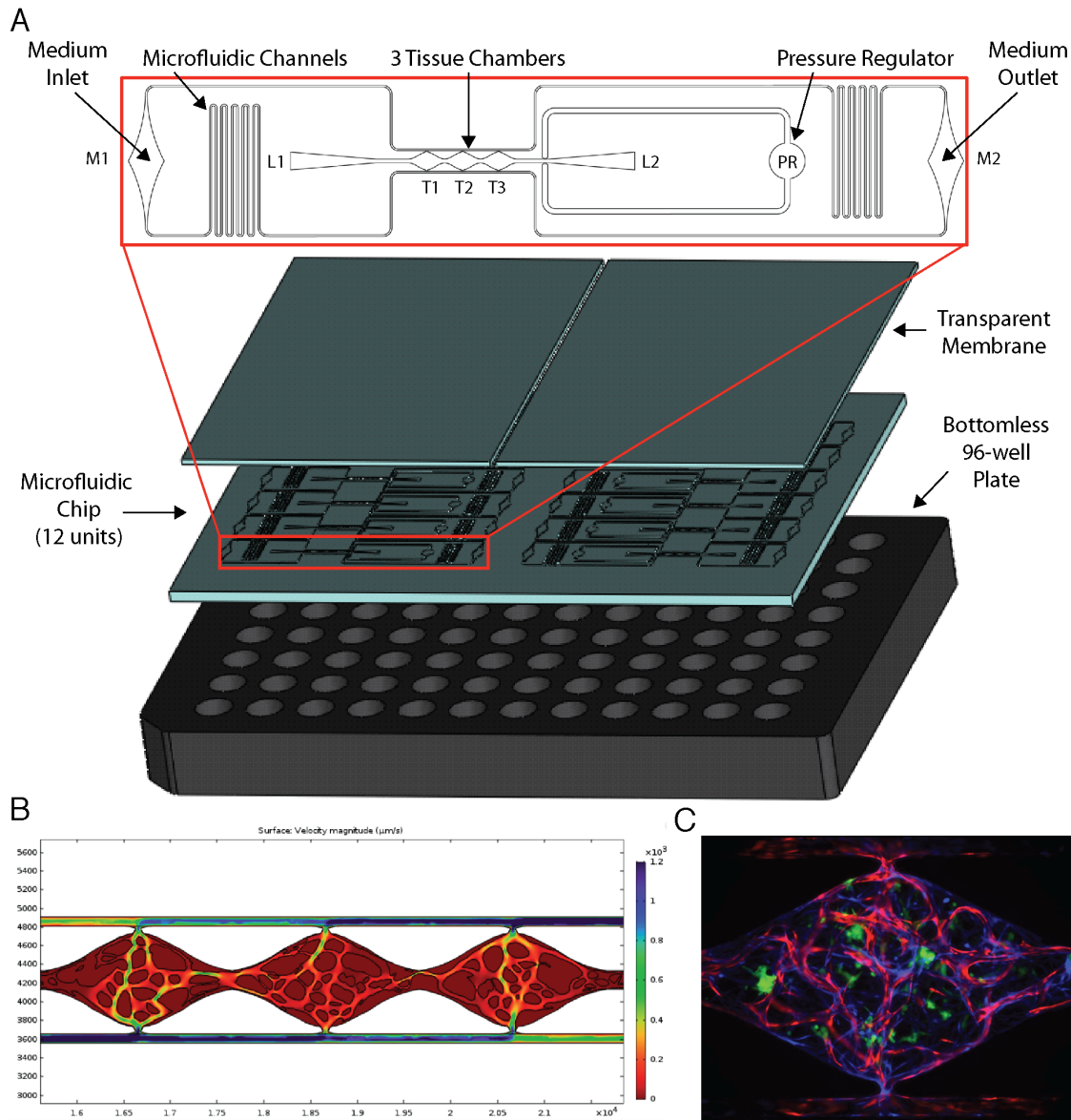


Figure 2.4 – Vascularized micro-tumors (VMTs) form in response to gravity-driven flow within a microfluidic platform arrayed for high throughput experiments (a) The microfluidic chip is bonded to a bottom-less 96-well plate via chemical glue and oxygen plasma. Zoom view shows a single device unit with 3 tissue chambers (T1-3) fed through microfluidic channels, 2 loading ports (L1-2), medium inlet and outlets (M1-2), and a pressure regulator (PR) to prevent gel bursting during loading. **(b)** COMSOL simulation on a perfused vascular network shows the surface velocity of medium flowing through the vessels. **(c)** Fluorescent image shows a vascularized micro-tumor with endothelial cells (mCherry, red) forming the vascular network, fibroblasts (Az, blue) supporting the tissue, and cancer cells (GFP, green). Chamber is 2 x 1 x .1 mm.

2.4.2 Vessels in the VMT are irregular and leaky, hallmarks of *in vivo* tumors.

Distinct changes in tumor-associated vascular architecture and function are known to occur during tumor progression. Although tumors recruit blood vessels to support their growth, the resulting vasculature is irregular, leaky, and ill-perfused due to tumor pathophysiology, contributed by highly proliferating, hypoxic and non-vascularized areas within the tumor[101, 280, 33]. Comparisons between vessels in our normal tissue platform, the VMO, and the VMT show that the vessels in the VMT recapitulate key features of *in vivo* tumor-associated vasculature. Furthermore, these features become more pronounced at later time points, as the tumors grow larger, compressing and displacing the existing vasculature within the tissue construct (Figure 2.5a). Overall, vessel density is significantly reduced in the VMT compared to the VMO due to reduced total vessel length (Figure 2.5b). The vessels in the VMT are highly disorganized, such that individual networks contain areas of both vessel dilation and vessel narrowing, although on average the vessels in the VMT are narrower than the vessels in the VMO (Figure 2.5c). The tumor-associated vasculature within the VMT also contains fewer vascular junctions (Figure 2.5d), and greater lacunarity, a measure of the non-vascularized spaces within the tissue chamber. Likely due to pro-angiogenic tumor signaling, we observe an increased number of vascular endpoints and tip cells in the tumor-associated vasculature compared to the VMO (Figure 2.5e). Perfusion experiments flowing 70 kD FITC dextran through the vascular networks in both the VMT and the VMO reveal that the vessels in the VMT are significantly leakier than vessels in the VMO, with areas of massive leak in the VMT compared to fully patent networks in the VMO (Figure 2.5f). Furthermore, as a result of structural heterogeneity in tumor-associated vasculature, the VMT shows differential patterns of perfusion, with highly leaky areas found adjacent to ill- or non-perfused areas. Overall, the vasculature within the VMT is significantly more leaky than the VMO (Figure 2.5g), indicating that the

vessels are affected by the presence of the tumor to model tumor-associated vasculature *in vivo*.

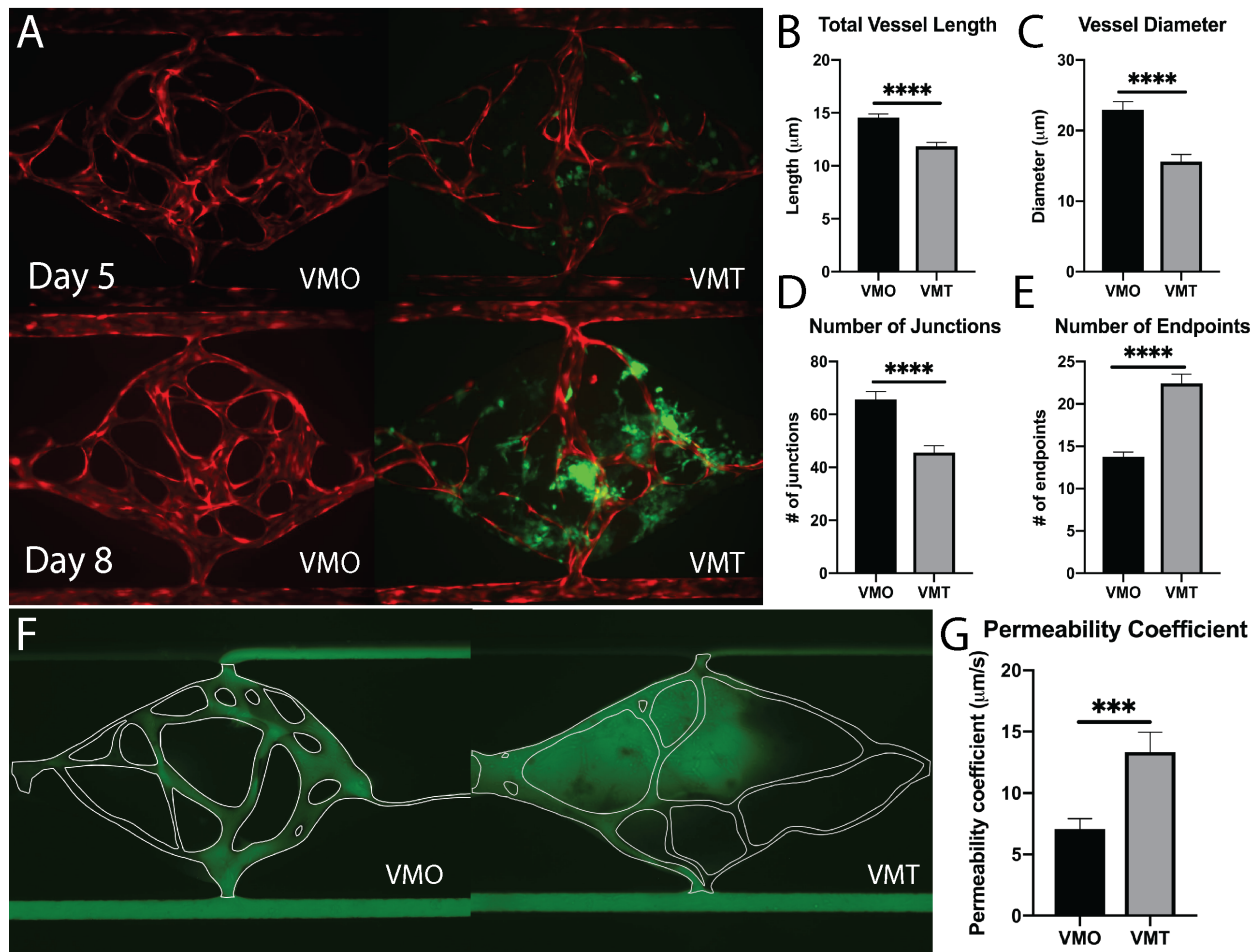


Figure 2.5 – VMT-associated stroma model key features of *in vivo* tumors. (a) Comparison of VMO and VMT on days 5 and 8 show irregular vasculature in the VMT that worsens over time. (b) Quantification of total vessel length, (c) vessel diameter, (d) number of junctions and (e) number of endpoints. While vessel length, diameter and density are decreased in the VMT, # of endpoints increases, suggesting angiogenic sprouting in response to the tumor. (f) Perfusion with 70 kD FITC dextran reveals fully patent networks in the VMO, with leaky and non-perfused vessels in the VMT. (g) Quantification of the permeability coefficient shows that the VMT is twice as leaky as the VMO.

Immunofluorescence staining reveals stark differences in collagen density and organization between the VMO and VMT, with collagen III highly prevalent in the VMT, enriched near tumor cells and fibroblasts and forming collagen fiber ‘tracks’ throughout the tissue. In contrast, collagen III is less abundant in the VMO, showing homogenous and diffuse staining patterns (Figure 2.6a–2.6c). Various collagens, including collagen III, show in-

creased deposition during tumor formation to promote cell survival and proliferation via upregulated integrin signaling[144]. In a recent study, serological detection of type III collagen degradation and formation fragments in CRC patients served as a biomarker to distinguish stage IV metastatic disease from all other stages, suggesting that collagen III deposition and remodeling may be a measure of tumor invasiveness[114]. Intriguingly, live imaging studies have shown that cancer cells migrate rapidly on collagen fiber tracks in areas enriched in collagen[173]. The VMT is uniquely well-suited for direct observation of spatially random and temporally rapid events, such as epithelial to mesenchymal transition (EMT). Via confocal microscopy time-lapse imaging of VMT development over the course of 10 days, we capture the coordinated self-organization of the VMT as it progresses from single cancer cells embedded in a stromal tissue niche to a fully-formed vascularized tumor mass. We observe a remarkable series of events: tumor cells extravasate into adjacent vessels and are swept through the vasculature by flow, and growing clusters of tumor cells suddenly explode into single cells that rapidly migrate radially from the origin, undergoing a coordinated EMT event. Taken together, defining features of the VMT are changes in ECM composition associated with *in vivo* tumor progression and the presence of an abnormal vasculature that closely models known characteristics of tumor-associated vasculature *in vivo*. Recapitulating these features is critical to faithfully model nutrient and drug delivery to the tumor, as well as changes in the microenvironment, extracellular matrix and stroma associated with tumor progression.

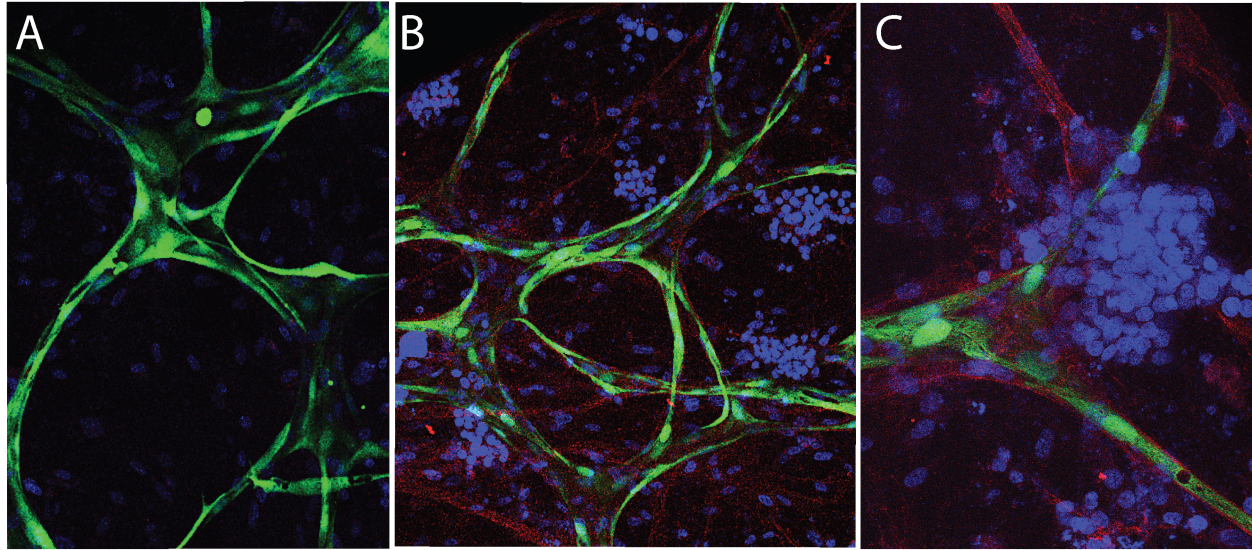


Figure 2.6 – Collagen tracks revealed within the VMT. (a) Collagen III staining (red) in the VMO vs (b) the VMT. Cancer cells blue, vessels green. (c) Zoom view reveals collagen fiber enrichment and ‘tracks’ in the VMT.

2.4.3 Transcriptomic comparison of cancer cells grown as monolayer culture, in the VMT and as xenograft tumors shows high correlation in gene expression between VMT and xenograft tumors, with significant divergence from monolayer cultures.

To determine if the VMT more closely models *in vivo* tumors than monolayer cultures, we carried out transcriptomic analysis of 770 cancer-related genes on HCT116 colorectal cancer (CRC) cells that had been grown in the VMT, as xenograft tumors and in 2D monocultures. The multiplex gene expression analysis included genes from 13 cancer-associated pathways, including: MAPK, STAT, PI3K, RAS, Hedgehog, Wnt, TGF- β 2, cell cycle, apoptosis, DNA damage control, transcriptional regulation, and chromatin modification (Nanostring, Inc.). Importantly, each biological replicate was established in parallel from a single vial and passage of HCT116 cells, cells grown in the VMT and in monolayer were cultured under

the same conditions, and HCT116 mCherry-labeled cells were isolated from all experimental groups by fluorescence activated cell sorting (FACS).

As anticipated, we found that the gene expression patterns of tumor cells derived from the VMT better matched *in vivo* tumor-derived cells than the HCT116 cells growing in the culture dish. A heat map comparing gene expression of HCT116 CRC cells derived from each of the three systems shows that the VMT clusters with the xenograft tumor, whereas cells grown in monolayer diverge in their gene expression patterns (Figure 2.7a). By assessing all genes together, we found that VMT were not significantly different in gene expression from the xenograft tumors (p-value = 0.6), whereas monolayer cultures displayed significantly different gene expression patterns compared to both the VMT and xenograft tumors (p-value = 0.001). The experiment was repeated with similar results. Interestingly, the variation between samples was highest for monolayer cultures (12.8%) and second highest for xenograft tumors (6.6%), with the VMT yielding the least variability between replicates (3.5%), highlighting the robustness and reproducibility of the VMT model. Pathways consistently enriched in the VMT and xenograft-derived CRC cells, but not in 2D monocultures, included PI3K-Akt signaling pathway, MAPK signaling pathway, Ras signaling, FGF signaling, chromosome and microsatellite instability in CRC, epithelial to mesenchymal transition in CRC and angiogenesis, among several other cancer-related pathways (Figure 2.7b). Interestingly, genes that were consistently differentially expressed in the VMT compared to xenograft were enriched for beta-1 signaling (COL1A1, COL3A1, FN1), urokinase-type plasminogen activator (uPA), uPAR-mediated signaling (PDGFRB, HGF, MMP3), and interleukin signaling pathways (IL11, IL1A, IL6, IL13RA2). However, it is important to note that the expression changes between the three model systems are relative, meaning the absolute expression of oncogenes in the 2D cultures is likely still higher than in normal epithelium.

2.4.4 The VMT recapitulates xenograft tumor growth and response to standard of care therapy, whereas monolayer cultures show significantly different growth patterns and drug sensitivity.

Based on the significant overlap in gene expression between HCT116-derived VMT and xenograft tumors, we next compared growth rates and drug responses between tumor cells grown as monolayer cultures, VMT and xenograft tumors. To capture the molecular landscape of CRC, we tested two established CRC cell lines originating from tumors of different subtypes: HCT116, which is a primary-derived, MSI-high (microsatellite unstable - high), KRAS-mutant CRC representing about 15% of clinical CRC cases; as well as SW480, a primary-derived, MSS (microsatellite stable), APC-mutant CRC representing the majority (85%) of clinical CRC cases. First-line treatment for advanced metastatic CRC is a combination of systemic cytotoxic chemotherapy (FOLFOX- a regimen of 5 fluorouracil (5FU), leucovorin and oxaliplatin). Therefore, we treated each system with pharmaceutical-grade FOLFOX at a dose, duration and frequency to approximate the clinical administration, plasma Cmax and clearance for each drug. In the VMT and monolayer cultures, 5FU was given as a 100 μm bolus for 2 hours in combination with 10 μm leucovorin, and followed by 5 μm oxaliplatin for an additional 48 hours. Drugs were delivered to the VMT by perfusing through the vasculature. Mice were treated weekly by intraperitoneal injection based on a moderate dosing schedule to limit toxicities and better mimic the clinical outcomes of FOLFOX treatment.

As shown, the growth and drug sensitivity of both HCT116- and SW480-derived VMT closely models the growth and sensitivity seen for xenograft tumors derived from those same cells, whereas monolayer cultures significantly diverge at the 48 hour time-point due to enhanced cell growth and increased FOLFOX sensitivity in 2D (Figure 2.7c–2.7f). HCT116-derived xenograft and VMT tumors show no statistically significant difference in growth for the

entire 6-day experimental period (day 6 fold change from baseline: 2.84 ± 1.31 vs 2.66 ± 0.35 , respectively) (Figure 2.7c, 2.7d). In contrast, monolayer cultures exceed the maximum growth observed in VMT and xenograft tumors in only 48 hours, to reach a fold change of 4.51 ± 0.21 . The 2D cultures were significantly different from both VMT and xenograft at the 2-day time point (p-value < 0.0001) (Figure 2.7c), and, due to rapid growth, were not sustainable for longer drug testing studies. For FOLFOX treatment, we observe that xenograft tumors and VMT show similar drug sensitivity (1.19 ± 0.27 and 1.12 ± 0.01 fold change, respectively) and thus similar effect size (approximately 58%) at 6 days post-treatment (Figure 2.7c). Monolayer cultures, however, show an approximate 96% reduction in tumor growth at the 48-hour time point (fold change from baseline for treated cultures 0.18 ± 0.01), which is significantly different from both xenograft and VMT response (p-value < 0.001) (Figure 2.7c).

We confirm similar findings in SW480-derived xenograft and VMT tumors, with respective fold change 3.03 ± 0.79 and 3.29 ± 0.56 above baseline on day 6, and no significant difference in growth between VMT and xenograft tumor at any time point (Figure 2.7e, 2.7f). FOLFOX treated xenograft and VMT-derived tumors also show similar drug sensitivity, with maximum response at 6 days post-treatment (1.48 ± 0.09 and 1.13 ± 0.03 fold change, respectively) and similar effect size (52-66%) (Figure 2.7e). Monolayer cultures showed significantly increased cell growth and drug sensitivity at the 48-hour time point (control fold change in tumor growth 3.91 ± 0.16 , treated fold change 0.47 ± 0.07) compared to xenograft and VMT (Figure 2.7e), with an effect size of approximately 88%. Intriguingly, SW480-derived spheroid cultures showed significantly reduced tumor growth compared to xenograft tumors (spheroid control fold change day 4: 1.41 ± 0.06 , xenograft control fold change day 4: 2.29 ± 0.53) while maintaining roughly the same effect size in response to FOLFOX treatment. However, the absolute response to FOLFOX was significantly different in the spheroid cultures compared to xenograft (0.85 ± 0.16 and 1.45 ± 0.02 fold change in tumor growth, respectively). Hence, for two different subtypes of CRC, we show that while 2D and

3D monocultures are poorly predictive of tumor growth and response to chemotherapy *in vivo*, the VMT recapitulates these important features.

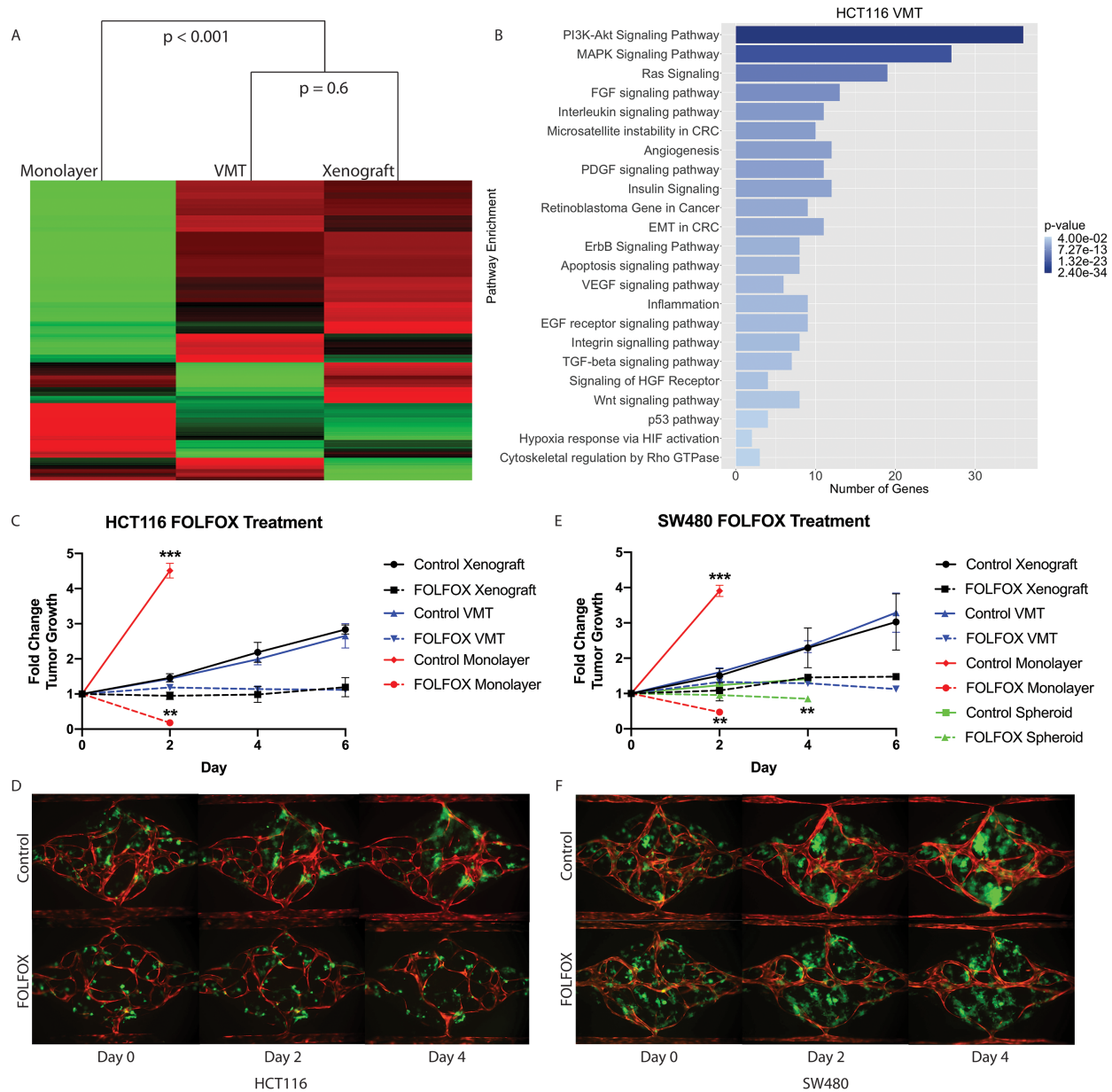


Figure 2.7 – Comparison of gene expression, tumor growth and response to drug treatment between VMT, 2D and 3D monocultures and xenograft tumors. (a) Bulk RNA sequencing of 770 cancer-related genes in HCT116 CRC cell line-derived mono-layers, VMT and xenograft tumors. **(b)** Pathway enrichment plot for VMT similarity to xenograft tumor. **(c)** Growth curves of HCT116 cells grown in mice or in the device and treated with standard of care, FOLFOX. **(d)** Representative images of HCT116-VMT. **(e)** Growth curves of SW480 cells in VMT, spheroids (working on this) and mice treated with FOLFOX. **(f)** Representative images of SW480-VMT.

2.4.5 Single-cell mRNA sequencing reveals that the transcriptome of stromal and tumor cells in the VMT retain features of *in vivo* tumor cell populations not seen in monolayer or spheroid cultures.

2.4.6 HCT116 CRC cell-derived VMT and matched monolayer cultures.

Based on stark differences in tumor growth and response to chemotherapy between 2D and 3D monocultures and the VMT, we next sought to explore the distinct gene expression changes that occur at the single cell level when cells are co-cultured within the dynamic 3D tumor microenvironment of the VMT. Here we used single-cell mRNA sequencing (scRNAseq) to profile the transcriptomes of cells isolated from HCT116-derived VMT and matched HCT116 CRC cells, endothelial cells and fibroblasts growing in 2D monocultures (Figure 2.8a). Unbiased clustering analysis using the Seurat pipeline[28] revealed distinct shifts in gene expression between the cells grown in the VMT and those grown in monolayer (Figure 2.8b). Guided by annotated lineage-specific markers in humans[284] and prior knowledge, two populations were identified as endothelial cells (EC A and EC B) by differential expression of PECAM1 (CD31+), two populations were derived from fibroblasts (fibroblast A and B) based on high expression of MMP2 and ACTA2, two populations were enriched for EPCAM and labeled as tumor (A and B), and a third tumor cluster highly expressed KRT5 (tumor C) (Figure 2.8c). Overall, the cells derived from the VMT showed higher expression of cell-type specific markers than the same cells grown in 2D cultures (Figure 2.8c). Higher KRT5 expression, characteristic of cells undergoing epithelial to mesenchymal transition (EMT)[194], was also observed in the VMT compared to monolayer (Figure 2.8c).

Intriguingly, one cluster of cells that was found exclusively in the VMT could not be readily characterized by querying marker expression distinctive to the other subpopulations.

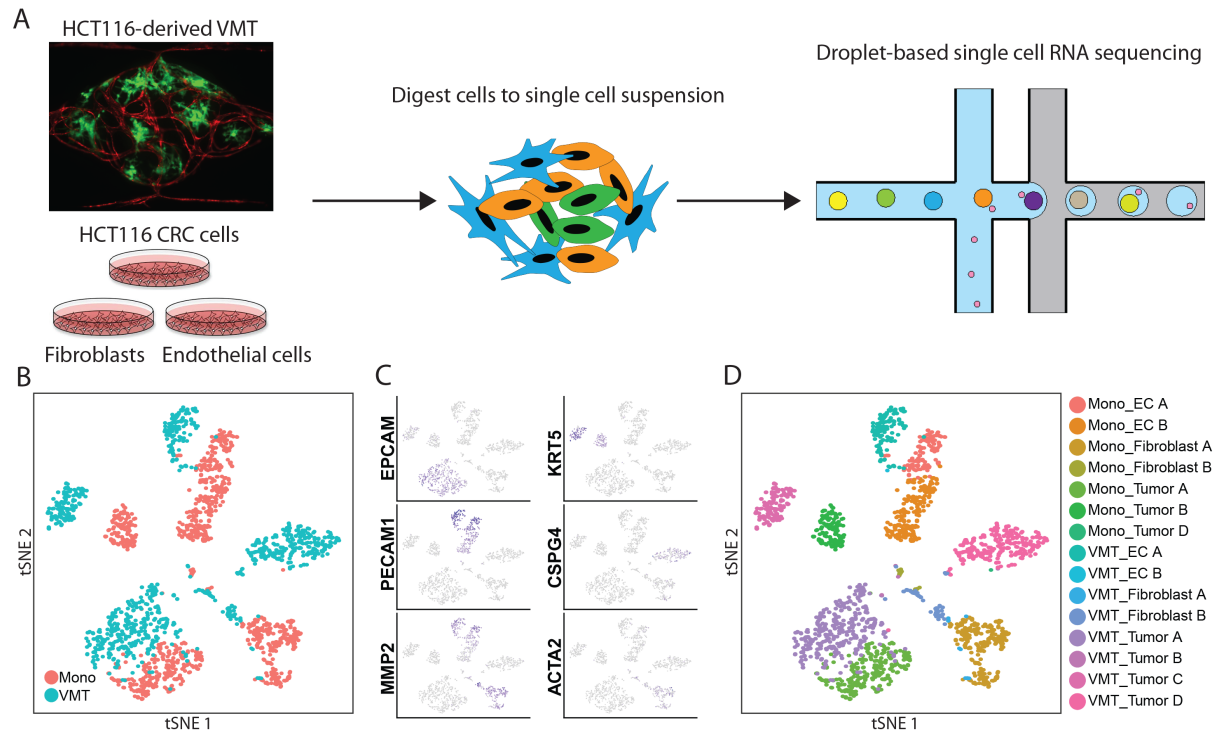


Figure 2.8 – Distinct changes in gene expression that better model *in vivo* tumors occur when cells previously grown in 2D monocultures are grown in the VMT. (a) Experimental design. HCT116 CRC cells, endothelial cells and fibroblasts were grown as 2D monocultures or co-cultured within the VMT, harvested on day 7 of culture and processed for droplet-based single cell RNA sequencing. (b) tSNE plot reveals marked shifts in gene expression between VMT and monolayer samples for all cell types. (c) Cell clusters are characterized into types by known markers and differential gene expression is displayed by tSNE plot. (d) tSNE plot shows each cluster annotated by group (Mono vs VMT) and cell type (EC A, EC B, Fibroblast A, Fibroblast B, Tumor A, Tumor B, Tumor C, Tumor D). Note that tumor C and D are absent from the monolayer culture (only 1 cell in tumor D).

Instead, the ‘unknown’ population showed differential expression of a unique panel of genes (Figure 2.9a). While CSPG4 (NG2+, a pericyte marker) was highly expressed, additional pericyte markers such as PDGFR β and DES were absent, and CD74 and HLA-DRA (immune modulation) were highly, and exclusively, expressed. Furthermore, expression of PAGE5 (a proposed tumor marker) and VGF (a neuroendocrine marker) were restricted to this population, hinting at a tumor origin. However, other markers of neuroendocrine differentiation (e.g. CHGA or SYP), a process that can occur in highly invasive and resistant CRC tumors[141, 78], were either absent or below the detection limit.

To confirm the origin of the unknown population, we performed single nucleotide variation (SNV) profiling of raw reads in order to barcode the different populations within the VMT using SNV found in HCT116 CRC cells. Further confirmation of these findings derived from additional barcoding based on Y-chromosome linked genes since HCT116 CRC cells are derived from a male patient, and the fibroblast line used in experiments were derived from a female patient. Further analyses were performed to look at copy number variations (CNV) between the different populations. Interestingly, the unknown population had a CNV signature distinctive of HCT116 CRC tumor origin, but with enrichment of CNV on chromosomes 1, 11 and 19 compared to the other tumor populations. While tumor populations A and B had a similar CNV profile, C clustered with tumor D and both showed distinguishing patterns of CNV enrichment, suggesting a greater degree of tumor heterogeneity within the VMT through selection of HCT116 CRC subclones. Taken together, these analyses confirmed that the unknown population (tumor D) was indeed originating from CRC cells and not from the stroma or EC, and also revealed a high degree of heterogeneity within VMT-derived tumor subpopulations relative to monolayer cultures (2.9).

In Figure 2.8d, tSNE plotting shows the degree to which subpopulations were unique to either VMT or monolayer culture, and a heat map with the combined top 10 cluster-discriminative genes for HCT116 populations showed that clusters were distinct in their gene signatures (Figure 2.10a). The distribution of cells from each sample based on cell type reveals distinct changes in the VMT compared to 2D monocultures (Figure 2.10b). The stromal cells within the VMT occupy only EC A and fibroblast B subpopulations, whereas monolayer contains cells of each subtype (EC A, ECB, fibroblast A and fibroblast B). In contrast, VMT-derived tumor cells were distributed to all four subtypes (tumor A-D), although only 3 cells occupied tumor B, whereas no monolayer cells were found in C and only 1 cell occupied tumor D, further highlighting the higher degree of tumor heterogeneity seen in VMT-derived HCT116 CRC cells compared to those derived from 2D monocultures. Immunofluorescence (IF) staining of HCT116-derived VMT and HCT116 CRC cells growing in

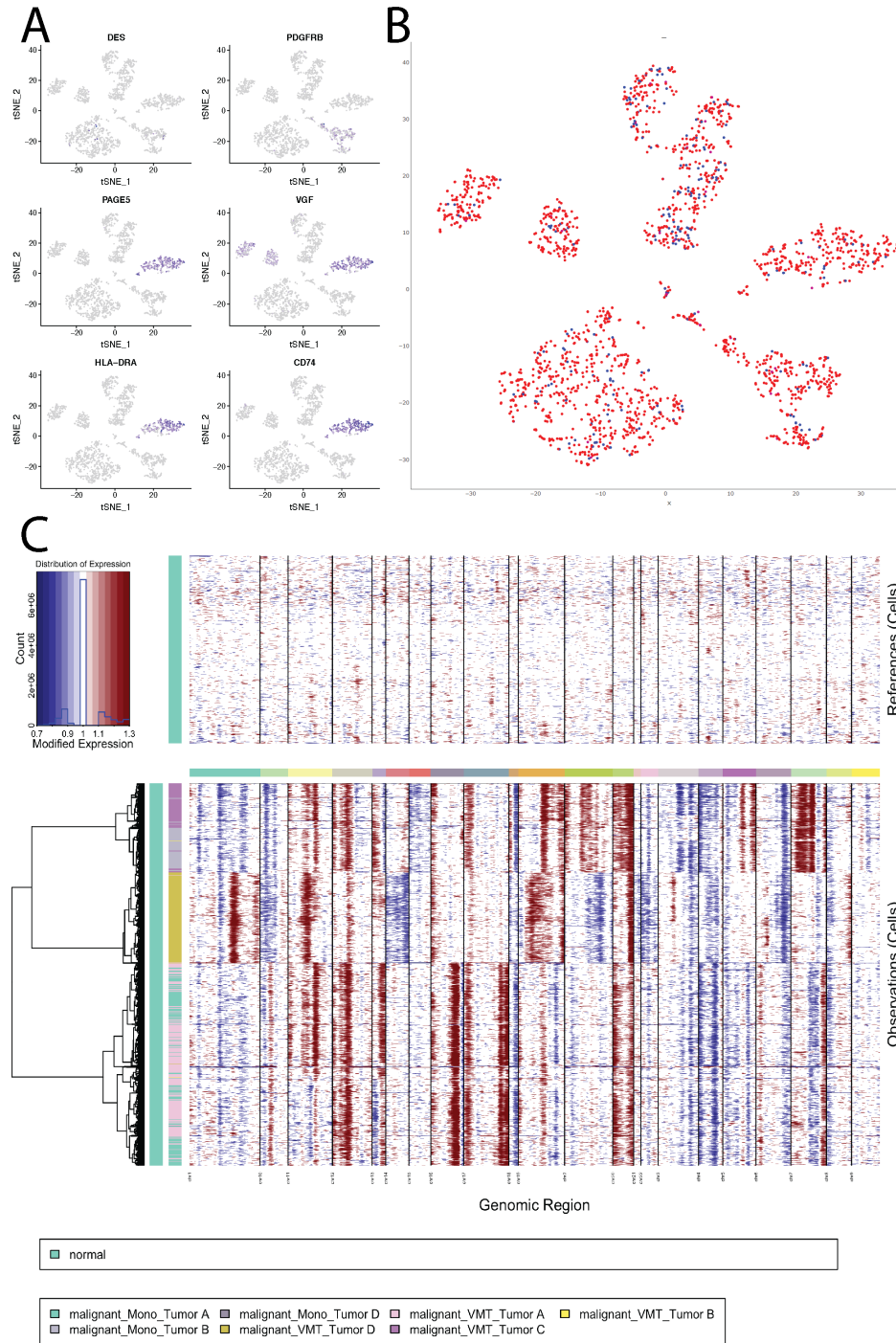


Figure 2.9 – Single nucleotide variation and copy number variation analyses for HCT116 . (a) tSNE plot showing marker gene expression for HCT116-derived VMT, highlighting the unique gene expression signature of tumor D. **(b)** SNV analyses. Red = greater proportion of HCT116-derived SNV present, blue = lower proportion. **(c)** CNV analyses showing that VMT-derived tumor D groups with known tumor-derived clusters A, B and C, whereas normal cells show greater chromosomal stability.

monolayer confirmed the presence of tumor subpopulations in the VMT (Epcam+, Cytokeratin 5+), with only a subset of the tumors expressing EPCAM in the VMT, and a proportion of cells expressing high levels of KRT5, compared to HCT116 CRC cells growing in 2D which showed lower levels of EPCAM expression in nearly all cells and low levels of KRT5 expression in a subpopulation (Figure 2.10c).

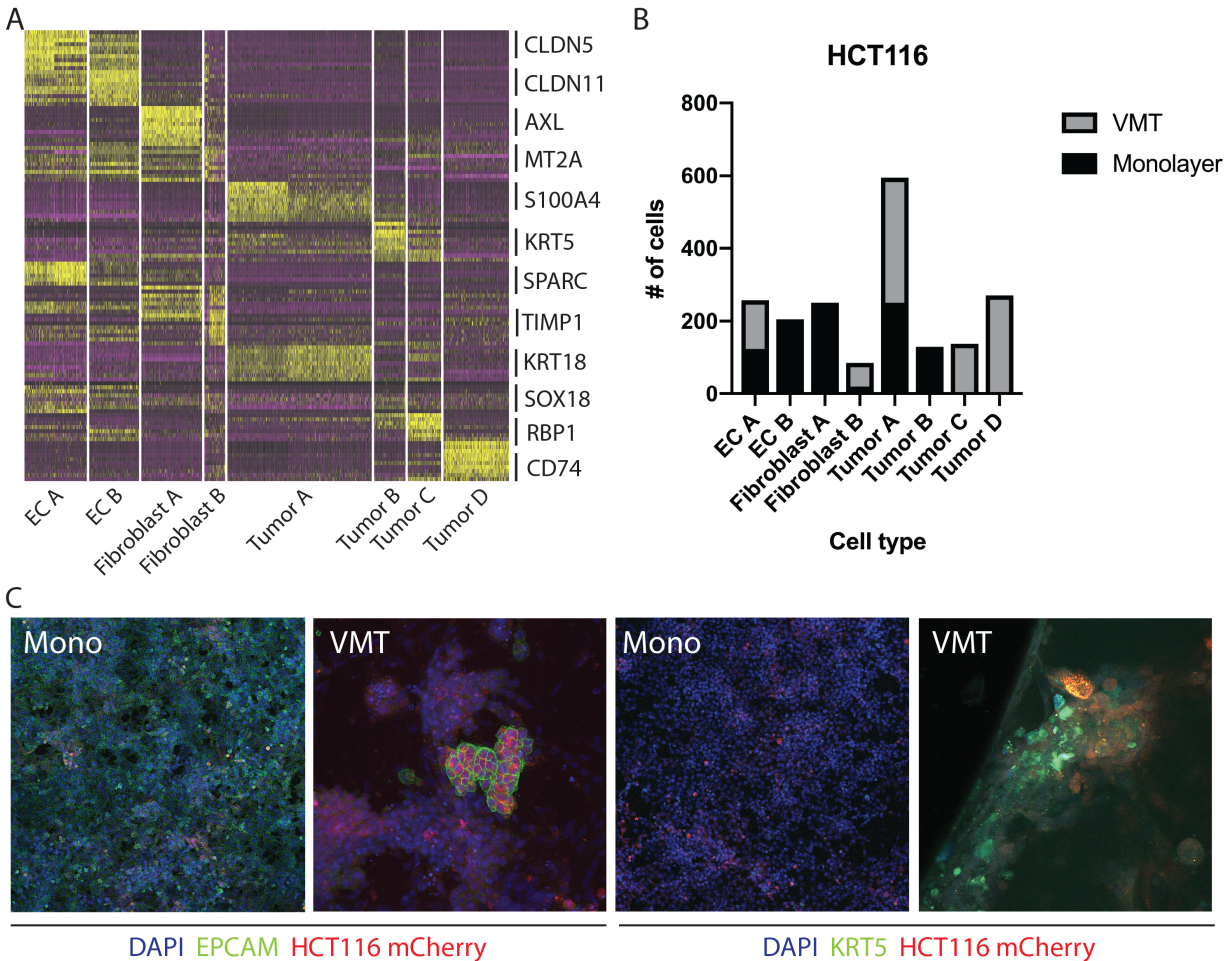


Figure 2.10 – Distinct changes in tumor heterogeneity that better model *in vivo* tumors occur when cells previously grown in 2D monocultures are grown in the VMT. (a) Heatmap of the top 10 differentially expressed genes in each cell type shows clear differentiation between sub-populations. (b) Plot showing distribution of cells from each sample (Mono or VMT) based on cell type. (c) Immunofluorescence staining of HCT116-derived VMT, 2D monocultures and xenograft tumors show that native tumor heterogeneity is reproduced in the VMT and not in monolayer, further supporting the scRNAseq data.

2.4.7 SW480 CRC cell-derived VMT, tumor spheroids and matched monolayer cultures.

Given that SW480 CRC cells represent the major subtype of colorectal cancers (~85%), we sought to validate the robustness of our system by performing scRNAseq on 1391 cells isolated from SW480-derived VMT, matched monolayer cultures, and tumor spheroids (Figure 2.11a). There is growing acknowledgement in the field that 3D cultures are more representative of actual tumors and we therefore wanted to test the physiological relevance of the VMT model compared to current standards. For SW480, we observe distinct shifts between the VMT and monolayer cultures for the endothelial cell and fibroblast populations (Figure 2.11b), as well as for the cancer cell populations, with some overlap between VMT, monolayer and spheroid cultures for SW480-derived tumor subpopulations. Populations were defined based on marker expression used in HCT116 (Figure 2.11c); with heat map and tSNE plot showing the discrimination between clusters (Figure 2.11d, 2.12a). Two populations were identified as endothelial cells (EC A and EC B) by differential expression of PECAM1 (CD31+), three populations were derived from fibroblasts (fibroblast A, B and C) based on high expression of MMP2 and ACTA2, three populations were enriched for EPCAM and labeled as tumor (A, B and C), and a third tumor cluster highly expressed EPCAM and KRT5 (tumor D) (Figure 2.11d). A heat map with the combined top 10 cluster-discriminative genes for SW480 populations showed that clusters were distinct in their gene signatures (Figure 2.12a).

The distribution of cells from each sample based on cell type revealed distinct changes in the VMT compared to both 2D and 3D monocultures (Figure 2.12b). The stromal cells within the VMT occupy only EC A, fibroblast B and fibroblast C subpopulations, whereas monolayer contains cells of each subtype with the exception of fibroblast B (i.e. EC A, EC B, fibroblast A and fibroblast C). In contrast, VMT-, 2D and 3D monoculture-derived tumor

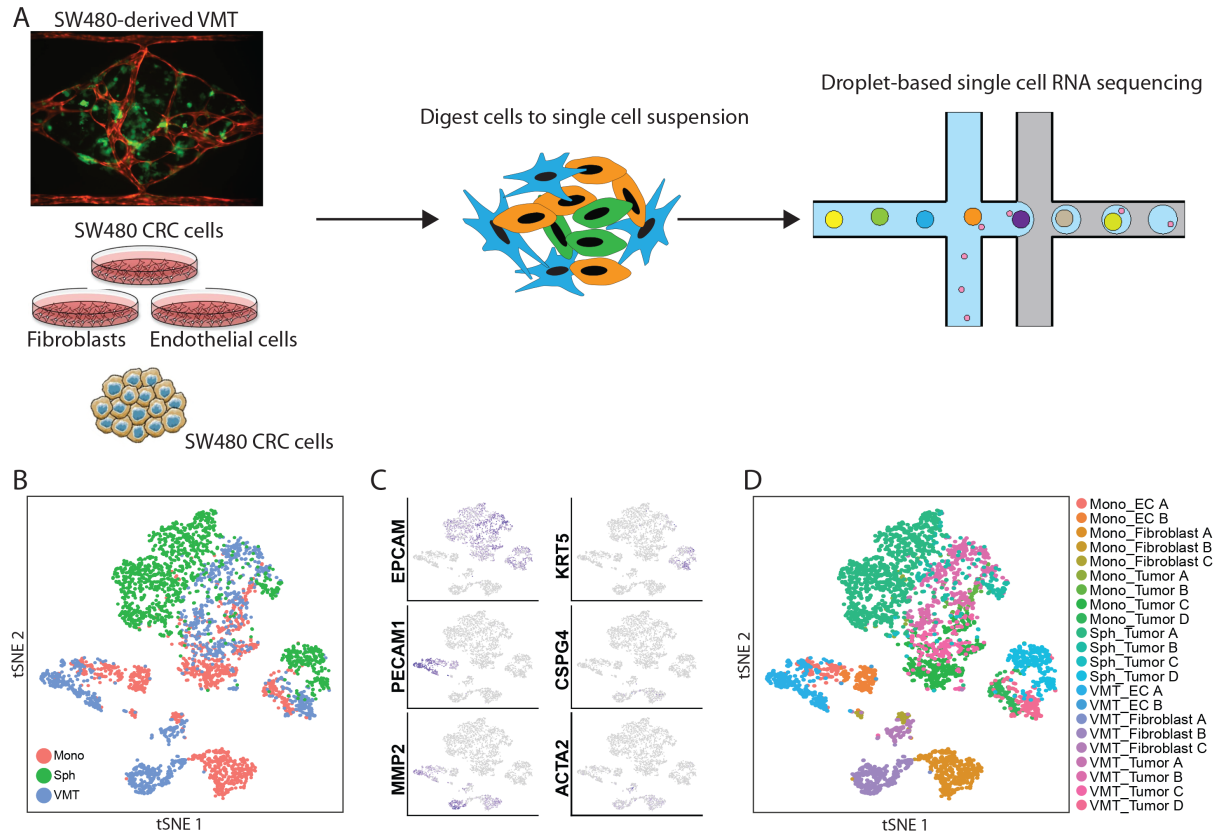


Figure 2.11 – Distinct changes in gene expression that better model *in vivo* tumors occur when cells previously grown in 2D or 3D monolayers are grown in the VMT. (a) Schematic of the experimental design. SW480 CRC cells were grown as 2D or 3D monolayers, endothelial cells and fibroblasts were grown as 2D monolayers or all 3 cell types were co-cultured within the VMT, harvested on day 7 of culture and processed for droplet-based single cell RNA sequencing. (b) tSNE plot reveals marked shifts in gene expression between VMT and monolayer samples for all cell types. (c) Cell clusters are characterized into types by known markers and differential gene expression is displayed by tSNE plot. (d) tSNE plot shows each cluster annotated by group (Mono vs VMT) and cell type (EC A, EC B, Fibroblast A, Fibroblast B, Fibroblast C, Tumor A, Tumor B, Tumor C, Tumor D). Note that tumor C and D are absent from the monolayer culture (only 1 cell in tumor D).

cells were distributed to all four subtypes (tumor A-D), in varying proportions. Interestingly, 70% of spheroid-derived tumor cells were categorized as tumor A with high GAPDH and SOX4 expression, whereas the majority of cells in the VMT (57%) were characterized as tumor B with high EPCAM and KRT8 expression. The majority of monolayer cells (64%) were found in tumor C, defined by high SDF2L1 expression and containing few spheroid-derived tumor cells. While few VMT- and monolayer-derived tumor cells occupied tumor A, the remaining cells were roughly equally distributed between subpopulations, includ-

ing tumor D which was characterized by high expression of RBP1 and KRT23. Interestingly, the CSPG4/CD74-enriched population seen in HCT116-derived VMT was absent from SW480. Similar to HCT116, we see upregulation of PECAM1 in the VMT compared to monolayer cultures, and KRT5 expression is enriched in the VMT compared to both 2D and 3D monocultures of SW480. EPCAM was not significantly enriched in a single group for the SW480 dataset. IF staining confirmed the presence of tumor populations expressing EPCAM or EPCAM/KRT5 in SW480 cells grown in monolayer and in the VMT (Figure 2.12c), with nearly ubiquitous expression of EPCAM in both systems, but higher expression of KRT5 seen in the VMT, confirming the scRNAseq data.

2.4.8 Lineage hierarchy reconstruction reveals a unique VMT-derived HCT116 tumor population with characteristics of invasive CRC.

To investigate the origins of the CD74+ tumor subpopulation observed solely in the HCT116-derived VMT, we performed pseudotemporal reconstruction of differentiation trajectories using Monocle[249]. To interrogate the hierarchical relationships between the tumor subpopulations, HCT116-derived VMT scRNAseq data were subset in Seurat to contain only tumor A-D by removing EC and fibroblast subpopulations. Applying Monocle to this subsampled population yielded a connected differentiation trajectory that separated into three main branches representing distinct cellular states – with tumor A and tumor C occupying distinct cell states, tumor B at the junction, and the CD74+/NG2+ tumor subpopulation D occupying the third state along pseudotime (Figure 2.14a). Repeating this process with fibroblast subpopulations present in the subsampled dataset yielded a surprising finding: that fibroblasts segregate with tumor D to occupy the same state that is not observable with SW480 (Figure 2.13).

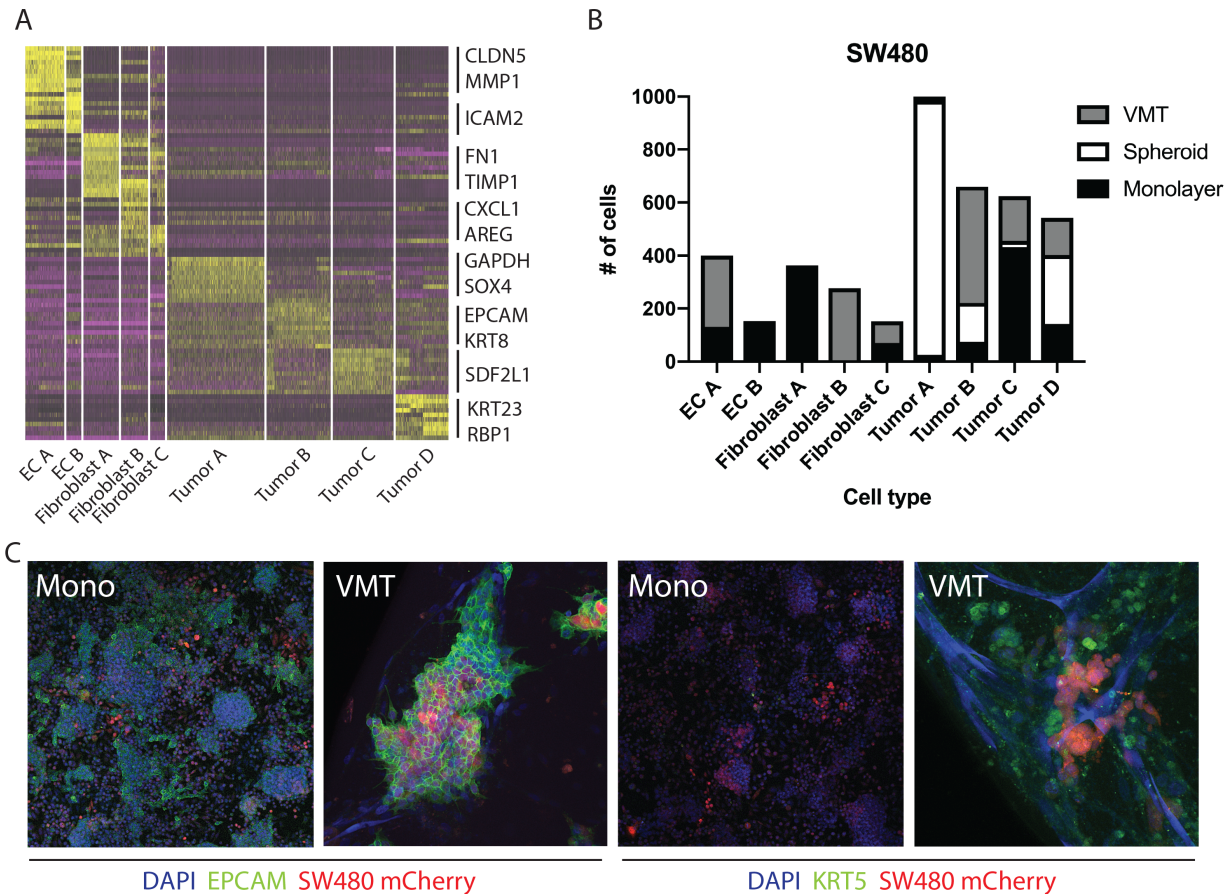


Figure 2.12 – Distinct changes in tumor heterogeneity that better model *in vivo* tumors occur when cells previously grown in 2D or 3D monocultures are grown in the VMT. (a) Heatmap of the top 10 differentially expressed genes in each cell type shows clear differentiation between sub-populations. (b) Plot showing cell distribution by cell type for each sample. (c) Immunofluorescence staining of sw480-derived VMT, 2D monocultures, tumor spheroids and xenograft tumors show that native tumor heterogeneity is reproduced in the VMT and not in monolayer or spheroid cultures, further supporting the scRNAseq data.

On further examination of this lineage hierarchy via pseudotemporal expression pattern gene clustering, we determined a list of genes that may be responsible for the transition of HCT116 CRC epithelial cells to a de-differentiated, mesenchymal state within the VMT (Figure 6B). While NG2 is considered a perivascular cell or pericyte marker, several other cell types also express NG2, including oligodendrocyte progenitor cells, chondroblasts, myoblasts, as well as several different tumors including glioblastoma and melanoma. CRC and breast cancer cells have been reported to upregulate CSPG4 (NG2) during epithelial-mesenchymal transition[212]. Indeed, we observe increases in EMT regulatory factors in

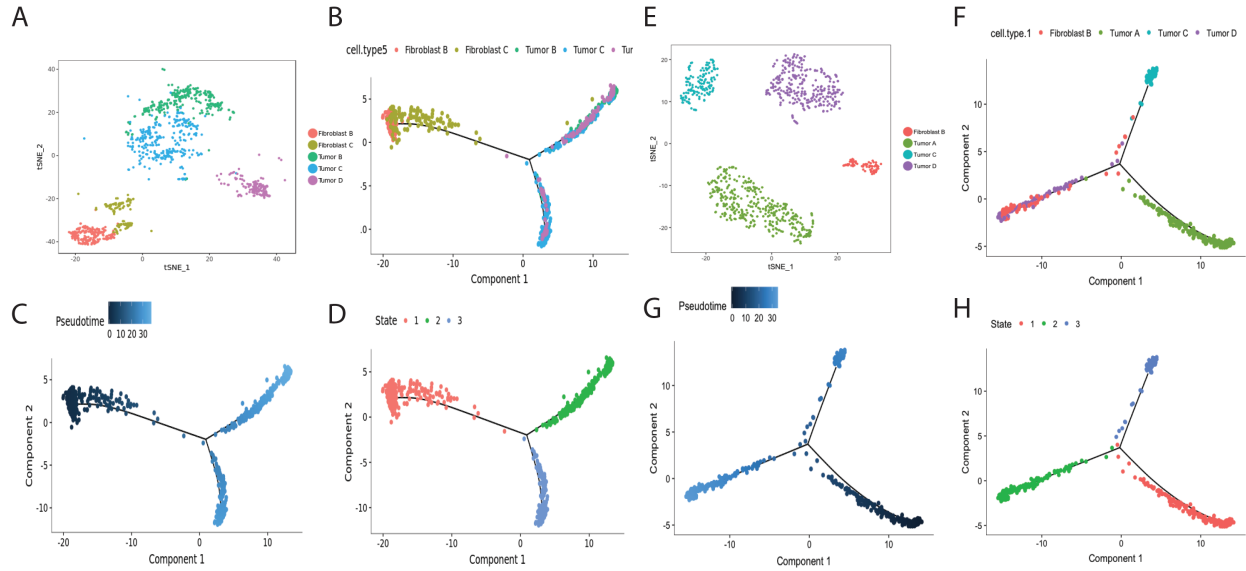


Figure 2.13 – Differential tumor states observed in VMT derived from SW480 and HCT116 . (a) Clustering for SW480 . **(b)** Monocle trajectory shows that tumor cells overlap and occupy two distinct states, and that fibroblasts segregate to a third branch for SW480 . **(c)** Pseudotime plot of SW480 . **(d)** Cell state plot for SW480 . **(e)** Clustering for HCT116 . **(f)** Monocle trajectory shows that tumor cells are distinct and occupy two distinct states, and that fibroblasts segregate to a third branch with tumor D to occupy the same state for HCT116 . **(g)** Pseudotime plot of HCT116 . **(h)** Cell state plot for HCT116 .

the CD74+/NG2+ tumor population, including TWIST1, VIM, TIMP1, and FN1, and decreased expression of differentiation and cellular adhesion markers, such as EPCAM, KRT8, KRT9 and KRT18 (Figure 2.14b). These findings suggest that HCT116 cells are undergoing EMT within the VMT, with each subpopulation occupying a distinct state. Indeed, we observe a collective EMT event within the VMT, with rapid and coordinated movement of cancer cells from the center of a tumor cluster within the span of an hour (Figure 2.14c). KRT5 and KRT23 serve as transitional markers for the tumor C population - midway between tumor A and tumor D/fibroblast populations, with low expression at the endpoints of pseudotime and high expression at the midpoint. While KRT5 is associated with metastasis[194], a recent study found that KRT23 activates CRC growth and migration, and that high KRT23 expression is prognostic of markedly shorter overall survival in CRC[283].

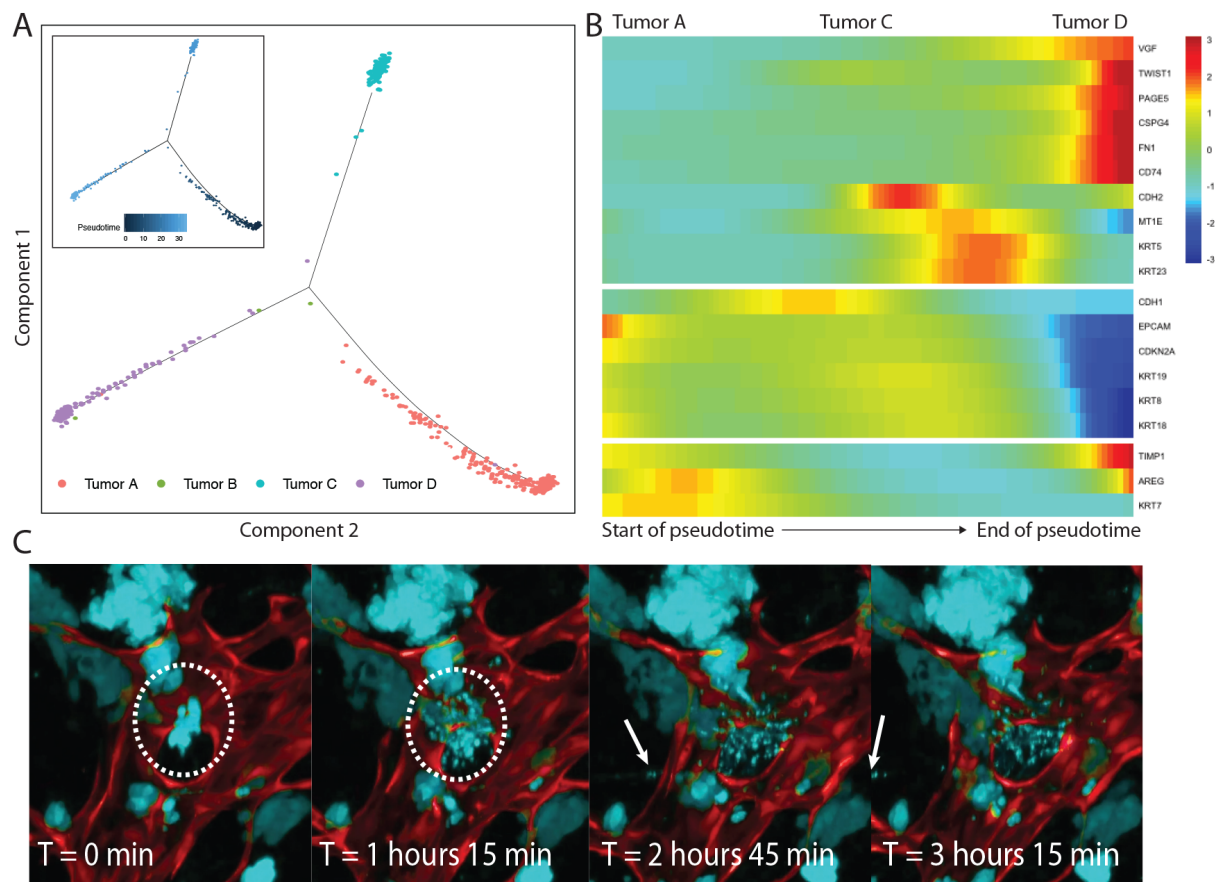


Figure 2.14 – Lineage hierarchy reconstruction reveals differential tumor states between HCT116- and SW480-derived VMT. (a) Monocle analyses for HCT116-derived VMT tumor subset showing monocle trajectory plot and pseudotime plot (inset). **(b)** Pseudotime heatmap for HCT116-derived VMT transition subset showing 3 differentially expressed clusters across the pseudotime trajectory. **(c)** Time-lapse confocal imaging showing an EMT event within the VMT. Arrow shows movement of an individual CRC cell.

2.4.9 Pathways implicated in tumor progression are upregulated in CRC cells grown in the VMT when compared to cells grown as 2D or 3D monocultures.

Comprehensive gene set enrichment analyses, based on cell type- and state-specific marker genes, revealed pathways that were significantly upregulated in cells grown in the VMT compared to 2D or 3D monocultures (Figure 2.15a). A key feature of cancer is the dysregulation of transcriptional programs[22], and indeed we observe transcriptional activation in

SW480-VMT derived tumor A and tumor D populations, as well as HCT116-VMT derived fibroblast A, evidenced by enhanced ribosomal biogenesis, increased eukaryotic transcription initiation, and high expression of ribosomal proteins and translation factors.

Both HCT116-VMT and SW480-VMT derived CRC cells showed enhanced growth factor signaling, upregulation of genes associated with colorectal cancer, activation of c-MYC, enhanced TNF signaling, and increased PDGFR- β signaling (Figure 2.15a). Notably, both HCT116- and SW480-VMT derived CRC cells displayed heterogeneity in intra-tumor patterning of metabolic gene expression by tumor cluster, a characteristic of *in vivo* tumors[172, 226]. Interestingly, two SW480 tumor populations (tumor B and tumor C) showed increased signaling downstream of IL-17, a pro-inflammatory cytokine that is elevated in several human tumors, including ovarian cancer, breast cancer, gastric cancer, and CRC[277]. Pro-growth, pro-survival pathways upregulated in the HCT116-VMT derived CRC cells included the RAC1 signaling pathway (ARPC2, ARPC3, ARPC1B, RAC1; adjusted p-value 0.016) and NF- κ B signaling pathway (LYN, VCAM1, TRAF1, LTB, CXCL2; adjusted p-value 0.037). In SW480-VMT derived CRC cells, we observed increased regulation of nuclear β -catenin signaling and target gene transcription (JUN, XPO1, YWHAQ, ID2, CUL1, SP5, SFN; adjusted p-value 0.011), regulation of telomerase (JUN, DKC1, NCL, E2F1, FOS, EGFR; adjusted p-value 0.016), and regulation of rb protein (CCND3, JUN, DNMT1, TFDP1, CEBPD, E2F1; adjusted p-value 0.016). Within the VMT, tumor populations with high expression of Wnt signaling effectors (HCT116 tumor A and SW480 tumor B) also showed the highest expression of stem-like markers (Figure 2.15b), in agreement with *in vivo* findings that suggest a critical role for Wnt signaling in CRC cancer stem cell maintenance[193].

Compared to SW480-derived VMT and monolayer cultures, spheroid cultures showed upregulation of genes involved in HIF1 α signaling and glycolysis; however, we found no other significantly enriched pathways, indicating that these 3D tumor spheroid models are limited in their ability to recapitulate features of *in vivo* tumors. While we observed significant

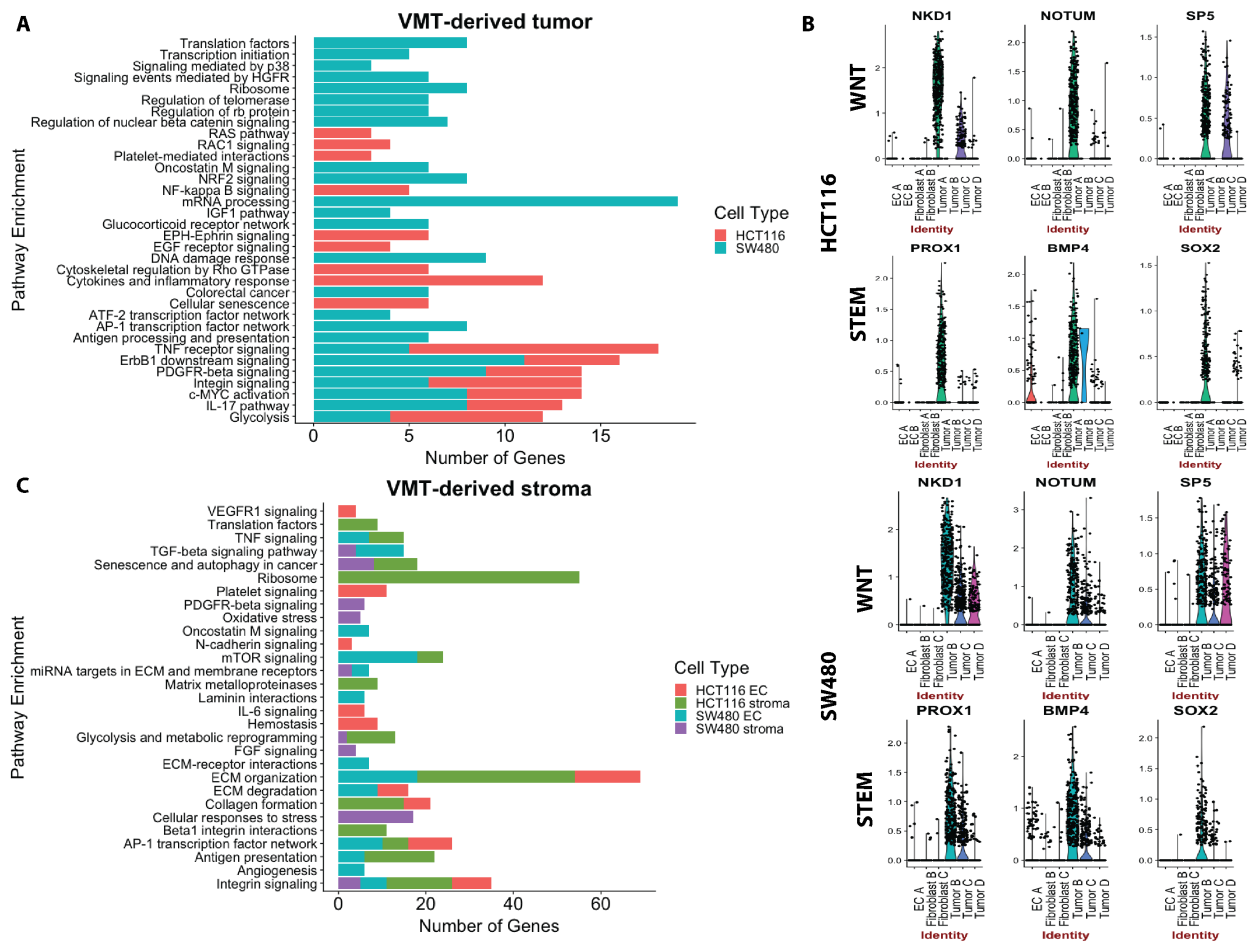


Figure 2.15 – Pathway enrichment for VMT-derived cells. (a) VMT-derived tumor pathway enrichment for HCT116 and SW480. **(b)** Violin plots for Wnt-related genes and stem-like signatures for HCT116 and SW480. **(c)** VMT-derived tumor pathway enrichment for HCT116 and SW480 EC and stroma.

PDGFR signaling enrichment in SW480-VMT derived CRC cells compared to both 2D and 3D monocultures of the same cells, HCT116-VMT derived CRC cells showed highly activated EGFR signaling compared to HCT116-derived monolayer cultures.

2.4.10 Dynamic intercellular cross talk within the VMT promotes extracellular matrix remodeling characteristic of malignancy.

The tumor microenvironment is comprised of many host cell types, including endothelial cells, perivascular cells, fibroblasts and inflammatory cells, which contribute to tumor progression by mediating angiogenesis, desmoplasia and inflammation[47]. Integrin-mediated remodeling of the tumor microenvironment is a key step in cancer progression[82]. Not only do integrins contribute to tumor cell migration and invasion by regulating the activity of matrix-degrading proteases, such as matrix metalloproteases (MMPs) and urokinase-type plasminogen activator (uPA), integrins also support the process by which tumors recruit new blood vessels via angiogenesis[52]. In SW480 and HCT116 VMT-derived stromal populations (EC and fibroblasts) and CRC cells, we observe enhanced integrin signaling compared to 2D and 3D monocultures. Extracellular matrix remodeling is controlled by integrins[82] and indeed we find that HCT116- and SW480-VMT derived EC and stromal subpopulations actively re-organize the extracellular matrix.

Pathways significantly enriched within the VMT-derived stroma include collagen formation and degradation, integrin signaling, laminin interactions, ECM-receptor interactions and miRNA targets in ECM and membrane receptors (Figure 2.15c). HCT116 VMT-derived fibroblasts display upregulated uPA and uPA receptor-mediated signaling (ITGB1, LRP1, ITGB5, ITGA3, FN1; adjusted p-value 0.01) and increased expression of MMPs (MMP14, BSG, TIMP2, TIMP1; adjusted p-value 0.02). Furthermore, we observe an increase in β 1 integrin cell surface interactions (ITGB1, CD81, COL4A1, LAMB2, ITGA3, COL6A2, COL6A1, FN1, COL6A3, LAMB1, LAMC1; adjusted p-value 0.000017). β 1 integrin has been implicated in CRC to promote hepatic invasion and metastasis in addition to supporting CRC cancer stem cells[176, 41].

Endothelial cells (EC) within both HCT116- and SW480-VMT highly express genes associated with angiogenic sprouting and tip-cell formation, including ANGPT2, NID2 and DLL4,

while expression of VWF, a marker of non-sprouting EC, was not differentially expressed between the VMT and monolayer cultures. Regulators of angiogenesis (JUN, FOS, ETS1, HIF1A, JAK1) were significantly upregulated in the VMT-derived endothelial cells compared to 2D monocultures. Fibroblasts derived from the VMT support vessel sprouting and formation via upregulation of integrins involved in angiogenesis, such as COL1A1, COL1A2, COL3A1, and COL4A1. Intriguingly, several cancer-associated pathways were also enriched in VMT-derived stroma, including focal adhesion-PI3K-Akt-mTOR-signaling, TNF signaling, N-cadherin signaling events, and senescence and autophagy in cancer (Figure 2.15c).

It is generally accepted that most solid tumors, including CRC, are linked to chronic inflammation and that inflammatory cells and cytokines create a microenvironment that supports disease progression[47]. Transcriptomic profiles obtained from VMT-derived fibroblasts suggest a hypoxic, pro-inflammatory, and tumorigenic microenvironment within the VMT. Several pathways associated with tumor progression, resistance and metastasis are highly activated in the VMT-derived stromal population compared to 2D monocultures: HIF1A regulation of glycolysis, the inflammatory response pathway and cellular responses to stress, oxidative stress and lncRNA-mediated mechanisms of therapeutic resistance (Figure 2.15c). Intriguingly, fibroblasts derived from both HCT116- and SW480-VMT, as well as HCT116-VMT derived EC A population, were distinguished by enhanced IL-6 expression and signaling. IL-6 is a pro-inflammatory cytokine reported to have an important role during CRC tumor development, and of which high expression is associated with drug resistance, advanced disease stage and decreased survival in CRC[260, 236, 156]. The pro-inflammatory cytokines CXCL1 and CXCL2 are also upregulated in HCT116- and SW480-VMT derived fibroblast populations and HCT116-VMT derived tumor D, respectively. Among enriched pathways within the VMT, glycolysis and metabolic reprogramming of CRC mediated by HIF1 α emerged within HCT116- and SW480-VMT derived stroma, with HIF1A highly expressed in EC and fibroblast subpopulations.

2.4.11 VMT-derived stroma model clinical characteristics of reactive stroma in CRC.

Both HCT116- and SW480-derived fibroblasts display active TGF- β signaling in the VMT (Figure 2.16a, 2.16b). Intriguingly, we observe significant upregulation of the TGF- β signaling pathway in fibroblasts derived from SW480-VMT compared to those same fibroblasts grown in monolayers, but do not observe enhanced TGF- β signaling in SW480-VMT tumor populations compared to both 2D and 3D monocultures. In contrast, HCT116 VMT-derived fibroblasts and tumor populations both show modest increases in TGF- β signaling over 2D monocultures. Importantly, we observe these differences in cancer-associated fibroblasts between SW480- and HCT116-derived VMT despite using the same line and passage of fibroblasts (derived from a single vial) in all experiments, suggesting that the tumor uniquely models the microenvironment and stromal compartment of the VMT. Indeed, these observations are consistent with recent literature defining the role of TGF- β -activated stroma in poor prognosis CRC[32]. Although most CRC display mutational inactivation of the TGF- β pathway, these tumors are paradoxically characterized by elevated TGF- β production. Functional studies show that cancer-associated fibroblasts support tumor-initiating cells via enhanced TGF- β signaling (Figure 2.17), and that poor clinical outcomes are predicted by a gene program induced by TGF- β in tumor-associated stromal cells[32].

TGF- β signaling is active between the tumor and fibroblast populations in both HCT116 and SW480 VMT. Since TGF- β activation in the stroma is known to promote CRC tumorigenesis, we sought to test whether targeting TGF- β signaling in the reactive stroma could suppress the tumor within the VMT. VMT were treated with the TGF- β receptor antagonist galunisertib, which is currently in clinical trials for hepatocellular cancer, within a physiologically-relevant range of doses. While galunisertib showed no effect for HCT116 grown in the VMT over the course of 6 days (Figure 2.16c), we observed potent inhibition of

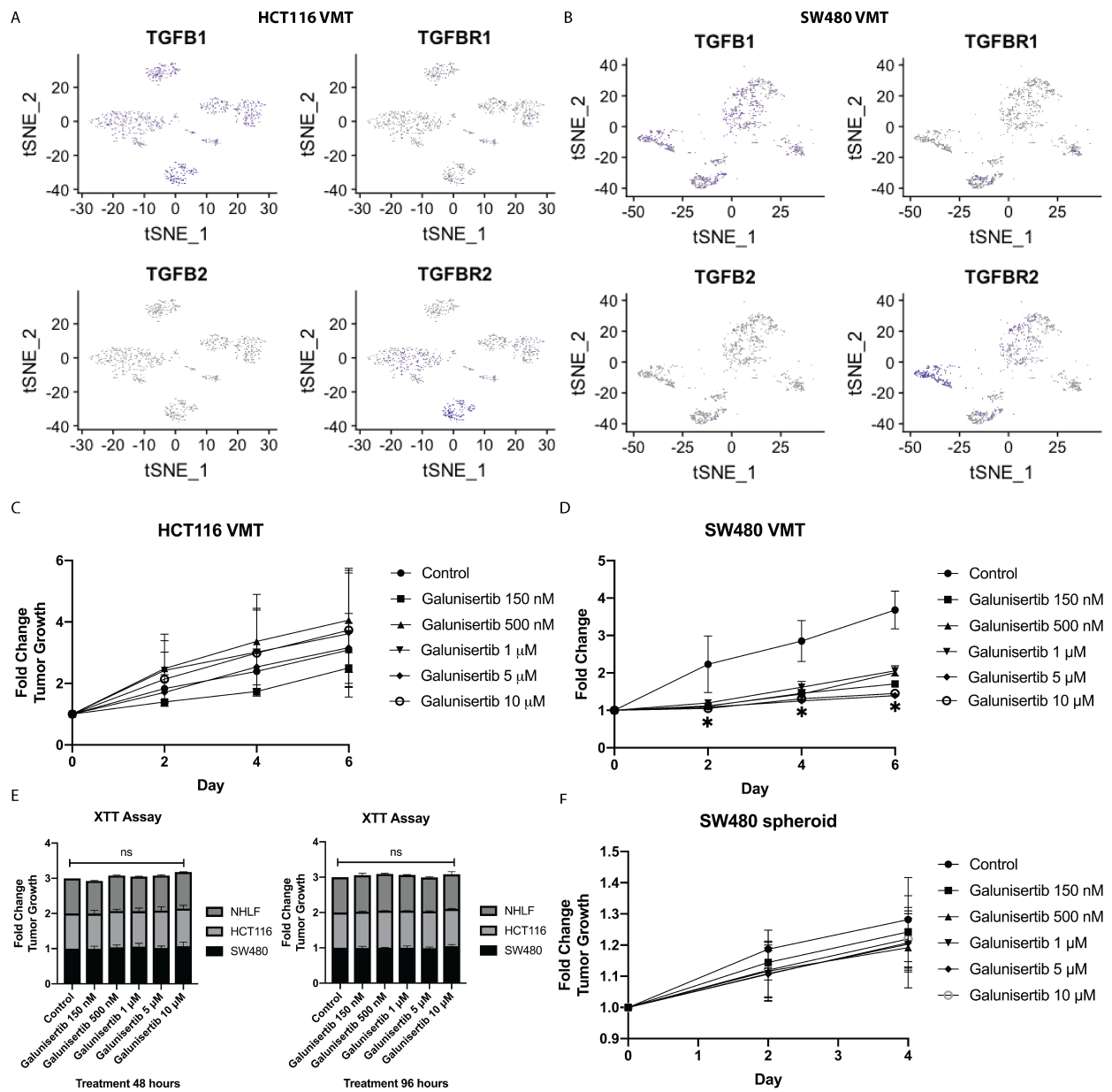


Figure 2.16 – TGF- β -activated stroma in VMT confers differential drug sensitivity. (a) tSNE plot of HCT116 VMT with TGF- β ligands and receptors highlighted. (b) tSNE plot of SW480 VMT with TGF- β ligands and receptors highlighted. (c) Dose response of galunisertib for HCT116-derived VMT. (d) Dose response of galunisertib for SW480-derived VMT. (e) Dose response of galunisertib for monolayer-derived HCT116, SW480 and NHLF at 48 hours and 96 hours. (f) Dose response of galunisertib for spheroid-derived SW480.

SW480 growth in the VMT with galunisertib treatment (Figure 2.16d). Interestingly, there were no responses observed for HCT116, SW480, or NHLF growing as 2D monocultures at any of the concentrations tested at 48 hours or 96 hours (Figure 2.16e). There were also no

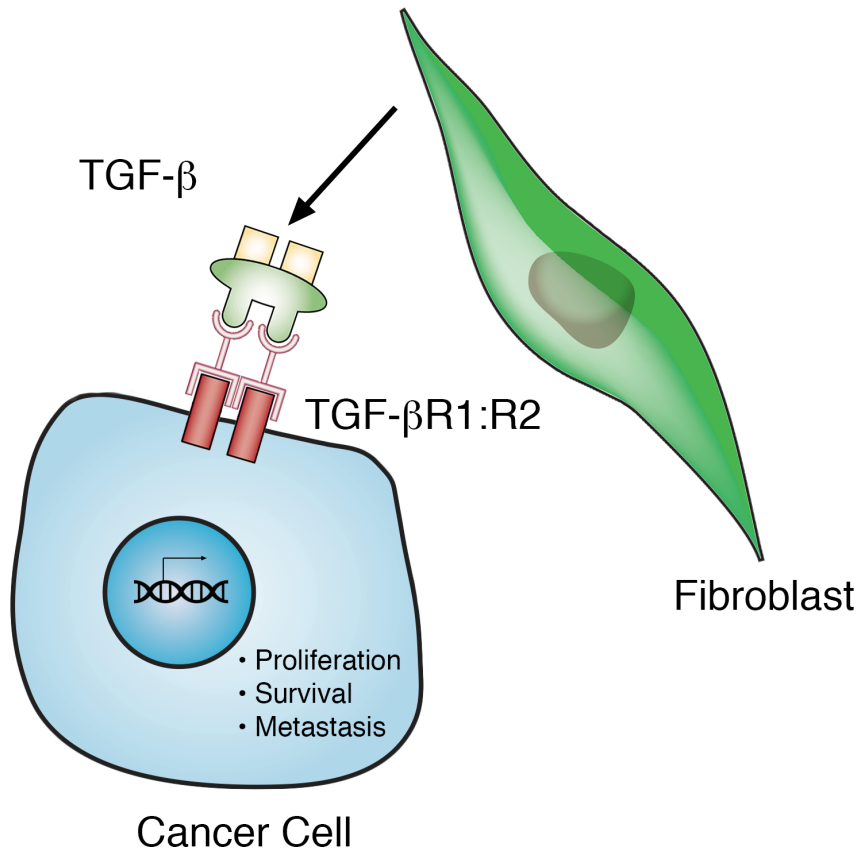


Figure 2.17 – TGF- β signaling promotes CRC progression. Stromal production of TGF- β supports CRC growth, survival, metastasis, and immune suppression.

effects on SW480-derived spheroid growth in response to treatment (Figure 2.16f). These findings suggest that SW480 cells, and not HCT116, become dependent on TGF- β signaling in the presence of TGF- β activated stroma, and that the stroma is a powerful regulator of tumor growth as well as suppression. The VMT model can serve as an important tool to further investigate molecular signatures of resistance or susceptibility to TGF- β antagonists toward tumor stratification and to interrogate other tumorigenic pathways.

2.4.12 VMT-derived SW480 CRC cells better model *in vivo* tumor heterogeneity than 2D and 3D monocultures.

To further validate the VMT as a physiologically relevant drug screening and disease modeling platform, we performed a reference-based integration using Seurat[235]. To run the cell anchoring pipeline, a scRNAseq dataset of SW480-derived xenograft tumors was used as reference and all other SW480 datasets (VMT, spheroid and monolayer) were used as query (Table 2.1). Out of the three model systems, VMT showed the greatest similarity to xenograft tumor, with 289 cells (38% of total) accurately mapping to the reference dataset. In contrast, monolayer cultures showed 27% fidelity, with 184 cells correctly mapping to the reference. Surprisingly, spheroid cultures showed the lowest concordance with xenograft tumors, with only 8% of cells (123 cells) correctly mapping to the reference. A potential explanation for the high rate of false matches in the spheroid sample may be because the spheroids displayed the least degree of heterogeneity of all the models, being almost entirely composed of a single clonal population. These results suggest that the VMT more closely resembles the cellular diversity found within a xenograft tumor than both 2D and 3D monocultures.

Sample	# True	# False	% True	% False
VMT	289	475	38	62
Spheroid	123	1268	8	92
Monolayer	184	490	27	73

Table 2.1 – Results from reference-based integration of SW480 scRNAseq datasets

2.5 Discussion

Anti-cancer drug development is a costly, time-consuming and inefficient process with a low success rate - only about 5% of drugs in the pipeline will ultimately gain FDA-approval. Recapitulating the complex intercellular crosstalk between the tumor and microenvironment is critical to capturing clinical tumor pathology toward novel therapeutic development. With the VMT model, we aim to improve clinical outcomes for patients and save resources by predicting which compounds will demonstrate efficacy in humans, detecting promising drug candidates that may be missed by standard assays, and eliminating toxic and ineffective drugs earlier in the pipeline. To this effect, we show that the VMT more closely models the growth and chemotherapeutic drug response observed in preclinical *in vivo* murine models than 2D and 3D monocultures. Indeed, FOLFOX, with IC₅₀ in the nanomolar range in standard assays, has significantly diminished anti-tumor effect in the VMT, with IC₅₀ shifted toward peak plasma concentrations observed in clinical trial settings. We find that numerous tumor-associated pathways are enriched in the VMT and xenograft tumors, but not in 2D monocultures, including PI3K-Akt signaling pathway, MAPK signaling pathway, Ras signaling, FGF signaling, chromosome and microsatellite instability in CRC, epithelial to mesenchymal transition in CRC and angiogenesis, among several other cancer-related pathways.

By recreating the tumor microenvironment *in vitro*, we begin to dissect the complex intercellular interactions occurring within a 3D, vascularized tumor mass that contribute to disease pathology and drug resistance. In the same way that malignancy progresses via aberrant signaling in the microenvironment, targeting key intercellular signaling pathways between cancer cells and stroma can abrogate malignant progression. In VMT-derived stromal populations, we observe significant upregulation of TGF- β signaling, that, when pharmacologically abrogated, suppresses tumor growth within the VMT but not in 2D or

3D monocultures, underscoring the critical role stromal cells play in disease progression and drug sensitivity. Here we show that both HCT116 and SW480 induce TGF- β activation in the stroma within the VMT model to recapitulate pathological features of poor-prognosis clinical CRC tumors. However, only VMT-derived SW480 CRC cells show sensitivity to TGF- β inhibition, indicating that the VMT captures tumor cell-type specific stromal dependencies within the VMT. Our findings reveal that stromal cell activating, prognostic *in vivo* phenomena are reproduced within the dynamic tumor microenvironment of the VMT and cannot be studied or targeted in simple 2D or 3D monocultures. High levels of TGF- β are associated with poor outcomes in CRC and a key hallmark of microsatellite-stable CRC is TGF- β activated stroma. Furthermore, TGF- β can act as a tumor suppressor or tumor promoter depending on the context[153], further emphasizing the importance of capturing cancer-specific disease characteristics in preclinical models. Our findings highlight the unique capability of the VMT to recapitulate human-specific and clinically relevant tumor pathologies *in vitro* that cannot be readily reproduced with standard cell culture or animal models.

Intriguingly, a CD74+/NG2+ mesenchymal-like population originating from HCT116 emerges only in HCT116-derived VMT, and is not seen in monolayer cultures or SW480 CRC cells. Further examination of this population (tumor D) revealed downregulation of epithelial markers and upregulation of mesenchymal-related genes such as VIM, TWIST1, FN1, ZEB1 and TIMP1, suggesting a subpopulation of HCT116 CRC cells undergo EMT within the VMT. These findings were confirmed by time-lapse confocal microscopy of VMT development and growth showing the coordinated, collective and rapid migration of CRC cells coupled with CRC cell intravasation into associated vasculature, highlighting the utility of the VMT to study tumor cell behaviors that result in metastatic spread toward development of targeted therapies. Intriguingly, based on CNV analyses and marker gene expression, HCT116 tumor D is likely derived from tumor C, another unique tumor population arising only within the VMT, which shows transitional metastatic markers and similar CNV profiles.

Interestingly, VGF (or VGF nerve growth factor inducible), a secreted protein and neuropeptide precursor, was enriched in the tumor D subpopulation. Usually expressed in nerve cells or neuroendocrine cells, high VGF expression also occurs in several types of malignant neuroendocrine tumors that confer unfavorable prognosis[97, 265]. In glioblastoma, VGF has been shown to promote tumor growth and cancer stem cell (CSC) survival and self-renewal via autocrine and paracrine signaling between differentiated glioblastoma cells and glioblastoma-specific CSC[265]. Further, a recent study found that high expression of VGF in a subset of lung cancer cells induces the transcription factor TWIST1 to facilitate EMT and resistance to EGFR inhibitors, and that VGF silencing attenuates tumor growth[97]. Notably, high VGF expression is associated with diminished survival in CRC and is prognostic for poor outcomes in endometrial cancer and malignant glioma/glioblastoma[252].

Although the consequences of VGF expression have not been widely studied in CRC, the role of VGF in the development and progression of CRC and other cancers warrants further study based on its potential utility as a biomarker and therapeutic target. To facilitate such studies, we show that the VMT captures tumor heterogeneity arising from differentiation trajectories and distinct cellular states not seen in 2D or 3D monocultures, and thus serves as a powerful tool to recapitulate the clinicopathology of human tumors *in vitro*. Notably, the CD74+/NG2+ tumor D population appears to arise through EMT, a phenomenon observed *in vivo* and within the VMT, but not in 2D or 3D monocultures. Therefore, the VMT can facilitate the study and targeting of resistance mechanisms related to this unique population that is not possible with other culture systems and not easily studied in mouse models. Importantly, the heterogeneity observed in the SW480-derived VMT was also found in SW480-derived xenograft tumors but not in 2D or 3D monocultures. Taken together, our findings demonstrate that the VMT not only recapitulates *in vivo* drug response, but also reconstitutes the cellular diversity of the tumor growing *in vivo*.

2.6 Conclusion

The tumor microenvironment forms a complex ecosystem that facilitates tumor progression and resistance. Only with the appropriate model system can the dynamic interplay within the tumor microenvironment begin to be defined for therapeutic targeting. Here we show that the VMT robustly reproduces clinicopathological features and drug response of CRC tumors. Furthermore, we demonstrate the VMT can be used as a powerful tool to study, and target, spatially random and temporally rapid events such as EMT that are not readily observable with other model systems. These results highlight the marked changes in gene expression, cellular diversity and drug sensitivity that occur when cells grown in simple 2D or 3D monocultures are co-cultured to form the complex 3D tumor architecture within the VMT.

Chapter 3

Automated Image Processing for a Vascularized Micro-Tumor Model Using ImageJ Scripting and Macros

3.1 Abstract

To address the need for improved preclinical models, our lab has designed and validated an advanced microfluidic device that allows long-term study of tissue engineered miniaturized organ constructs. Through the co-culture of multiple cell types in a dynamic flow environment, perfused microvascular networks self-assemble within the tissue chambers of the device to enable realistic modeling and real-time monitoring of physiologic and disease states. The VMO is a base platform that can be adapted to virtually any organ system or cultured with cancer cells to create a VMT. By replicating *in vivo* delivery of nutrients and drugs in a complex 3D microenvironment, the VMO/VMT platform is arguably the most physiologically relevant *in vitro* model in which to perform drug screening, in-

terrogate complex pathological processes and study cancer, vascular or organ-specific biology. The microfluidic platform is optically transparent for real-time image acquisition of fluorescently labeled cells or molecules within the tissue construct, allowing the user to interrogate drug response, inter-cellular interactions and temporally rapid, spatially random phenomena such as epithelial to mesenchymal transition. Since these studies can lead to the generation of enormous amounts of imaging data, robust and standard workflows for analysis are critical. Typically, micrographs of vessels and tumors can be processed manually in the open-source software ImageJ using repetitive functions. Here we describe how this time-consuming process can be greatly streamlined using ImageJ scripts, a simplified and standardized method for efficient image processing and data extraction from the novel VMO/VMT model.

3.2 Introduction

Our lab has developed a novel drug-screening platform in which living, perfused microvessel networks form *de novo* within a microfluidic device [80, 224, 179, 263, 177]. This base organ-on-a-chip platform, hereby termed the VMO, can be adapted to virtually any organ system to replicate tissue physiology for disease modeling and drug screening or personalized medicine applications. The VMO can also be established as a cancer model system by co-culturing tumor cells with associated stroma to create a VMT. Endothelial cells, fibroblasts and, in the VMT, tumor cells are embedded in a 3D extracellular matrix within the tissue chambers of the device and subjected to gravity-driven fluid flow through the microfluidic channels. Within days, a perfused vascular network forms and, in the case of the VMT, begins to feed the growing tumor mass just as it occurs *in vivo* – *i.e.* nutrients and drugs are delivered through the microvessels. Unlike any other drug-screening platform, the VMO/VMT model establishes a complex microenvironment complete with

stromal and/or tumor cell interactions within a capillary bed. As such, it is arguably one of the most physiologically relevant platforms to screen drugs and model disease.

In addition to being low cost, easily established and arrayed for high throughput experiments, the platform is fully optically compatible for real-time imaging of stromal and tumor response to stimuli and drug treatment. By labeling each cell type in the system with a different fluorescent marker, we can directly visualize and track cell behavior throughout the entire experiment, thus allowing a window into the dynamic tissue microenvironment. Our methods for establishing and imaging the VMO/VMT model have been described previously[224, 179]. The complex spatial and temporal information derived from VMO/VMT images requires a robust and highly reproducible method for extracting data. Yet normally to assess tumor response, vessel remodeling or flow dynamics, a series of images must first be processed and analyzed through ImageJ software by applying repetitive functions individually to each image. By automating these processes in ImageJ, the macro can extract thousands of data points from series of images in a matter of seconds, thus requiring very little effort or time from the investigator. Here we describe an ImageJ script designed to automate image processing and analyses for high throughput applications in the VMO/VMT model that can be readily adapted to other common research applications.

3.3 Materials and methods

3.3.1 Script development

Git source control[77] was used during the development of the macro. The complete version history can be found on Github.

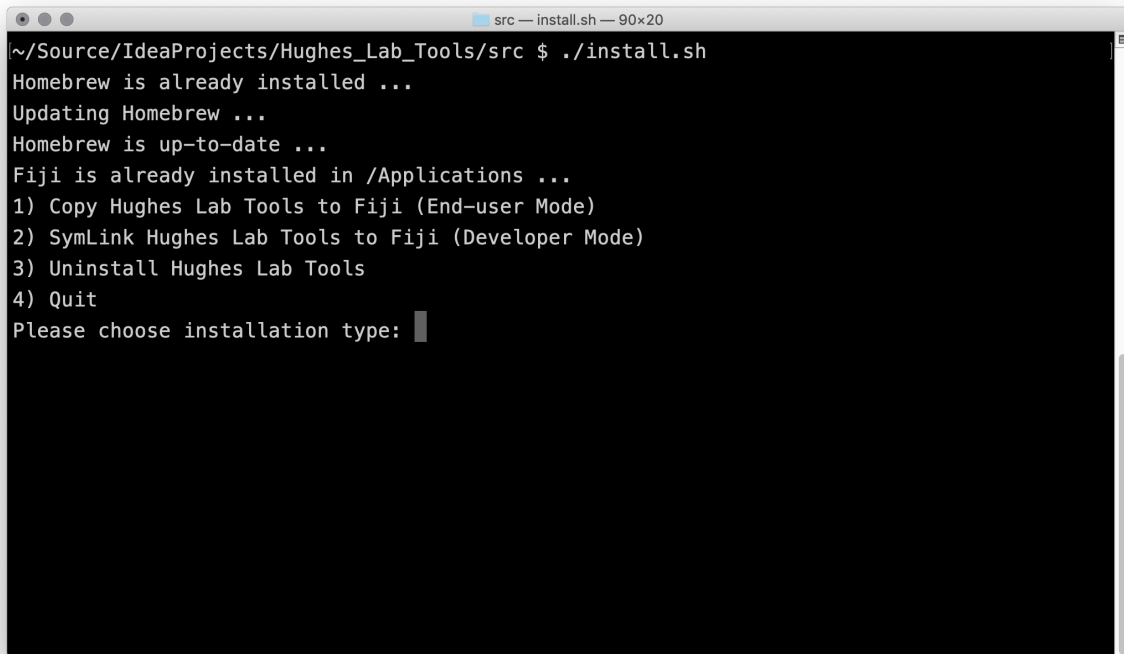
ImageJ and the Fiji Distribution of ImageJ[206] include tools for developing ImageJ macros and scripts[207]. The development tools included with both ImageJ and Fiji are reasonably well-suited for simple macro and script development. Likewise, they include a Macro Recorder that is helpful in identifying the commands needed to execute operations typically invoked from the ImageJ user interface. During script development, we opted to use an Integrated Development Environment (IDE) for its advanced development and code debugging tool set. The IDE used was IntelliJ IDEA Community from JetBrains. IntelliJ IDEA is a Java Virtual Machine (JVM)[139] development environment that offers the ability to create JVM compatible programs using the Java language, Java derivative languages such as Groovy, and various other languages such as Python, which we used as our primary development language.

3.3.2 Script installation

The Hughes Lab Tools suite is compatible with ImageJ and has been tested with the Fiji[206] distribution of ImageJ2 on MacOS 10.14.4. It is recommended that the tools be used with Fiji as some functions rely on plugins not installed by default with the base ImageJ distribution. Manual installation of Fiji on MacOS is easily accomplished using the Homebrew package management system[87] using the terminal command `brew cask install fiji`. To simplify installation of the tools, a shell script has been included with the suite to test for the presence of both Homebrew and Fiji and then install the Hughes Lab Tools scripts and macros into the appropriate locations.

To install the Hughes Lab Tools, the user should download the tools from GitHub, decompress the downloaded zip file, and navigate to the resulting directory using the terminal. To run installer script the user should run the command `./install.sh`. During the installation the user will be prompted to “Copy Hughes Lab Tools to Fiji (End-user Mode)” or

“SymLink Hughes Lab Tools to Fiji (Developer Mode)” (Supplemental figure 3.1). These installation options will either copy the Hughes Lab Tools source files into Fiji or create symbolic links to them from their current location. For most users, the copy option is the appropriate choice as this will install all files needed inside the Fiji.app package on their computer. However, developers debugging or extending the tools may find it convenient to symbolically link to the location of the tools install folder since this directory can be opened directly in IntelliJ, the source code modified, and tested simply by restarting Fiji. A third option in the installer allows files created during install to be removed from Fiji.app if desired.



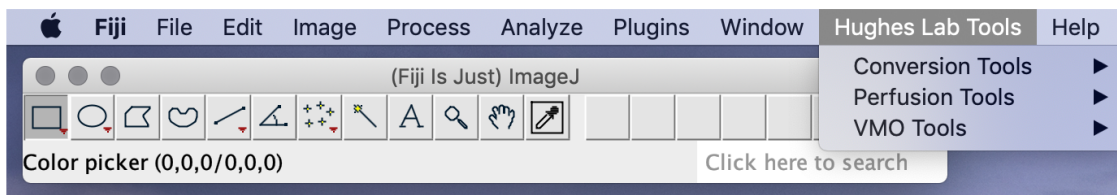
```
src — install.sh — 90x20
~/Source/IdeaProjects/Hughes_Lab_Tools/src $ ./install.sh
Homebrew is already installed ...
Updating Homebrew ...
Homebrew is up-to-date ...
Fiji is already installed in /Applications ...
1) Copy Hughes Lab Tools to Fiji (End-user Mode)
2) SymLink Hughes Lab Tools to Fiji (Developer Mode)
3) Uninstall Hughes Lab Tools
4) Quit
Please choose installation type: █
```

Figure 3.1 – Options presented during installation of Hughes Lab Tools

After the installation is complete the user will find a new “Hughes Lab Tools” menu item in the menu bar of Fiji (Supplemental figure 3.2a). A keyboard shortcut to quickly execute any of the tools can be created using the “Add Shortcut ...” command found under “Plugins >Shortcuts” menu (Supplemental figure 3.2b). Using this command the end user can

specify keyboard shortcuts of their preference and assign them to any of the menu items found under Hughes Lab Tools.

A



B

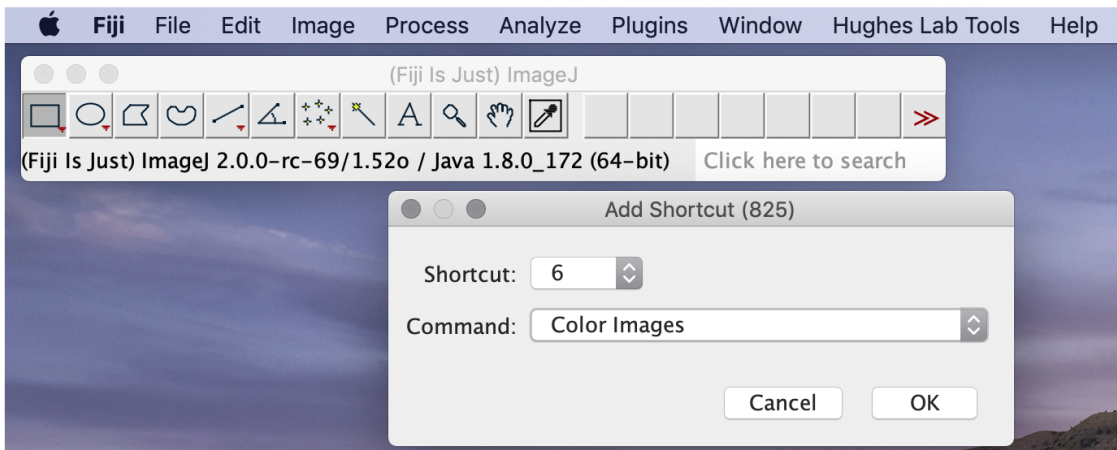


Figure 3.2 – Hughes Lab Tools Menu. (a) Hughes Lab Tools menu bar item in Fiji. (b) Dialog box to specify a keyboard shortcut function using the “Add Shortcut ...” command.

3.3.3 Device fabrication

A detailed description of device fabrication can be found in our earlier publications[224, 179]. Briefly, the high throughput platforms used in the experiments were fabricated with polydimethylsiloxane (PDMS) by mixing 10:1 parts base to curing agent (Sylgard 184 elastomer kit, Dow Corning). The PDMS is then degassed in a vacuum chamber and poured into a polyurethane master mold replicated from a soft lithographic designed silicon wafer. The PDMS device is then cured in a 70°C oven for 4 hours before holes are punched to

create media inlets/outlets and loading ports. Next, the device is bonded to a chemically treated bottomless 96-well plate by oxygen plasma treatment. Finally, the high-throughput platform is bonded to a thin PDMS membrane and placed under UV light for 20 minutes to sterilize the device prior to loading cells.

3.3.4 Cell culture

Human CRC cell lines SW480, SW620 and HCT116 (gifts from the University of California, Irvine (UCI) Chao Family Comprehensive Cancer Center), and NHLF (purchased from Lonza) were cultured in Dulbecco's modified Eagle medium (DMEM) supplemented with 10% DMEM. ECFC-EC were isolated from cord blood according to an Institutional Review Board-approved protocol and cultured on gelatin-coated flasks in endothelial growth medium-2 (EGM-2). All cells were incubated in a 37°C and 5% CO₂ environment. Cancer cells, ECFC-EC and NHLF were transduced with lentivirus to express either GFP, mCherry or Azurite fluorescent markers. All ECFC-EC were used between passage 5–7 and NHLF were used between passage 7–10.

3.3.5 VMO/VMT establishment

To load the device and establish the VMO model, ECFC-EC and NHLF were harvested, counted and resuspended with 10 mg/mL solution of 70% clottable fibrinogen in basal media to a concentration of 7 million cells/mL. To establish the VMT model, CRC cells were also harvested, counted, and resuspended with the ECFC-EC/NHLF fibrinogen mix. The cell slurry was then mixed with 2 U/ μ L thrombin to catalyze fibrin clotting and quickly introduced into the tissue chambers of the device. In order to culture VMO/VMT, the microfluidic

channels were coated with laminin to promote vessel anastomosis and the media inlets were fed with EGM-2.

3.3.6 Fluorescent imaging, perfusion and bead tracking

Fluorescently labeled tumors, stromal cells and vessels were imaged using a SPOT Pursuit High Speed Cooled CCD camera on an Olympus IX70 microscope with X-Cite 120LED. Vessels were perfused with 70 kD FITC- or rhodamine-dextran and imaged using a Nikon confocal microscope. Permeability coefficient is calculated by using Eq 3.1:

$$P_D = \frac{1}{I_i - I_b} \left(\frac{I_f - I_i}{\Delta t} \right) \times \frac{d}{4} \quad (3.1)$$

where I_i , I_f and I_b represent the initial, final and background average intensities, respectively, Δt is the time interval between two captured images and d is the average diameter of the vessel[106].

To induce vascular leak, VMOs were first perfused for 2 hours with basal medium, and then perfused with thrombin (10 U/mL) for an hour before addition of fluorescent-dextran. To track bead velocity, 2 μm fluorescent beads were introduced into the media inlets and sequential vessel images were taken at a shutter speed of 2.5 frames/second. Each image pair in the series was differentially colored and merged to measure the distance a specific bead traveled through any given vessel segment. Velocity was then calculated by dividing the distance traveled in μm by the frame rate.

3.3.7 COMSOL Multiphysics simulation

COMSOL Multiphysics 5.2a was used to perform finite element simulations for the interstitial flow and bead tracking inside a developed microvascular network. The geometry of the vessel network was first integrated into the geometry of the microfluidic channel. Thresholded vessel images were smoothed and processed into outlines using ImageJ software, then converted into a .dxf file using Img2cad software. After the vessel outline was closed and redundant fragments removed using AutoCAD software, the complete vessel outline was scaled and integrated into the geometry of the microfluidic device. The refined CAD vessel diagram was then built into a 2D free and porous media flow model in COMSOL Multiphysics. Water was chosen as the material to model the flow of culture media through the vascular network. The porosity and permeability of fibrin gel were estimated to be 0.99 and $1.5 \times 10^{-13} \text{ m}^2$ based on our published result[224]. Inlet/outlet were designated at the media reservoir boundaries, with pressure specified as 98 and 0.001 Pa, respectively, based on calculated gravity-driven pressure difference in the device. The particle tracking for fluidic flow module of COMSOL Multiphysics was used to simulate the beads perfusion in the vascular network. The properties of polystyrene bead were set as 1040 kg/m^3 in density and $2 \text{ }\mu\text{m}$ in diameter. Stokes' law and the flow velocity field from the previous model was used for the drag force, and bounce wall condition is applied for this model. 9 beads were released near the inlet at T_0 from 3×3 grid with $200 \text{ }\mu\text{m}$ spacing. A movie was recorded for this bead perfusion process.

3.3.8 Statistical analysis

Three biological replicates were performed for each experiment. GraphPad Prism Version 8.1.1 was utilized to perform students t-test for permeability comparisons with significance set at $p < 0.05$. Spearman's rank correlation coefficient was used to determine the degree

of correlation between COMSOL simulated fluid flow velocity and actual bead velocity determined through experimental tracking. Significance was determined by plotting the correlation coefficient on Spearman's rank significance graph with $p < 0.05$.

3.4 Results

3.4.1 Overview

ImageJ is a Java-based image processing program developed at the National Institutes of Health and the Laboratory for Optical and Computational Instrumentation, University of Wisconsin (LOCI)[207]. ImageJ was designed with an open architecture that provides extensibility via Java plugins, scripts capable of being written in various programming languages, and recordable macros using the built-in ImageJ macro language. Using scripting and macro capabilities within ImageJ, we have created a series of tools to automate and standardize image processing for our VMO/VMT tissue constructs. Our suite of Jython[188] scripts and ImageJ macros, collectively called Hughes Lab Tools, incorporates user interface driven tools to execute one or more common tasks while also providing flexibility to quickly batch process large numbers of images in nested folders.

The primary functions of the tool are to:

1. Color monochromatic micrographs
2. Merge two or more colored micrographs into a single image
3. Measure the mean gray levels of the tumor images
4. Measure the diameter of the VMO/VMT vessels
5. Segment the tumor structures for further image analysis

6. Threshold micrographs of the VMO/VMT vessel structure for further image analysis
7. Batch convert Nikon ND2 files to tiff files
8. Measure the perfusion coefficient for images of the VMO/VMT vessel structure

The scripts are capable of being executed in either a completely automatic manner or a semi-automatic mode where the operator is able to verify the intermediate results. In addition, images can be processed in a single directory or a series of nested directories, allowing for flexibility in the image acquisition and organization. Script functions can be individually chosen or a series of functions can be run in series on each batch of images, which vastly improves throughput over manual image processing. Furthermore, the tools can be easily modified or adapted to address a broad range of experimental questions, either in the VMO/VMT platform or other model systems.

3.4.2 Functionality

3.4.2.1 VMO Tools

Found under the Hughes Lab Tools>VMO Tools menu item, the VMO tools is a set of tools that can be run individually or in sequence to process fluorescently labeled tumors, stromal cells and vessels images. The functions that can be performed are to color the monochromatic images, merge multiple colored images in to a single image, measure tumor image mean gray levels as a read-out of tumor growth and regression, segment the tumor structures for further image analysis, and threshold micrographs of the VMO/VMT vessel structure for further image analysis. From the Hughes Lab Tools >VMO Tools >All VMO Scripts menu item (Figure 3.3a), one or more of the functions can be invoked from a unified VMO function selection dialog box (Figure 3.3b).

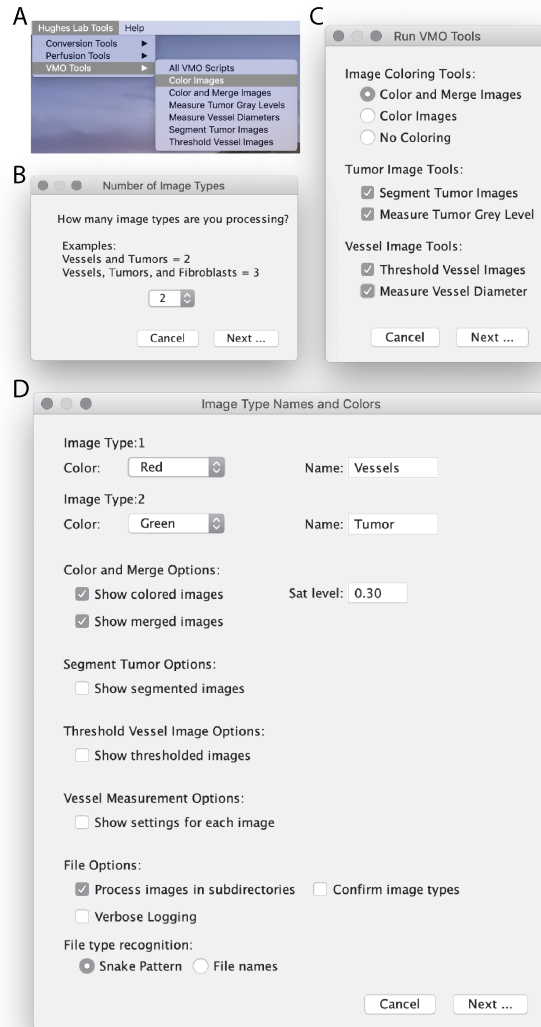


Figure 3.3 – Hughes Lab Tools User Interface (a) Tool selection drop-down menu. (b) Unified VMO function selection dialog box. (c) Dialog box for the selection of the number of image types. (d) Dialog box with functions specific options.

After one or more functions have been selected and the user clicks the Next button, the user is prompted to indicate the number of image types in the sub-directories to be processed (Figure 3.3c). For instance, if the sub-directories contain only vessel images then the image type would be 1, however, if the sub-directories contain images of both vessels and tumors then the image type would be 2. All sub-directories to be processed must contain the same number of image types.

The script offers two methods of identifying the cell type of each image. The first is based on a common procedure used when photographing the cells on the microscope. Often each cell type requires a different microscope configuration to be photographed, and in order to minimize reconfiguration of the microscope, images are usually captured in a “snake” pattern. For example, if there are two image types, and three chambers were photographed, the sequence of image types would be Vessel, Tumor, Tumor, Vessel, Vessel, Tumor. Using the snake pattern image classification method there is an assumption that the images will be placed in one or more folders where the images will be numbered sequentially corresponding to the pattern. Alternatively, the image files can be named with a hint about the image type. Using the File Name Recognition Image File Classification Method option the user must name each image file using the following basename template : d#-c#-x, where d stands for device, c stands for chamber, # are the device and chamber numbers and x is the first letter of the image type. For example, a series of images may be named d1-c1-v.tif, d1-c1-t.tif, d1-c2-v.tif, d1-c2-t.tif, d1-c3-v.tif, d1-c3-t.tif.

With either image classification method, the results can be verified, and overridden if necessary, by checking “Confirm image types”. When checked the user will be presented with a dialog box as each image is opened to confirm the image type has been identified correctly. After choosing the number of image types contained in the folders to be processed, the user is presented with a dialog box containing options for the selected functions. Only options relevant to the functions selected will be presented to the user. Figure 3.3d shows options for the various functions to be run. The dialog box includes options to specify how images should be colored, assign names to the images, show various processed image types, specify whether the operations should be applied to only the images in the chosen directory or recursively to all sub-directories, whether each image should be presented to the user to confirm the image type or not, and whether or not to present a verbose log of all operations performed to the user. Depending on the options selected, the user can quickly process hundreds or thousands of images with no intervention, or monitor inter-

mediate results to confirm image processing is progressing as expected. Upon clicking Next the user is presented a directory chooser to specify the location of the images, and optionally sub-directories, to be processed.

3.4.2.1.1 Running a single function

If it is desirable to run a single function (e.g. Color Images) rather than multiple functions on each image, a series of shortcut scripts (Figure 3.3a) are included in the Hughes Lab Tools >VMO Tools menu. Each script bypasses the initial unified VMO function selection dialog box and immediately presents the dialog box for selecting the number of image types. Next, a function specific set of options is presented to the user. These scripts are provided as a convenient way to skip the functions dialog box, further reducing the time required for a user to process a large number of images.

3.4.3 Convert ND2

Found under the Hughes Lab Tools >Conversion Tools menu item, this function batch converts Nikon ND2 microscope images to TIFF format for ease of processing. The conversion tool is dependent on the BioFormats^[140] plugin included with Fiji. When run, the user will be prompted for the location of the ND2 files to be converted. After a location has been chosen, the Fiji Log window will show the detailed progress of the tool and an indication of when the tool has completed. The tools will recursively process all ND2 files under the directory chosen so care should be taken to choose the appropriate root directory. An example of the log window output of the Convert ND2 tool can be seen in Supplemental Figure 3.4.

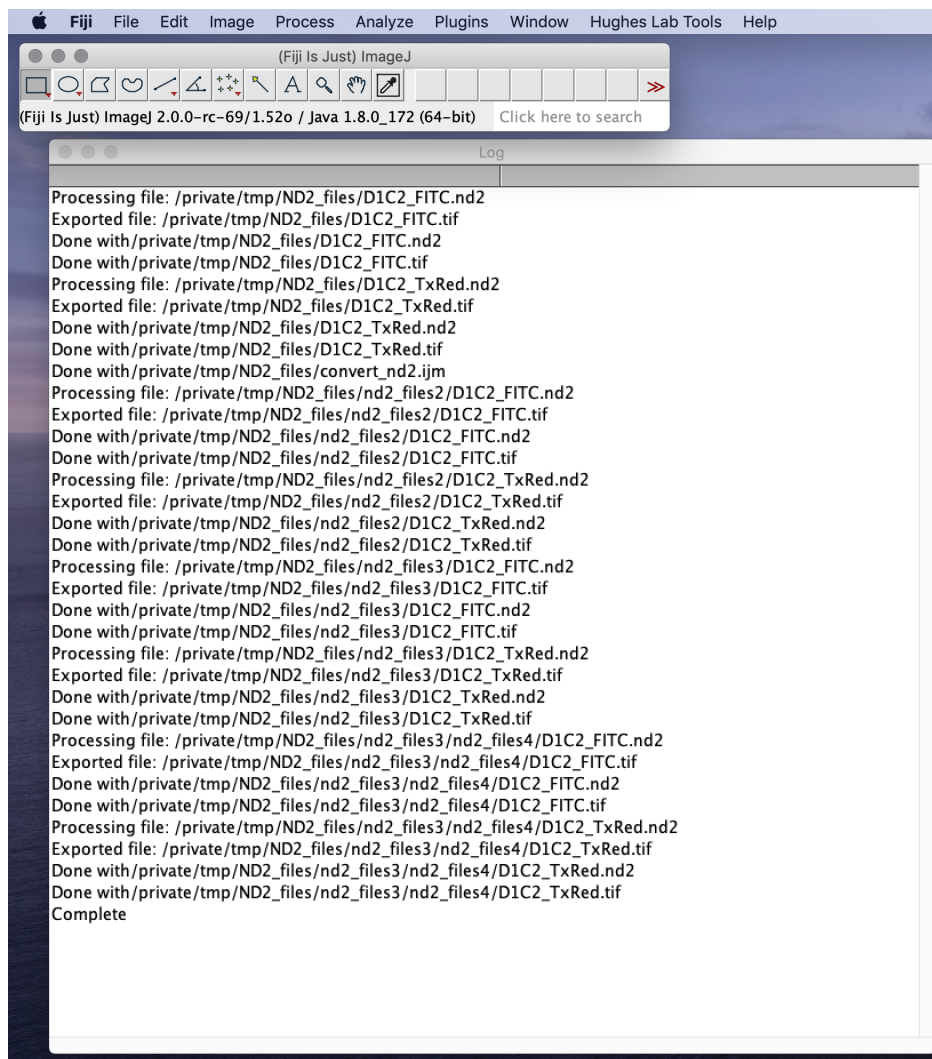


Figure 3.4 – ND2 Convert tool log window

3.4.4 Color and Merge Images Module

FITC- and mCherry-labeled cells grown in the VMT are standardly photographed as monochromatic images. The Color and Merge Module of VMO Tools colors monochrome micrograph images. As suggested in the options dialog, the color of each image type can be specified. The resulting colored images are saved in a sub-directory named “Colored” using the JPEG[167][168] file format. After one of each image type specified has been colored, the Color and Merge Module can optionally merge those images into a new image. The resulting merged images are saved as JPEGs in a sub-directory named “Merged.” Figure

3.5a and 3.5b show examples of unprocessed and colored Vessel, Tumor and Stromal Cell images. Figure 3.5c shows the results when the three images are colored and merged into a single composite image. Composite images are saved into a sub-directory named “merged” with the file name “composite_#” where # is incremented starting with 1 for each composite image saved.

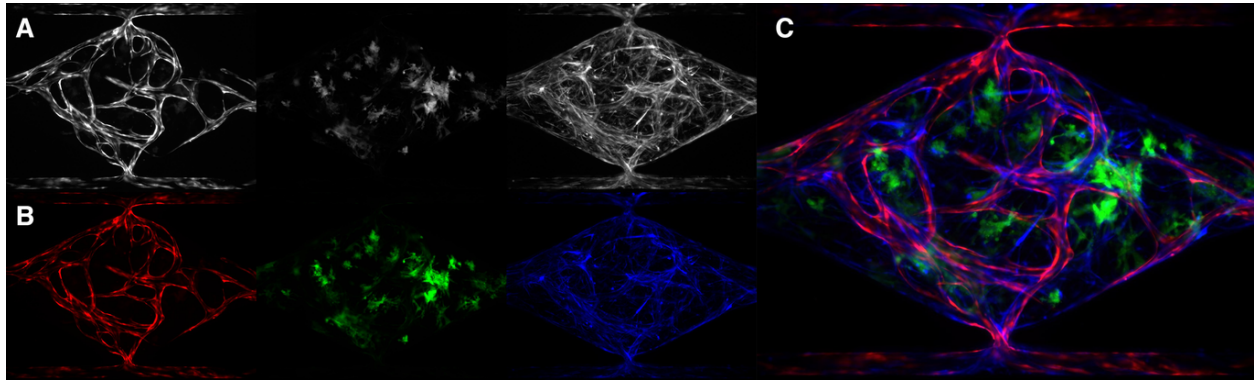


Figure 3.5 – Color and Merge Images function (a) unprocessed images. (b) resulting colored Images from 3.5a (c) composite image from merging colored vessel (red), tumor (green), and stromal cell (blue) images shown in 3.5b

3.4.5 Segment Tumor Images Module

The Segment Tumor Images Module of VMO Tools segments the tumor portion of the photomicrograph from the background and the total area, mean gray value, and total integrated density are measured. Each tumor image undergoes thresholding using an iterative minimum cross entropy thresholding algorithm[136] and converted to a mask. The resulting images are saved in a sub-directory named “Segmented” as JPEGs and the measurement results are saved to a Comma Separated Values (CSV) file. Figure 3.6 shows an example tumor image before and after segmentation and the resulting data in a spreadsheet.

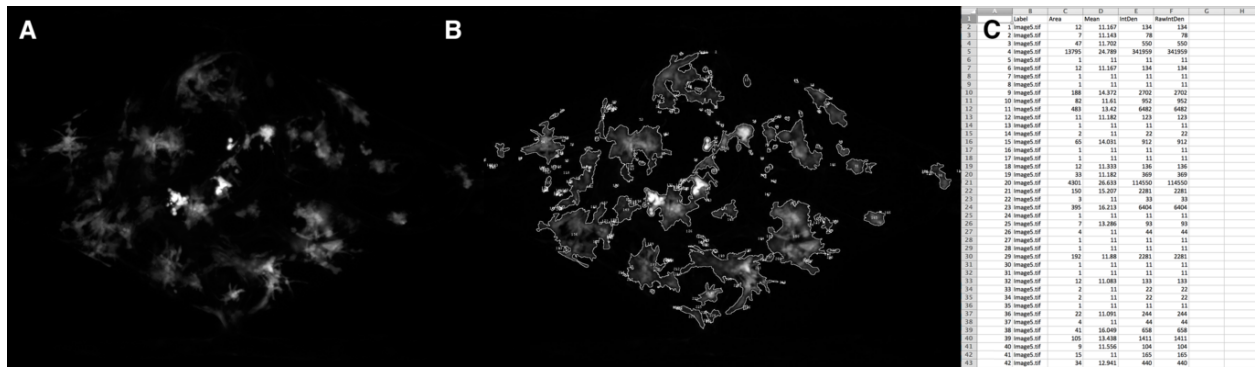


Figure 3.6 – Tumor Segmentation and Measurement function. (a) Tumor image prior to segmentation (b) Segmented tumor image (c) Resulting data

3.4.6 Measure Tumor Gray Level

The Measure Tumor Gray Level Module of the VMO tools measures the mean gray value, modal gray value, minimum gray value, and the standard deviation of the gray value for an entire tumor image. The measurement results are saved to a CSV file in a sub-directory named “measured_gray”.

3.4.7 Threshold Vessel Images

The Threshold Vessel Images of the VMO tools thresholds each vessel image using an iterative minimum cross entropy thresholding algorithm[136] and converts the threshold to a mask. This process greatly standardizes and simplifies downstream image manipulation for measurements of vessel structure and fluid flow simulations. The resulting images are saved as JPEGs to a sub-directory named “threshold” with the file name corresponding to the original file name appended with “_threshold”. Figure 3.7 shows an example vessel image before and after thresholding.

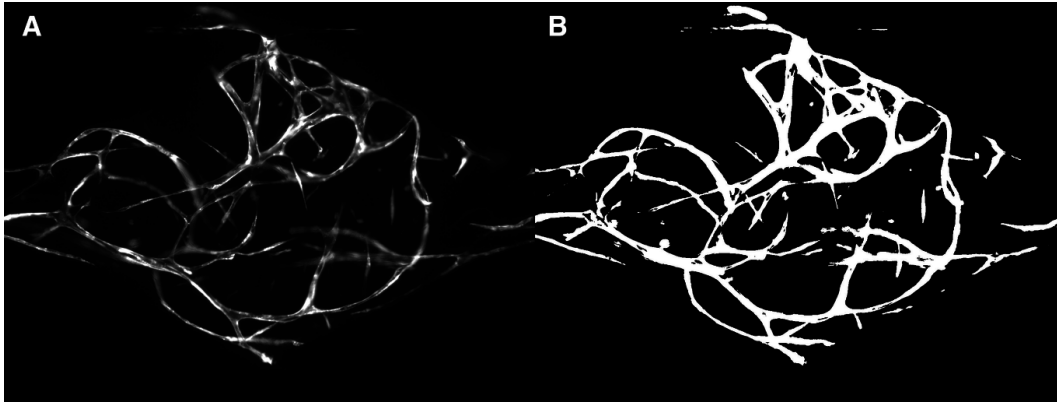


Figure 3.7 – Vessel Thresholding function. (a) Unprocessed vessel image (b) Resulting threshold vessel image

3.4.8 Measure Vessel Diameter

Mean vessel diameter is a measurement that describes the mean width of sampled blood vessels in an imaged blood vessel network. Although vascular biologists frequently rely upon this quantitation to describe blood vessel networks *in vivo* and *in vitro*, there are few existing tools available to automatically and systematically measure mean blood vessel diameter; instead, individual vessel diameter are often measured manually in image analysis software like ImageJ. However, given the tedious nature of manual measurements as well as the inherent subjectivity of manual methods, manual measurements of vessel diameter are time-consuming, prone to low sampling number, and vulnerable to investigator bias in sampling.

To address these issues, we have developed a tool to automatically detect the coordinates of blood vessel objects in segmented network images and to measure the corresponding vessel diameters of each object coordinate. In brief, the segmented image is scanned in the horizontal and vertical directions to detect and store the coordinates of positive vessel objects by comparing positive signal against mean background signal. Next, the boundaries of vessel objects in the horizontal direction at each measurement coordinate is identified, and a line selection is set at the midpoint of each vessel object and rotated

to identify the shortest vessel diameter that can be measured at that coordinate; vessel diameter is determined by comparing positive signal along the length of the line selection against background. Each vessel diameter measurement is then output into the Results window in pixel units and saved in a tab delimited CSV file, and the vector of the measured vessel diameter is stored as an image overlay on a duplicate results image that is created and saved by this tool.

Users can modify the function of this tool in the initial dialogue window (Figure 3.8a) by setting the maximum number of measurements to record, the minimum and maximum size of vessel objects to include in the analysis, the vertical (vertical scan step) and horizontal (scanning resolution) step sizes used in scanning for vessel objects, and the sensitivity of the tool to LUT values at object boundaries. Using the default settings for these values, a representative network image was analyzed. 248 vessel diameter measurements were collected and the resulting results images showing the measurement vector overlay is displayed in Figure 3.8b–3.8c. Figure 3.8b shows that the tool is able to discriminate between linear vessel segments and branchpoints where several segments converge, and that it only samples in linear regions to minimize sampling artifacts; however, the tool settings can be adapted to encourage sampling in areas of vessel convergence if the user so desires. In Figure 3.8c, an analyzed vessel segment is highlighted to show that automatically determined diameter measurement vectors are reasonably placed, and that each vessel segment is sampled across its entire length. Each vector is also labeled with its corresponding coordinate number to allow users to perform post-hoc removal of unwanted measurements from the dataset. The tool shows no bias towards horizontally vs. vertically-oriented vessels; instead, the tool samples evenly across the entire imaged network.

The strength of this tool is that it significantly increases sampling rate (number of measurements / analysis time) (Figure 3.8e) while generating data comparable to conventional,

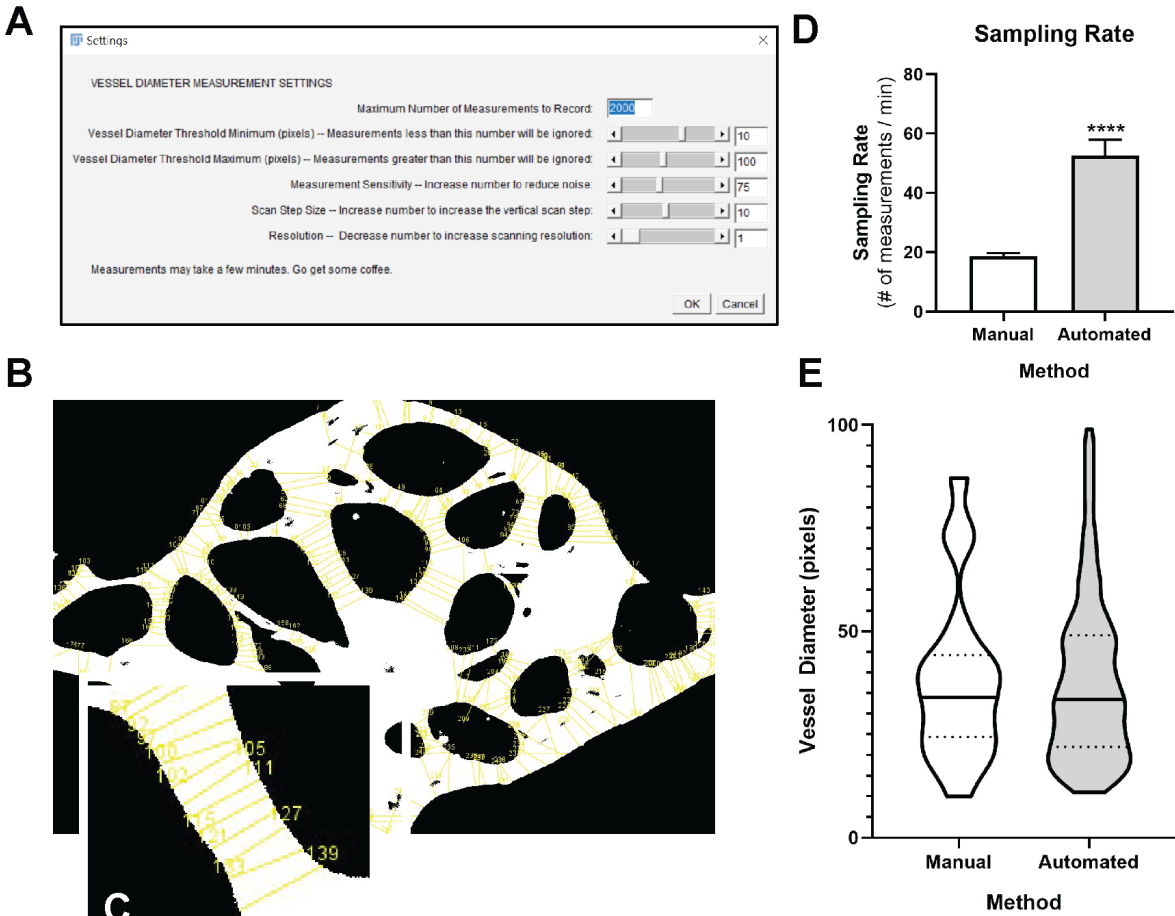


Figure 3.8 – An Automated Method of Measuring Vessel Diameter is Comparable to Manual Methods. (a) Dialog window showing variable parameters for our automated script. (b) Representative output of a segmented vessel network image following measurement of mean vessel diameter using our automated script and its default settings. (c) Inset showing the automatically placed vessel diameter vectors along the length of a blood vessel in the network. (d) Sampling rate is significantly increased in the automated method compared to manual measurement. (f) For the network shown in 3.8c, both automated (>350 measurements) and manual (~50 measurements) methods of measuring mean vessel diameter yield a comparable set of diameter measurements, with a similar mean, median, and standard deviation.

manual methods of analysis. Automatically measured vessel diameter datasets are comparable to those generated manually (Figure 3.8f): a representative network measured by both methods yields vessel diameter datasets with similar means, medians, and distributions, even though the automated dataset includes more than ten times as many measured vessel coordinates. Across many sampled networks measured by both manual

and automated methods, the mean vessel diameters measured by either approach are nearly equivalent.

3.4.8.1 Perfusion Coefficient

Perfusion Coefficient, found under the Hughes Lab Tools Perfusion Tools menu item, allows the user to select a region of interest (ROI) outside the microvascular network to be measured for permeability coefficient calculation. Permeability is a functional readout of vascular patency in the VMO/VMT models, as well as in *in vivo* assays, and is visualized by leak of small molecular weight fluorescent-dextran into the extracellular space outside the vasculature. The first dialog box will prompt the user to choose an ROI radius, in pixels, with default set to 25. Depending on the density of the microvascular network, an ROI radius in the range of 15–50 pixels is likely appropriate. In the next dialog box, the user will specify the number of images in the time course, with 3 as the default setting, after which the user will be prompted to find the location of the images and sequentially open each image within the function. Next, the user is given the option to run the manual aligner to specify the chamber coordinates, in case the chamber is misaligned in any of the time-course images. If run, the user will be prompted to adjust the lines in each image to the center of the communication pore and the center of the chamber. Once alignment is completed, the user will be prompted to choose areas to place the ROIs, and a confirmatory dialog box will then allow the user to either proceed with the analysis or change the ROIs. In the latter situation, the user can move the placement of the ROIs by clicking and dragging existing ROIs to a different position or adding additional ROIs by clicking in an unoccupied area. By proceeding, all ROIs will be measured and results output into a CSV file and a stack of ROI labeled images within a folder named “Perfusion”.

Our VMO/VMT model is currently the only *in vitro* assay to incorporate a living and perfused vascular network that transports nutrients to the tissue construct, mimicking *in vivo*

capillary bed function as well as drug delivery. We standardly perfuse the networks with 70 kD FITC- or rhodamine-dextran to confirm the patency of the microvessels and detect changes in permeability. By visualizing perfusion throughout the tissue chamber, we can then note changes due to disease condition (e.g. increased permeability or “leaky” vessels in the presence of high grade tumors). To show the responsiveness of the microvessels formed within the device, thrombin, a known vascular disruptor, was perfused through the VMO-associated vessels and perfusion measured via Perfusion Coefficient tool. Figure 3.9a shows VMO perfusion at time 0, 10 and 20 minutes under control and thrombin-treated conditions. Resulting images with selected ROIs are shown in Figure 3.9b, with quantification of images confirming the increase in vascular permeability induced by thrombin in the VMO.

3.4.8.2 Fluid flow simulations on living vessel network

After creating and further processing threshold vessel images, fluid or cell flow dynamics through the vascular network can be simulated using COMSOL Multiphysics Modeling software. To determine whether the COMSOL simulation on a 2D projection of the vessel network is representative of actual fluid velocity in our system, we perfused VMOs with 2 μm fluorescent beads and simulated the process using COMSOL (Figure 3.10). In Figure 3.10a, resulting fluid velocity and streamline profiles are shown for a living and perfused vascular network. Individual beads were then tracked, both in the simulation (Figure 3.10b) and experimentally (Figure 3.10c), flowing through the vascular network. In the VMO, the fluid velocity was calculated in each vessel segment per given time frame (distance bead traveled in $\mu\text{m/s}$ determined by imaging frame rate), and these values were then directly compared with the COMSOL simulation results. By using the Hughes Lab Tools threshold vessel image as input, the resulting simulation realistically modeled the actual fluid flow and velocities in the vascular network. We measured the distance 100

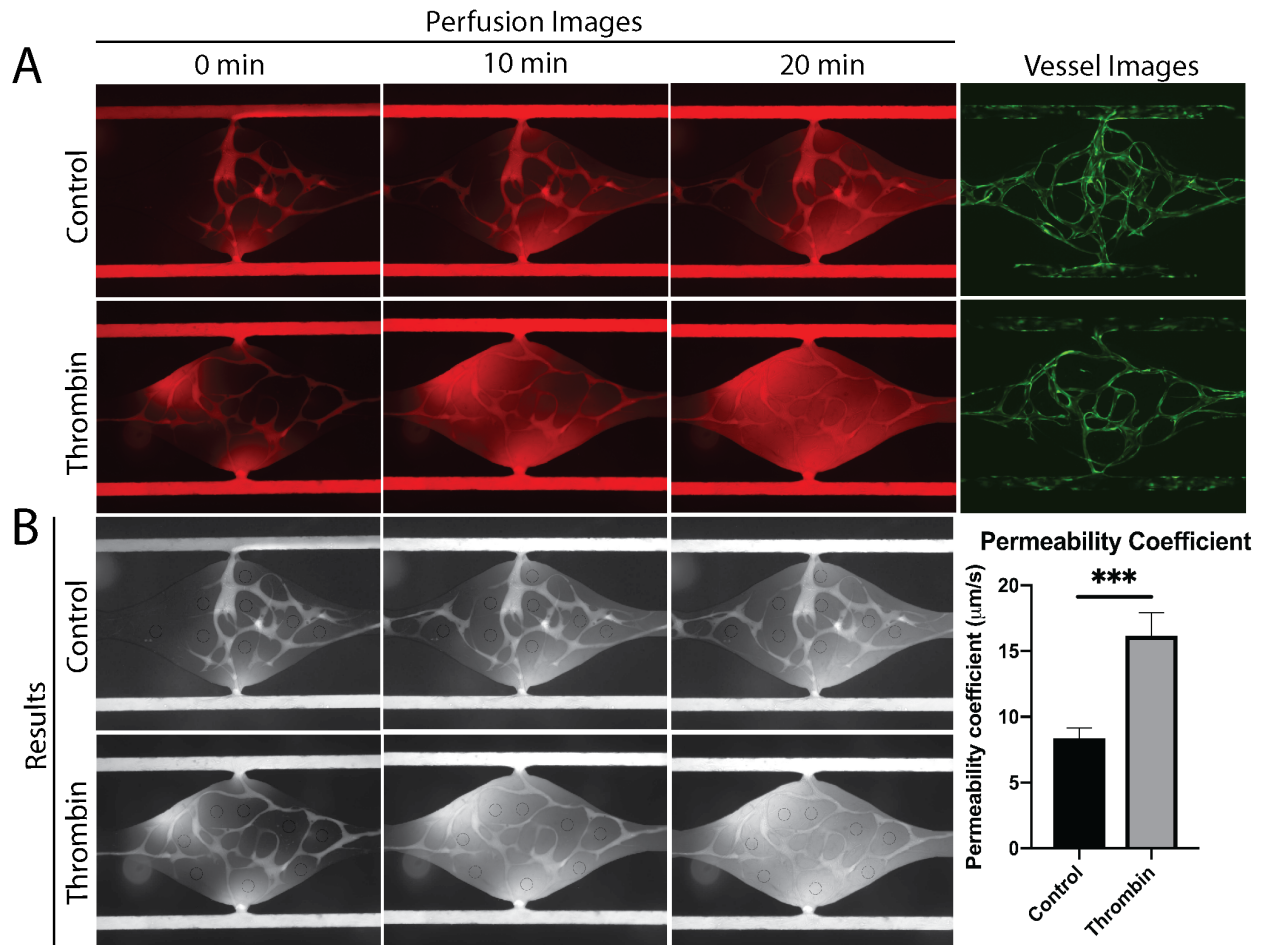


Figure 3.9 – Thrombin-induced vascular leak in the VMO (a) Perfusion of 70 kD rhodamine-dextran through the vasculature of control and thrombin-treated VMO at 0, 10 and 20 minutes. Associated GFP-labeled vessel images on the right. (b) Images resulting from the Perfusion Coefficient processing and quantification of results.

single beads traveled through each segment in the vascular network and found that, with direct comparison to velocity values simulated in COMSOL for the same segments, the Spearman’s rank correlation coefficient indicated strong correlation at $r = 0.8$ ($p < 0.001$) (Figure 3.10d). This serves as validation that Hughes Lab Tools vessel threshold images input into COMSOL Multiphysics modeling is a robust and reliable method for determining fluid flow velocity through the vasculature of the VMO.

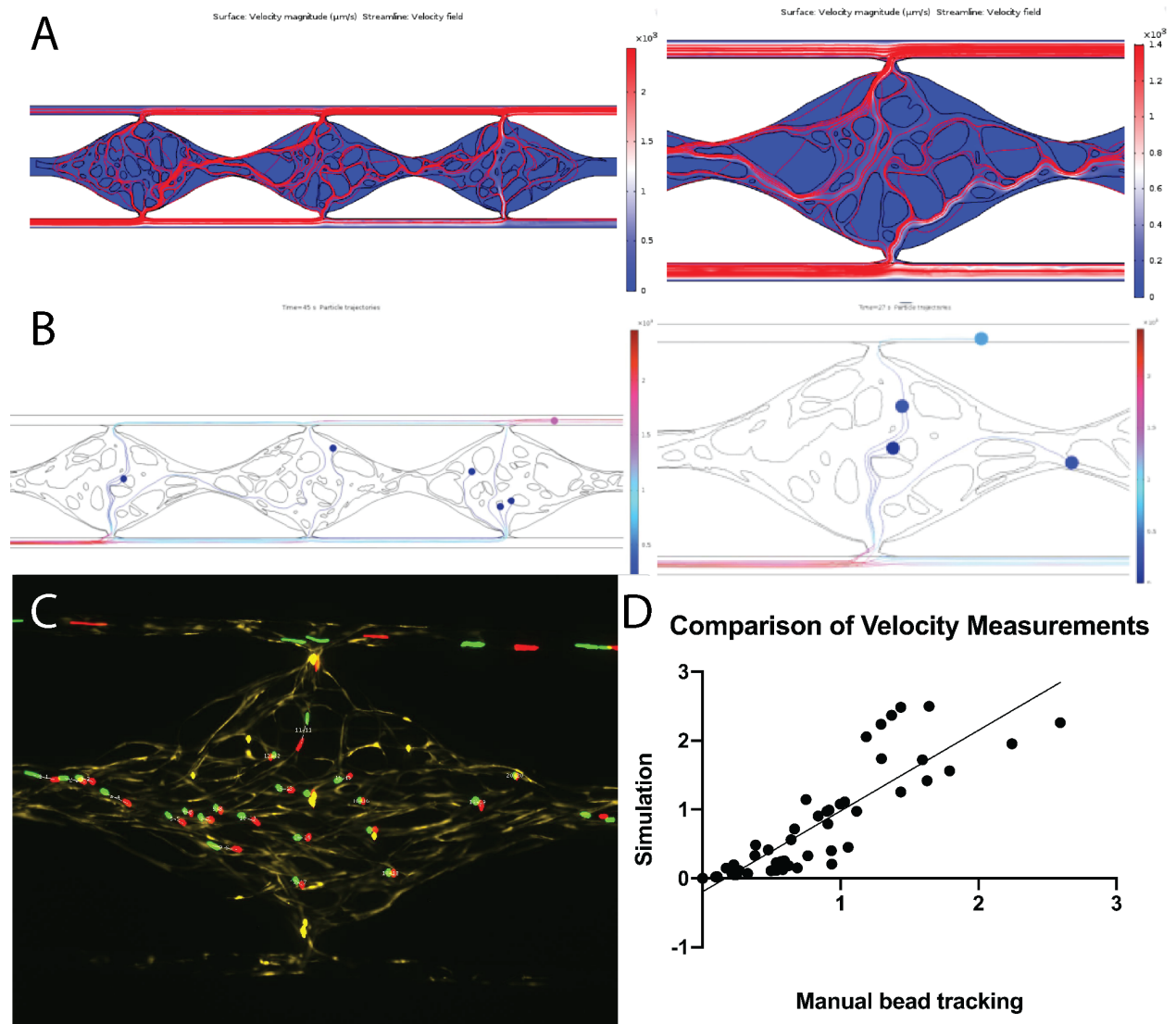


Figure 3.10 – Streamline profile and bead tracking simulation using thresholded vessel images. (a) Color map of fluid flow velocity magnitude through the VM0 in $\mu\text{m/s}$ with streamlines in red. Right: Close-up of a single tissue chamber. (b) Bead tracking simulation still with close-up of a single tissue chamber on the right. (c) Merged fluorescent image of middle tissue chamber. FITC-labeled $2 \mu\text{m}$ beads were perfused through the network and tracked to determine velocity in $\mu\text{m/s}$. Images of later time-points were pseudo-colored red, merged with earlier time-points in green, and distance between green and red beads were measured in ImageJ. (d) Quantitation of comparison between bead velocities by manual tracking vs simulation. A high degree of correlation is observed ($r = 0.8$).

3.5 Discussion

We have outlined the use of an ImageJ suite to automate repetitive tasks for the processing and analysis of VMO/VMT micrographs. The Hughes Lab Tools provides a simplified, user-friendly and standardized method to efficiently extract imaging data for large scale analyses. This computational tool is especially suitable for high throughput applications such as drug screening because the end-user has the option to choose the location of the images or to process images in sub-directories to allow for an extensive series of images to be processed in seconds. For reference, using a 2014 Macbook Pro 11.3 with a 2.8GHz Intel Core i7 processor with 16GB of RAM, a 1TB Apple SM1024F SSD, and an NVIDIA GeForce GT 750M GPU, the Hughes Lab Tools was able to process (color, merge, threshold) 600 images (300 tumor/vessel pairs) in 48.029 seconds. The time required for a trained, expert end-user to manually process a single tumor/vessel pair was approximately 3 minutes. Extrapolating, this would mean the same 600 images would require a minimum of 15 hours for the trained, expert end-user to process. That time only includes active time clicking in ImageJ and does not include breaks, slow downs due to fatigue, and correction time required for inevitable mistakes associated with doing a repetitive task.

Segmenting and measuring tumors adds a significant amount of time to manually process the images. The time required for a trained, expert end-user to manually process a single tumor/vessel pair was approximately 6 minutes, extending the extrapolated time for 600 images to approximately 30 hours. In contrast, the Hughes Lab Tools suite was able to color, merge, threshold, and measure the tumors of 600 images (300 tumor/vessel pairs) in 72.423 seconds. The significant amount of time saved by using the macro to automate repetitive tasks vs processing the images manually is especially critical for high throughput applications of the VMO/VMT. By contrast, for an expertly trained user, the same manual routine takes approximately 6 minutes to process only 1 vessel/tumor image pair.

The range of functions and user-friendly interface provided by Hughes Lab Tools allows the investigator flexibility to meet experimental needs while also maximizing data output. ImageJ is an open-source and freely distributed software that is commonly used for research applications to process biological images. Here we show the Hughes Lab Tools to be a robust, reliable and flexible tool for high throughput analyses and disease modeling applications in the VMO/VMT model. Hughes Lab Tools can also be used to simply process a large dataset of VMO/VMT images by quickly coloring and merging images for experimental reference and publication. Importantly, the vessel thresholding function of our macro creates images that can be imported into COMSOL Multiphysics software for realistic fluid flow modeling, which we have validated by comparing simulated velocity with actual fluid velocity measurements. The correlation between predicted and actual velocity values was found to be strong, with $r = 0.8$ ($p < 0.001$). Importantly, the script structure allows the user flexibility to easily add additional functionality to tailor data processing and analyses to specific research questions.

3.6 Conclusion

Nearly every tissue in the body receives nutrients and oxygen through the vasculature, making it a critical component for realistic disease modeling and drug screening. Moreover, several malignancies and disease states are defined by vascular endothelial dysfunction and hyperpermeability, such as diabetic retinopathy and cancer. Our lab has validated a microphysiological system that supports the formation of a living, perfused vascularized micro-organ (VMO) or micro-tumor (VMT) for disease modeling, drug screening and personalized medicine approaches. Yet the huge amount of imaging data that can be derived from each VMO or VMT tissue chamber micrograph, especially in the context of high throughput experiments, is too onerous for the investigator to extract manually.

We have developed the Hughes Lab Tools to aid researchers in efficiently processing and analyzing complex sets of images in a standardized manner. As the VMO/VMT platform sees wider adoption, we anticipate the Hughes Lab Tools to have broad applicability as an easy-to-use tool to accelerate VMO/VMT data analyses to answer complex physiological questions.

Chapter 4

A Vascularized Micro-Tumor Model to Study Patient-Derived Colorectal Cancer Cells

4.1 Introduction

Approximately 95% of anti-cancer agents fail to demonstrate efficacy in clinical trials despite showing promise during preclinical study, and those that do gain FDA-approval confer marginal survival gains at best[223]. The low rates of effective preclinical compounds reaching the clinic can be largely attributed to drawbacks in current model systems that are poor predictors of drug response in patients[80]. Moreover, efforts to develop individualized treatment regimens that lead to durable responses have been hampered considerably by inter- and intra-patient tumor heterogeneity and the complexity of underlying biologic pathways[49]. Although clinical benefit derived from current biomarker-guided therapeutic strategies is limited, most therapy decisions in oncology are still carried out

at the population level. A major obstacle to personalized cancer treatment is the lack of a technology that can identify drug sensitivity, and predict clinical benefit, to guide cancer management for each individual patient. Indeed, current model systems for drug screening fail to recapitulate the complex, heterogeneous 3D cell-cell interactions and microenvironment of a vascularized human tumor *in vivo*. Moreover, standard research practice involves testing established cell lines that, after maintenance in cell culture for years, are no longer representative of the disease from which they were derived and do not yield individualized information about drug response for each patient. Failure of pre-clinical models to mimic the patient-specific disease condition leads to the development and clinical testing of ineffective, and often harmful, drugs on patients. Moreover, current standards for personalized medicine involve physicians choosing drugs for their patients based on aggregated data, which does not mean that, because a drug works on many patients, it will work on any given individual. A new approach to personalized medicine is necessary to ensure that the most clinical benefit, with the least toxicity, is consistently achieved from therapy for each individual patient.

The ability to directly grow and study samples from patient tumors is a crucial technology in the development and testing of new therapies toward personalized medicine in oncology. Several groups now report reliable derivation of tumor cultures for drug screening and molecular studies. To date, contributions to the field include the establishment of patient-derived cancer cell and fibroblast monolayer co-cultures[127, 48], explant cultures in which primary resected tumors are thinly sectioned onto an extracellular matrix[145], and organoids, which are cultured 3D tumors derived from cancer cells seeded into a basement membrane extract such as Matrigel[204, 256]. While these models reproduce certain features of primary-derived tumors and have been used for drug sensitivity studies, these same models fail to recapitulate the complex and dynamic cell-cell interactions and architecture of a vascularized tumor mass growing *in vivo*. Furthermore, the static

culture systems utilized in such models preclude long-term molecular and drug screening studies, since limited nutrient and oxygen diffusion restricts cell growth and survival.

To address the need for improved preclinical models, we have designed, fabricated and validated a microfluidic device that supports the formation of a dynamic tumor ecosystem – the vascularized micro-tumor (VMT)[224, 180]. Via co-culture of multiple cell types in an extracellular matrix under dynamic flow conditions, a perfused vascular network forms *de novo* and feeds the growing tumor mass just as it occurs *in vivo*. This is a truly novel platform as it is the only one where survival and growth of the tumor is entirely dependent on flow of nutrients through the living vascular network. We have previously shown that, in contrast to 2D and 3D monocultures, the VMT reproduces the growth and drug sensitivity of *in vivo* tumors and recapitulates expected drug response based on subtype-specific molecular programs activated in the tumor stroma. Furthermore, the VMT closely models gene expression profiles of *in vivo* tumors at bulk and single-cell RNA sequencing resolution, capturing clinically relevant tumor heterogeneity not seen in 2D or 3D monocultures. We now show that the VMT model reproducibly supports the growth and long-term culture of patient-specific tumor cells derived from small fresh CRC biopsies and surgical resections, and that the VMT accurately models tumor heterogeneity and drug response seen in clinical specimens. Herein we outline our methods for generating patient-derived VMT (pVMT) and demonstrate the ability to interrogate *ex vivo* response to standard chemotherapeutics and novel compounds using pVMT. A translational infrastructure providing real-time information from patient-derived tumor cells in our VMT, as established in this study, will support efforts to improve patient outcomes. Most importantly, our system will allow patients to avoid months taking drugs that are not going to work.

4.2 Methods

4.2.1 Sample collection

Tissue was collected under protocols approved by UCI IRB in accordance with the principles of ethical human subjects research. Written informed consent was obtained from all patients prior to enrollment in the study. The population was sampled from patients >18 years of age treated for CRC at UCI Medical Center (MC) in Orange, California. Patients with a known diagnosis of CRC who were already planned to undergo medically necessary endoscopic sampling or operative tumor resection were approached by their treating physician to provide written informed consent. Willing and eligible patients underwent an additional endoscopic biopsy from visualized tumor during endoscopy or, from surgical specimens, excess tissue not needed for diagnostic purposes was donated to the Hughes lab. Samples were deposited directly into a conical tube with basal cell culture media on ice for immediate transport to UCI Main Campus for processing. All samples were deidentified to the Hughes lab.

4.2.2 Tissue processing

Laboratory personnel are trained annually in the safe handling of bloodborne pathogens and observe biosafety level III precautions while handling biohazardous or toxic materials. Surgical specimens were cut into ~1 mm pieces using a scalpel and biopsies were broken into small pieces with pipetting. Tissue pieces were portioned for RNA and DNA isolation, fixation with 4% PFA for immunostaining, with at least 50% of the tissue reserved for cell culture. Portions reserved for cell culture were then resuspended in a 300 U/mL collagenase type III HBSS solution and digested at room temperature with vigorous shaking

for 30 minutes at a time. Every 30 minutes, single cells and cell clusters were removed from the digestion, neutralized with medium and collected by centrifugation at 340 x g for 3 minutes. Cells were then resuspended into colorectal cancer initiating-cell (CCIC) supplemented media[218] and plated into ultra-low attachment plates. The procedure was repeated until all the tissue was fully digested.

4.2.3 Cell culture

Tissues were transported in serum-free DMEM with 4.5 g/L glucose, sodium pyruvate and L-glutamine with 1x P/S and antimetabolic/antimycotic. CCIC media consisted of DMEM F12 50:50 media with L-glutamine supplemented as indicated in 4.1 and 4.2 below:

Reagent	[Original]	[Final]	Volume for 50 ml
DMEM F12 50:50 media	n/a	n/a	48 ml
Non-essential amino acids	100x (10 mM)	1x (0.1 mM)	500 µl
Pen-strep	100x	1x	500 µl
B27 supplement	50x	0.2x	200 µl
Heparin	2 µg/µl	4 µg/ml	100 µl
Sodium pyruvate	100x	1x	500 µl

Table 4.1 – CCIC basal media

The following were added freshly to basal CCIC media:

Reagent	[Original]	[Final]	Volume for 50 ml
DMEM F12 supplemented as above	n/a	n/a	50 μ l
bFGF	100 ng/ μ l	20 ng/ml	10 μ l
EGF	0.5 μ g/ μ l	40 ng/ml	4 μ l
N2	100X	1X	500 μ l

Table 4.2 – CCIC complete media

Endothelial growth medium-2 (EGM2) was obtained from Lonza (Basel, Switzerland), DMEM was from Corning (Corning, New York), and Fetal Bovine Serum (FBS) was from Gemini Bio Products (Sacramento, California). Endothelial colony forming cells (ECFC, hereafter termed EPC for endothelial progenitor cells or EC for differentiated endothelial cells) were isolated from human umbilical cords obtained from the UCIMC under an approved IRB protocol. Normal human lung fibroblasts (NHLF, hereafter termed LF) were purchased from Lonza (Basel, Switzerland), CRC cell lines (SW480 , HCT116) were given to the lab from UCI’s Chao Family Comprehensive Cancer Center and previously established CCIC lines (1024, 5707, 5823-3, J774, J906, and J919[231]) were from Dr. Steven Lipkin at Cornell University. EPC were cultured in EGM2 and used between passages 4–8. LF (used between passages 4–9), SW620, SW480 and HCT116 were cultured in DMEM containing 10% FBS. Cells were cultured at 37 °C in a 5% CO₂ incubator. The EPC and cancer cells were transduced with lentivirus expressing mCherry (LeGO-C2 (plasmid # 27339)) or green fluorescent protein (GFP) (LeGO-V2 (plasmid # 27340), from Boris Fehse (Addgene, Massachusetts). Cells were washed with HBSS (Thermo Fisher Scientific), harvested using TrypLE express enzyme and collected by centrifugation at 340 x g, 22 °C for 3 minutes. Primary tumor cells were fed with fresh organoid media supplemented with 10 μ m Rho kinase inhibitor Y-27683 every 2–3 days and expanded for no more than 7–10 days prior to device loading. Isolated tumor cells are labeled with membrane dye (CellBrite Cytoplasmic Membrane

Dye, Biotium) for visualization and mixed with fluorescently labeled endothelial cells and fibroblasts in ECM within the device.

4.2.4 Immunofluorescent staining

The VMTs are fixed for immunostaining by perfusing 4% paraformaldehyde (PFA) through the medium inlet for 30 minutes at room temperature. After fixing, PFA is replaced with 1X DPBS to wash for 1 hour at room temperature, or overnight at 4 °C. The platform is inverted and the bottom polymer membrane is carefully removed. Each VMT is washed with 1X DPBS once before permeabilizing for 15 minutes with 0.5% Triton-X100 diluted in DPBS. After permeabilization, VMTs are blocked with 10% goat serum for 1 hour at room temperature and then incubated with primary antibody overnight at 4 °C. After washing with 1X DPBS, VMTs are incubated with goat anti-rabbit secondary antibody (1:2000 dilution in 5% serum) for 2 hours at room temperature before washing with DPBS and counter-staining with DAPI. Finally, anti-fade solution is added on top of each VMT before mounting with a glass cover slip. Established cell lines were seeded into multi-well slide chambers and subsequently processed by the same protocol. Paraffin embedded and sectioned xenograft tumors were processed by the same protocol, starting at the blocking step.

4.2.5 Fluorescent imaging

Objective tumor and stromal response was monitored in real-time using fluorescence microscopy. Fluorescence images were acquired with an Olympus IX70 inverted microscope using SPOT software (SPOT Imaging, Sterling Heights, Michigan). Confocal images were obtained using a Leica TCS SP8 (Leica) microscope. Fluorescence lifetime imaging microscopy (FLIM) was performed on a Zeiss LSM 710 (Carl Zeiss, Jena, Germany) micro-

scope using an EC Plan-Neofluar 20x/0.50 N.A. objective (Carl Zeiss, Oberkochen, Germany). NADH was excited by an 80 MHz Titanium:Sapphire Mai Tai Laser (Spectra-Physics) at 740 nm. Individual cells were imaged with a size of 256 x 256 pixels and a scan speed of 25.21 μ sec/pixel. A total of 50 frames were collected and integrated for each fluorescence lifetime image. The excitation and emission signals were separated by a 690 nm dichroic mirror, and a 460/80 bandpass filter and photomultiplier tube (H7422P-40, Hamamatsu Photonics, Hamamatsu, Japan) were used for detection. Frequency domain FLIM data was acquired by the A320 FastFLIM FLIMbox (ISS, Champaign, Illinois) and analyzed by SimFCS software (LFD, Irvine, California, www.lfd.uci.edu).

4.2.6 Fluorescent image analysis

AngioTool software (National Cancer Institute) was used to quantify vessel area, vessel length, number of vascular junctions and endpoints in the VMT. ImageJ software (National Institutes of Health) was utilized to measure the total fluorescence intensity (i.e. mean grey value) for each tumor image to quantify tumor growth. Each chamber was normalized to time zero baseline. Vessels are routinely perfused with 150 kD FITC-dextran to calculate vessel permeability as an indication of vascular integrity. FLIM images were analyzed by the phasor approach as previously described[50]. Briefly, every pixel of the integrated FLIM image is transformed into a point on the phasor plot. The g and s coordinates in the phasor plot are calculated from the sine and cosine components of the Fourier transform of the fluorescence intensity decay of each pixel in the image. By NADH FLIM phasor analysis, we mapped the free to protein bound NADH distribution in the images, which has been correlated to the metabolic state of the biological sample[50].

4.2.7 Microfluidic device fabrication

Device fabrication has been described previously[224, 180]. Briefly, polydimethylsiloxane (PDMS, Sigma-Aldrich) is poured into a customized polyurethane master mold of the VMT device design and allowed to polymerize overnight in a 70 °C oven. The PDMS replicate layer is removed and holes are punched to create inlet and outlets for the media reservoirs and loading chambers. A thin PDMS membrane is then bonded to the device using oxygenated plasma cleaner (Harrick Plasma). The high throughput system (HTS) is further attached to a 96-well open-bottom plastic culture plate via chemical gluing and oxygen plasma bonding.

4.2.8 Loading the microfluidic device

Patient-derived CCIC (2×10^6 cells/mL), EPC and LF (7×10^6 cells/mL) were resuspended in fibrinogen (10 mg/mL in EBM₂). The cell slurry was then mixed with 6 U thrombin (3 U/ μ L) to catalyze gel solidification and quickly loaded into the VMT. Fibrin ECM was allowed to solidify at 37 °C for 15 minutes prior to introducing laminin into the microfluidic channels to promote vessel anastomosis. VMT were fed with EGM₂ and cultured at 37 °C, in either a 5% CO₂/20% O₂ incubator (normoxic condition) or in a 4% O₂ incubator (for low oxygen culture). Media was changed every other day in the VMT and media flow restored every day in the HTS.

4.2.9 DNA and RNA isolation

RNA is isolated from each sample via RNeasy Mini kit (Qiagen) according to the manufacturer's protocol. DNA is isolated using the Zymo MicroDNA kit (Zymo) according to the manufacturer's protocol.

4.3 Results

4.3.1 The VMT model supports the growth of patient-derived tumor tissue.

We have previously validated our VMT model system for cancer-specific disease modeling and drug screening studies using established tumor cell lines[225, 178]. A rational next step in validating the VMT model as a clinically relevant predictive tool in the field of oncology entailed obtaining fresh, treatment-naive colon cancer biopsy and surgical samples from patients during routine, clinically indicated endoscopic or surgical procedures. Cancer stem cells are isolated from primary tissues via gentle digestion and cultured non-adherent in serum-free stem cell media for no more than a week prior to device loading (Figure 4.1).

Once cell numbers are expanded, tumor spheroids are harvested, mixed with endothelial cells and fibroblasts in extracellular matrix slurry, and introduced quickly into the platform. The single unit wide-chamber is arrayed onto a multi-unit chip for high throughput experiments (Figure 4.2a. In response to physiological flow, cells self-assemble into patient-derived vascularized micro-tumors (pVMTs) fed through a fully perfused, living vascular network (Figure 4.2b. Zoom views of fluorescently-labeled, primary-isolated CRC

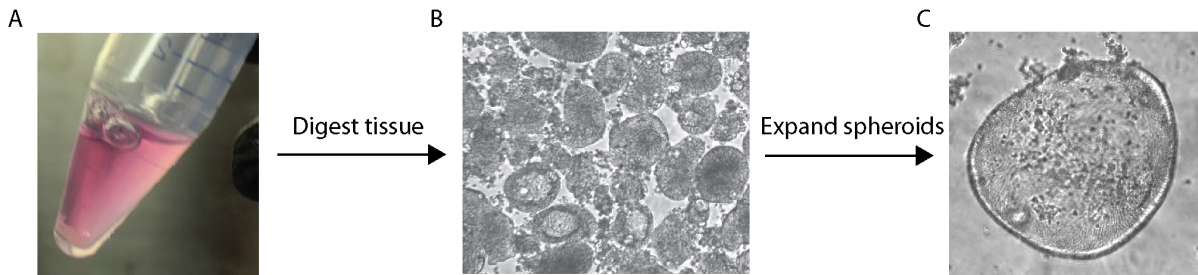


Figure 4.1 – Isolation of primary colorectal cancer-initiating cells (a) Colorectal cancer-derived 1 mm punch biopsies or surgical tissues are freshly collected during routine, clinically-necessary endoscopic sampling or tumor debulking. (b) Tissues are digested and cultured in specialized stem cell medium. (c) Spheroids are expanded briefly in culture and loaded into the device for primary VMT establishment.

initiating cells (CCIC) growing within replicate device units show the tumors integrating with microvessels within the pVMT (Figure 4.2c). Interestingly, the patient-derived samples demonstrate vastly different morphology in the pVMT compared to spheroid culture, with an invasive/mesenchymal phenotype observed in the pVMT that is not seen in the well plates. pVMTs are grown for up to 3 weeks and form fully perfused and functional vasculature by day 5 for drug screening and other molecular analyses.

While we have previously utilized a chip design with three chambers per individual device unit (Figure 4.3a), in order to facilitate loading and distribution of CCIC spheroids, a single, wide channel design was used instead (Figure 4.3b). Dimensions between the two devices are similar, except, to accommodate loading spheroids, the single chamber device has a wider loading channel (0.50 mm compared to 0.20 mm) and contains only one compartment.

The VMT robustly supports the survival and growth of patient-derived CRC tumors from different individuals (Figure 4.4). Via the co-culture of multiple cell types within an extracellular matrix, the dynamic microenvironment of an actual tumor is recapitulated within the pVMTs to support primary CRC tumor histology (Figure 4.5a,4.5b) and growth characteristics (Figure 4.5c) based on pathology and grade. We are currently in the process of

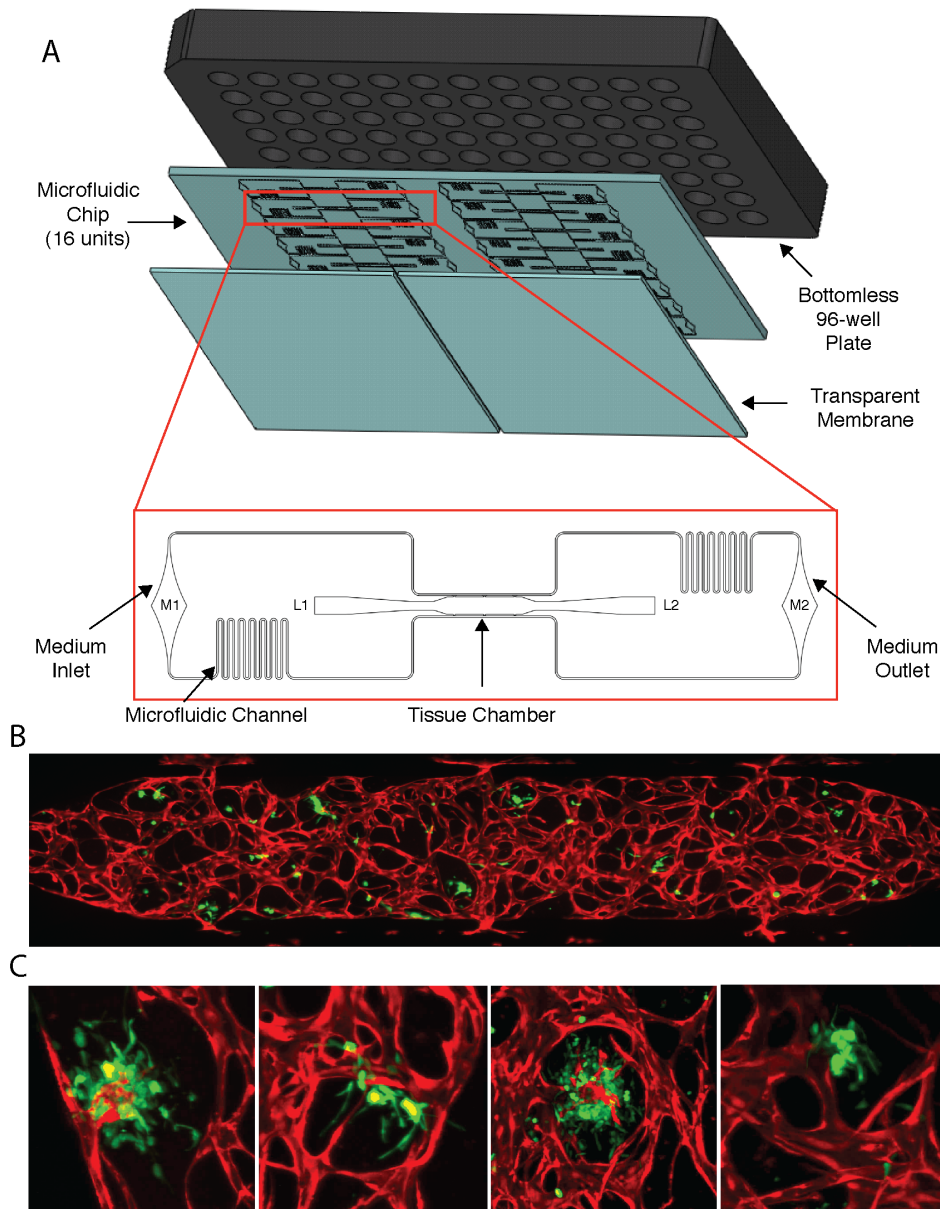


Figure 4.2 – Primary CRC cells grow in a vascularized micro-tumor model arrayed for high throughput experiments. (a) The microfluidic chip is bonded to a bottom-less 96-well plate via chemical glue and oxygen plasma. Zoom view shows a single device unit with a single tissue chamber fed through microfluidic channels, 2 loading ports (L1-2), and medium inlet and outlets (M1-2). (b) Fluorescent image of a patient-derived VMT. P54 CRC primary tumor in green, vessels in red. (c) Zoom views of four individual P54 pVMT replicates. As shown, the tumor closely associates and integrates with the vasculature.

assessing these features for each individually-derived pVMT. Notably, the pVMT not only readily supports tumors derived from advanced stage disease, but also the growth of stage I CRC tumors for which growth has proven to be a major challenge in current culture systems and mouse models.

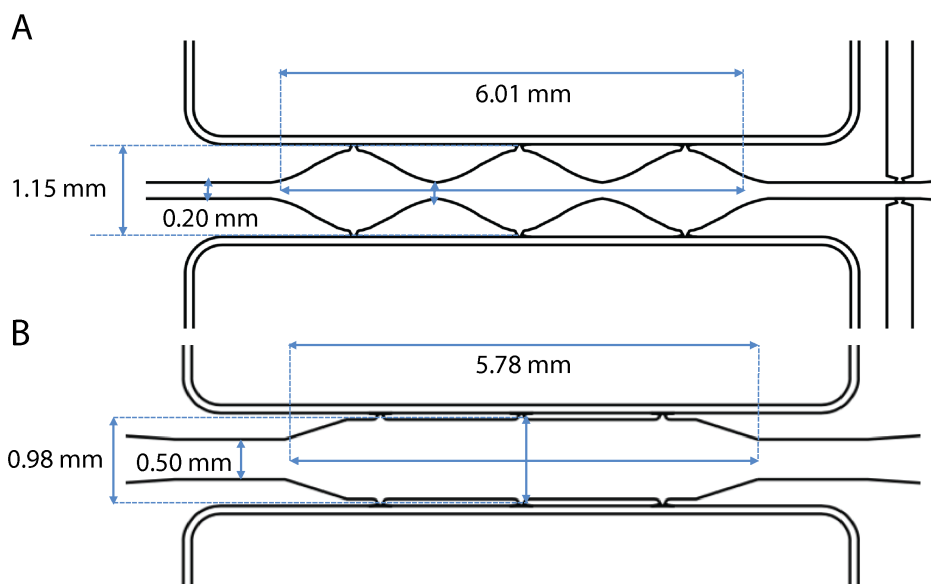


Figure 4.3 – Wide chamber design allows ease of ccic loading. (a) The microfluidic chip is bonded to a bottom-less 96-well plate via chemical glue and oxygen plasma. Zoom view shows a single device unit with a single tissue chamber fed through microfluidic channels, 2 loading ports (L1-2), and medium inlet and outlets (M1-2). (b) Comparison between the standard 3 chamber device and the single, wide chamber device. While height and width are roughly the same, the loading channel is greater in the wide chamber device (0.5 mm vs 0.2 mm) and also lacks narrowing within the chamber.

4.3.2 FLIM detects metabolomic heterogeneity in pVMT.

Cancer cells often utilize glycolysis to fulfill their metabolic and energy demands rather than oxidative phosphorylation (OxPhos), regardless of oxygen availability, a phenomenon known as the Warburg effect[83]. This balance between glycolysis and OxPhos can be visualized using fluorescence lifetime imaging microscopy (FLIM), a label-free and non-invasive method to measure metabolic activity in living cells using differences in the fluorescence lifetime of free vs. protein-bound NADH, the key co-factor in many metabolic pathways[20, 50]. Free NADH correlates with a more glycolytic environment, while the bound form correlates with less glycolysis. FLIM reveals glycolytic gradients throughout the tissue, thereby providing a metabolic signature[50]. We have shown this method to be highly sensitive in distinguishing the metabolic state between different cell types in the VMT[224]. High-resolution FLIM imaging demonstrates that the tumor is more glycolytic in areas associated with endothelium and stroma (Figure 4.6), as well as the core of the

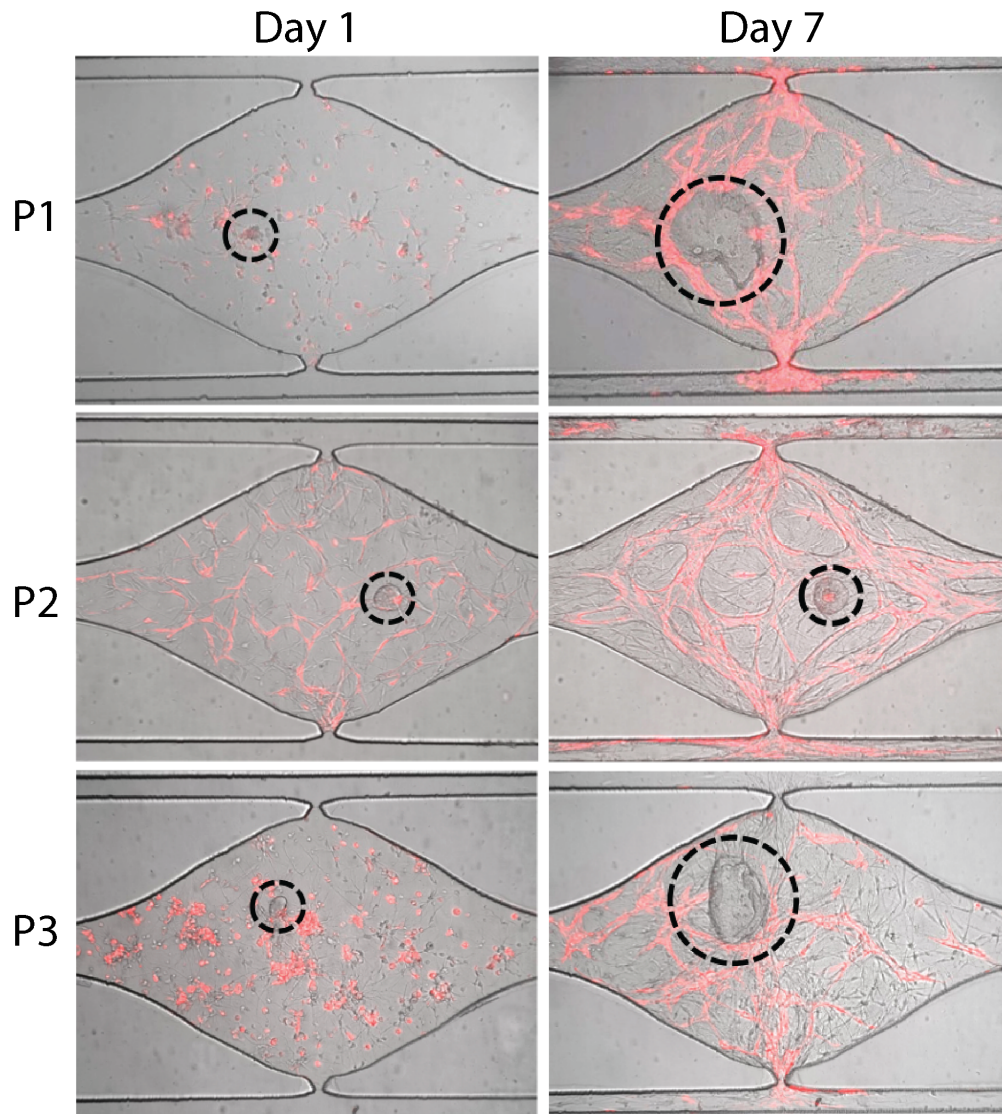


Figure 4.4 - The vMT supports the survival and growth of patient-derived CRC cells from different individuals. Brightfield/fluorescent merged images of pVMT. Patient-derived CRC tissue (unlabeled, circled) is seeded into each device unit with endothelial cells (mCherry, red fluorescence) and fibroblasts (unlabeled). Shown are 3 primary CRC tumors derived from different individuals (P1, P2, and P3). The left column shows the pVMT on day 1 of culture and the right column shows the same pVMT on day 7 of culture.

tumor mass, with a high degree of spatially patterned heterogeneity. We observe a top-down pattern of metabolic heterogeneity that models patterns observed in colon crypts *in vivo*[234]. Metabolic heterogeneity is revealed within the tumor, with distinct areas of high free NADH interspersed with high bound NADH, similar to what has been observed in solid tumors *in vivo*[234]. Our findings demonstrate that cells in the pVMTs are behaving as they

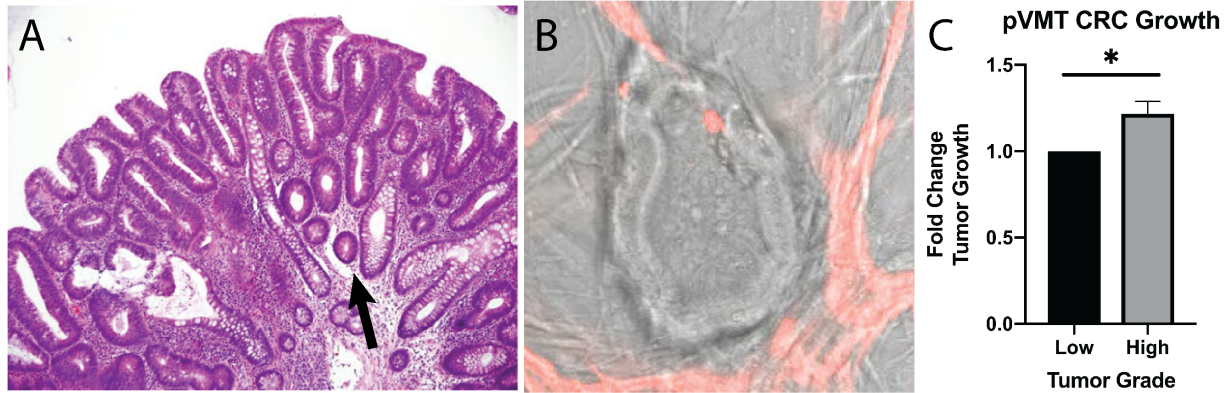


Figure 4.5 – pVMTs model histological and growth characteristics of primary tumors from which they were derived. (a) Example H&E stained tubulovillous adenoma. Arrow shows an area with tubular histology that mimics the structure of tumor in 4.5b. (b) pVMT derived from patient 3 (P3), who had a tubulovillous adenoma (stage I). Shows a portion of tumor growing within the VMT that recapitulates the parent tumor histology in 4.5a. (c) Quantitation of growth for low grade and high grade tumors seeded into the pVMT.

would *in vivo*, and that the system will be useful for further studies using patient-derived cells.

4.4 Discussion

The need for improved therapies in CRC is immense. Despite the large global burden and poor prognosis, our molecular understanding and ability to predict response to therapy has been slow to translate to clinical benefit. Accurately modeling tumor biology and testing novel therapies on patient-derived cells is critically important to developing therapeutic regimens personalized to a patient's specific disease to improve clinical outcomes. We have optimized culture conditions to grow patient-derived tumor samples in the VMT by dissociating fresh cancer biopsy or surgical tissue and then positively selecting for cancer-initiating cells using a specialized stem cell media. Although growing cancer cells from clinical tissue is notoriously unpredictable, VMTs replicate the *in vivo* condition more closely than standard monolayer or spheroid cultures and, as such, foster higher rates of successful growth. We see nearly 100% success rate for engraftment of primary-derived

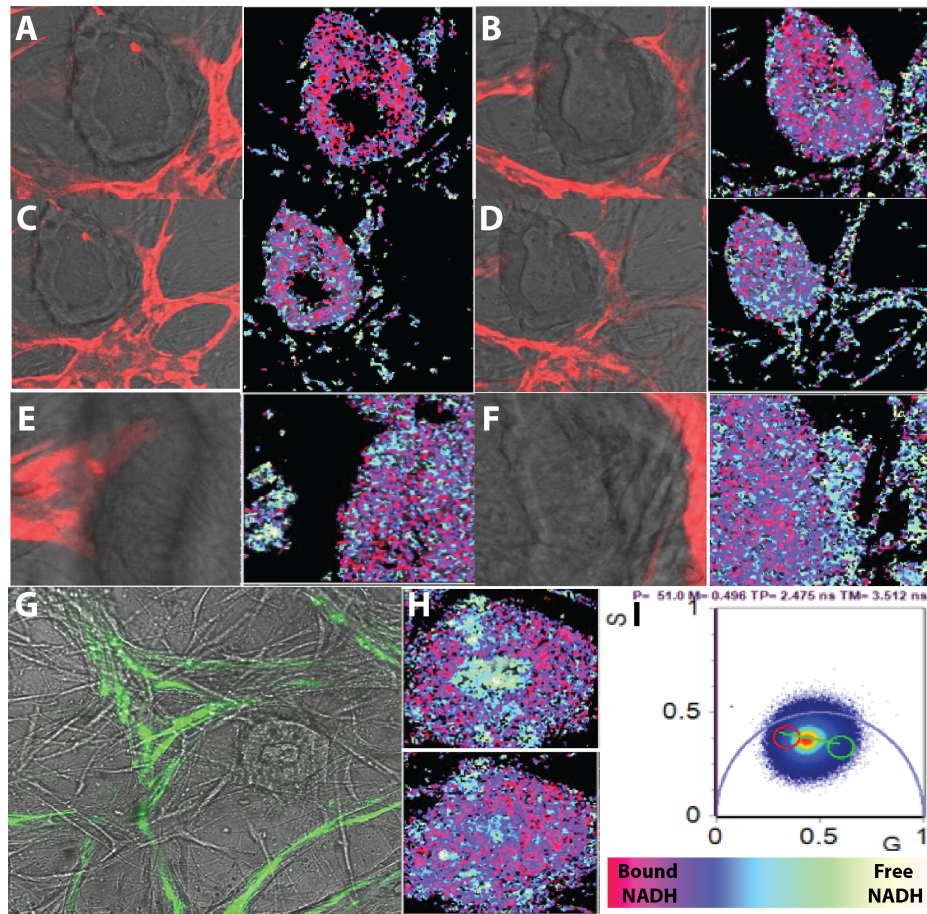


Figure 4.6 – FLIM metabolomics imaging of pvMT reveals heterogeneity. (a) Left: Top plane merged bright-field/fluorescence images of P3 grown in the pvMT on day 7 of culture with mCherry labeled EC. Right: Resulting metabolomic profile. (b) Left: Bottom plane of P3 with resulting FLIM image on the right. (c) Top and (d) bottom planes of P3 with resulting FLIM images. (e) Zoom view of vessel interaction with patient-derived CRC tissue in the top and (f) bottom planes with resulting images. (g) P39 growing in the pvMT with vessels labeled with GFP. (h) Top: Resulting FLIM image of top plane of P40. Bottom: Resulting FLIM image of bottom plane of P40. (i) Phasor plot with color legend.

tumors in our system, whereas in immunodeficient mice, engraftment success typically ranges from 10-50% depending on tumor type and often requires months to establish (ref). The VMT can be established within days of tissue collection, is low cost, and is much easier to monitor and manipulate than xenograft models, allowing for results to be acquired and interpreted in real-time and within a clinically actionable time frame. Furthermore, the pvMT incorporates only human cells and requires very few cells for establishment, such that drug testing can be performed in a rapid and high throughput manner using tumor cells derived from a small biopsy. Based on these data, we conclude that the VMT serves

as an accurate and physiologically relevant model for drug screening and personalized medicine applications.

Here we show that we can reliably establish patient-derived VMT, the growth characteristics of which model *in vivo* characteristics based on stage and grade. Although growing cancer cells from clinical tissue is notoriously unpredictable, pVMTs replicate *in vivo* condition more closely than standard monolayer or spheroid cultures and, therefore, foster higher rates of successful growth, especially with early stage disease tissue in which primary cultures are otherwise unattainable. We are now testing targeted and standard of care treatment response in the pVMT and comparing those results with clinical trials data based on the mutation status of the tumor. Furthermore, we are assessing whether heterogeneity of the parent tumor is maintained in the VMT by performing immunofluorescent (IF) staining for cell-specific markers, as well as H&E staining to look at gross histology. We aim to show that the primary-derived tumor cells show greater cell viability and better retain primary tumor heterogeneity when cultured in the VMT vs spheroid cultures. A direct comparison between histology of the primary tumors and matched pVMTs is expected to reveal whether the pVMT culture conditions are optimal for maintenance of primary tumor heterogeneity. However, we recognize that the tumors we generate in our platforms are small and thus may miss some of the large-scale heterogeneity present in human tumors. This is probably unavoidable and is a limitation that the field is grappling with - from the sampling of tumors by biopsy, to the establishment of xenografts in mice, to the various culture models currently in use. However, generating multiple micro-tumors from a single sample as we propose may aid in capturing the original heterogeneity, so that several pVMT can be tested in parallel to determine the drug sensitivities for each unique clonal population across multiple replicates.

In future studies, we plan to use the patient-derived VMT model to study different stages of tumor progression and dissemination, develop novel therapeutic approaches tailored

to individual patients, and, ultimately, to use as a diagnostic tool to guide clinical management. An important step toward realizing these goals is to perform drug testing in the pVMT as part of a clinical trial to see if 1) the responses in the pVMT match responses seen in individual patients and 2) to determine if results from the pVMT are predictive of patient outcomes. The overarching goal of these efforts is to inform clinical management for patients by testing drug efficacy on their own tumor cells growing in the pVMT before they receive treatment in the clinic. We envision the pVMT to facilitate choosing the most effective drug regimen for eradicating their particular tumor. Improving the preclinical prediction efficacy of human drug responses and stratifying patients in clinical trials based on molecular profile are both critical to reducing costly failures in drug development and to ensuring that each patient receives the optimal treatment regimen for their disease given malignancy. Our goal with this pilot clinical study is to generate sufficient data to justify a larger clinical trial in order to validate the pVMT platform as a companion diagnostic and move closer to realizing precision medicine in oncology.

4.5 Conclusion

To date, we have shown that the VMT grows, responds to drugs, and has similar patterns of gene expression when compared to *in vivo* tumors, in stark contrast to those same cells growing in 2D or 3D monocultures. Although recent molecular insights have begun to pave the way for disease stratification and development of targeted cancer therapies for improved patient outcomes, the full potential of current research efforts has yet to be realized in the clinic.

A rational next step in validating the VMT model as a clinically relevant predictive tool in the field of oncology entailed obtaining fresh, treatment-naive colon cancer biopsy samples from patients during routine, clinically indicated endoscopic or surgical procedures.

Here we establish proof-of-concept that patient-derived CRC cells can be maintained in the device for drug screening purposes, to serve as a platform that can, in the future, accelerate personalized treatments to the clinic. If the platform is clinically validated, both the research and health care fields aim to benefit from this broadly applicable translational technology. This new approach to personalized medicine is necessary to ensure that the most clinical benefit, with the least toxicity, is consistently achieved from therapy for each individual patient.

Chapter 5

Considerations

5.1 Establishment of culture conditions

5.1.1 Oxygen tension

Many different niche factors contribute to the *in vivo* microenvironment of the native tumor, and since the tumor has adapted to these conditions while growing *in vivo* it is imperative to recapitulate this microenvironment *in vitro*. While cells are standardly cultured in atmospheric oxygen conditions (20% O₂), oxygen in the body can range from 1-12% with oxygen tension in capillaries reaching 4%[33]. On the other hand, tumors often become hypoxic (<1% O₂) with enhanced generation of lactate as metabolic demands outgrow the blood supply. Therefore, oxygen tension is an important factor in cell culture for cells to maintain endogenous functions, proliferative capacity, metabolic function and innate response to drugs. Intriguingly, we observe significantly increased growth of SW480 CRC cells in the VMT when cultured in 4% O₂ compared to atmospheric O₂ (Figure 5.1a, 5.1b), which warrants further study as well as testing with patient-derived tumor tissue.

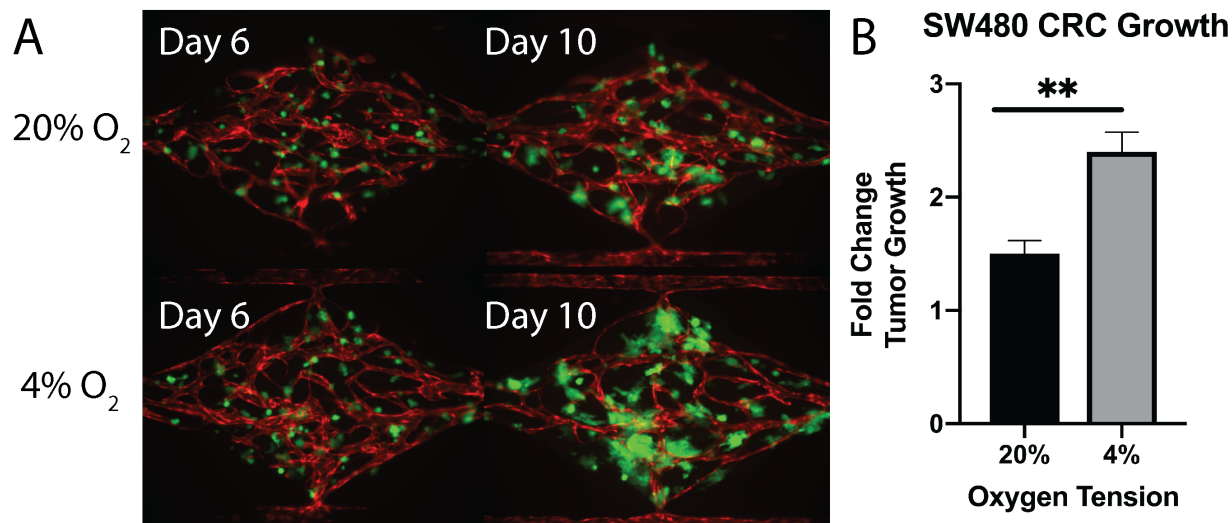


Figure 5.1 – Oxygen tension affects growth of CRC cells within the VMT. (a) SW480 CRC cells (GFP) growing within the VMT in 20% O₂ or 4% O₂. Day 6 shown on the left and day 10 on the right. (b) Quantification of SW480 CRC cells growing in different oxygen tension conditions. ** = p < 0.01.

5.1.2 Human-derived serum

A diverse network of oncogenic signaling pathways is induced *in vivo* by endogenous ligands found in patient sera[145]. Several recent studies have shown that growth factors in serum have the ability to impact tumor heterogeneity[26]. Moreover, use of human-derived serum (HS), whether it is autologous in origin or pooled, in place of fetal bovine serum (FBS) has been shown to not only enhance the growth of primary tumor cultures but also significantly alter receptor tyrosine kinase activation and the tumor cell response to drugs to more accurately mimic the parent tumor[145]. Those findings demonstrate a more precise representation of patient biology when the source of serum is derived from increasingly individualized sources (i.e. autologous serum shows the greatest degree of correlation in phenotype between cultured tumor and parent tumor). FBS is standardly used in culture media, but a set back to using FBS in drug screening applications is that it does not stimulate the signaling networks and survival cascades native to patient-derived cancer cells since it lacks the growth factors enriched in patient sera that contribute to

these autocrine-paracrine loops. Further, effects of FBS on tumor growth in culture are largely unknown[148]. The first step toward using autologous serum in the VMT was to show that replacing FBS with HS can have an effect on CRC growth. Growth of CRC cell line HCT116 was assessed with standard EGM2 media containing 2% FBS and compared to growth with EGM2 media containing 2% HS in place of FBS (Figure 5.1a). As shown, there was no difference in tumor growth (Figure 5.1b). However, when SW480 was seeded into the VMT to test these same conditions (Figure 5.1a), we saw significantly increased tumor growth with EGM2 2% HS vs 2% FBS at every time point (Figure 5.1b). These results suggest that tumor cells differ in their sensitivities to the growth factors present in serum and that there is a difference between human and bovine serums that can alter cell proliferative capacity. Previous research also supports that more individualized serum sources are warranted to obtain accurate results from drug screening, which we aim to test further in the VMT. Patient-derived tumors may be especially sensitive to serum factors to allow optimal adaptation to culture conditions.

5.1.3 Treatment with bevacizumab

First-line treatment for advanced metastatic CRC is a combination of systemic cytotoxic chemotherapy (FOLFOX or FOLFIRI – a regimen of 5 fluorouracil (5FU), leucovorin and either oxaliplatin or irinotecan) and a biologic: patients with CRC harboring a KRAS mutation receive the angiogenesis inhibitor bevacizumab[192]. Bevacizumab is an anti-angiogenic monoclonal antibody specific for vascular endothelial growth factor (VEGF) that inhibits the growth of tumor blood vessels, thereby ‘starving’ the tumor of nutrients and blood supply[162]. However, the efficacy of bevacizumab is limited and treatment extends the overall survival of patients by just five months[14]. We currently do not see significant anti-vascular or anti-tumor effects in response to bevacizumab in the VMT when treated at day 5 – even at supraphysiologic doses (10 μ M) (Figure 5.3). Intriguingly, when bevacizumab

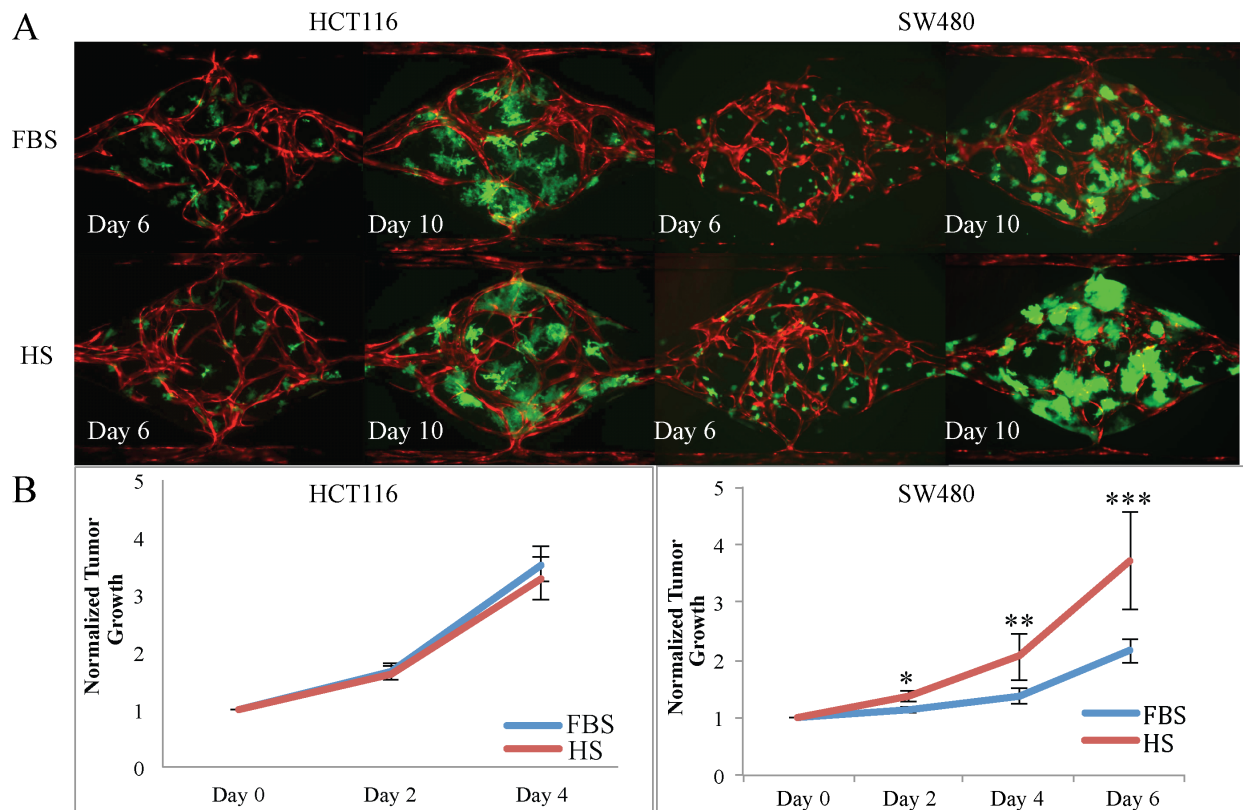


Figure 5.2 – Replacing FBS with human serum promotes differential growth of CRC-derived VMT. (a) Left panels show HCT116 on day 6 and day 10 fed with medium supplemented with FBS or HS. Right panels show the same conditions for SW480. (b) Quantification of results showing significant increase in growth in SW480 in response to HS.

is introduced at day 0 of VMT culture (Figure 5.3b), the endothelial cells fail to migrate out and line the outer channels, suggesting that bevacizumab may alter laminin receptor interactions.

However, an explanation for the lack of observable anti-angiogenic response to bevacizumab may be that we observe only vasculogenesis, and not angiogenesis, in our three-chamber device. Vasculogenesis is the process by which endothelial progenitor cells self-assemble to form new vasculature, mostly during development, whereas angiogenesis is the process by which new vessels sprout from existing vasculature in response to injury, during tissue regeneration or in disease states such as tumor progression [33, 102]. While both vasculogenesis and angiogenesis are important for vessel development, these

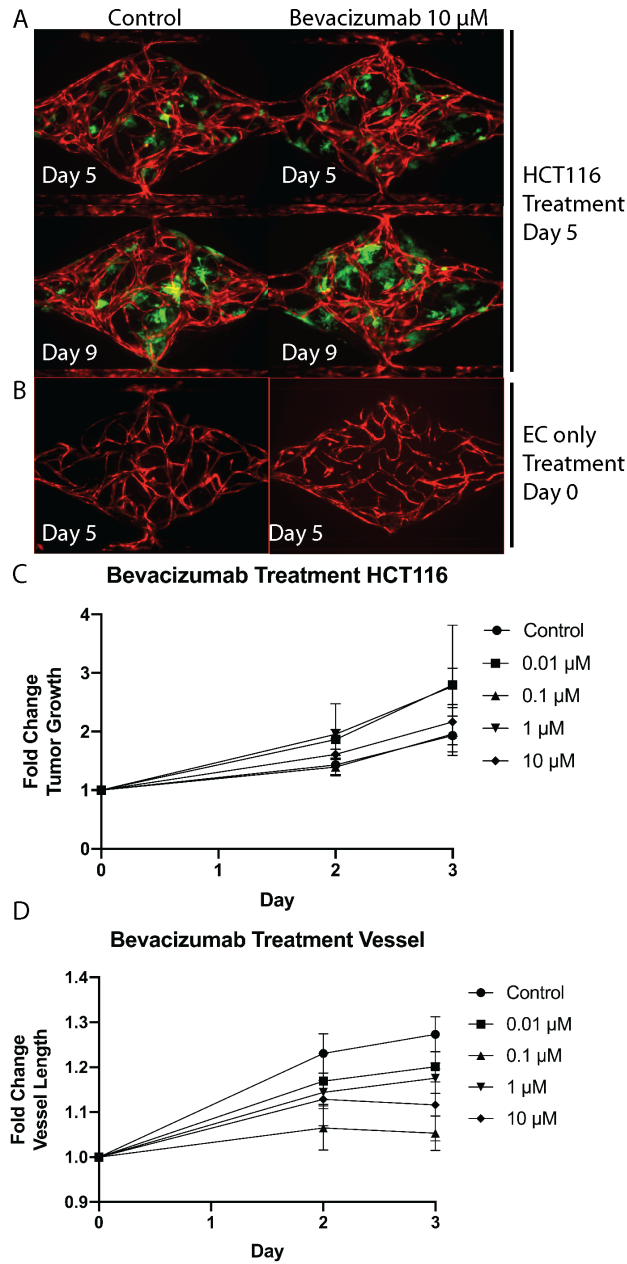


Figure 5.3 – Bevacizumab shows no significant anti-angiogenic or anti-tumor effects in the VMT. (a) Left panels show control HCT116 VMT on day 5 and day 9. Right panels show bevacizumab treated (day 5) HCT116 VMT on day 5 and day 9. Vessels in red and tumor in green. **(b)** Left panel shows control VMO and right panel shows bevacizumab treated VMO. VMO treated starting on day 0 of culture. Note the lack of anastomosis and endothelial cell migration into the outer channels. **(c)** Quantification of tumor response to treatment. **(d)** Quantification of vessel response to treatment.

processes are biologically distinct and may differentially rely on VEGF signaling. To test the true anti-angiogenic potency of bevacizumab within the VMT, an important step is to test vessel sensitivity in the dual chamber platform (Figure 5.4). The dual chamber is a new

device iteration developed by the Lee lab that incorporates two chambers, fed through separate microfluidic channels and media reservoirs, partitioned by a central channel (Figure 5.4a). Tumor cells can be loaded into either of the chambers or the central channel, initially away from the forming vessels, and each compartment fed with different media – allowing ‘independent’ growth of each component until the tumor cells recruit the vessels and promote endothelial sprouting via angiogenesis (Figure 5.4b, 5.4c).

Another consideration is that bevacizumab has been proposed to have a vascular ‘normalizing’ effect, meaning the decrease in hyper-angiogenic signaling in response to bevacizumab treatment causes the vessels to adopt a mature, quiescent phenotype rather than regress[102], and it may be possible that this is what we are observing in the VMT. These findings warrant further investigation into factors that influence vascular and tumor response to bevacizumab. Doing so may reveal novel combination therapeutic strategies or predictive biomarkers to allow patient stratification in the clinic. Our platform is uniquely suited to address the efficacy of novel combination therapies through direct observation of not just tumor growth, but also vascular response and cell-cell interactions within the tumor microenvironment.

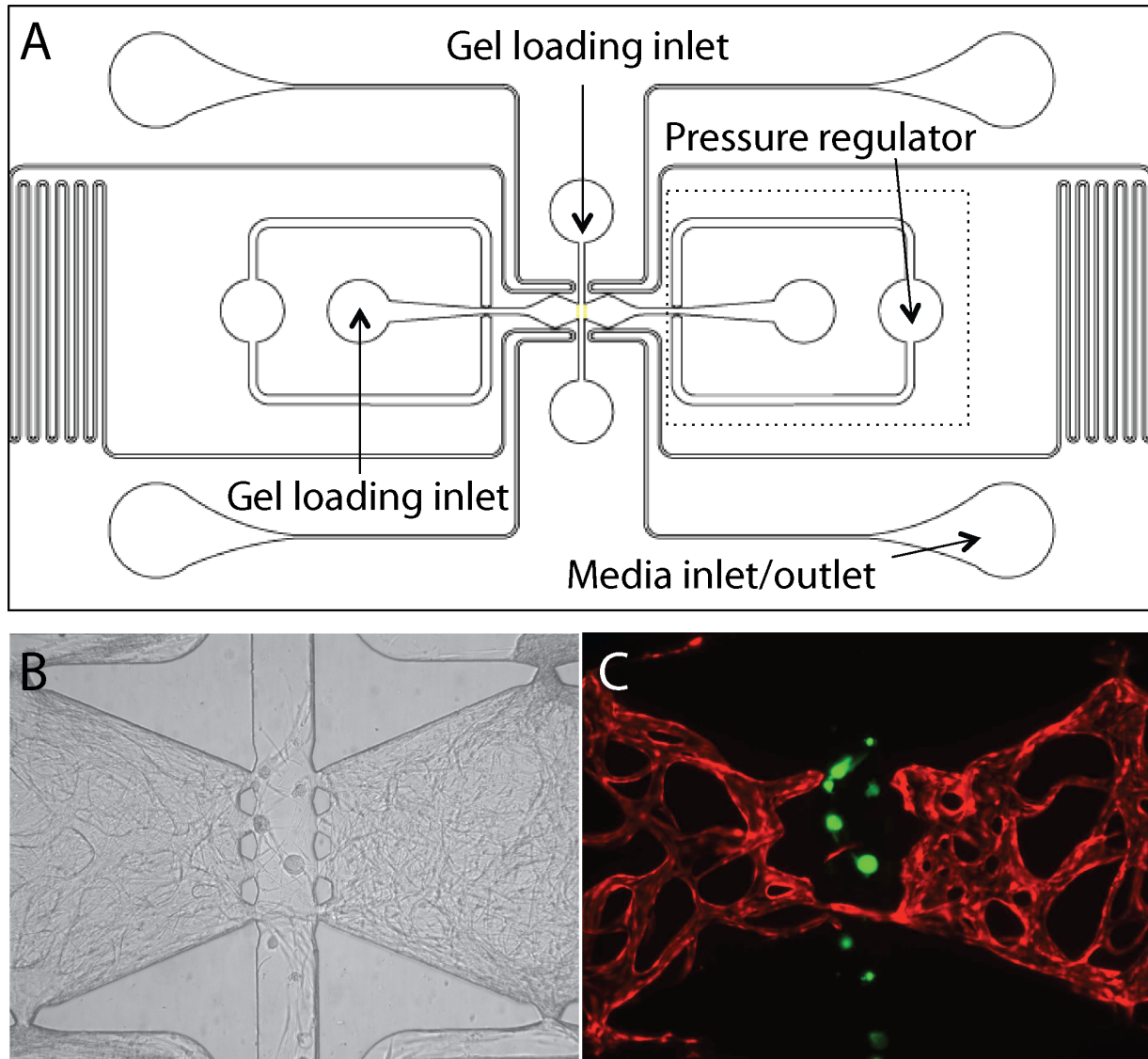


Figure 5.4 – Dual chamber device supports angiogenic sprouting toward tumor cells. (a) Schematic of the dual chamber microfluidic device. Two diamond-shaped chambers flank a central channel that is 100 μm wide. Each chamber is independently fed through separate medium inlet/outlets. A pressure regulator aids with loading. (b) Brightfield image of a dual chamber with vasculature established in each diamond chamber and cancer cells in the central channel. (c) Fluorescent image of 5.4b. Vasculature in red and tumor in green.

Chapter 6

Future Directions

6.1 Significance

CRC represents a major source of morbidity and mortality as the second leading cause of cancer-related deaths in the US and the third most common cancer worldwide, with over a million diagnoses and half a million deaths each year[216]. Alarming, CRC incidence is rising among patients under the age of 50[159]. While the majority (75%) of patients present with localized (stage I and II) disease and undergo intentionally curative surgery, more than half of these patients will develop, and ultimately die from, metastatic disease[217]. First-line treatment for advanced metastatic CRC is a combination of systemic cytotoxic chemotherapy (FOLFOX or FOLFIRI - a regimen of 5 fluorouracil (5FU), leucovorin and either oxaliplatin or irinotecan) and a biologic. Bevacizumab, a monoclonal antibody specific for vascular endothelial growth factor (VEGF), is an anti-angiogenic biologic typically administered in CRC to inhibit the growth of blood vessels and 'starve' the tumor of nutrients and blood supply[254]. However, the efficacy of bevacizumab is limited and treatment extends the overall survival of patients by just three months[271].

Further, chemotherapies are largely ineffective and highly toxic. With a 5-year survival rate for stage IV CRC at a mere 10%, new approaches are needed to facilitate targeted drug development for this common and lethal malignancy.

Immunotherapies are revolutionizing medical oncology due to the remarkable and, in some cases, unprecedented outcomes observed in a subset of patients. Cancer immunotherapies can unleash antitumor activity and lead to long-term clinical responses in patients with advanced cancer, including those with disease that is highly resistant to traditional therapies[195]. However, patients with CRC usually do not benefit from immunotherapies to the same extent as patients with other solid tumors, such as melanoma or non-small cell lung cancer, except in cases where the tumor belongs to the group of microsatellite instable (MSI) disease that make up only about 15% of CRCs[112]. Antibodies targeting immune checkpoint inhibitors are FDA-approved for use in microsatellite instable (MSI) high tumors and several other malignancies[230], and breakthrough strategies are quickly advancing. Adoptive cell transfer (ACT) of naturally occurring or gene-engineered T cells, in which tumor-specific lymphocytes are expanded *ex vivo* and transferred back into the patient, has been shown to trigger complete tumor eradication in some instances – leading to durable and complete remission in select patients, even those with heavily pretreated disease[200]. Yet currently, few patients with CRC benefit from immunotherapy treatment, overcoming innate resistance remains a major challenge and biomarkers to guide treatment decisions are lacking. These barriers highlight the need to elucidate mechanisms of response and resistance to immunotherapy in CRC.

Recent studies in CRC have shown an association between immune reactivity within the tumor and lack of metastatic spread[73]. Intriguingly, increased density of activated immune cells within the tumor is better prognostic of improved clinical outcomes and longer overall survival in CRC than criteria based on anatomic extent of disease[73]. However, the majority of CRCs do not show evidence of a productive immune cell infiltrate[66], contribut-

ing to poor clinical outcomes and further hampering immune-therapeutic approaches. It is well recognized that dynamic interactions between the tumor and the immune system influence clinical outcomes and response to immunotherapies, yet appropriate model systems to study tumor-immune interactions are lacking. Although organoid cultures capture the 3D structure of a tumor, these models typically lack stroma and do not reproduce barriers to drug or immune cell delivery to the tumor[255]. Xenograft tumor models are a cornerstone in cancer research, but are time consuming, expensive, not easily manipulated and contain non-human cells. Further, xenograft tumors are often established in immune-suppressed animals to improve graft rate, which precludes studies of human immune-tumor interaction[40].

Allograft, or syngeneic, mouse models are established via engraftment of cancer cells that have been induced, or originated spontaneously, in a murine host[56]. Strengths and limitations of the syngeneic mouse model are similar to the xenograft model, with the exception of an intact immune system in the syngeneic model that allows immunological studies. Yet both models lack the significant genomic and microenvironmental heterogeneity that define human cancers. Indeed, the cell lines used for engraftment lack mutational patterns that recapitulate human intra-patient clonal heterogeneity and are implanted into a limited number of inbred strains of mice that fail to model the human inter-patient heterogeneity[166]. In contrast, genetically-engineered mouse models (GEMMs) form tumors *de novo* via introduction of tissue- or cell-specific oncogenic mutations and/or tumor suppressor gene knock-outs[115]. While GEMMs are immunocompetent and better reproduce the evolution and heterogeneity of an actual tumor, central challenges when using GEMMs include a lack of penetrance of the tumor phenotype and extended latency of neoplastic development [115, 166]. However, the clinical translatability of murine models is often limited by species-specific differences in tumor progression, metabolism and immunology. Cross-reactivity between mouse and human may differ due to absence of antigens and surface markers on murine cells that are present on human

cells[166]. Further, differences in antigen processing, T cell signaling pathway activation, and chemokine/chemokine receptor expression can also affect cross-reactivity with human epitopes, illustrating the underlying challenges with using murine models for immuno-oncology research[158].

Given the importance of the tumor microenvironment in modulating immune cell function, we propose using a tumor model that incorporates key features of the native human tumor microenvironment. To this end, we have created and validated a vascularized micro-tumor (VMT) model that forms *de novo* within a microfluidic platform via co-culture of multiple cell types under dynamic, physiological flow conditions. In this tissue engineered micro-tumor construct, a living vascular network forms within days and begins to feed the growing tumor mass just as it occurs *in vivo*. The VMT is optically transparent for high resolution imaging of dynamic processes and direct visualization of fluorescently labeled cells within the tissue. Not only does the VMT allow real-time imaging and interrogation of cell-cell interactions, the model can be established within days for rapid turnaround of results and contains only cells of human origin. Furthermore, the microfluidic design provides experimental control to address specific research questions. We have shown that the VMT, in contrast to current 2D and 3D models, retains *in vivo* tumor heterogeneity, gene expression signatures, drug response, and subtype-specific activated stromal compartments. Importantly, we have optimized methods to derive cancer-initiating cells from fresh CRC biopsy and surgical tissue that grow and respond to drug treatment in the VMT.

6.2 Aims

Myriad factors contribute to clinical failure of immunotherapies, which, while interdependent, can be broadly categorized by: 1) a lack of immune cell penetration into the tumor; 2) immunosuppression of immune cells that do penetrate the tumor; and, 3) an inability of

immune cells to target the heterogeneous cellular populations within a tumor[112]. Here we outline our strategies to address the first two challenges by using our advanced VMT model to find novel immunotherapeutic approaches for CRC. An approach to address the third challenge will be proposed in a future funding application.

6.2.1 Aim 1: Promote enhanced immune cell infiltration into the tumor via vascular normalization.

Just like nearly all healthy tissues, tumors rely on blood vessels for nutrient and oxygen delivery and the removal of metabolic wastes. Although tumors recruit blood vessels to support their growth, the resulting vasculature is irregular, leaky, and ill-perfused due to tumor pathophysiology that induces the continued production of pro-angiogenic factors, leading to rapid but aberrant tumor blood vessel formation[33, 51]. Solid tumors are composed of highly proliferating, fibrotic and non-vascularized areas that are not only hypoxic and acidic, but also surrounded by high interstitial pressure[208, 19, 46]. Indeed, histological analyses of CRC tumors reveal that tumor-associated blood vessels are spatially aggregated in a limited belt-like zone at the periphery of the tumor and are almost completely absent from the center of the tumor[113]. These features lead to an immunosuppressive microenvironment and form a physical barrier to effective drug delivery and immune destruction of the tumor[54]. Tumor-associated endothelial cells also express lower levels of cell adhesion molecules, which further reduce the trafficking of immune cells into tumors[91]. Current anti-angiogenic approaches in oncology (e.g. bevacizumab as standard treatment for CRC) aim to suppress new blood vessel formation and destroy pre-existing tumor vessels to starve tumor cells[43]. Yet anti-angiogenic treatments often cause extreme hypoxia in tumors due to vessel regression that eventually leads to increased drug resistance and metastasis[191]. Instead, studies have shown that restoring the functional integrity of tumor blood vessels via vascular normalization results in

enhanced tissue perfusion to alleviate hypoxia[91, 33]. As a result, an increase in oxygen delivery to the tumor reconditions the microenvironment to sensitize resistant tumor populations, potentiate immune response and, ultimately, reduce tumor growth, invasion and metastasis[117]. Importantly, stabilizing tumor vasculature improves drug and immune cell penetration into the tumor to facilitate anti-tumor activity[54]. Evidence further suggests a positive feedback loop, whereby stimulation of immune cell functions also helps to normalize tumor vasculature, and vice versa[91]. However, effective therapeutic agents that can promote vascular normalization and restore function to tumor-associated vessels are an unmet need.

The angiopoietin (ANGPT)-TIE2/TEK signaling pathway is essential for vascular homeostasis and, in disease, ANGPT2-mediated inhibition of TIE2 in blood vessels causes aberrant blood vessel formation and vascular leak[170, 229]. Notably, high expression of ANGPT2 is prognostic of poor outcomes in several malignancies[252]. ANGPT2 is enriched at the invasive front, but not the central regions, of tumors where increased levels of matrix metalloproteinase-2 and angiogenesis are also evident[229]. Co-opted vessels display striking upregulation of ANGPT2, which is not detectable in vessels of adjacent normal tissue[82]. In our studies, we performed single cell RNA-sequencing analyses of VMT-derived endothelial cells (EC), fibroblasts, and CRC (HCT116 and SW480) and compared gene expression at single cell resolution with those cells growing as 2D or 3D monocultures. Intriguingly, we find upregulation of ANGPT2 in microvascular EC within the VMT compared to those EC growing as monolayers. Functionally, we observe leaky and ill-perfused vessels in the VMT when compared to the vascularized micro-organ (VMO), with associated structural irregularities. Since ANGPT2 is an antagonist of ANGPT1 that competes for binding to the TIE2 receptor (TEK), and ANGPT1-induces TIE2 autophosphorylation and activation, we aim to compare the phosphorylation of TEK between extsmallerHCT116-VMT and VMO. We expect, based on our findings, to observe a greater amount of phosphorylated TEK in the

VMO compared with extsmallerHCT116-VMT, suggesting that the vascular leak induced in the VMT may be attributable to ANGPT2 antagonism of TEK phosphorylation.

A recent study shows that endothelial-specific phosphatase VEPTP (vascular endothelial protein tyrosine phosphatase) determines TIE2 response to ANGPT2, and that inhibition of VEPTP converts ANGPT2 into a potent TIE2 activator in blood endothelium, thereby promoting a mature, quiescent vascular phenotype[229]. Based on these findings, we propose a novel strategy to stabilize tumor vessels by treating with a small-molecule inhibitor of VEPTP (AKB-9785, Aerpio Pharmaceuticals). We predict that therapeutic induction of vascular normalization will: 1) restore tumor vascular patency; and, 2) increase immune cell homing and extravasation to the tumor. To assess patency, we will first perfuse the vasculature of VMT, treated with AKB-9785 treated or non-treated, with 70 kDa FITC dextran to visualize and quantitate vascular leak. If therapeutic effect is evident through reduction of tumor vessel permeability, we will then perform immunofluorescence staining to look for expression of cell adhesion molecules such as vascular cell adhesion protein 1 (VCAM1) and intercellular adhesion molecule 1 (ICAM1). The VMT model is ideal for studying tumor-immune-vascular interactions, and we aim to show that freshly isolated peripheral blood mononuclear cells (PBMCs) can extravasate and seed within the VMT. To determine if stabilization of vessels with AKB-9785 enhances immune cell homing and extravasation to the tumor, PBMCs will be perfused in AKB-9785 treated and non-treated VMT and the number of PBMCs that have extravasated under each condition will be quantitated. If AKB-9785 is successful in normalizing tumor-associated vasculature, we expect that immune cell homing and extravasation will increase in the VMT. If AKB-9785 is not successful in inducing normalization, we can therapeutically block ANGPT2 itself, activate TIE2, or combine ANGPT2 inhibition with TIE2 activation[170]. Alternatively, from our single cell RNA-seq dataset, we have identified several oncogenic pathways specifically upregulated in VMT-associated endothelium, including TNF signaling, mTOR signaling and TGF- β signaling, that can be

pharmacologically targeted to potentially induce vascular normalization and promote immune cell extravasation[124, 32].

6.2.2 Aim 2: Analyze transcriptome of CRC tumor-immune microenvironment at single cell resolution to derive novel immunotherapy targets.

Knowledge of tumor, stromal and immune cell phenotypes within the tumor microenvironment is essential for understanding mechanisms of disease progression and immune evasion to enable development of novel therapies. While recent studies have characterized significant intratumoral heterogeneity in CRC at the single-cell level[17, 137], these efforts have been largely limited to tumor cells and analyses of the immune component have been neglected. Here we propose to profile malignant, stromal and immune cell populations from five CRC tumors, as well as matched normal colon tissue and blood using single-cell RNA sequencing. T cells that have been exposed to tumor-associated antigens via presentation by antigen-loaded dendritic cells, and expanded in culture, will be subjected to VDJ sequencing. By analyzing cells from tumors, matching non-malignant tissue and blood, we expect to uncover a large degree of cellular heterogeneity, distinguished by mechanisms with which those populations adapt to the tumor that may be therapeutically exploited. Further, VDJ sequencing is anticipated to reveal novel TCRs specific to tumor neoantigens that can direct engineering of CAR-T cell therapies.

Each characterized cell subtype will be confirmed by immunostaining for selected markers and an associated marker gene panel will be assessed in bulk RNA-sequencing data to determine how gene expression signatures correlate with immunotherapy response in CRC. To reveal the combinatorial impact of T cell receptor (TCR) utilization on phenotypic T cell diversity in CRC, we will analyze paired single-cell RNA and TCR sequencing

data from T cells. These analyses are anticipated to identify T-cell differentiation states and additional immunosuppressive mechanisms in the CRC tumor microenvironment that can be therapeutically exploited. We further aim to identify T-cell clonotypes specific to tumor neoantigens that may be used for ACT. An overarching goal of these analyses is to generate a comprehensive catalog of the CRC stroma and immune compartments to better understand CRC disease progression and to guide targeted- and immune-therapeutic development. The strategies that result from these analyses can then be tested for efficacy in the VMT using patient-derived cells to determine feasibility and efficacy.

6.3 Conclusion

The University of California, Irvine (UCI) Chao Family Comprehensive Cancer Center's Gastrointestinal Disease Oriented Team (GI-DOT) is a multidisciplinary group of GI cancer researchers spanning the clinical, translational, and basic research expertise of the institution (representing 4 schools and 12 departments) that continually inform our research design. An ongoing collaboration between the Hughes lab and the GI-DOT along with a concerted effort by all involved parties at the UCI Medical Center has led to the establishment of a standard pipeline for successful procurement of fresh CRC biopsy and surgical tissue. Furthermore, the partnership has allowed free exchange of ideas across the Schools of Biological Sciences and Medicine in our effort to accelerate translation of the novel VMT into a tangible clinical application with health benefits. The translational infrastructure we have established providing real-time information from patient-derived tumor cells in our VMT will support efforts to improve patient outcomes in CRC.

Herein, we have shown that the VMT is uniquely suited to facilitate the development of personalized medicine because few cells are needed from the patient and rapid, automated results can be obtained within a clinically actionable timeframe. The VMT supports

the survival and growth of CRC biopsy and surgically excised tissues, for which the morphology and growth of the tissues within the VMT models characteristics of the primary tumors. Our studies provide insights into the crosstalk between tumor and stromal cells, and demonstrate that modeling the dynamic, complex and heterogeneous cell-cell interactions of a vascularized tumor mass are necessary to recapitulate the tumor growing *in vivo*. The tumor-associated vasculature within the VMT models the immature and leaky vessels of an actual tumor mass, thereby mimicking nutrient delivery to the tumor, acting as a physiological barrier to drug delivery, promoting pro-tumorigenic signaling, and serving as a conduit through which cancer cells or stromal cells can intravasate/extravasate. Compared to 2D and 3D monocultures, the VMT more closely models the architecture, gene expression, tumor heterogeneity, and drug response of an actual tumor for two CRC cell lines representing the molecular landscape of the disease. For the first time to our knowledge, we analyze the cellular diversity and gene expression in a tumor chip model at single cell resolution, and find that the VMT more closely mimics the single cell gene expression signatures of *in vivo* tumors than current standard model systems. The VMT platform allowed real-time visualization of the dynamic tumor–stromal interactions involved in disease progression and revealed distinct cellular populations undergoing metastasis, an observation not readily made in other systems. We aim to target these cellular behaviors as a future research direction, as well as study the tumor-immune microenvironment to guide therapeutic development and personalized medicine strategies in oncology.

Bibliography

- [1] 10XGenomics. Vartrix single-cell genotyping tool.
- [2] M. A. Acosta, X. Jiang, P.-K. Huang, K. B. Cutler, C. S. Grant, G. M. Walker, and M. P. Gamcsik. A microfluidic device to study cancer metastasis under chronic and intermittent hypoxia. *Biomicrofluidics*, 8(5):054117, 2014.
- [3] B. A. Aguado, G. G. Bushnell, S. S. Rao, J. S. Jeruss, and L. D. Shea. Engineering the pre-metastatic niche. *Nature Biomedical Engineering*, 1(6):1–12, 2017.
- [4] M. Andersen, H. Anderson, J. C. Bailar, K. Boekelheide, R. Brent, G. Charnley, V. G. Cheung, S. Green, K. T. Kelsey, N. I. Kerkvliet, A. a. Li, L. McCray, O. Meyer, R. D. Patterson, W. Pennie, R. a. Scala, G. M. Solomon, M. Stephens, J. Yager, L. Zeise, Daniel Krewski, Daniel Acosta Jr., Melvin Andersen, Henry Anderson, John C. Bailar III, Kim Boekelheide, Robert Brent, Gail Charnley, Vivian G. Cheung, Sidney Green Jr., Karl T. Kelsey, Nancy I. Kerkvliet, Abby A. Li, Lawrence McCray, and L. Zeise. Toxicity Testing in the 21st Century: a Vision and a Strategy. *Natl. Acad. Sci.*, 13(0):51–138, 2007.
- [5] S. Aparicio, M. Hidalgo, and A. L. Kung. Examining the utility of patient-derived xenograft mouse models. *Nature Reviews Cancer*, 15(5):311–316, 2015.
- [6] K. Asano, C. M. Nelson, S. Nandadasa, N. Aramaki-Hattori, D. J. Lindner, T. Alban, J. Inagaki, T. Ohtsuki, T. Oohashi, S. S. Apte, and S. Hirohata. Stromal Versican Regulates Tumor Growth by Promoting Angiogenesis. *Sci. Rep.*, 7(1):17225, dec 2017.
- [7] E. A. Ashley. Towards precision medicine. *Nat. Rev. Genet.*, 17(9):507–522, sep 2016.
- [8] M. Astolfi, B. Péant, M. A. Lateef, N. Rousset, J. Kendall-Dupont, E. Carmona, F. Monet, F. Saad, D. Provencher, A.-M. Mes-Masson, and T. Gervais. Micro-dissected tumor tissues on chip: an ex vivo method for drug testing and personalized therapy. *Lab Chip*, 16(2):312–325, 2016.
- [9] M. Baker. Tissue models: A living system on a chip. *Nature*, 471(7340):661–665, 2011.
- [10] S. Bashir, M. Bashir, X. Casadevall i Solvas, J. M. Rees, and W. B. Zimmerman. Hydrophilic surface modification of PDMS microchannel for O/W and W/O/W emulsions. *Micromachines*, 6(10):1445–1458, 2015.

- [11] C. H. Beckwitt, A. M. Clark, S. Wheeler, D. L. Taylor, D. B. Stolz, L. Griffith, and A. Wells. Liver 'organ on a chip'. *Exp. Cell Res.*, 363(1):15–25, feb 2018.
- [12] D. G. Belair, J. A. Whisler, J. Valdez, J. Velazquez, J. A. Molenda, V. Vickerman, R. Lewis, C. Daigh, T. D. Hansen, D. A. Mann, J. A. Thomson, L. G. Griffith, R. D. Kamm, M. P. Schwartz, and W. L. Murphy. Human Vascular Tissue Models Formed from Human Induced Pluripotent Stem Cell Derived Endothelial Cells. *Stem Cell Rev. Reports*, 11(3):511–525, 2015.
- [13] U. Ben-David, G. Ha, Y. Y. Tseng, N. F. Greenwald, C. Oh, J. Shih, J. M. McFarland, B. Wong, J. S. Boehm, R. Beroukhi, and T. R. Golub. Patient-derived xenografts undergo mouse-specific tumor evolution. *Nat. Genet.*, 49(11):1567–1575, 2017.
- [14] G. Bergers and D. Hanahan. Modes of resistance to anti-angiogenic therapy. *Nature Reviews Cancer*, 8(8):592–603, aug 2008.
- [15] S. N. Bhatia and D. E. Ingber. Microfluidic organs-on-chips. *Nat. Biotechnol.*, 32(8):760–772, 2014.
- [16] N. S. Bhise, J. Ribas, V. Manoharan, Y. S. Zhang, A. Polini, S. Massa, M. R. Dokmeci, and A. Khademhosseini. Organ-on-a-chip platforms for studying drug delivery systems. *J. Control. Release*, 190:82–93, 2014.
- [17] S. Bian, Y. Hou, X. Zhou, X. Li, J. Yong, Y. Wang, W. Wang, J. Yan, B. Hu, H. Guo, J. Wang, S. Gao, Y. Mao, J. Dong, P. Zhu, D. Xiu, L. Yan, L. Wen, J. Qiao, F. Tang, and W. Fu. Single-cell multiomics sequencing and analyses of human colorectal cancer. *Science*, 362(6418):1060–1063, nov 2018.
- [18] M. J. Bissell and D. Radisky. Putting tumours in context. *Nat. Rev. Cancer*, 1(1):46–54, 2001.
- [19] M. J. Bissell, A. Rizki, and I. S. Mian. Tissue architecture: the ultimate regulator of breast epithelial function. *Curr. Opin. Cell Biol.*, 15(6):753–62, dec 2003.
- [20] T. S. Blacker, Z. F. Mann, J. E. Gale, M. Ziegler, A. J. Bain, G. Szabadkai, and M. R. Duchon. Separating NADH and NADPH fluorescence in live cells and tissues using FLIM. *Nature Communications*, 5(1):3936, sep 2014.
- [21] A. Boussommier-Calleja, R. Li, M. B. Chen, S. C. Wong, and R. D. Kamm. Microfluidics: A new tool for modeling cancer-immune interactions. *Trends in cancer*, 2(1):6–19, jan 2016.
- [22] J. E. Bradner, D. Hnisz, and R. A. Young. Transcriptional Addiction in Cancer. *Cell*, 168(4):629–643, feb 2017.
- [23] M. D. Brennan, M. L. Rexius-Hall, L. J. Elgass, and D. T. Eddington. Oxygen control with microfluidics. *Lab Chip*, 14(22):4305–18, nov 2014.

- [24] A. Bruce, R. Evans, R. Mezan, L. Shi, B. S. Moses, K. H. Martin, L. F. Gibson, and Y. Yang. Three-dimensional microfluidic tri-culture model of the bone marrow microenvironment for study of acute lymphoblastic leukemia. *PLoS ONE*, 10(10):1–16, 2015.
- [25] A. Bruna, O. M. Rueda, W. Greenwood, A. S. Batra, M. Callari, R. N. Batra, K. Pogrebniak, J. Sandoval, J. W. Cassidy, A. Tufegdžic-Vidakovic, S. J. Sammut, L. Jones, E. Provenzano, R. Baird, P. Eirew, J. Hadfield, M. Eldridge, A. McLaren-Douglas, A. Barthorpe, H. Lightfoot, M. J. O’Connor, J. Gray, J. Cortes, J. Baselga, E. Marangoni, A. L. Welm, S. Aparicio, V. Serra, M. J. Garnett, and C. Caldas. A Biobank of Breast Cancer Explants with Preserved Intra-tumor Heterogeneity to Screen Anticancer Compounds. *Cell*, 167(1):260–274.e22, sep 2016.
- [26] R. A. Burrell, N. McGranahan, J. Bartek, and C. Swanton. The causes and consequences of genetic heterogeneity in cancer evolution. *Nature*, 501(7467):338–345, sep 2013.
- [27] P. W. BurrIDGE, Y. F. Li, E. Matsa, H. Wu, S. G. Ong, A. Sharma, A. Holmström, A. C. Chang, M. J. Coronado, A. D. Ebert, J. W. Knowles, M. L. Telli, R. M. Witteles, H. M. Blau, D. Bernstein, R. B. Altman, and J. C. Wu. Human induced pluripotent stem cell-derived cardiomyocytes recapitulate the predilection of breast cancer patients to doxorubicin-induced cardiotoxicity. *Nature Medicine*, 22(5):547–556, 2016.
- [28] A. Butler, P. Hoffman, P. Smibert, E. Papalexli, and R. Satija. Integrating single-cell transcriptomic data across different conditions, technologies, and species. *Nature Biotechnology*, 36(5):411–420, may 2018.
- [29] A. T. Byrne, D. G. Alférez, F. Amant, D. Annibaldi, J. Arribas, A. V. Biankin, A. Bruna, E. Budinská, C. Caldas, D. K. Chang, R. B. Clarke, H. Clevers, G. Coukos, V. Dangles-Marie, S. Gail Eckhardt, E. Gonzalez-Suarez, E. Hermans, M. Hidalgo, M. A. Jarzabek, S. De Jong, J. Jonkers, K. Kemper, L. Lanfrancone, G. M. Mælandsmo, E. Marangoni, J. C. Marine, E. Medico, J. H. Norum, H. G. Palmer, D. S. Peeper, P. G. Pelicci, A. Piris-Gimenez, S. Roman-Roman, O. M. Rueda, J. Seoane, V. Serra, L. Soucek, D. Vanhecke, A. Villanueva, E. Vinolo, A. Bertotti, and L. Trusolino. Interrogating open issues in cancer precision medicine with patient-derived xenografts. *Nature Reviews Cancer*, 17(4):254–268, 2017.
- [30] D. Caballero, S. M. Blackburn, M. de Pablo, J. Samitier, and L. Albertazzi. Tumour-vessel-on-a-chip models for drug delivery. *Lab Chip*, 17(22):3760–3771, 2017.
- [31] D. Caballero, S. Kaushik, V. Correló, J. Oliveira, R. Reis, and S. Kundu. Organ-on-chip models of cancer metastasis for future personalized medicine: From chip to the patient. *Biomaterials*, 149:98–115, dec 2017.
- [32] A. Calon, E. Espinet, S. Palomo-Ponce, D. V. Tauriello, M. Iglesias, M. V. Céspedes, M. Sevillano, C. Nadal, P. Jung, X. H.-F. Zhang, D. Byrom, A. Riera, D. Rossell, R. Mangues, J. Massagué, E. Sancho, and E. Batlle. Dependency of Colorectal Cancer

- on a TGF- β -Driven Program in Stromal Cells for Metastasis Initiation. *Cancer Cell*, 22(5):571–584, nov 2012.
- [33] P. Carmeliet and R. K. Jain. Molecular mechanisms and clinical applications of angiogenesis. *Nature*, 473(7347):298–307, may 2011.
- [34] A. Carreau, B. E. Hafny-Rahbi, A. Matejuk, C. Grillon, and C. Kieda. Why is the partial oxygen pressure of human tissues a crucial parameter? Small molecules and hypoxia. *J. Cell. Mol. Med.*, 15(6):1239–1253, 2011.
- [35] J. M. Chan, I. K. Zervantonakis, T. Rimchala, W. J. Polacheck, J. Whisler, and R. D. Kamm. Engineering of In Vitro 3D Capillary Beds by Self-Directed Angiogenic Sprouting. *PLoS One*, 7(12):1–11, 2012.
- [36] M. B. Chen, J. A. Whisler, J. Fröse, C. Yu, Y. Shin, and R. D. Kamm. On-chip human microvasculature assay for visualization and quantification of tumor cell extravasation dynamics. *Nat. Protoc.*, 12(5):865–880, 2017.
- [37] M. B. Chen, J. A. Whisler, J. S. Jeon, and R. D. Kamm. Mechanisms of tumor cell extravasation in an in vitro microvascular network platform. *Integr. Biol.*, 5(10):1262, 2013.
- [38] X. Chen, A. S. Aledia, S. a. Popson, L. Him, C. C. Hughes, and S. C. George. Rapid Anastomosis of Endothelial Progenitor Cell-Derived Vessels with Host Vasculature Is Promoted by a High Density of Cotransplanted Fibroblasts. *Tissue Eng. Part A*, 16(2):585–594, feb 2010.
- [39] Y.-A. Chen, A. D. King, H.-C. Shih, C.-C. Peng, C.-Y. Wu, W.-H. Liao, and Y.-C. Tung. Generation of oxygen gradients in microfluidic devices for cell culture using spatially confined chemical reactions. *Lab Chip*, 11(21):3626, 2011.
- [40] D.-J. Cheon and S. Orsulic. Mouse Models of Cancer. *Annual Review of Pathology: Mechanisms of Disease*, 6(1):95–119, feb 2011.
- [41] I. Cherciu, A. Bărbălan, D. Pirici, C. Mărgăritescu, and A. Săftoiu. Stem cells, colorectal cancer and cancer stem cell markers correlations. *Current health sciences journal*, 40(3):153–61, 2014.
- [42] S. Y. C. Choi, D. Lin, P. W. Gout, C. C. Collins, Y. Xu, and Y. Wang. Lessons from patient-derived xenografts for better in vitro modeling of human cancer. *Advanced Drug Delivery Reviews*, 79:222–237, 2014.
- [43] A. S. Chung, J. Lee, and N. Ferrara. Targeting the tumour vasculature: Insights from physiological angiogenesis. *Nat. Rev. Cancer*, 10(7):505–514, jul 2010.
- [44] M. Cirit and C. L. Stokes. Maximizing the impact of microphysiological systems with *in vitro* – *in vivo* translation. *Lab on a Chip*, 18:1831–1837, 2018.

- [45] J. G. Clohessy and P. P. Pandolfi. Mouse hospital and co-clinical trial project-from bench to bedside. *Nature Reviews Clinical Oncology*, 12(8):491–498, 2015.
- [46] A. L. Correia and M. J. Bissell. The tumor microenvironment is a dominant force in multidrug resistance. *Drug Resistance Updates*, 15(1-2):39–49, 2012.
- [47] L. M. Coussens and Z. Werb. Inflammation and cancer. *Nature*, 420(6917):860–867, 2002.
- [48] A. S. Crystal, A. T. Shaw, L. V. Sequist, L. Friboulet, M. J. Niederst, E. L. Lockerman, R. L. Frias, J. F. Gainor, A. Amzallag, P. Greninger, D. Lee, A. Kalsy, M. Gomez-Caraballo, L. Elamine, E. Howe, W. Hur, E. Lifshits, H. E. Robinson, R. Katayama, A. C. Faber, M. M. Awad, S. Ramaswamy, M. Mino-Kenudson, A. J. Iafrate, C. H. Benes, and J. A. Engelman. Patient-derived models of acquired resistance can identify effective drug combinations for cancer. *Science*, 346(6216):1480–1486, 2014.
- [49] I. Dagogo-Jack and A. T. Shaw. Tumour heterogeneity and resistance to cancer therapies. *Nature Reviews Clinical Oncology*, 15(2):81–94, 2018.
- [50] R. Datta, A. Alfonso-García, R. Cinco, and E. Gratton. Fluorescence lifetime imaging of endogenous biomarker of oxidative stress. *Scientific Reports*, 5(1):9848, sep 2015.
- [51] M. De Palma, D. Biziato, and T. V. Petrova. Microenvironmental regulation of tumour angiogenesis. *Nature Reviews Cancer*, 17(8):457–474, aug 2017.
- [52] J. S. Desgrosellier and D. A. Cheresh. Integrins in cancer: biological implications and therapeutic opportunities. *Nature Reviews Cancer*, 10(1):9–22, jan 2010.
- [53] M. Devarasetty, E. Wang, S. Soker, and A. Skardal. Mesenchymal stem cells support growth and organization of host-liver colorectal-tumor organoids and possibly resistance to chemotherapy. *Biofabrication*, 9(2):21002, 2017.
- [54] M. W. Dewhirst and T. W. Secomb. Transport of drugs from blood vessels to tumour tissue. *Nature Reviews Cancer*, 17(12):738–750, dec 2017.
- [55] J. A. DiMasi, H. G. Grabowski, and R. W. Hansen. Innovation in the pharmaceutical industry: New estimates of R&D costs. *J. Health Econ.*, 47:20–33, 2016.
- [56] G. Dranoff. Experimental mouse tumour models: what can be learnt about human cancer immunology? *Nature Reviews Immunology*, 12(1):61–66, jan 2012.
- [57] L. Drew. Pharmacogenetics: The right drug for you. *Nature*, 537(7619):S60–S62, sep 2016.
- [58] J. Drost and H. Clevers. Organoids in cancer research. *Nat. Rev. Cancer*, 18(7):407–418, jul 2018.

- [59] C. D. Edington, W. L. K. Chen, E. Geishecker, T. Kassis, L. R. Soenksen, B. M. Bhushan, D. Freake, J. Kirschner, C. Maass, N. Tsamandouras, J. Valdez, C. D. Cook, T. Parent, S. Snyder, J. Yu, E. Suter, M. Shockley, J. Velazquez, J. J. Velazquez, L. Stockdale, J. P. Papps, I. Lee, N. Vann, M. Gamboa, M. E. LaBarge, Z. Zhong, X. Wang, L. A. Boyer, D. A. Lauffenburger, R. L. Carrier, C. Communal, S. R. Tannenbaum, C. L. Stokes, D. J. Hughes, G. Rohatgi, D. L. Trumper, M. Cirit, and L. G. Griffith. Interconnected Microphysiological Systems for Quantitative Biology and Pharmacology Studies. *Sci. Rep.*, 8(1):4530, dec 2018.
- [60] R. Edmondson, J. J. Broglie, A. F. Adcock, and L. Yang. Three-Dimensional Cell Culture Systems and Their Applications in Drug Discovery and Cell-Based Biosensors. *ASSAY and Drug Development Technologies*, 12(4):207–218, 2014.
- [61] S. M. Ehsan and S. C. George. Vessel network formation in response to intermittent hypoxia is frequency dependent. *J. Biosci. Bioeng.*, 120(3):347–350, sep 2015.
- [62] S. M. Ehsan, K. M. Welch-Reardon, M. L. Waterman, C. C. W. Hughes, and S. C. George. A three-dimensional in vitro model of tumor cell intravasation. *Integr. Biol.*, 6(6):603–610, 2014.
- [63] P. Eirew, A. Steif, J. Khattra, G. Ha, D. Yap, H. Farahani, K. Gelmon, S. Chia, C. Mar, A. Wan, E. Laks, J. Biele, K. Shumansky, J. Rosner, A. McPherson, C. Nielsen, A. J. Roth, C. Lefebvre, A. Bashashati, C. De Souza, C. Siu, R. Aniba, J. Brimhall, A. Oloumi, T. Osako, A. Bruna, J. L. Sandoval, T. Algara, W. Greenwood, K. Leung, H. Cheng, H. Xue, Y. Wang, D. Lin, A. J. Mungall, R. Moore, Y. Zhao, J. Lorette, L. Nguyen, D. Huntsman, C. J. Eaves, C. Hansen, M. A. Marra, C. Caldas, S. P. Shah, and S. Aparicio. Dynamics of genomic clones in breast cancer patient xenografts at single-cell resolution. *Nature*, 518(7539):422–426, 2015.
- [64] N. T. Elliott and F. Yuan. A review of three-dimensional in vitro tissue models for drug discovery and transport studies. *J. Pharm. Sci.*, 100(1):59–74, 2011.
- [65] E. W. Esch, A. Bahinski, and D. Huh. Organs-on-chips at the frontiers of drug discovery. *Nat. Rev. Drug Discov.*, 14(4):248–260, 2015.
- [66] J. Fan, D. Shang, B. Han, J. Song, H. Chen, and J.-m. Yang. Adoptive Cell Transfer: Is it a Promising Immunotherapy for Colorectal Cancer? *Theranostics*, 8(20):5784–5800, 2018.
- [67] Y. Fang and R. M. Eglén. Three-Dimensional Cell Cultures in Drug Discovery and Development. *SLAS DISCOVERY: Advancing Life Sciences R&D*, page 247255521769679, 2017.
- [68] S. Farkona, E. P. Diamandis, and I. M. Blasutig. Cancer immunotherapy: the beginning of the end of cancer? *BMC Med.*, 14(1):73, may 2016.
- [69] C. Fellmann, B. G. Gowen, P. C. Lin, J. A. Doudna, and J. E. Corn. Cornerstones of CRISPR-Cas in drug discovery and therapy. *Nature Reviews Drug Discovery*, 16(2):89–100, 2017.

- [70] J. Folkman. Angiogenesis: An organizing principle for drug discovery? *Nat. Rev. Drug Discov.*, 6(4):273–286, apr 2007.
- [71] A. H. Fong, M. Romero-López, C. M. Heylman, M. Keating, D. Tran, A. Sobrino, A. Q. Tran, H. H. Pham, C. Fimbres, P. D. Gershon, E. L. Botvinick, S. C. George, and C. C. Hughes. Three-Dimensional Adult Cardiac Extracellular Matrix Promotes Maturation of Human Induced Pluripotent Stem Cell-Derived Cardiomyocytes. *Tissue Engineering Part A*, 22(15-16):1016–1025, 2016.
- [72] P. Friedl and S. Alexander. Cancer invasion and the microenvironment: Plasticity and reciprocity. *Cell*, 147(5):992–1009, 2011.
- [73] J. Galon, A. Costes, F. Sanchez-Cabo, A. Kirilovsky, B. Mlecnik, C. Lagorce-Pagès, M. Tosolini, M. Camus, A. Berger, P. Wind, F. Zinzindohoué, P. Bruneval, P.-H. Cugnenc, Z. Trajanoski, W.-H. Fridman, and F. Pagès. Type, density, and location of immune cells within human colorectal tumors predict clinical outcome. *Science*, 313(5795):1960–1964, 2006.
- [74] A. M. Ghaemmaghami, M. J. Hancock, H. Harrington, H. Kaji, and A. Khademhosseini. Biomimetic tissues on a chip for drug discovery. *Drug Discov. Today*, 17(3-4):173–181, 2012.
- [75] M. Ghandi, F. W. Huang, J. Jané-Valbuena, G. V. Kryukov, C. C. Lo, E. R. McDonald, J. Barretina, E. T. Gelfand, C. M. Bielski, H. Li, et al. Next-generation characterization of the cancer cell line encyclopedia. *Nature*, 569(7757):503, 2019.
- [76] C. Giese, A. Lubitz, C. D. Demmler, J. Reuschel, K. Bergner, and U. Marx. Immunological substance testing on human lymphatic micro-organoids in vitro. *Journal of Biotechnology*, 148(1):38–45, 2010.
- [77] Git source control. <http://git-scm.com/>. Accessed: 2018-08-23.
- [78] P. Grabowski, I. Schindler, I. Anagnostopoulos, H.-D. Foss, E.-O. Riecken, U. Mansmann, H. Stein, G. Berger, H.-J. Buhr, and H. Scherübl. Neuroendocrine differentiation is a relevant prognostic factor in stage III–IV colorectal cancer. *European Journal of Gastroenterology & Hepatology*, 13(4):405–411, apr 2001.
- [79] L. G. Griffith and M. A. Swartz. Capturing complex 3D tissue physiology in vitro. *Nature reviews Molecular cell biology*, 7(3):211–24, 2006.
- [80] S. J. Hachey and C. C. Hughes. Applications of tumor chip technology. *Lab on a Chip*, 18(19):2893–2912, 2018.
- [81] S. J. Hachey and C. C. W. Hughes. Applications of tumor chip technology. *Lab on a Chip*, 18(19):2893–2912, 2018.
- [82] H. Hamidi and J. Ivaska. Every step of the way: integrins in cancer progression and metastasis. *Nature Reviews Cancer*, 18(9):533–548, sep 2018.

- [83] D. Hanahan and R. A. Weinberg. Hallmarks of cancer: The next generation. *Cell*, 144(5):646–674, 2011.
- [84] B. A. Hassell, G. Goyal, E. Lee, A. Sontheimer-Phelps, O. Levy, C. S. Chen, and D. E. Ingber. Human Organ Chip Models Recapitulate Orthotopic Lung Cancer Growth, Therapeutic Responses, and Tumor Dormancy In Vitro. *Cell Rep.*, 21(2):508–516, 2017.
- [85] C. Heylman, A. Sobrino, V. S. Shirure, C. C. Hughes, and S. C. George. A strategy for integrating essential three-dimensional microphysiological systems of human organs for realistic anticancer drug screening. *Experimental biology and medicine (Maywood, N.J.)*, 239(9):1240–54, 2014.
- [86] C. Heylman, A. Sobrino, V. S. Shirure, C. C. W. Hughes, and S. C. George. A strategy for integrating essential three-dimensional microphysiological systems of human organs for realistic anticancer drug screening. *Exp. Biol. Med.*, 239(9):1240–1254, 2014.
- [87] Homebrew. <http://brew.sh/>. Accessed: 2018-08-23.
- [88] T.-H. Hsu, Y.-L. Kao, W.-L. Lin, J.-L. Xiao, P.-L. Kuo, C.-W. Wu, W.-Y. Liao, and C.-H. Lee. The migration speed of cancer cells influenced by macrophages and myofibroblasts co-cultured in a microfluidic chip. *Integr. Biol. (Camb.)*, 4(2):177–82, feb 2012.
- [89] Y. H. Hsu, M. L. Moya, P. Abiri, C. C. Hughes, S. C. George, and A. P. Lee. Full range physiological mass transport control in 3D tissue cultures. *Lab on a Chip*, 13(1):81–89, 2013.
- [90] Y.-H. Hsu, M. L. Moya, C. C. W. Hughes, S. C. Georgea, and A. P. Lee. A microfluidic platform for generating large-scale nearly identical human microphysiological system arrays. *Lab Chip*, 13(15):2990–2998, 2013.
- [91] Y. Huang, B. Y. S. Kim, C. K. Chan, S. M. Hahn, I. L. Weissman, and W. Jiang. Improving immune–vascular crosstalk for cancer immunotherapy. *Nature Reviews Immunology*, 18(3):195–203, mar 2018.
- [92] N. Huebsch, P. Loskill, N. Deveshwar, C. I. Spencer, L. M. Judge, M. A. Mandegar, C. B. Fox, T. M. Mohamed, Z. Ma, A. Mathur, A. M. Sheehan, A. Truong, M. Saxton, J. Yoo, D. Srivastava, T. A. Desai, P.-L. So, K. E. Healy, and B. R. Conklin. Miniaturized iPSC-Derived Cardiac Muscles for Physiologically Relevant Drug Response Analyses. *Sci. Rep.*, 6(1):24726, jul 2016.
- [93] C. C. Hughes., C. O. Savage, and J. S. Pober. The Endothelial Cell as a Regulator of TâCell Function. *Immunol. Rev.*, 117(1):85–102, 1990.
- [94] D. Huh, D. C. Leslie, B. D. Matthews, J. P. Fraser, S. Jurek, G. a. Hamilton, K. S. Thorneloe, M. A. Mcalexander, and D. E. Ingber. A Human Disease Model of Drug

- Toxicity à Induced Pulmonary Edema in a Lung-on-a-Chip Microdevice. *Sci. Transl. Med.*, 4(159):1–9, 2012.
- [95] D. Huh, B. D. Matthews, A. Mammoto, M. Montoya-Zavala, H. Y. Hsin, and D. E. Ingber. Reconstituting Organ-Level Lung Functions on a Chip. *Science (80-.)*, 328(5986):1662–1668, jun 2010.
- [96] L. Hutchinson and R. Kirk. High drug attrition rates—where are we going wrong? *Nature reviews. Clinical oncology*, 8(4):189–90, 2011.
- [97] W. Hwang, Y.-F. Chiu, M.-H. Kuo, K.-L. Lee, A.-C. Lee, C.-C. Yu, J.-L. Chang, W.-C. Huang, S.-H. Hsiao, S.-E. Lin, and Y.-T. Chou. Expression of Neuroendocrine Factor VGF in Lung Cancer Cells Confers Resistance to EGFR Kinase Inhibitors and Triggers Epithelial-to-Mesenchymal Transition. *Cancer Research*, 77(11):3013–3026, jun 2017.
- [98] D. E. Ingber. Reverse Engineering Human Pathophysiology with Organs-on-Chips. *Cell*, 164(6):1105–1109, 2016.
- [99] J. L. Inman, C. Robertson, J. D. Mott, and M. J. Bissell. Mammary gland development: cell fate specification, stem cells and the microenvironment. *Development*, 142(6):1028–1042, 2015.
- [100] E. Izumchenko, K. Paz, D. Ciznadija, I. Sloma, A. Katz, D. Vasquez-Dunddel, I. Ben-Zvi, J. Stebbing, W. McGuire, W. Harris, R. Maki, A. Gaya, A. Bedi, S. Zacharoulis, R. Ravi, L. H. Wexler, M. O. Hoque, C. Rodriguez-Galindo, H. Pass, N. Peled, A. Davies, R. Morris, M. Hidalgo, and D. Sidransky. Patient-derived xenografts effectively capture responses to oncology therapy in a heterogeneous cohort of patients with solid tumors. *Annals of Oncology*, 28(10):2595–2605, 2017.
- [101] R. K. Jain. Molecular regulation of vessel maturation. *Nature Medicine*, 9(6):685–693, jun 2003.
- [102] R. K. Jain. Normalization of tumor vasculature: An emerging concept in antiangiogenic therapy. *Science*, 307(5706):58–62, 2005.
- [103] M. Jang, I. Koh, S. J. Lee, J.-H. Cheong, and P. Kim. Droplet-based microtumor model to assess cell-ECM interactions and drug resistance of gastric cancer cells. *Sci. Rep.*, 7(December 2016):41541, jan 2017.
- [104] W. Jawaaid. *enrichR: Provides an R Interface to 'Enrichr'*, 2019. R package version 2.0.
- [105] R. W. Jenkins, A. R. Aref, P. H. Lizotte, E. Ivanova, S. Stinson, C. W. Zhou, M. Bowden, J. Deng, H. Liu, D. Miao, M. X. He, W. Walker, G. Zhang, T. Tian, C. Cheng, Z. Wei, S. Palakurthi, M. Bittinger, H. Vitzthum, J. W. Kim, A. Merlino, M. Quinn, C. Venkataramani, J. A. Kaplan, A. Portell, P. C. Gokhale, B. Phillips, A. Smart, A. Rotem, R. E. Jones, L. Keogh, M. Anguiano, L. Stapleton, Z. Jia, M. Barzily-Rokni, I. Cañadas, T. C. Thai, M. R. Hammond, R. Vlahos, E. S. Wang, H. Zhang, S. Li, G. J. Hanna, W. Huang, M. P. Hoang, A. Piris, J.-P. Eliane, A. O. Stemmer-Rachamimov,

- L. Cameron, M.-J. Su, P. Shah, B. Izar, M. Thakuria, N. R. LeBoeuf, G. Rabinowitz, V. Gunda, S. Parangi, J. M. Cleary, B. C. Miller, S. Kitajima, R. Thummalapalli, B. Miao, T. U. Barbie, V. Sivathanu, J. Wong, W. G. Richards, R. Bueno, C. H. Yoon, J. Miret, M. Herlyn, L. A. Garraway, E. M. Van Allen, G. J. Freeman, P. T. Kirschmeier, J. H. Lorch, P. A. Ott, F. S. Hodi, K. T. Flaherty, R. D. Kamm, G. M. Boland, K.-K. Wong, D. Dornan, C. P. Paweletz, and D. A. Barbie. Ex Vivo Profiling of PD-1 Blockade Using Organotypic Tumor Spheroids. *Cancer Discov.*, 8(2):196–215, feb 2018.
- [106] J. S. Jeon, S. Bersini, J. A. Whisler, M. B. Chen, G. Dubini, J. L. Charest, M. Moretti, and R. D. Kamm. Generation of 3D functional microvascular networks with human mesenchymal stem cells in microfluidic systems. *Integr. Biol. (Camb)*., 6(5):555–63, may 2014.
- [107] S. Y. Jeong, J. H. Lee, Y. Shin, S. Chung, and H. J. Kuh. Co-culture of tumor spheroids and fibroblasts in a collagen matrix-incorporated microfluidic chip mimics reciprocal activation in solid tumor microenvironment. *PLoS One*, 11(7):1–17, 2016.
- [108] H. Jiang, S. Hegde, B. L. Knolhoff, Y. Zhu, J. M. Herndon, M. A. Meyer, T. M. Nywening, W. G. Hawkins, I. M. Shapiro, D. T. Weaver, J. A. Pachter, A. Wang-Gillam, and D. G. DeNardo. Targeting focal adhesion kinase renders pancreatic cancers responsive to checkpoint immunotherapy. *Nat. Med.*, 22(8):851–60, 2016.
- [109] A. Junaid, A. Mashaghi, T. Hankemeier, and P. Vulto. An end-user perspective on Organ-on-a-Chip: Assays and usability aspects. *Current Opinion in Biomedical Engineering*, 1:15–22, 2017.
- [110] L. Kang, B. G. Chung, R. Langer, and A. Khademhosseini. Microfluidics for drug discovery and development: From target selection to product lifecycle management. *Drug Discov. Today*, 13(1-2):1–13, 2008.
- [111] M. Kasendra, A. Tovagliari, A. Sontheimer-Phelps, S. Jalili-Firoozinezhad, A. Bein, A. Chalkiadaki, W. Scholl, C. Zhang, H. Rickner, C. A. Richmond, H. Li, D. T. Breault, and D. E. Ingber. Development of a primary human Small Intestine-on-a-Chip using biopsy-derived organoids. *Scientific Reports*, 8(1):1–14, 2018.
- [112] J. N. Kather, N. Halama, and D. Jaeger. Genomics and emerging biomarkers for immunotherapy of colorectal cancer. *Seminars in Cancer Biology*, 52(February):189–197, oct 2018.
- [113] J. N. Kather, F. G. Zöllner, L. R. Schad, S. M. Melchers, H.-p. Sinn, A. Marx, T. Gaiser, and C.-a. Weis. Identification of a characteristic vascular belt zone in human colorectal cancer. *PLOS ONE*, 12(3):e0171378, mar 2017.
- [114] S. N. Kehlet, R. Sanz-Pamplona, S. Brix, D. J. Leeming, M. A. Karsdal, and V. Moreno. Excessive collagen turnover products are released during colorectal cancer progression and elevated in serum from metastatic colorectal cancer patients. *Scientific Reports*, 6(1):30599, nov 2016.

- [115] K. Kersten, K. E. Visser, M. H. Miltenburg, and J. Jonkers. Genetically engineered mouse models in oncology research and cancer medicine. *EMBO Molecular Medicine*, 9(2):137–153, feb 2017.
- [116] K. Kessenbrock, V. Plaks, and Z. Werb. Matrix Metalloproteinases: Regulators of the Tumor Microenvironment. *Cell*, 141(1):52–67, apr 2010.
- [117] K. A. Khan and R. S. Kerbel. Improving immunotherapy outcomes with anti-angiogenic treatments and vice versa. *Nature Reviews Clinical Oncology*, 15(5):310–324, may 2018.
- [118] A. S. Khazali, A. M. Clark, and A. Wells. A Pathway to Personalizing Therapy for Metastases Using Liver-on-a-Chip Platforms. *Stem Cell Rev. Reports*, 13(3):364–380, 2017.
- [119] C. Kim, J. Kasuya, J. Jeon, S. Chung, and R. D. Kamm. A quantitative microfluidic angiogenesis screen for studying anti-angiogenic therapeutic drugs. *Lab Chip*, 15(1):301–310, jan 2015.
- [120] H. J. Kim, D. Huh, G. Hamilton, and D. E. Ingber. Human gut-on-a-chip inhabited by microbial flora that experiences intestinal peristalsis-like motions and flow. *Lab Chip*, 12(12):2165, 2012.
- [121] H. J. Kim, H. Li, J. J. Collins, and D. E. Ingber. Contributions of microbiome and mechanical deformation to intestinal bacterial overgrowth and inflammation in a human gut-on-a-chip. *Proceedings of the National Academy of Sciences*, 113(1):E7–E15, 2016.
- [122] J. Kim, M. Chung, S. Kim, D. H. Jo, J. H. Kim, and N. L. Jeon. Engineering of a biomimetic pericyte-covered 3D microvascular network. *PLoS One*, 10(7):1–15, 2015.
- [123] S. Kim, H. Lee, M. Chung, and N. L. Jeon. Engineering of functional, perfusable 3D microvascular networks on a chip. *Lab Chip*, 13(8):1489, 2013.
- [124] S. J. Kim, K. H. Jung, M. K. Son, J. H. Park, H. H. Yan, Z. Fang, Y. W. Kang, B. Han, J. H. Lim, and S.-S. Hong. Tumor vessel normalization by the pi3k inhibitor hs-173 enhances drug delivery. *Cancer letters*, 403:339–353, 2017.
- [125] J. Kimmelman and C. Federico. Consider drug efficacy before first-in-human trials. *Nature*, 542(7639):25–27, jan 2017.
- [126] L. Knezevic, M. Schaupper, S. Mühleder, K. Schimek, T. Hasenberg, U. Marx, E. Priglinger, H. Redl, and W. Holnthoner. Engineering Blood and Lymphatic Microvascular Networks in Fibrin Matrices. *Frontiers in Bioengineering and Biotechnology*, 5(April):1–12, 2017.
- [127] D. P. Kodack, A. F. Farago, A. Dastur, M. A. Held, L. Dardaei, L. Friboulet, F. von Flotow, L. J. Damon, D. Lee, M. Parks, R. Dicecca, M. Greenberg, K. E. Kattermann, A. K. Riley, F. J. Fintelmann, C. Rizzo, Z. Piotrowska, A. T. Shaw, J. F. Gainor, L. V.

- Sequist, M. J. Niederst, J. A. Engelman, and C. H. Benes. Primary patient-derived cancer cells and their potential for personalized cancer patient care. *Cell Reports*, 21(11):3298 – 3309, 2017.
- [128] I. Kola and J. Landis. Can the pharmaceutical industry reduce attrition rates? *Nat. Rev. Drug Discov.*, 3(8):711–716, aug 2004.
- [129] Y. K. Kurokawa, R. T. Yin, M. R. Shang, V. S. Shirure, M. L. Moya, and S. C. George. Human Induced Pluripotent Stem Cell-Derived Endothelial Cells for Three-Dimensional Microphysiological Systems. *Tissue Eng. Part C Methods*, 23(8):474–484, 2017.
- [130] S. Lamouille, J. Xu, and R. Derynck. Molecular mechanisms of epithelial-mesenchymal transition. *Nat. Rev. Mol. Cell Biol.*, 15(3):178–196, 2014.
- [131] M. A. Lancaster and J. A. Knoblich. Organogenesis in a dish: Modeling development and disease using organoid technologies. *Science*, 345(6194):1247125–1247125, jul 2014.
- [132] M. Landgraf, J. A. McGovern, P. Friedl, and D. W. Huttmacher. Rational Design of Mouse Models for Cancer Research. *Trends in Biotechnology*, 36(3), 2018.
- [133] R. R. Langley and I. J. Fidler. Tumor cell-organ microenvironment interactions in the pathogenesis of cancer metastasis. *Endocr. Rev.*, 28(3):297–321, 2007.
- [134] G. Y. Lee, P. a. Kenny, E. H. Lee, and M. J. Bissell. Three-dimensional culture models of normal and malignant breast epithelial cells. *Nat. Methods*, 4(4):359–365, apr 2007.
- [135] S. H. Lee, W. Hu, J. T. Matulay, M. V. Silva, T. B. Owczarek, K. Kim, C. W. Chua, L. M. J. Barlow, C. Kandoth, A. B. Williams, S. K. Bergren, E. J. Pietzak, C. B. Anderson, M. C. Benson, J. A. Coleman, B. S. Taylor, C. Abate-Shen, J. M. McKiernan, H. Al-Ahmadie, D. B. Solit, and M. M. Shen. Tumor Evolution and Drug Response in Patient-Derived Organoid Models of Bladder Cancer. *Cell*, 173(2):515–528.e17, 2018.
- [136] C. H. Li and C. Lee. Minimum cross entropy thresholding. *Pattern recognition*, 26(4):617–625, 1993.
- [137] H. Li, E. T. Courtois, D. Sengupta, Y. Tan, K. H. Chen, J. J. L. Goh, S. L. Kong, C. Chua, L. K. Hon, W. S. Tan, M. Wong, P. J. Choi, L. J. K. Wee, A. M. Hillmer, I. B. Tan, P. Robson, and S. Prabhakar. Reference component analysis of single-cell transcriptomes elucidates cellular heterogeneity in human colorectal tumors. *Nature Genetics*, 49(5):708–718, may 2017.
- [138] M. L. Li, J. Aggeler, D. A. Farson, C. Hatier, J. Hassell, and M. J. Bissell. Influence of a reconstituted basement membrane and its components on casein gene expression and secretion in mouse mammary epithelial cells. *Proc. Natl. Acad. Sci. U. S. A.*, 84(1):136–40, 1987.

- [139] T. Lindholm, F. Yellin, G. Bracha, and A. Buckley. *The Java Virtual Machine Specification, Java SE 8 Edition*. Addison-Wesley Professional, 1st edition, 2014.
- [140] M. Linkert, C. T. Rueden, C. Allan, J.-M. Burel, W. Moore, A. Patterson, B. Loranger, J. Moore, C. Neves, D. MacDonald, et al. Metadata matters: access to image data in the real world. *The Journal of cell biology*, 189(5):777–782, 2010.
- [141] Y. Liu, J. He, J. Xu, J. Li, Y. Jiao, D. Bei, Y. Hu, H. Chen, Q. Xiao, and K. Ding. Neuroendocrine differentiation is predictive of poor survival in patients with stage II colorectal cancer. *Oncology Letters*, 13(4):2230–2236, apr 2017.
- [142] L. A. Low and D. A. Tagle. Tissue chips - innovative tools for drug development and disease modeling. *Lab Chip*, 17(18):3026–3036, sep 2017.
- [143] L. A. Low and D. A. Tagle. ‘You-on-a-chip’ for precision medicine. *Expert Review of Precision Medicine and Drug Development*, 3(2):137–146, 2018.
- [144] P. Lu, V. M. Weaver, and Z. Werb. The extracellular matrix: A dynamic niche in cancer progression. *J. Cell Biol.*, 196(4):395–406, feb 2012.
- [145] B. Majumder, U. Baraneedharan, S. Thiyagarajan, P. Radhakrishnan, H. Narasimhan, M. Dhandapani, N. Brijwani, D. D. Pinto, A. Prasath, B. U. Shanthappa, A. Thayakumar, R. Surendran, G. K. Babu, A. M. Shenoy, M. A. Kuriakose, G. Bergthold, P. Horowitz, M. Loda, R. Beroukhim, S. Agarwal, S. Sengupta, M. Sundaram, and P. K. Majumder. Predicting clinical response to anticancer drugs using an ex vivo platform that captures tumour heterogeneity. *Nature Communications*, 6(1):6169, may 2015.
- [146] I. W. Mak, N. Evaniew, and M. Ghert. Lost in translation: animal models and clinical trials in cancer treatment. *Am. J. Transl. Res.*, 6(2):114–8, 2014.
- [147] C. C. Maley, A. Aktipis, T. A. Graham, A. Sottoriva, A. M. Boddy, M. Janiszewska, A. S. Silva, M. Gerlinger, Y. Yuan, K. J. Pienta, K. S. Anderson, R. Gatenby, C. Swanton, D. Posada, C. I. Wu, J. D. Schiffman, E. S. Hwang, K. Polyak, A. R. Anderson, J. S. Brown, M. Greaves, and D. Shibata. Classifying the evolutionary and ecological features of neoplasms. *Nature Reviews Cancer*, 17(10):605–619, 2017.
- [148] F. Mannello and G. A. Tonti. Concise review: No breakthroughs for human mesenchymal and embryonic stem cell culture: Conditioned medium, feeder layer, or feeder-free; medium with fetal calf serum, human serum, or enriched plasma; serum-free, serum replacement nonconditioned medium, or ad hoc formula? all that glitters is not gold! *STEM CELLS*, 25(7):1603–1609, 2007.
- [149] F. Marcucci, G. Stassi, and R. De Maria. Epithelial-mesenchymal transition: A new target in anticancer drug discovery. *Nat. Rev. Drug Discov.*, 15(5):311–325, 2016.

- [150] A. Marturano-Kruik, M. M. Nava, K. Yeager, A. Chramiec, L. Hao, S. Robinson, E. Guo, M. T. Raimondi, and G. Vunjak-Novakovic. Human bone perivascular niche-on-a-chip for studying metastatic colonization. *Proceedings of the National Academy of Sciences*, 115(6):1256–1261, 2018.
- [151] A. Marturano-Kruik, A. Villasante, K. Yeager, S. R. Ambati, A. Chramiec, M. T. Raimondi, and G. Vunjak-Novakovic. Biomechanical regulation of drug sensitivity in an engineered model of human tumor. *Biomaterials*, 150:150–161, 2018.
- [152] U. Marx, T. B. Andersson, A. Bahinski, M. Beilmann, S. Beken, F. R. Cassee, M. Cirit, M. Daneshian, S. Fitzpatrick, O. Frey, C. Gaertner, C. Giese, L. Griffith, T. Hartung, M. B. Heringa, J. Hoeng, W. H. De Jong, H. Kojima, J. Kuehnl, M. Leist, A. Luch, I. Maschmeyer, D. Sakharov, A. J. Sips, T. Steger-Hartmann, D. A. Tagle, A. Tonevitsky, T. Tralau, S. Tsyb, A. Van De Stolpe, R. Vandebriel, P. Vulto, J. Wang, J. Wiest, M. Rodenburg, and A. Roth. Biology-inspired microphysiological system approaches to solve the prediction dilemma of substance testing. *Altex*, 33(3):272–321, 2016.
- [153] J. Massagué. TGF β in Cancer. *Cell*, 134(2):215–230, jul 2008.
- [154] A. Mathur, P. Loskill, S. Hong, J. Y. Lee, S. G. Marcus, L. Dumont, B. R. Conklin, H. Willenbring, L. P. Lee, and K. E. Healy. Human induced pluripotent stem cell-based microphysiological tissue models of myocardium and liver for drug development. *Stem Cell Res. Ther.*, 4 Suppl 1(Suppl 1):S14, 2013.
- [155] A. Mathur, P. Loskill, K. Shao, N. Huebsch, S. Hong, S. G. Marcus, N. Marks, M. Mandegar, B. R. Conklin, L. P. Lee, and K. E. Healy. Human iPSC-based Cardiac Microphysiological System For Drug Screening Applications. *Sci. Rep.*, 5(1):8883, aug 2015.
- [156] M. B. Meads, R. A. Gatenby, and W. S. Dalton. Environment-mediated drug resistance: a major contributor to minimal residual disease. *Nature Reviews Cancer*, 9(9):665–674, sep 2009.
- [157] M. A. Mena, T. P. Treynor, S. L. Mayo, and P. S. Daugherty. Blue fluorescent proteins with enhanced brightness and photostability from a structurally targeted library. *Nature Biotechnology*, 24(12):1569–1571, dec 2006.
- [158] J. Mestas and C. C. W. Hughes. Of Mice and Not Men: Differences between Mouse and Human Immunology. *J. Immunol.*, 172(5):2731–2738, mar 2004.
- [159] Z. Moghadamyeghaneh, R. F. Alizadeh, M. Phelan, J. C. Carmichael, S. Mills, A. Pigazzi, J. A. Zell, and M. J. Stamos. Trends in colorectal cancer admissions and stage at presentation: impact of screening. *Surgical Endoscopy*, 30(8):3604–3610, aug 2016.
- [160] M. L. Moya, Y.-H. Hsu, A. P. Lee, C. C. Hughes, and S. C. George. In Vitro Perfused Human Capillary Networks. *Tissue Eng. Part C Methods*, 19(9):730–737, sep 2013.

- [161] M. L. Moya, Y.-H. Hsu, A. P. Lee, C. C. Hughes, and S. C. George. *In Vitro* Perfused Human Capillary Networks. *Tissue Engineering Part C: Methods*, 19(9):730–737, 2013.
- [162] M. Muhsin, J. Graham, and P. Kirkpatrick. Bevacizumab. *Nature Reviews Drug Discovery*, 3(12):995–996, dec 2004.
- [163] E. S. Nakasone, H. A. Askautrud, T. Kees, J. H. Park, V. Plaks, A. J. Ewald, M. Fein, M. G. Rasch, Y. X. Tan, J. Qiu, J. Park, P. Sinha, M. J. Bissell, E. Frengen, Z. Werb, and M. Egeblad. Imaging Tumor-Stroma Interactions during Chemotherapy Reveals Contributions of the Microenvironment to Resistance. *Cancer Cell*, 21(4):488–503, 2012.
- [164] D.-H. T. Nguyen, S. C. Stapleton, M. T. Yang, S. S. Cha, C. K. Choi, P. A. Galie, and C. S. Chen. Biomimetic model to reconstitute angiogenic sprouting morphogenesis in vitro. *Proc. Natl. Acad. Sci.*, 110(17):6712–6717, apr 2013.
- [165] D. T. Odom, R. D. Dowell, E. S. Jacobsen, W. Gordon, T. W. Danford, K. D. MacIsaac, P. A. Rolfe, C. M. Conboy, D. K. Gifford, and E. Fraenkel. Tissue-specific transcriptional regulation has diverged significantly between human and mouse. *Nat. Genet.*, 39(6):730–732, 2007.
- [166] B. Olson, Y. Li, Y. Lin, E. T. Liu, and A. Patnaik. Mouse models for cancer immunotherapy research. *Cancer Discovery*, 8(11):1358–1365, 2018.
- [167] I. S. Organization. ISO 10918-1:1994 - Information technology – Digital compression and coding of continuous-tone still images: Requirements and guidelines. Standard, International Organization for Standardization, Geneva, CH, Feb. 1995.
- [168] I. S. Organization. ISO 10918-5:2013 - Information technology – Digital compression and coding of continuous-tone still images: JPEG File Interchange Format (JFIF). Standard, International Organization for Standardization, Geneva, CH, May 2013.
- [169] E. P. Papapetrou. Patient-derived induced pluripotent stem cells in cancer research and precision oncology. *Nat. Med.*, 22(12):1392–1401, 2016.
- [170] J.-s. Park, I.-K. Kim, S. Han, I. Park, C. Kim, J. Bae, S. J. Oh, S. Lee, J. H. Kim, D.-C. Woo, Y. He, H. G. Augustin, I. Kim, D. Lee, and G. Y. Koh. Normalization of Tumor Vessels by Tie2 Activation and Ang2 Inhibition Enhances Drug Delivery and Produces a Favorable Tumor Microenvironment. *Cancer Cell*, 30(6):953–967, dec 2016.
- [171] S. Parlato, A. De Ninno, R. Molfetta, E. Toschi, D. Salerno, A. Mencattini, G. Romagnoli, A. Fragale, L. Roccazzello, M. Buoncervello, I. Canini, E. Bentivegna, M. Falchi, F. R. Bertani, A. Gerardino, E. Martinelli, C. Natale, R. Paolini, L. Businaro, and L. Gabriele. 3D Microfluidic model for evaluating immunotherapy efficacy by tracking dendritic cell behaviour toward tumor cells. *Sci. Rep.*, 7(1):1093, apr 2017.

- [172] K. T. Pate, C. Stringari, S. Sprowl-Tanio, K. Wang, T. TeSlaa, N. P. Hoverter, M. M. McQuade, C. Garner, M. A. Digman, M. A. Teitell, R. A. Edwards, E. Gratton, and M. L. Waterman. Wnt signaling directs a metabolic program of glycolysis and angiogenesis in colon cancer. *The EMBO Journal*, 33(13):1454–1473, may 2014.
- [173] C. D. Paul, P. Mistriotis, and K. Konstantopoulos. Cancer cell motility: lessons from migration in confined spaces. *Nature Reviews Cancer*, 17(2):131–140, feb 2017.
- [174] A. Pavesi, G. Adriani, A. Tay, M. E. Warkiani, W. H. Yeap, S. C. Wong, and R. D. Kamm. Engineering a 3D microfluidic culture platform for tumor-treating field application. *Sci. Rep.*, 6(1):26584, jul 2016.
- [175] P. Perel, I. Roberts, E. Sena, P. Wheble, C. Briscoe, P. Sandercock, M. Macleod, L. E. Mignini, P. Jayaram, and K. S. Khan. Comparison of treatment effects between animal experiments and clinical trials: systematic review. *Br. Med. J.*, 334(7586):197–200, 2007.
- [176] J. Y. Perentes, T. D. McKee, C. D. Ley, H. Mathiew, M. Dawson, T. P. Padera, L. L. Munn, R. K. Jain, and Y. Boucher. In vivo imaging of extracellular matrix remodeling by tumor-associated fibroblasts. *Nature Methods*, 6(2):143–145, feb 2009.
- [177] D. T. Phan, R. H. F. Bender, J. W. Andrejcsk, A. Sobrino, S. J. Hachey, S. C. George, and C. C. Hughes. Blood–brain barrier-on-a-chip: Microphysiological systems that capture the complexity of the blood–central nervous system interface. *Experimental Biology and Medicine*, 242(17):1669–1678, 2017.
- [178] D. T. Phan, R. H. F. Bender, J. W. Andrejcsk, A. Sobrino, S. J. Hachey, S. C. George, and C. C. Hughes. Bloodâbrain barrier-on-a-chip: Microphysiological systems that capture the complexity of the bloodâcentral nervous system interface. *Exp. Biol. Med.*, 242(17):1669–1678, nov 2017.
- [179] D. T. Phan, X. Wang, B. M. Craver, A. Sobrino, D. Zhao, J. C. Chen, L. Y. Lee, S. C. George, A. P. Lee, and C. C. Hughes. A vascularized and perfused organ-on-a-chip platform for large-scale drug screening applications. *Lab on a Chip*, 17(3):511–520, 2017.
- [180] D. T. T. Phan, X. Wang, B. M. Craver, A. Sobrino, D. Zhao, J. C. Chen, L. Y. N. Lee, S. C. George, A. P. Lee, and C. C. W. Hughes. A vascularized and perfused organ-on-a-chip platform for large-scale drug screening applications. *Lab Chip*, 17(3):511–520, 2017.
- [181] M. W. Pickup, J. K. Mouw, and V. M. Weaver. The extracellular matrix modulates the hallmarks of cancer. *EMBO Rep*, 15(12):1243–1253, 2014.
- [182] A. S. Piotrowski-Daspit, A. K. Simi, M.-F. Pang, J. Tien, and C. M. Nelson. A 3D Culture Model to Study How Fluid Pressure and Flow Affect the Behavior of Aggregates of Epithelial Cells. In F. Martin, T. Stein, and J. Howlin, editors, *Mammary Gland Dev. Methods Protoc.*, pages 245–257. Springer New York, New York, NY, 2017.

- [183] W. J. Polacheck, A. E. German, A. Mammoto, D. E. Ingber, and R. D. Kamm. Mechanotransduction of fluid stresses governs 3D cell migration. *Proc. Natl. Acad. Sci.*, 111(7):2447–2452, 2014.
- [184] R. Portillo-Lara and N. Annabi. Microengineered cancer-on-a-chip platforms to study the metastatic microenvironment. *Lab Chip*, 16(21):4063–4081, 2016.
- [185] M. Potente, H. Gerhardt, and P. Carmeliet. Basic and therapeutic aspects of angiogenesis. *Cell*, 146(6):873–887, 2011.
- [186] R. Prantil-Baun, R. Novak, D. Das, M. R. Somayaji, A. Przekwas, and D. E. Ingber. Physiologically-Based Pharmacokinetic and Pharmacodynamic Analysis Enabled by Microfluidically Linked Organs-on-Chips. *Annu. Rev. Pharmacol. Toxicol.*, 58:37–64, 2016.
- [187] I. Puig, I. Chicote, S. P. Tenbaum, O. Arqués, J. R. Herance, J. D. Gispert, J. Jimenez, S. Landolfi, K. Caci, H. Allende, L. Mendizabal, D. Moreno, R. Charco, E. Espín, A. Prat, M. E. Elez, G. Argilés, A. Vivancos, J. Taberner, S. Rojas, and H. G. Palmer. A personalized preclinical model to evaluate the metastatic potential of patient-derived colon cancer initiating cells. *Clin. Cancer Res.*, 19(24):6787–6801, 2013.
- [188] Python Software Foundation. Jython. <http://www.jython.org/>. Accessed: 2018-08-23.
- [189] J. A. Ramilowski, T. Goldberg, J. Harshbarger, E. Kloppmann, M. Lizio, V. P. Satagopam, M. Itoh, H. Kawaji, P. Carninci, B. Rost, and A. R. R. Forrest. A draft network of ligand–receptor-mediated multicellular signalling in human. *Nature Communications*, 6(1):7866, nov 2015.
- [190] A. Rangarajan and R. A. Weinberg. Opinion: Comparative biology of mouse versus human cells: modelling human cancer in mice. *Nat. Rev. Cancer*, 3(12):952–959, 2003.
- [191] E. B. Rankin and A. J. Giaccia. Hypoxic control of metastasis. *Science*, 352(6282):175–180, apr 2016.
- [192] P. Rawla, A. Barsouk, A. V. Hadjinicolaou, and A. Barsouk. Immunotherapies and targeted therapies in the treatment of metastatic colorectal cancer. *Medical Sciences*, 7(8), 2019.
- [193] T. Reya and H. Clevers. Wnt signalling in stem cells and cancer. *Nature*, 434(7035):843–850, apr 2005.
- [194] C. Ricciardelli, N. A. Lokman, C. E. Pyragius, M. P. Ween, A. M. Macpherson, A. Ruzkiewicz, P. Hoffmann, and M. K. Oehler. Keratin 5 overexpression is associated with serous ovarian cancer recurrence and chemotherapy resistance. *Oncotarget*, 8(11):17819–17832, mar 2017.

- [195] R. S. Riley, C. H. June, R. Langer, and M. J. Mitchell. Delivery technologies for cancer immunotherapy. *Nature Reviews Drug Discovery*, 18(3):175–196, mar 2019.
- [196] A. C. Rios and H. Clevers. Imaging organoids: A bright future ahead. *Nat. Methods*, 15(1):24–26, 2018.
- [197] M. Romero-López, A. L. Trinh, A. Sobrino, M. M. Hatch, M. T. Keating, C. Fimbres, D. E. Lewis, P. D. Gershon, E. L. Botvinick, M. Digman, J. S. Lowengrub, and C. C. Hughes. Recapitulating the human tumor microenvironment: Colon tumor-derived extracellular matrix promotes angiogenesis and tumor cell growth. *Biomaterials*, 116:118–129, 2017.
- [198] M. Romero-López, A. L. Trinh, A. Sobrino, M. M. Hatch, M. T. Keating, C. Fimbres, D. E. Lewis, P. D. Gershon, E. L. Botvinick, M. Digman, J. S. Lowengrub, and C. C. Hughes. Recapitulating the human tumor microenvironment: Colon tumor-derived extracellular matrix promotes angiogenesis and tumor cell growth. *Biomaterials*, 116:118–129, 2017.
- [199] K. Ronaldson-Bouchard and G. Vunjak-Novakovic. Organs-on-a-Chip: A Fast Track for Engineered Human Tissues in Drug Development. *Cell Stem Cell*, 22(3):310–324, 2018.
- [200] S. A. Rosenberg, N. P. Restifo, J. C. Yang, R. A. Morgan, and M. E. Dudley. Adoptive cell transfer: a clinical path to effective cancer immunotherapy. *Nature Reviews Cancer*, 8(4):299–308, apr 2008.
- [201] RStudio Team. *RStudio: Integrated Development Environment for R*. RStudio, Inc., Boston, MA, 2016.
- [202] B. A. Ruggeri, F. Camp, and S. Miknyoczki. Animal models of disease: Pre-clinical animal models of cancer and their applications and utility in drug discovery. *Biochem. Pharmacol.*, 87(1):150–161, 2014.
- [203] J. Ruppen, F. D. Wildhaber, C. Strub, S. R. R. Hall, R. A. Schmid, T. Geiser, and O. T. Guenat. Towards personalized medicine: chemosensitivity assays of patient lung cancer cell spheroids in a perfused microfluidic platform. *Lab Chip*, 15(14):3076–3085, 2015.
- [204] N. Sachs and H. Clevers. Organoid cultures for the analysis of cancer phenotypes. *Current Opinion in Genetics & Development*, 24:68 – 73, 2014. Cancer genomics.
- [205] E. K. Sackmann, A. L. Fulton, and D. J. Beebe. The present and future role of microfluidics in biomedical research. *Nature*, 507(7491):181–189, mar 2014.
- [206] J. Schindelin, I. Arganda-Carreras, E. Frise, V. Kaynig, M. Longair, T. Pietzsch, S. Preibisch, C. Rueden, S. Saalfeld, B. Schmid, et al. Fiji: an open-source platform for biological-image analysis. *Nature methods*, 9(7):676, 2012.

- [207] C. A. Schneider, W. S. Rasband, and K. W. Eliceiri. NIH Image to ImageJ: 25 years of image analysis. *Nature methods*, 9(7):671, 2012.
- [208] G. L. Semenza. HIF-1 and mechanisms of hypoxia sensing. *Curr. Opin. Cell Biol.*, 13(2):167–171, apr 2001.
- [209] J. Seok, H. S. Warren, A. G. Cuenca, M. N. Mindrinos, H. V. Baker, W. Xu, D. R. Richards, G. P. McDonald-Smith, H. Gao, L. Hennessy, C. C. Finnerty, C. M. López, S. Honari, E. E. Moore, J. P. Minei, J. Cuschieri, P. E. Bankey, J. L. Johnson, J. Sperry, A. B. Nathens, T. R. Billiar, M. A. West, M. G. Jeschke, M. B. Klein, R. L. Gamelli, N. S. Gibran, B. H. Brownstein, C. Miller-Graziano, S. E. Calvano, P. H. Mason, J. P. Cobb, L. G. Rahme, S. F. Lowry, R. V. Maier, L. L. Moldawer, D. N. Herndon, R. W. Davis, W. Xiao, and R. G. Tompkins. Genomic responses in mouse models poorly mimic human inflammatory diseases. *Proc. Natl. Acad. Sci.*, 110(9):3507–3512, feb 2013.
- [210] G. Sharma and G. Stein-O’Brien. *projectR: Functions for the projection of weights from PCA, CoGAPS, NMF, correlation, and clustering*, 2016. R package version 1.0.045.
- [211] P. Sharma, S. Hu-Lieskovan, J. A. Wargo, and A. Ribas. Primary, Adaptive, and Acquired Resistance to Cancer Immunotherapy. *Cell*, 168(4):707–723, feb 2017.
- [212] A. K. Shenoy, Y. Jin, H. Luo, M. Tang, C. Pampo, R. Shao, D. W. Siemann, L. Wu, C. D. Heldermon, B. K. Law, L.-J. Chang, and J. Lu. Epithelial-to-mesenchymal transition confers pericyte properties on cancer cells. *Journal of Clinical Investigation*, 126(11):4174–4186, oct 2016.
- [213] S. T. Sherry, M.-H. Ward, M. Kholodov, J. Baker, L. Phan, E. M. Smigielski, and K. Sirotkin. dbsnp: the ncbi database of genetic variation. *Nucleic acids research*, 29(1):308–311, 2001.
- [214] V. S. Shirure, A. Lezia, A. Tao, L. F. Alonzo, and S. C. George. Low levels of physiological interstitial flow eliminate morphogen gradients and guide angiogenesis. *Angiogenesis*, 20(4):493–504, nov 2017.
- [215] M. L. Shuler. Organ-, body- and disease-on-a-chip systems. *Lab Chip*, 17(14):2345–2346, 2017.
- [216] R. L. Siegel, K. D. Miller, and A. Jemal. Cancer statistics, 2018. *CA. Cancer J. Clin.*, 68(1):7–30, jan 2018.
- [217] R. L. Siegel, K. D. Miller, and A. Jemal. Cancer statistics, 2019. *CA: a cancer journal for clinicians*, 69(1):7–34, 2019.
- [218] S. S. Sikandar, K. T. Pate, S. Anderson, D. Dizon, R. A. Edwards, M. L. Waterman, and S. M. Lipkin. NOTCH Signaling Is Required for Formation and Self-Renewal of Tumor-Initiating Cells and for Repression of Secretory Cell Differentiation in Colon Cancer. *Cancer Research*, 70(4):1469–1478, feb 2010.

- [219] A. Skardal, M. Devarasetty, S. Forsythe, A. Atala, and S. Soker. A reductionist metastasis-on-a-chip platform for in vitro tumor progression modeling and drug screening. *Biotechnol. Bioeng.*, 113(9):2020–2032, 2016.
- [220] A. Skardal, S. V. Murphy, M. Devarasetty, I. Mead, H.-W. Kang, Y.-J. Seol, Y. Shrike Zhang, S.-R. Shin, L. Zhao, J. Aleman, A. R. Hall, T. D. Shupe, A. Kleensang, M. R. Dokmeci, S. Jin Lee, J. D. Jackson, J. J. Yoo, T. Hartung, A. Khademhosseini, S. Soker, C. E. Bishop, and A. Atala. Multi-tissue interactions in an integrated three-tissue organ-on-a-chip platform. *Sci. Rep.*, 7(1):8837, dec 2017.
- [221] A. Skardal, T. Shupe, and A. Atala. Organoid-on-a-chip and body-on-a-chip systems for drug screening and disease modeling. *Drug Discov. Today*, 21(9):1399–1411, sep 2016.
- [222] D. A. Skelly, G. T. Squiers, M. A. McLellan, M. T. Bolisetty, P. Robson, N. A. Rosenthal, and A. R. Pinto. Single-Cell Transcriptional Profiling Reveals Cellular Diversity and Intercommunication in the Mouse Heart. *Cell Reports*, 22(3):600–610, jan 2018.
- [223] K. Smietana, M. Siatkowski, and M. Møller. Trends in clinical success rates. *Nat. Rev. Drug Discov.*, 15(6):379–380, jun 2016.
- [224] A. Sobrino, D. T. Phan, R. Datta, X. Wang, S. J. Hachey, M. Romero-Lopez, E. Gratton, A. P. Lee, S. C. George, and C. C. Hughes. 3d microtumors in vitro supported by perfused vascular networks. *Scientific reports*, 6:31589, 2016.
- [225] A. Sobrino, D. T. T. Phan, R. Datta, X. Wang, S. J. Hachey, M. Romero-López, E. Gratton, A. P. Lee, S. C. George, and C. C. W. Hughes. 3D microtumors in vitro supported by perfused vascular networks. *Sci. Rep.*, 6(1):31589, aug 2016.
- [226] A. Sobrino, D. T. T. Phan, R. Datta, X. Wang, S. J. Hachey, M. Romero-Lopez, E. Gratton, A. P. Lee, S. C. George, and C. C. W. Hughes. 3D microtumors in vitro supported by perfused vascular networks. *Scientific Reports*, 6(1):31589, aug 2016.
- [227] J. W. Song and L. L. Munn. Fluid forces control endothelial sprouting. *Proc. Natl. Acad. Sci.*, 108(37):15342–15347, 2011.
- [228] M. S. Sosa, P. Bragado, and J. A. Aguirre-Ghiso. Mechanisms of disseminated cancer cell dormancy: An awakening field. *Nature Reviews Cancer*, 14(9):611–622, 2014.
- [229] T. Souma, B. R. Thomson, S. Heinen, I. Anna, and S. Yamaguchi. Context-dependent functions of angiopoietin 2 are determined by the endothelial phosphatase VEPTP. *Proceedings of the National Academy of Sciences*, 115(6), 2018.
- [230] S. Spranger and T. F. Gajewski. Impact of oncogenic pathways on evasion of antitumour immune responses. *Nature Reviews Cancer*, 18(3):139–147, mar 2018.
- [231] T. Srinivasan, J. Walters, P. Bu, E. B. Than, K. L. Tung, K. Y. Chen, N. Panarelli, J. Milsom, L. Augenlicht, S. M. Lipkin, and X. Shen. NOTCH signaling regulates asymmetric cell fate of fast- and slow-cycling colon cancer-initiating cells. *Cancer Res.*, 76(11):3411–3421, jun 2016.

- [232] K. Stock, M. F. Estrada, S. Vidic, K. Gjerde, A. Rudisch, V. E. Santo, M. Barbier, S. Blom, S. C. Arundkar, I. Selvam, A. Osswald, Y. Stein, S. Gruenewald, C. Brito, W. Van Weerden, V. Rotter, E. Boghaert, M. Oren, W. Sommergruber, Y. Chong, R. De Hoogt, and R. Graeser. Capturing tumor complexity in vitro: Comparative analysis of 2D and 3D tumor models for drug discovery. *Sci. Rep.*, 6(1):28951, jul 2016.
- [233] R. Straussman, T. Morikawa, K. Shee, M. Barzily-Rokni, Z. R. Qian, J. Du, A. Davis, M. M. Mongare, J. Gould, D. T. Frederick, Z. A. Cooper, P. B. Chapman, D. B. Solit, A. Ribas, R. S. Lo, K. T. Flaherty, S. Ogino, J. A. Wargo, and T. R. Golub. Tumour micro-environment elicits innate resistance to RAF inhibitors through HGF secretion. *Nature*, 487(7408):500–4, 2012.
- [234] C. Stringari, R. A. Edwards, K. T. Pate, M. L. Waterman, P. J. Donovan, and E. Gratton. Metabolic trajectory of cellular differentiation in small intestine by Phasor Fluorescence Lifetime Microscopy of NADH. *Scientific Reports*, 2(1):568, dec 2012.
- [235] T. Stuart, A. Butler, P. Hoffman, C. Hafemeister, E. Papalexi, W. M. Mauck, Y. Hao, M. Stoeckius, P. Smibert, and R. Satija. Comprehensive Integration of Single-Cell Data. *Cell*, 177(7):1888–1902.e21, jun 2019.
- [236] S. Su, J. Chen, H. Yao, J. Liu, S. Yu, L. Lao, M. Wang, M. Luo, Y. Xing, F. Chen, D. Huang, J. Zhao, L. Yang, D. Liao, F. Su, M. Li, Q. Liu, and E. Song. CD10+GPR77+ Cancer-Associated Fibroblasts Promote Cancer Formation and Chemoresistance by Sustaining Cancer Stemness. *Cell*, 172(4):841–856.e16, feb 2018.
- [237] J. H. Sung, M. B. Esch, J.-M. Prot, C. J. Long, A. Smith, J. J. Hickman, and M. L. Shuler. Microfabricated mammalian organ systems and their integration into models of whole animals and humans. *Lab on a Chip*, 13(7):1201, 2013.
- [238] J. H. Sung, C. Kam, and M. L. Shuler. A microfluidic device for a pharmacokinetic-pharmacodynamic (PK&PD) model on a chip. *Lab Chip*, 10(4):446, 2010.
- [239] R. M. Sutherland, J. A. McCreddie, and W. R. Inch. Growth of multicell spheroids in tissue culture as a model of nodular carcinomas. *J. Natl. Cancer Inst.*, 46(1):113–120, 1971.
- [240] K. Takahashi and S. Yamanaka. Induced pluripotent stem cells in medicine and biology. *Development*, 140(12):2457–2461, 2013.
- [241] A. Takai, V. Fako, H. Dang, M. Forgues, Z. Yu, A. Budhu, and X. W. Wang. Three-dimensional Organotypic Culture Models of Human Hepatocellular Carcinoma. *Sci. Rep.*, 6(June 2015):21174, feb 2016.
- [242] T. Takebe, B. Zhang, and M. Radisic. Synergistic Engineering: Organoids Meet Organs-on-a-Chip. *Cell Stem Cell*, 21(3):297–300, 2017.
- [243] T. Takebe, B. Zhang, and M. Radisic. Synergistic Engineering: Organoids Meet Organs-on-a-Chip. *Cell Stem Cell*, 21(3):297–300, 2017.

- [244] J. Tannenbaum and B. T. Bennett. Russell and Burch's 3Rs then and now: the need for clarity in definition and purpose. *J. Am. Assoc. Lab. Anim. Sci.*, 54(2):120–32, mar 2015.
- [245] D. V. F. Tauriello and E. Batlle. Targeting the Microenvironment in Advanced Colorectal Cancer. *Trends in cancer*, 2(9):495–504, sep 2016.
- [246] B. Tavora, L. E. Reynolds, S. Batista, F. Demircioglu, I. Fernandez, T. Lechertier, D. M. Lees, P.-P. Wong, A. Alexopoulou, G. Elia, A. Clear, A. Ledoux, J. Hunter, N. Perkins, J. G. Gribben, and K. M. Hodivala-Dilke. Endothelial-cell FAK targeting sensitizes tumours to DNA-damaging therapy. *Nature*, 514(7520):112–6, oct 2014.
- [247] T. Tickle, I. Tirosh, C. Georgescu, M. Brown, and B. Haas. *inferCNV of the Trinity CTAT Project*. Klarman Cell Observatory, Broad Institute of MIT and Harvard, Cambridge, MA, USA, 2019.
- [248] Y. S. Torisawa, C. S. Spina, T. Mammoto, A. Mammoto, J. C. Weaver, T. Tat, J. J. Collins, and D. E. Ingber. Bone marrow-on-a-chip replicates hematopoietic niche physiology in vitro. *Nature Methods*, 11(6):663–669, 2014.
- [249] C. Trapnell, D. Cacchiarelli, J. Grimsby, P. Pokharel, S. Li, M. Morse, N. J. Lennon, K. J. Livak, T. S. Mikkelsen, and J. L. Rinn. The dynamics and regulators of cell fate decisions are revealed by pseudotemporal ordering of single cells. *Nature Biotechnology*, 32(4):381–386, apr 2014.
- [250] H.-F. Tsai, A. Trubelja, A. Q. Shen, and G. Bao. Tumour-on-a-chip: microfluidic models of tumour morphology, growth and microenvironment. *J. R. Soc. Interface*, 14(131):20170137, 2017.
- [251] N. Tsamandouras, W. L. K. Chen, C. D. Edington, C. L. Stokes, L. G. Griffith, and M. Cirit. Integrated Gut and Liver Microphysiological Systems for Quantitative In Vitro Pharmacokinetic Studies. *AAPS J.*, 19(5):1499–1512, sep 2017.
- [252] M. Uhlen, C. Zhang, S. Lee, E. Sjöstedt, L. Fagerberg, G. Bidkhori, R. Benfeitas, M. Arif, Z. Liu, F. Edfors, K. Sanli, K. von Feilitzen, P. Oksvold, E. Lundberg, S. Hober, P. Nilsson, J. Mattsson, J. M. Schwenk, H. Brunnström, B. Glimelius, T. Sjöblom, P.-H. Edqvist, D. Djureinovic, P. Micke, C. Lindskog, A. Mardinoglu, and F. Ponten. A pathology atlas of the human cancer transcriptome. *Science*, 357(6352):eaan2507, aug 2017.
- [253] G. Urban, K. M. Bache, D. Phan, A. Sobrino, A. K. Shmakov, S. J. Hachey, C. Hughes, and P. Baldi. Deep Learning for Drug Discovery and Cancer Research: Automated Analysis of Vascularization Images. *IEEE/ACM Transactions on Computational Biology and Bioinformatics*, pages 1–1, 2018.
- [254] E. Van Cutsem, D. Lambrechts, H. Prenen, R. K. Jain, and P. Carmeliet. Lessons From the Adjuvant Bevacizumab Trial on Colon Cancer: What Next? *Journal of Clinical Oncology*, 29(1):1–4, jan 2011.

- [255] A. Van De Stolpe and R. H. Kauffmann. Innovative human-specific investigational approaches to autoimmune disease. *RSC Advances*, 5(24):18451–18453, 2015.
- [256] M. Van De Wetering, H. E. Francies, J. M. Francis, G. Bounova, F. Iorio, A. Pronk, W. Van Houdt, J. Van Gorp, A. Taylor-Weiner, L. Kester, A. McLaren-Douglas, J. Blokker, S. Jaksani, S. Bartfeld, R. Volckman, P. Van Sluis, V. S. Li, S. Seepo, C. Sekhar Pedamallu, K. Cibulskis, S. L. Carter, A. McKenna, M. S. Lawrence, L. Lichtenstein, C. Stewart, J. Koster, R. Versteeg, A. Van Oudenaarden, J. Saez-Rodriguez, R. G. Vries, G. Getz, L. Wessels, M. R. Stratton, U. McDermott, M. Meyerson, M. J. Garnett, and H. Clevers. Prospective derivation of a living organoid biobank of colorectal cancer patients. *Cell*, 161(4):933–945, 2015.
- [257] E.-T. Verjans, J. Doijen, W. Luyten, B. Landuyt, and L. Schoofs. Three-dimensional cell culture models for anticancer drug screening: Worth the effort? *J. Cell. Physiol.*, 233(4):2993–3003, apr 2018.
- [258] K. H. Vining and D. J. Mooney. Mechanical forces direct stem cell behaviour in development and regeneration. *Nat. Rev. Mol. Cell Biol.*, 18(12):728–742, nov 2017.
- [259] G. Vlachogiannis, S. Hedayat, A. Vatsiou, Y. Jamin, J. Fernández-Mateos, K. Khan, A. Lampis, K. Eason, I. Huntingford, R. Burke, M. Rata, D.-m. Koh, N. Tunariu, D. Collins, S. Hulkki-Wilson, C. Ragulan, I. Spiteri, S. Y. Moorcraft, I. Chau, S. Rao, D. Watkins, N. Fotiadis, M. Bali, M. Darvish-Damavandi, H. Lote, Z. Eltahir, E. C. Smyth, R. Begum, P. A. Clarke, J. C. Hahne, M. Dowsett, J. de Bono, P. Workman, A. Sadanandam, M. Fassan, O. J. Sansom, S. Eccles, N. Starling, C. Bracconi, A. Sottoriva, S. P. Robinson, D. Cunningham, and N. Valeri. Patient-derived organoids model treatment response of metastatic gastrointestinal cancers. *Science*, 359(6378):920–926, feb 2018.
- [260] M. J. Waldner, S. Foersch, and M. F. Neurath. Interleukin-6 - A Key Regulator of Colorectal Cancer Development. *International Journal of Biological Sciences*, 8(9):1248–1253, 2012.
- [261] L. Wan, J. Skoko, J. Yu, P. R. Leduc, and C. A. Neumann. Mimicking Embedded Vasculature Structure for 3D Cancer on a Chip Approaches through Micromilling. *Sci. Rep.*, 7(1):1–8, dec 2017.
- [262] M. Wang, J. Zhao, L. Zhang, F. Wei, Y. Lian, Y. Wu, Z. Gong, S. Zhang, J. Zhou, K. Cao, X. Li, W. Xiong, G. Li, Z. Zeng, and C. Guo. Role of tumor microenvironment in tumorigenesis. *J. Cancer*, 8(5):761–773, 2017.
- [263] X. Wang, D. T. Phan, S. C. George, C. C. Hughes, and A. P. Lee. 3d anastomosed microvascular network model with living capillary networks and endothelial cell-lined microfluidic channels. In *3D Cell Culture*, pages 325–344. Springer, 2017.
- [264] X. Wang, D. T. T. Phan, S. C. George, C. C. W. Hughes, and A. P. Lee. *3D Cell Culture - Methods and Protocols*, volume 1612 of *Methods in Molecular Biology*. Springer New York, New York, NY, 2017.

- [265] X. Wang, B. C. Prager, Q. Wu, L. J. Kim, R. C. Gimple, Y. Shi, K. Yang, A. R. Morton, W. Zhou, Z. Zhu, E. A. A. Obara, T. E. Miller, A. Song, S. Lai, C. G. Hubert, X. Jin, Z. Huang, X. Fang, D. Dixit, W. Tao, K. Zhai, C. Chen, Z. Dong, G. Zhang, S. M. Dombrowski, P. Hamerlik, S. C. Mack, S. Bao, and J. N. Rich. Reciprocal Signaling between Glioblastoma Stem Cells and Differentiated Tumor Cells Promotes Malignant Progression. *Cell Stem Cell*, 22(4):514–528.e5, apr 2018.
- [266] Y. Wang, L. Wang, Y. Zhu, and J. Qin. Human brain organoid-on-a-chip to model prenatal nicotine exposure. *Lab on a Chip*, 18(6):851–860, 2018.
- [267] Y. I. Wang, C. Carmona, J. J. Hickman, and M. L. Shuler. Multiorgan Microphysiological Systems for Drug Development: Strategies, Advances, and Challenges. *Adv. Healthc. Mater.*, 1701000:1–29, 2017.
- [268] Y. I. Wang, C. Oleaga, C. J. Long, M. B. Esch, C. W. McAleer, P. G. Miller, J. J. Hickman, and M. L. Shuler. Self-contained, low-cost Body-on-a-Chip systems for drug development. *Exp. Biol. Med.*, 242(17):1701–1713, 2017.
- [269] M. J. Waring, J. Arrowsmith, A. R. Leach, P. D. Leeson, S. Mandrell, R. M. Owen, G. Pairaudeau, W. D. Pennie, S. D. Pickett, J. Wang, O. Wallace, and A. Weir. An analysis of the attrition of drug candidates from four major pharmaceutical companies. *Nat. Rev. Drug Discov.*, 14(7):475–486, 2015.
- [270] K. Weber, U. Bartsch, C. Stocking, and B. Fehse. A Multicolor Panel of Novel Lentiviral “Gene Ontology” (LeGO) Vectors for Functional Gene Analysis. *Molecular Therapy*, 16(4):698–706, apr 2008.
- [271] S. Welch, K. Spithoff, R. B. Rumble, and J. Maroun. Bevacizumab combined with chemotherapy for patients with advanced colorectal cancer: a systematic review. *Annals of Oncology*, 21(6):1152–1162, jun 2010.
- [272] J. A. Whisler, M. B. Chen, and R. D. Kamm. Control of Perfusable Microvascular Network Morphology Using a Multiculture Microfluidic System. *Tissue Eng. Part C Methods*, 20(7):543–552, jul 2014.
- [273] J. P. Wikswo, E. L. Curtis, Z. E. Eagleton, B. C. Evans, A. Kole, L. H. Hofmeister, and W. J. Matloff. Scaling and systems biology for integrating multiple organs-on-a-chip. *Lab Chip*, 13(18):3496, 2013.
- [274] C. B. Williams, E. S. Yeh, and A. C. Soloff. Tumor-associated macrophages: unwitting accomplices in breast cancer malignancy. *NPJ breast cancer*, 2(1):15025, dec 2016.
- [275] M. J. Wilmer, C. P. Ng, H. L. Lanz, P. Vulto, L. Suter-Dick, and R. Masereeuw. Kidney-on-a-Chip Technology for Drug-Induced Nephrotoxicity Screening. *Trends Biotechnol.*, 34(2):156–170, 2016.
- [276] D. K. Wood, A. Soriano, L. Mahadevan, J. M. Higgins, and S. N. Bhatia. A Biophysical Indicator of Vaso-occlusive Risk in Sickle Cell Disease. *Sci. Transl. Med.*, 4(123):123ra26–123ra26, feb 2012.

- [277] D. Wu, P. Wu, Q. Huang, Y. Liu, J. Ye, and J. Huang. Interleukin-17: A Promoter in Colorectal Cancer Progression. *Clinical and Developmental Immunology*, 2013:1–7, 2013.
- [278] S. Xiao, J. R. Coppeta, H. B. Rogers, B. C. Isenberg, J. Zhu, S. A. Olalekan, K. E. McKinnon, D. Dokic, A. S. Rashedi, D. J. Haiseneder, S. S. Malpani, C. A. Arnold-Murray, K. Chen, M. Jiang, L. Bai, C. T. Nguyen, J. Zhang, M. M. Laronda, T. J. Hope, K. P. Maniar, M. E. Pavone, M. J. Avram, E. C. Sefton, S. Getsios, J. E. Burdette, J. J. Kim, J. T. Borenstein, and T. K. Woodruff. A microfluidic culture model of the human reproductive tract and 28-day menstrual cycle. *Nat. Commun.*, 8:14584, mar 2017.
- [279] T. M. Yeung, S. C. Gandhi, J. L. Wilding, R. Muschel, and W. F. Bodmer. Cancer stem cells from colorectal cancer-derived cell lines. *Proc. Natl. Acad. Sci.*, 107(8):3722–3727, 2010.
- [280] J. L. Yu, J. W. Rak, P. Carmeliet, A. Nagy, R. S. Kerbel, and B. L. Coomber. Heterogeneous Vascular Dependence of Tumor Cell Populations. *The American Journal of Pathology*, 158(4):1325–1334, apr 2001.
- [281] I. K. Zervantonakis, S. K. Hughes-Alford, J. L. Charest, J. S. Condeelis, F. B. Gertler, and R. D. Kamm. Three-dimensional microfluidic model for tumor cell intravasation and endothelial barrier function. *Proc. Natl. Acad. Sci.*, 109(34):13515–13520, aug 2012.
- [282] B. Zhang and M. Radisic. Organ-on-a-chip devices advance to market. *Lab Chip*, 17(14):2395–2420, 2017.
- [283] N. Zhang, R. Zhang, K. Zou, W. Yu, W. Guo, Y. Gao, J. Li, M. Li, Y. Tai, W. Huang, C. Song, W. Deng, and X. Cui. Keratin 23 promotes telomerase reverse transcriptase expression and human colorectal cancer growth. *Cell Death & Disease*, 8(7):e2961–e2961, jul 2017.
- [284] X. Zhang, Y. Lan, J. Xu, F. Quan, E. Zhao, C. Deng, T. Luo, L. Xu, G. Liao, M. Yan, Y. Ping, F. Li, A. Shi, J. Bai, T. Zhao, X. Li, and Y. Xiao. CellMarker: a manually curated resource of cell markers in human and mouse. *Nucleic Acids Research*, 47(D1):D721–D728, jan 2019.
- [285] Y. S. Zhang, Y. N. Zhang, and W. Zhang. Cancer-on-a-chip systems at the frontier of nanomedicine. *Drug Discov. Today*, 22(9):1392–1399, 2017.
- [286] L. Zitvogel, J. M. Pitt, R. Daillère, M. J. Smyth, and G. Kroemer. Mouse models in oncoimmunology. *Nat. Rev. Cancer*, 16(12):759–773, 2016.